Investigations of Factors that Control Retinal Axon Growth during Mouse Optic Pathway Development

LI, Jia

A Thesis Submitted in Partial Fulfillment

of the Requirements for the Degree of

Doctor of Philosophy

in

Anatomy

The Chinese University of Hong Kong

September 2010

Thesis/ Assessment Committee

Professor CHO Yu Pang (Chair)

Professor CHAN Sun On (Thesis Supervisor)

Professor KWONG Wing Hang (Committee Member)

Professor SHUM Kwok Yan (External Examiner)

Abstract of thesis entitled:

Investigations of factors that control retinal axon growth during mouse optic pathway development

Submitted by Li Jia

for the degree of Doctor of Philosophy

at The Chinese University of Hong Kong in July 2010

Abstract

During development, retinal ganglion cell axons grow from the eye to the ventral diencephalon, where axons from the two eyes converge and segregate into crossed and uncrossed projections, forming the optic chiasm. This pattern is critical for binocular vision. Although significant progress has been obtained over the past decades, how retinal axon growth and guidance are regulated at the chiasm is largely unknown. Our research will focus on those problems.

Chiasm cells, which include glia and neurons, are generated early before any retinal axon arrives at the midline of the mouse ventral diencephalon. These cells have been shown to affect retinal axon growth and patterning in the optic chiasm. In this study, we used EdU (5-ethynyl-2′-deoxyuridine) for birthdating these chiasm cells, aiming to find out when these cells are generated; then we tried to trace their fates at later stages of development. EdU injection at embryonic day (E) 9.5 to E11 labeled a number of chiasmatic neurons and radial glial cells at E13, which were immunoreactive for SSEA-1 and RC2, respectively. After colocalization studies, we found that most of these neurons were born as early as E9.5, while a large number of radial glial cells were born as from E11. Both E9.5-born chiasmatic neurons and E11-born radial glia decreased by E14-E16; the radial glia even disappeared finally from the midline. Furthermore, we found that some chiasmatic neurons underwent

apoptotic cell death as from E14, and that the radial glia likely differentiated into other cell types after finishing their retinal axon guidance mission at the midline. So it is reasonable that some of the earliest born chiasm cells disappear during development.

N-methyl-D-aspartate (NMDA) receptor is one of the ionotropic glutamate receptors, which are important in synaptic plasticity, apart from implications in dendritic spine remodeling, neurite outgrowth, elongation and branching and glutamate neurotoxicity. There are several subtypes of NMDA receptor channel subunits, NR1, NR2A-D, NR3A&B. The functional diversity of NMDA receptor resides in the different assembly of subunits. In this study, we used RT-PCR to analyze the mRNA expression of all the NMDA receptor subunits in mouse embryos. After that we chose the NR1, NR2B and NR3A antibodies to investigate NMDA receptor subunit expression in the optic pathway during mouse optic pathway development. Using immunohistochemistry, we found that NR1, NR2B and NR3A were expressed in the mouse retina and optic pathway as from E13 when the optic chiasm is forming. Expression of the NMDA receptor subunits were found in the inner cell layers and along retinal axons. Colocalization studies showed that NR1, NR2B and NR3A were localized on the ganglion cells and their axons. In the ventral diencephalon, these subunits were expressed extensively, but NR1 and NR3A were particularly strong along the optic nerve and optic tract. Furthermore, to identify the function of NMDA receptor during optic chiasm development, we cultured E14 retinal explants on laminin and poly-D-ornithine in the presence of the NMDA receptor antagonists MK-801 or Dextrorphan-D-tartrate. These two antagonists can significantly inhibit the retinal axon outgrowth, suggesting that the NMDA receptor promotes retinal axon outgrowth in the retinofugal pathway during optic chiasm

development.

In the last part of this thesis, we investigated the retinal axon pathway in the ventral diencephalon of the *Sox10*^{Dom} mutant embryos and γA-crystallin mutant embryos. Our findings indicate that *Sox10* may not contribute to axon guidance in the developing optic pathway whereas γA-crystallin may only play a role in the later uncrossed axons.

論文摘要

在發育過程中，視網膜神經節細胞的軸突從眼睛一直延伸到腹側間腦，在那裡來自兩只眼睛的軸突先會聚然後分離到交叉和非交叉投射，從而形成了視交叉。視交叉對雙眼視覺的形成至關重要。雖然在過去的幾十年對視交叉的研究已經有了非常顯著的進展，但是視網膜軸突是如何在視交叉裡生長和調節走向仍然還不是很清楚。我們的研究就是致力於這些未解決的問題。

視交叉細胞，包括神經膠質細胞和神經元，在視網膜軸突還未到達小鼠腹側間腦中線的時候就已經產生了。這些細胞可以影響視網膜軸突在視交叉的生長和走向。在此研究中我們先用 EdU (5-ethynyl-2′-deoxyuridine) 找出這些視交叉細胞的產生時間，然後再試着追踪它們在發育晚期的命運。從胚胎發育第 9.5 天 (E9.5) 到 E11 注射 EdU 可以在 E13 標記到一定數量的視交叉神經元和放射狀膠質細胞，分別可用 SSEA-1 和 RC2 來做免疫染色。共區域化研究發現，絕大多數的視交叉神經元產生於 E9.5，而大量的放射狀膠質細胞則從 E11 開始產生。這些 E9.5 出生的神經元和 E11 出生的放射狀膠質細胞都在 E14 到 E16 的時候變得越來越少，而到最後中線的膠質細胞甚至完全消失。進一步的研究發現，一些視交叉神經元從 E14 開始凋亡，而放射狀膠質細胞則很有可能在完成它們在中線位置知道視網膜軸突走向的使命後轉變成其他細胞。這就是為什麼這些最早產生的視交叉細胞消失在其後的發育過程中。

NMDA 受體是谷氨酸離子型受體的一種，對神經元的可塑性，神經軸突的生長以及谷氨酸的神經毒性都起到重要作用。 NMDA 受體有 7 個亞型：NR1，NR2A-D 和 NR3A，B。不同亞型的結合賦予 NMDA 受體功能的多樣性。在這部分的研究中，我們用 RT-PCR 來分析所有亞型在小鼠胚胎發育中的 mRNA

表達，之後我們選擇了 NR1，NR2B 和 NR3A 三個抗體來研究 NMDA 受體在小鼠視覺通路發育過程中的表達。運用免疫組織化學技術我們發現 NR1，NR2B 和 NR3A 從 E13 開始就在小鼠的視網膜和視覺通路上表達，而且這些亞型都存在於視網膜內層細胞和軸突上。共區域化研究發現，NR1 和 NR3A 表達在視網膜神經節細胞胞體及其軸突上，而 NR2B 只在軸突上表達。在腹側間腦上這三個亞型表達則非常廣泛，但 NR1 和 NR3A 在視神經和視束上表達更高。進一步我們用 NMDA 受體的拮抗劑 MK801 或 Dextrorphan-D-tartrate 來研究 NMDA 受體的功能，結果發現這兩種拮抗劑都可以在 E14 視網膜組織培養中顯著抑制軸突的外向生長，提示我們 NMDA 受體在視交叉的發育中可以促進視網膜軸突沿視覺通途的生長。

在論文的最後一部分我們研究了在兩個小鼠突變模型 *Sox10*^{Dom} 和 γA-crystallin 基因突變胚胎中視網膜軸突在腹側間腦的軌跡，結果發現 *Sox10* 對胚胎髮育期視網膜軸突在間腦內的走向不起作用，而 γA-crystallin 則有可能只作用於發育後期的非交叉軸突。

Acknowledgements

It would not have been possible to write this doctoral thesis without the help and support of the kind people around me, to only some of whom it is possible to give particular mention here.

First and foremost I offer my sincerest gratitude to my supervisor, Professor Sun-on Chan, who has supported me throughout my thesis with his patience, kindness and knowledge. Thanks a lot for his support in my scientific research during the past three years. His expert guidance, continuous encouragement, creative ideas and invaluable suggestions have inspired me throughout the course of this project. His profound knowledge, his attitude of research and skill of presentation have been the precious resources to me. He is an admirable professor and will always be a role model for me.

I also would like to express my deepest appreciation to Professor Woody Chan, Professor Eric Cho, and Professor Zhao Hui for their suggestions and instructions in the Journal club. I want to show my gratitude to Anny Cheung and Peggy Leung for their kind help in retinal culture, Western-blot and preparation for the experiments. My warmest thanks also go to my colleagues, Dr Amy Chung, Dr Wang liqing, Dr Wang xia, Dr Wong Wai Kai, Cheng Xiaojing, Florence Yat, Jason Chan, Liu xia, Bao lihua and Shi chun for their support and suggestions on my studies. I am indebted to the technical assistance in my research from Corinna Au, Jenny Hou, Jean Kung, Simon Tong and Samuel Wong.

Finally, I own my deepest gratitude to my family for their deep love, understanding, endless patience and encouragement when it was most required.

Table of Abbreviations

AF488	Alexa Fluor 488
AMPA	α-amino-3-hydroxy-5-methylisoxazole-4-proionate
BMPs	bone morphogenetic proteins
BrdU	5-bromo-2′-deoxyuridine
CMZ	ciliary margin zone
CNS	central nervous system
CSPGs	chondroitin sulfate proteoglycans
Cy3	Cyanine 3
DC	dorsal central
DCC	deleted in colorectal cancer
DiI	1,1'-Dioctadecyl-3,3,3',3'-tetramethylindo-carbocyanine perchlorate
DN	dorsal nasal
E	embryonic day
EdU	5-ethynyl-2'-deoxyuridine
FITC	Fluorescein isothiocyanate
GAP43	growth-associated protein-43
GluRs	Glutamate receptors
iGluRs	ionotropic glutamate receptors
LGN	lateral geniculate nucleus
MAP2	microtubule-associated protein
mGluRs	metabotropic glutamate receptors
NC	neural crest
NCAM	neural cell adhesion molecule
NCCs	neural crest cells
NMDA	N-methyl-D-aspartate
NR	N-methyl-D-aspartate receptor

OC	optic chiasm
OS	optic stalk
OT	optic tract
PB	phosphate buffer
PBS	phosphate buffered saline
RGC	retinal ganglion cell
SC	superior colliculus
Shh	Sonic hedgehog
SSEA1	stage specific embryonic antigen 1
VT	ventral temporal

Table of Contents

CHAPTER 1
General Introduction

In the mammalian visual system, there is an X-shaped axonal pathway intersection located in the ventral diencephalon. It is formed by the retinal ganglion cell (RGC) axons, which grow towards each other from the two optic nerves and encounter at the ventral midline. This structure is very important for the binocular vision and known as the optic chiasm (Mason & Sretavan, 1997). The main function of the optic chiasm is to transmit the inputs from the same visual point received by each retina to the same position in the visual cortex. Then in the visual cortex, the two images are integrated together and revealed as a three-dimensional representation (Herrera & Garcia-Frigola, 2008).

However, in the binocular vision animals, RGC axons arise from the two retinas do not merely project contralaterally at the optic chiasm. It has long been known that the optic chiasm also represents a decision point in the retinofugal pathway (Mason & Sretavan, 1997; Sretavan et al, 1994). In the adult visual pathway, retinal axons arising from the nasal retina of each eye cross the midline to project into the contralateral optic tract, innervating targets on the contralateral side of the brain (Sretavan et al, 1994). While, a group of retinal axons from the temporal retina do not cross, but turn away from the midline region and project into the ipsilateral optic tract, innervating targets on the same side of the brain (Sretavan et al, 1994). This highly specific axon routing pattern makes sure that visual information perceived by two retinas is directed to the target nuclei for processing the binocular vision (Guillery et al, 1995; Mann et al, 2004; Petros et al, 2008; Williams et al, 2004).

The earliest axonal growth pattern in the optic pathway is different from the adult pattern: (1) the earliest uncrossed axons arise from the dorsocentral (DC) retina instead of ventrotemporal (VT) retina in adult; (2) early uncrossed axons project into the ipsilateral optic tract directly, without first growing toward to the midline as the later uncrossed axons do; (3) interactions between axons from each eye, which is important for the uncrossed projection of ventrotemporal axons, are not necessary for establishing the early ipsilateral pathways (Marcus & Mason, 1995; Mason & Sretavan, 1997).

Therefore, the mechanisms controlling the early optic axon trajectory differ from that in later development. The rules, which govern the retinal axon projection at chiasm, critically depend upon retinal and chiasmatic factors. Furthermore, both the cellular environment and other axons within the chiasm are very important in the guidance mechanisms (Erskine & Herrera, 2007; Guillery et al, 1995; Petros et al, 2008; Williams et al, 2004).

1. DEVELOPMENT OF THE MOUSE OPTIC CHIASM

Visual pathway in the mouse is a good model used commonly to study the development of the optic chiasm in mammals. The formation of the mouse optic chiasm has been demonstrated to occur in three sequential phases.

1.1 The early phase of chiasm formation

In the first phase, from E 12.5-E 13.5, earliest-born RGC axons, originating from the dorsocentral retina, grow into the optic stalk to enter the ventral diencephalon, where they form an X-shaped pattern containing both crossed and uncrossed projection (Petros et al, 2008). The cellular environment of the developing ventral diencephalon is very important for the RGC axon guidance. There are two populations of cells in this environment, radial glia and neurons, which are generated

early before any retinal axons arrive at the midline of the mouse ventral diencephalon. These cells have been shown to affect retinal axon growth and patterning in the optic chiasm, so they are also called chiasm cells (Marcus & Mason, 1995; Mason & Sretavan, 1997; Petros et al, 2008).

One population of the chiasm cells is a palisade of radial glia located at the ventricular zone, which extend long processes that straddle the midline. These cells in the mouse can be labeled by RC2 antibody. Previous study indicated that this RC2-positive palisade contacting both ipsilateral and contralateral retinal axons serves as a boundary during the initial chiasm formation, playing permissive or inhibitory roles to the RGC axons (Marcus et al, 1995; Marcus & Mason, 1995).

A second population consists of a group of early differentiating neurons which are immunoreactive for the stage-specific embryonic antigen 1(SSEA-1), which is also expressed by stem cells (Capela & Temple, 2002; Muramatsu & Muramatsu, 2004). SSEA-1-positive cells form a characteristic "V" shaped array which marks the posterior boundary of the future chiasm, acting as a border for RGC axon growth (Herrera & Garcia-Frigola, 2008; Mason & Sretavan, 1997). These neurons also express a number of other different epitopes, including L1 (an immunoglobulin superfamily molecule), CD44 (a cell surface molecule in the immune system) (Sretavan et al, 1994), microtubule-associated protein (MAP2) and TuJ1 (both of them are neuronal marker). From in vitro and vivo studies of the cell surface molecules expressed by SSEA-1 neurons, it was found that these cells have complex interactions with the RGC axons. This neuronal population inhibits retinal axon growth, serving as a posterior boundary during chiasm formation (Sretavan et al, 1994). On the other hand, they may also serve to promote the axon growth into the ventral diencephalon, since in the absence of these neurons retinal axons fail to grow

in to the ventral diencephalon (Mason & Sretavan, 1997; Sretavan et al, 1995).

The interactions between chiasmatic radial glia and neurons are very important for pathfinding of crossed and uncrossed axons. Early uncrossed axons, originating from the dorsocentral retina, enter the ipsilateral optic tract directly. These early uncrossed axons never enter the radial glial palisade; whereas the early crossed axons enter its caudal border. For chiasmatic neurons, early crossed axons turn medially and rostrally along their anterior border (Marcus & Mason, 1995; Mason & Sretavan, 1997; Petros et al, 2008).

1.2 The peak phase of chiasm formation

The second phase, also called the peak phase, in the mouse is from E14 to E17. During this phase, the late uncrossed axons, originating from the ventrotemporal retina, first grow toward the chiasmatic midline and then turn laterally to enter the ipsilateral optic tract; while the crossed axons, originating from all other retina regions, traverse the chiasmatic midline and grow into the contralateral projection (Marcus et al, 1995; Marcus & Mason, 1995; Petros et al, 2008). For chiasmatic radial glia, later crossed and uncrossed optic axons only enter the rostral half of the glial palisade. For chiasmatic neurons, the conformation of these neurons elongates rostrocaudally during this phase; late crossed and uncrossed axons encounter them only near the midline (Guillery et al, 1995; Petros et al, 2008).

The correspondence between the retinal axon projections with the specialized cellular arrangement formed by the chiasm cells strongly suggests that cells localized within the ventral diencephalon contribute an important role in the retinal axon divergence and establishment of the visual pathway (Marcus & Mason, 1995; Mason & Sretavan, 1997; Williams et al, 2004).

1.3 The late phase of chiasm formation

In the third phase, from E17.5-P0, most RGC axons from the ventrotemporal retina project contralaterally rather than ipsilaterally. Thereafter, in this phase, all ganglion cells extend a crossed axon whether they are born in the ventrotemporal or nasal retina (Drager, 1985; Petros et al, 2008).

All these sequential processes are the result of a combination of tissue patterning event and axon guidance decisions taken by RGC axons at the midline of the ventral diencephalon.

2. AXON GUIDANCE IN THE OPTIC PATHWAY

After their final differentiation, RGCs send out axons into the optic fiber layer at the inner surface of the retina where they navigate towards their exit point from the eye, the optic disc. From here, they enter the optic nerve and travel towards the ventral midline of the diencephalon where they meet the axons from the contralateral eye and form the optic chiasm. At the chiasm a portion of axons cross the midline to project to the contralateral targets, including the superior colliculus and lateral geniculate nucleus, while some axons grow away from the midline to project to the ipsilateral brain targets (Haupt & Huber, 2008).

2.1 Guidance within retina

For differentiation and survival of RGCs, the Brn3 POU domain transcription factors play essential roles. In the mouse the Brn3 family consists of Brn3a, Brn3b and Brn3c. These factors have similar functions in neuronal differentiation, as they share more than 95% identity within the POU domain. In the developing retina, Brn3b starts to express from E11.5 in the mouse, when the first RGCs are generated, followed by Brn3a and Brn3c (Pan et al, 2005; Wang et al, 2002; Xiang et al, 1995). The mutation or deficiency of these genes will cause disorganized axonal outgrowth. For example, in Brn3b deficient mice, RGCs undergo enhanced apoptosis leading to

thinner optic nerves (Gan et al, 1999; Gan et al, 1996); in Brn3b/c deficient mice, RGCs fail to send out axons in vitro (Wang et al, 2000).

After differentiation, RGCs send out their axons into the optic fiber layer of the retina and project towards their exit point, the optic disc. This process is driven by the balance of the growth promoting properties, mediated by some inhibitory factors and positive factors (Brittis & Silver, 1995; Haupt & Huber, 2008). The inhibitory factors prevent RGC axons growth into retinal periphery and positive factors promote axons growth centrally. These factors act together to make sure that the RGC axons extend directly to the optic disc when they grow within the optic fiber layer.

Slits is an evolutionary conserved family providing axon guidance cues in this process. Slits act though their receptor Roundabouts. In mice, Slit1 and Slit2 are detected in the RGCs and retina inner nuclear layer, while Robo2 is expressed on the RGCs (Erskine et al, 2000). In vitro, Slit1 and Slit2 inhibit the RGC axon outgrowth (Erskine et al, 2000; Plump et al, 2002), while in Slit1/2 deficient mice, a subset of RGC axons extend to the outer layer of the retina instead of the optic fiber layer (Erskine & Herrera, 2007; Thompson et al, 2006). These findings imply that Slit-signaling play a role in restricting RGC axons to the optic fiber layer in the ventral retina.

Chondroitin sulphate proteoglycan (CSPG), which is also expressed in the retina, is involved in mediating the timing and initial direction of retinal axon outgrowth (Brittis et al, 1992; Brittis & Silver, 1995; Haupt & Huber, 2008). There are some cell adhesion molecules, such as L1, BEN, NrCAM, acting in a positive way to promote RGC axons growing directly towards the optic disc(Erskine & Herrera, 2007). L1, a transmembrane glycoprotein, is involved in the axon

pathfinding and fasciculation within the retina (Demyanenko & Maness, 2003). BEN might help L1 in the RGC axons fasciculation (Weiner et al, 2004). In developing retina, NrCAM plays a crucial role in promoting RGC axon growth towards the optic disc, and also for projecting into the optic nerve (Zelina et al, 2005).

Once RGC axons reach the optic disc, RGC axons have to exit the eye and enter the optic stalk, which is then called the optic nerve. The key players in this process are the axon guidance molecule netrin-1 and its receptor DCC (deleted in colorectal cancer) (Erskine & Herrera, 2007; Inatani, 2005; Meriane et al, 2004). Netrin-1 is highly expressed in the glia cells which are located at the optic disc surrounding RGC axons, while its receptor DCC is detected on the RGC axons (Deiner et al, 1997; Manitt et al, 2009). Netrin-1 or DCC deficiency will lead to the failure of RGC axons exiting the eye, which result in optic nerve hypoplasia. Thus, in the developing retina, netrin/DCC signaling has a local function at optic disc to direct axon outgrowth (Haupt & Huber, 2008; Hopker et al, 1999).

Several other factors, like EphBs, BMP receptor 1B and NrCAM also contribute to the targeting of RGC axons to the optic disc and subsequent exit from the eye (Birgbauer et al, 2000; Liu et al, 2003; Zelina et al, 2005).

2.2 Guidance at the optic chiasm

After leaving the eye, RGC axons navigate into the developing optic stalk, and grow toward the ventral midline in the diencephalon. Axons from the two eyes grow towards each other to encounter at the midline and form the x-shaped optic chiasm there. There are several factors determining the formation of the optic chiasm.

Sonic hedgehog (Shh), which is first found in the notochord and floor plate, is a member of hedgehog family (Marti et al, 1995). It has been proved that Shh plays

an important role in the formation of the eye (Macdonald et al, 1995), generation of retinal ganglion cells (Dakubo et al, 2003) and the development of the optic chiasm (Hao et al, 2007; Torres et al, 1996). In the chick, Shh induces the differentiation of the ventral forebrain neurons, which include the early differentiating chiasmatic neurons (Ericson et al, 1995). The determination of the ventral midline in the diencephalon requires Shh as well (Dale et al, 1997). Therefore, the initial positioning of the chiasm might depend on shh signaling. Sonic Hedgehog (Shh) is expressed in the entire ventral midline before retinal axons arrive. At the preoptic region, the expression of Shh is downregulated when the RGC axons are approaching, whereas at the border of chiasm, Shh still remains (Trousse et al, 2001). This suggests that Shh may take part in chiasm formation. In the *Pax2* null mice, the optic chiasm fails to develop due to absence of the contralateral projection of the RGC axons. This morphological alteration of the chiasm is associated with persistent expression of Shh at the optic disc (Macdonald et al, 1997). It is very likely that the patterning events directed by Pax2 are highly dependent on Shh expression at the midline which is crucial to establishing the correct projection of the RGC axons (Sanchez-Camacho & Bovolenta, 2008). So, in contrast to the retina, where Shh promotes retinal axon growth towards the optic disc, Shh serves as an inhibitor of RGC axon growth in the chiasmatic region (Erskine & Herrera, 2007).

The slit family, which is discussed above, also highly influences the position of the optic chiasm in mice. Slits guide retinal axon divergence with their receptor Robos (Haupt & Huber, 2008). In mice, Slit1 and Slit2 are expressed in the ventral diencephalon, while Robo2 is present in RGCs (Erskine et al, 2000). In Slit1 or Slit2 single deficient mice, the axon pathfinding at the optic chiasm are quite normal. But Slit1/Slit2 double mutant mice display an ectopic commissure rostral to the normal

chiasm, and misguidance of RGC axons into the contralateral projection and ventral diencephalon (Petros et al, 2008; Plump et al, 2002). These results suggest that Slit1 and Slit2 collaborate to channel RGC axons into the proper pathway and determine the location of future chiasm in the mouse.

The interactions between ephrinBs and their receptor EphBs are very important for the RGC axon divergence at the optic chiasm. In mice, EphB1 and ephrinB2 receptor-ligand system is crucial for the ipsilateral projection. During the early phase of chiasm formation, EphB1 is expressed in the DC retina; while during the peak phase, EphB1 is found exclusively in the VT retina. Then the expression of EphB1 is downregulated at the VT retina after E17.5, the time of late midline divergence. At the mouse chiasmatic midline, ephrinB2 is expressed in the chiasmatic radial glia and become most intense during the peak phase of chiasm development (Petros et al, 2008; Williams et al, 2003). In the EphB1 null mice, VT retinal axons ectopically cross the midline, revealing a reduced ipsilateral projection (Williams et al, 2003). Furthermore, ephrinB2's premature ectopic expression in chiasm causes a precocious uncrossed projection, indicating that ephrinB provides inhibitory information for axon divergence (Nakagawa et al, 2000). So ephrinB2/EphB1 signaling inhibits the VT RGC axons at the midline and make them project ipsilaterally. In the late phase of chiasm development, RGC axons from the VT retina also cross the midline and grow into the contralateral optic tract, due to the downregulation of EphB1 in the VT RGCs (Petros et al, 2008).

The zinc finger transcription factors Zic2, which is a vertebrate homolog of the Drosophila gene old-paired, is transiently expressed in the VT RGCs, which form the ipsilateral projection, during the peak phase of the midline divergence (Herrera et al, 2003; Petros et al, 2008). In the Zic2 knockdown mice, heterozygous animals

display a reduced uncrossed projection while most homozygous animals show the absence of the uncrossed projection (Herrera et al, 2003; Herrera & Garcia-Frigola, 2008; Nagai et al, 2000). This shows that Zic2 is required for the formation of ipsilateral projection at the optic chiasm. In mice, as both Zic2 and EphB1 are expressed in the VT retina and are crucial in guiding the ipsilateral axon projection at the chiasmatic midline, is there any relationship between the two factors? The ectopic expression of Zic2 in RGCs causes the axon avoidance at the chiasmatic midline, and this misguidance has been showed largely EphB1-dependent (Garcia-Frigola et al, 2008). In addition, in the Zic2 null mice, the expression of ephrinB2 is changed as well, making Zic2 a potential downstream candidate of ephrinB2 (Herrera et al, 2003). These findings indicate that Zic2 and EphB1/ephrinB2 are involved in the same pathway (Herrera & Garcia-Frigola, 2008; Petros et al, 2008). The lim homeodomain transcription factor Islet2 also takes part in the axon divergence in the optic chiasm. In contrast to Zic2, Islet2 is expressed specifically in RGCs which send contralateral projection. In the Islet2 deficient mice, the expression of both Zic2 and EphB1 is increased and associate with an increase of ipsilateral axon projection, indicating that Islet2 is involved in Zic2 and EphB1 pathway (Haupt & Huber, 2008; Pak et al, 2004; Petros et al, 2008).

CD44, a molecule involved in cell-cell interaction in the immune system, is expressed on a population of early born neurons, which arrange in an inverted V-shaped pattern at the future chiasm. This molecule has been shown to inhibit RGC axon outgrowth in vitro (Haupt & Huber, 2008; Sretavan et al, 1994). After in vivo ablation of CD44 from the chiasmatic neurons using the monoclonal antibodies against CD44, RGC axons fail to form the optic chiasm because of stalling at the approximate entry site into the optic chiasm (Sretavan et al, 1995). Application of

anti-CD44 antibodies in the brain slice preparation of E13 and E14 retinofugal pathway causes a significant reduction of crossed axons projection in the optic chiasm, while this change does not occur in the E15 brain slice preparation suggesting that CD44 has no influence to the lately generated crossed axons. But in E15 brain slice preparation, the anti-CD44 treatment led to a reduction of uncrossed projection (Lin & Chan, 2003). Therefore, CD44 is essential for axon crossing and divergence at the optic chiasm due to its selective responses to different kinds of retinal axons. Hyaluronan, the major ligand of CD44, was colocalized with CD44 only at the midline but not in the lateral domains of the chiasmatic neurons (Lin et al, 2007b). In E13 brain slice culture, exogenous hyaluronan leads to a dose-dependent reduction in midline crossing during the early phase of chiasm formation. In E15 brain slice culture, an obvious reduction of uncrossed axons is revealed after hyaluronan treatment. However, hyaluronan does not affect the retinal neurite outgrowth and extension in the retinal explants culture studies (Lin et al, 2007a). Taken together, hyaluronan plays a role in regulating midline crossing and axon divergence at the optic chiasm due to the interaction with CD44.

The winged helix transcription factors Foxg1 and Foxd1 belong to the forkhead family of transcription factors. Foxg1 is detected in most nasal RGCs, some temporal RGCs and at the chiasm. Foxg1 mutant mice display an increased ipsilateral projection, generating from RGCs in both nasal and temporal retina, suggesting that Foxg1 takes part in the establishment of the correct ipsilateral projection (Herrera & Garcia-Frigola, 2008; Pratt et al, 2004). Foxd1 is expressed in the VT retina and the ventral diencephalon during the chiasm development. In the Foxd1 lacking embryos, both the retinal development and chiasm morphologies appear to be abnormal. In the Foxd1 deficient mice, some factors contributing to the

ipsilateral projection, such as Zic2 and EphB1, are totally missing in the retina, and the Foxg1 expression expanding form the nasal RGCs to the VT ones. Foxd1 deficiency leads to the VT RGC axons grow aberrantly to the contralateral projection, while the ipsilateral projection is also increased, even though the ipsilateral program is malfunction (Haupt & Huber, 2008; Herrera et al, 2004). In Foxd1 deficient ventral diencephalon, Foxg1 invades into the Foxd1 region, meanwhile the expression of Zic2 is minimized. Thus, in the developing optic pathway, Foxg1 acts as an upstream protein in uncrossed projecting program, contributing in patterning of retina and takes part in patterning the ventral diencephalon where chiasm is formed (Haupt & Huber, 2008; Herrera et al, 2004).

Chondroitin sulfate proteoglycans (CSPGs), a population of extracellular matrix molecules, are involved in cell-cell and cell-matrix interactions and axon guidance in the developing neural pathway (Haupt & Huber, 2008). In mouse ventral diencephalon, CSPGs are first detected at E12, prior to any axon arrival. Then CSPGs are expressed in the caudal half of the ventral diencephalon and revealed as an inverted V-shaped array, marking the caudal boundary of the RGC axons in the optic chiasm. These findings indicate that CSPGs may be involved in the guidance mechanism regulating retinal axon pathfinding at the optic chiasm (Chung et al, 2000a). Enzymatic removal of CSPGs at different embryonic stages showed different effects on axon routing. At E13, morphological change in growth cone and aberrant position of axon crossing at the midline were observed. At later embryonic stages, enzyme treatments reduced the uncrossed projection obviously, but had no effect on the crossed axons (Chung et al, 2000b). Therefore, CSPGs provide two different guidance cues during the development of the optic chiasm, directing midline crossing of the early-generated axons and governing divergence of the late-generated axons.

The guidance mechanisms that make the RGC axons project contralaterally are still unclear. The molecules involved in this process are known much less known than the uncrossed program. So far, only two guidance molecules have been proved working in this crossed program(Erskine & Herrera, 2007). They are a cell adhesion molecule NrCAM and a secreted Semaphorin. NrCAM is expressed in the non-VT retina from E12 to E17, then it is found to express in the VT retina as well, when the crossed axons arise from the VT retina at the late phase of chiasm formation (Petros et al, 2008). In the ventral diencephalon, NrCAM is located at the chiasmatic midline (Petros et al, 2008; Williams et al, 2006). Thus, NrCAM is very likely to mediate the crossed projection. In addition, blocking the function of NrCAM causes a poor crossing ability of RGC axons, and Nr CAM null mice get an increased ipsilateral projection, which are strictly generated from the late-born VT retina. In vitro, blocking NrCAM function leads to a reduction of uncrossed axon outgrowth on chiasm cells (Erskine & Herrera, 2007; Williams et al, 2006). In zebrafish, Sema3D is expressed at the chiasm region and contributes to guiding the retinal axons into the contralateral optic tract (Sakai & Halloran, 2006). In mice, Sema5A has been shown to channel retinal axons along the optic nerve (Oster et al, 2003), but the expression and functions of other Semaphorin receptors remain largely unknown. Some researches also suggest that semphorins may interact with CAMs to promote axon crossing at the midline (Castellani et al, 2002; Falk et al, 2005). However, this possibility still needs to be investigated in the mouse optic chiasm.

2.3 Guidance in the optic tract

After crossing the chiasmatic midline, RGC axons grow into the optic tract and extend towards the brain targets. In this guidance process only a few molecules have been identified directing axon growth in the optic tract. One of them is the

highly peripheral membrane protein GAP-43, which is expressed in growth cones (Sretavan & Kruger, 1998). Mouse embryos deficient in GAP-43 reveal an enlarged optic chiasm, because of a temporal delay of retinal axons in the midline region and a misrouting from chiasm to optic tract, characterized by abnormal randomized axon growth extending into crossed and uncrossed projection. This abnormality causes a duplicated representation of the visual field on both sides of the brain (Haupt & Huber, 2008; Sretavan & Kruger, 1998). Growing from chiasm to optic tract, RGC axons need cell autonomous GAP-43 function to overcome inhibitory signals in this transition region. The cellular element of the ventral diencephalon and transition zone, such as chiasmatic neurons, is not necessary for the development of optic tract (Erskine & Herrera, 2007; Kruger et al, 1998). In addition to GAP-43, Slits, which contribute to axon guidance within retina and chiasm, also take part in the guidance process in the optic tract, as Slit deficient mice revealing abnormal axon routing at the optic tract (Thompson et al, 2006). CSPGs involve in this guidance process as well through inhibiting outgrowth and restricting axons to the optic tract (Ichijo & Kawabata, 2001).

2.4 Guidance at the visual targets

After growing into the optic tract, the axons navigate to project to the subcortical targets, superior colliculus (SC) and lateral geniculate nucleus (LGN). The map development in these two main visual targets is a good model to understand the general mapping processes.

1) Axon mapping in the superior colliculus

In the SC, RGC axon projections navigate along two orthogonally oriented axes. Nasal – temporal retinal axis is mapped onto the posterior – anterior axis of the SC, while dorsal – ventral axis of retina is mapped onto lateral – medial axis of the

SC. Two ephrin/Eph signaling systems are involved in these two topographic mappings of RGC axons in the SC respectively, as ephrinA/EphA signaling determines the mapping along the posterior – anterior axis while ephrinB/EphB signaling plays a role in medial – lateral axis mapping (Erskine & Herrera, 2007; Haupt & Huber, 2008; McLaughlin & O'Leary, 2005; Wilkinson, 2000).

EphAs are expressed in a high-to-low gradient from temporal to nasal retinal axons, while their ligands ephrinAs reveal a low-to-high gradient of expression from anterior to posterior SC (Erskine & Herrera, 2007; Haupt & Huber, 2008; Wilkinson, 2000). This expression pattern suggests that receptor high expressed retinal axons are not allowed to terminate in the ligands rich posterior region, in contrast receptor low expressed axons succeed to project in this region of SC. In addition, mice deficient for ephrinA5, ephrinA2 or both display errors on this anterior – posterior mapping (Feldheim et al, 2000; Frisen et al, 1998). Together with these findings, ephrinA/EphA signaling is essential for the correct mapping along the anterior – posterior axis of the SC.

As mentioned above, ephrinB/EphB signaling is involved in lateral – medial axis mapping of the SC. EphBs reveal a low-to-high expression gradient from dorsal to ventral RGC axons, while ephrinBs show a low-to-high gradient of expression along lateral – medial axis of the SC (Erskine & Herrera, 2007). Furthermore EphB2/EphB3 double mutant mice have defects in topographic mapping along the lateral – medial axis of the SC (Hindges et al, 2002). So ephrinB/EphB signaling provides an important function to map the lateral – medial axis, and this function is counterbalanced by the Wnt/Ryk signaling(Erskine & Herrera, 2007). In the mouse SC, Wnt3, one member of Wnt family, show an increasing gradient expression along lateral – medial axis. This is similar to the expression pattern of ephrinB1. Ryk, the

receptor of Wnt3 in this process, is found to exist as an increasing gradient from dorsal to ventral RGC axons which is matched with the expression pattern of EphBs. Overexpressing Wnt3 in the chick tectum leads to RGC axons avoiding their terminate zone in vivo. Expression of a dominant negative Ryk in dorsal retinal axons leads to RGC axons shifting their lateral termination to the medial region of the tectum (Erskine & Herrera, 2007; Schmitt et al, 2006).

In the SC, ephrinA/EphA and EphrinB/EphB signaling are not only contributing to the anterior – posterior and lateral – medial axes, but also playing a role in dorsal – ventral and nasal – temporal mapping respectively (Feldheim et al, 2000; Haupt & Huber, 2008; Hindges et al, 2002). Therefore, the retinotopic map in the SC is more likely fulfilled by a group of interacting factors in different signaling systems, but not a single signaling pathway (Haupt & Huber, 2008).

This retinotopic map experiences refinement after the rough map along the anterior – posterior and lateral – medial axes has been formed. The refinement requires electrical activity-driven effects mediated by Ca^{2+} entry through NMDA receptors (Isa & Saito, 2001; Schmidt, 2004). Here, the functions of NMDA receptors are also modulated by EphB receptors (Dalva et al, 2000; Schmidt, 2004). So the accomplishment of the complete retinotopic map needs all these factor work together in a proper way.

2) Axon mapping in the lateral geniculate nucleus

In the mouse LGN, crossed and uncrossed RGC axon projections display overlapped terminal spaces during the first postnatal week, but these retinal arbors are reduced between first and second week, then these retinal projections occupy distinct eye-specific laminae by the time of natural eye opening (Jaubert-Miazza et al, 2005). As in the SC, this map refinement also needs spontaneous activities occurring

in the RGCs. The spontaneous activities between neighboring cells correlate as waves of activities that sweeping across the developing retina (Wong, 1999). Blocking the retinal waves leads to the abolishment of axons projecting into eye-specific layers in the LGN (Huberman et al, 2002; Penn et al, 1998).

There are several mechanisms involved in the regulation of retinal waves. In the early stage (P0-P11 in mice), retinal wave generation is mediated by nAChRs neurotransmitter receptors, while at the late stage (P11-P21 in mice), the responsible neurotransmitter receptor switch to glutamate receptors (Feller, 2002; Wong, 1999). Besides the fast excitatory neurotransmitter ACh, retinal wave propagation requires the function of neuromodulator adenosine working through a cAMP/PKA second messenger cascade (Firth et al, 2005; Stellwagen et al, 1999). Finally, gap junction coupling may also take part in retinal wave propagation, as using junction blockers lead to wave abnormalities (Firth et al, 2005; Singer et al, 2001).

Here we emphasis on the functions of glutamate receptors in the development of retinogeniculate pathway, as L-glutamate is the most prevalent excitatory neurotransmitter in the retina (Thoreson & Witkovsky, 1999). As mentioned above, in the developing retinogeniculate pathway, the large-scale regionalization of eye specific areas in the early phase requires cholinergic transmission, while the local patterns of segregation occurring in the late phase is governed by glutamate signaling (Ebara et al, 2004; Feller, 2002; Jaubert-Miazza et al, 2005; Muir-Robinson et al, 2002). Two subtypes of glutamate receptors, NMDA receptor and AMPA receptor, are found to involve in the glutamatergic synapse transmission during the developmental remodeling of the LGN (Chen & Regehr, 2000; Liu & Chen, 2008). Furthermore, NMDA receptor contributes to the immature synapse transmission (before eyes open), while AMPA receptor significantly contributes to the mature

synapse transmission (Liu & Chen, 2008). This age related synaptic change of NMDA receptor may be the result of different subunit composition of NMDA receptor (Clarke & Johnson, 2006; Liu & Chen, 2008). In addition, the LGN inputs to the visual cortex are predominantly glutaminergic, while NMDA receptor is also involved in this process (Constantine-Paton et al, 1990; Giannakopoulos et al, 2010; Li et al, 2009), indicating that glutamate signaling is crucial for the development of visual pathway.

3. SUMMARY

The mechanisms underlying the development of the optic pathway in binocular species are really complicated. Only some of them have been identified. The processes of optic chiasm development occur sequentially, and every step starts at an exact time controlled by several effective factors. Many transcription factors have been shown to be involved in the formation of the optic chiasm. These factors help to guide the RGC axons as they grow toward the optic disc, exit the eye and enter the optic nerve, cross the ventral midline or otherwise, navigate toward the optic tract, and finally project to the brain targets. In this retinofugal pathway, some of these factors were demonstrated to be inhibitory, while others act as positive factors to promote the chiasm development. Even more intriguing is that these factors interact with each other. But it is unclear how these known factors interact with each other. So this is the challenging task for the further research.

CHAPTER 2
Birthdating of chiasmatic neurons in the mouse optic chiasm and tracing their fates

Introduction

In the mammalian visual system, retinal ganglion cell (RGC) axons from each eye converge and segregate into crossed and uncrossed projections at the optic chiasm. This structure is very important for the binocular vision. The growth pattern of RGC axons during the optic chiasm development is quite different at different embryonic stages, and it can be divided into 3 phases. In the first phase, the earliest RGCs arise from the dorsocentral (DC) retina and began to enter the ventral diencephalon at E12. Then at E13 the significant numbers of retinal axons have crossed the midline and projected to the opposite side. At this stage, the uncrossed axons grew directly into the ipsilateral optic tract, rather than growing toward the ventral midline. Thus the optic chiasm is formed (Colello & Guillery, 1990; Mason & Sretavan, 1997). The second phase is also the peak phase of axon growth, and starts from E14 to E17. During this phase, RGC axons from the ventrotemporal retina first approach the ventral midline at the chiasm, then turn laterally to the ipsilateral optic tract. On the other hand, the RGC axons from the other part of the retina do not turn back but grow into the contralateral optic tract directly (Guillery et al, 1995; Petros et al, 2008). In the third phase, from E17.5 to P0 in mice, retinal axons from the ventrotemporal retina project to the contralateral optic tract instead of ipsilateral projection in the second phase (Drager, 1985; Petros et al, 2008).

What are the guidance mechanisms directing the RGC axons into crossed and

uncrossed pathways? There are two populations of chiasm cells, one is a group of early differentiating neurons immunoreactive for stage-specific embryonic antigen1 (SSEA-1), the other is a palisade of radial glia that straddles the chiasmatic midline. These two groups of cells are generated early before any retinal axons arrive at the midline of the mouse ventral diencephalon, and have been shown to affect retinal axon growth and patterning in the optic chiasm (Marcus et al, 1995; Mason & Sretavan, 1997; Petros et al, 2008; Sretavan et al, 1994).

In this chapter, we emphasize on the chiasmatic neurons. Their distribution pattern and interaction with the RGC axons are different during the optic chiasm formation. During the early phase, chiasmatic neurons form a characteristic V-shaped configuration at the ventral diencephalon and serve as boundary for both crossed and uncrossed RGC axons (Lin et al, 2005; Mason & Sretavan, 1997). During the peak phase, these chiasmatic neurons extend anteriorly into the midline of the developing chiasm; both crossed and uncrossed retinal axons encounter them only near the midline, but only the ventral-temporal retinal axons turn away from the midline and make the ipsilateral projection. During the late phase, RGC axons from the ventral-temporal retina encounter the rostro-anterior part of the chiasmatic neurons and cross the midline (Marcus & Mason, 1995; Mason & Sretavan, 1997; Petros et al, 2008). Previous study suggested that interactions of RGC axons with these cells may be complex. In the developing chiasm, these cells may serve as a posterior boundary to RGC axons growth; on the other hand, they may promote the axon ingrowth as well (Mason & Sretavan, 1997; Sretavan et al, 1994). Therefore, chiasmatic neurons play a very important role in the development of mouse optic chiasm.

However, until now it is still unclear when these chiasmatic neurons are generated, and what the fates of these cells are in the adult mouse brain. As the

commonly used BrdU assay has some defects, in this study we used EdU (5-ethynyl-2'-deoxyuridine) instead of BrdU (5-bromo-2′-deoxyuridine) to do the pulse label birthdating experiment to birthdate chiasmatic neurons first and then try to find out what the fates of these chiasmatic neurons are at the later stages of development.

Materials and Methods

Animal

Time-mated pregnant pigmented C57 mice were obtained from the Laboratory Animals Services Center of the Chinese University of Hong Kong. The day on which the vaginal plug was found was considered as embryonic day 0 (E0). Experimental procedures in the present study were approved by the University Animal Ethic Committee.

EdU injections

In order to take advantage of a sharp window for labeling newly differentiated cells in the chiasm, time pregnant female C57 mice were given two intraperitoneal injections at one-hour interval of 50 mg/kg EdU (5-ethynyl-2'-deoxyuridine) dissolved at 5 mg/mL in the warm normal sterile saline on different embryonic days. The concentration of EdU used was as reported for BrdU or EdU in mice experiments (Chehrehasa et al, 2009; Wojtowicz & Kee, 2006). At each time point of analysis, embryos were taken from at least three different litters.

1) To check the efficiency of EdU labeling

EdU was injected at E11 or E13, the pregnant females were killed one hour after second injection.

2) Birthdating the chiasmatic neurons

EdU was injected either on E8, E9, E9.5, E10 or E11. For the E8, E9, E10 and E11 the first injection was at 9am and the second injection was at 10am; for the E9.5 the first injection was at 9pm and the second injection was at 10pm. The day of detecting EdU positive cells was fixed at E13, when the optic axons start to innervate the ventral midline of the diencephalon.

3) Tracing the fates of the chiasmatic neurons

For tracing the fates of chiasmatic neurons, the injection day was fixed at E9.5; then the pregnant mice were allowed to survive up to E14, E15, E16, E17 or E18.

Detecting EdU positive cells

All pregnant mice were killed by cervical dislocation, embryos at the stage from E13-E18 were removed by Cesarean section and killed by decapitation. The heads of the embryos were fixed with 4% paraformaldehyde in 0.1M phosphate buffer (PB, pH 7.4) overnight at 4°C.

The heads were embedded in a gelatin-albumen mixture and sectioned on a vibratome at the thickness of 100μm. Horizontal or frontal sections containing the retinofugal pathway from the eyes to the proximal parts of the optic tract were collected in 0.1M phosphate buffer saline (PBS, pH 7.4).

The method of detection of EdU was modified from the protocol of the Click-iT®EdU Alexa Fluor®488 Imaging Kit (Invitrogen, cat. No. C10337). The sections were washed thoroughly twice with 3% bovine serum albumin (BSA) in PBS (pH 7.4) each for 15min. Then the sections were incubated with 0.5% Triton® X-100 in PBS for 30 min at room temperature. After removing the permeabilization buffer, the sections were washed with 3% BSA twice. Then the sections were

incubated with the Click-iT™ reaction cocktail for 30 min at room temperature, protected from light. The sections were washed with 0.1M PBS. The components of the Click-iT™ reaction cocktail were 1X Click-iT™ reaction buffer (make the final volume to 250μl per well), $CuSO_4$ (1:25), Alexa Fluor azide (1: 650), Reaction buffer additive (1:10). To make sure the efficiency of the Click-iT™ reaction cocktail, the ingredients should be added in the order as listed.

Double staining of EdU together with chiasmatic neuron marker

After the EdU procedure, the horizontal sections were blocked with 10% normal goat serum in 0.1M PBS for 90 minutes to reduce the background signals; they were then incubated with stage-specific antigen (SSEA-1) antibody (mouse IgM, 1:5; Developmental Studies Hybridoma Bank (DSHB), USA) overnight at 4°C. Anti-SSEA-1 is an antibody labeling the chiasmatic neurons in the mouse diencephalon. In the following day sections were washed thoroughly with 0.1M PBS for three times, incubated with secondary antibodies Cy3-conjugated goat anti-mouse IgM (1:200, Jackson Laboratories) for 2 hours at room temperature. After thorough washing with 0.1M PBS, the sections were mounted on glass slides with mounting medium (Biomeda). Fluorescent signals on sections were imaged by the confocal microscope (FV300, Olympus Co, Japan). Control sections were prepared with the same procedures but with the absence of the primary antibody. No obvious staining was found in any of these control preparations.

Cell counting and statistical analyses

For birthdating the chiasmatic neurons, E13 sections containing the double labeled cells at the level of the typical "V-shaped" array were observed at 40x magnification on the confocal microscope. Using the MetaMorph software (Universal Imaging Corp, USA), we drew the outline of the "V-shaped" array on the

confocal images. Then we counted all the double labeled cells in this array at 400 magnification (Fig. 9A-C).

For tracing the fate of chiasmatic neurons, the double labeled cells were counted at the level of chiasm at different stages from E13 to E15 (Fig. 18A-D).

In this part of study we used Kruskal-Wallis nonparametric ANOVA test of the InStat software (Grapph-Pad Inc., USA) to compare the cell number in different groups.

Double staining of chiasmatic neurons with neural stem cell marker

To examine the characteristic of chiasm cells, a series of double staining experiment was performed in this study. Horizontal sections containing the chiasm were collected in 0.1M PBS and washed with 0.1M PBS for three times. The slices were blocked with 10% normal goat serum (horizontal sections) in 0.1M PBS for 90 min to reduce the background signals, and incubated with the primary antibodies against SSEA-1 and Nestin (1:1000, mouse IgG, Abcam, UK, cat. No. ab6142) overnight at 4℃. Nestin is a neural stem cell marker, widely used in the CNS (Jose & Krishnan, 2010; Pongpudpunth et al, 2010; Suzuki et al, 2010). After rinsing with 0.1M PBS, the sections were incubated in secondary antibodies at room temperature for 2 hours. The secondaries for SSEA-1 and Nestin were Cyanine 3 (Cy3) conjugated goat anti-mouse IgM (1:200) and AF488 conjugated goat anti-mouse IgG (1:200), respectively. After washing for three times with 0.1M PBS, the sections were mounted on glass slides and took imaged by the confocal microscope.

Double staining of chiasmatic neurons with cell apoptosis marker

To investigate whether there is extensive cell death in the chiasm cells, chiasmatic neurons were double stained with caspase 3, the method was already described above. Here we used the primary antibodies against SSEA-1 and caspase 3

(1:1000, Rabbit IgG, R&D, Cat. No. AF835). Caspase 3 is cell apoptosis marker, which can distinguish apoptotic cells from non-apoptotic cells (Egeland et al, 2010; Suganuma et al, 2010). The secondaries for SSEA-1 and caspase 3 were Cy3 conjugated goat anti-mouse IgM (1:200) and AF488 conjugated goat anti-rabbit IgG (1:200), respectively.

Cell counting analyses of apoptotic cells

The double labeled cells of caspase 3 and SSEA-1 were counted in the SSEA-1 positive region at the level of the chiasm from E13 to E15. Kruskal-Wallis nonparametric ANOVA test of the InStat software (Grapph-Pad Inc., USA) was used to compare the cell number in different groups.

Results

The efficiency of EdU labeling

In order to check the efficiency of EdU labeling, EdU was injected twice intraperitoneally into the pregnant mice at E11 or E13. The mice were killed 1 hour after the final injection. After the EdU detection, most EdU positive cells were found at the ventricular layer lining the third ventricle when EdU was injected at E11 (n=5) (Fig. 1A). When EdU was injected at E13 (n=4), most EdU positive cells were observed in the ventricular layer, but a few were also detected in other regions of the diencephalon (Fig. 1C). If looked at higher magnification, EdU labels were found strictly in the nuclei (Fig. 1B, D).

The first postmitotic cells in the mouse ventral diencephalon were generated around E9.5

Cells in the diencephalon are generated from the ventricular zone during embryonic development. After undergoing the last mitotic division, the cells migrate

from the ventricular layer to take up their final destinations in the brain (Hashimoto & Mikoshiba, 2004). The time point at which a cell leaves the cell cycle and becomes forever postmitotic is defined as its birthdate (Messersmith et al, 1997). Consequently, cells that are exposed to EdU at their birthdate will incorporate EdU into their DNA permanently, yielding intense signal of EdU incorporation at all subsequent stages. Contrarily, for those cells that keep dividing, EdU will be gradually diluted and reveals only a weak labeling.

When EdU was injected at E8 (n=5), no trace of EdU staining was detected in the E13 ventral diencephalon (not shown). This indicates that no neuron go through terminal mitosis at this embryonic stage. When EdU was injected at E9 (n=6), punctate, dot-like staining was detected in the ventral diencephalon of E13 embryos (Fig. 2A-D), indicating that these labeled cells kept dividing after EdU incorporation.

When EdU was injected at E9.5 (n=10), EdU heavily labeled cells were observed initially in the ventral diencephalon at E13. Here we took a series of sections through the optic chiasm to examine distribution of the EdU positive cells. At the level about 400μm above the ventral pial surface, only a few EdU positive cells were observed in the ventral diencephalon (Fig. 3A, B). At a lower level, more EdU positive cells were detected (Fig. 3C, D). At the level of the chiasm, about 200μm above the ventral pial surface, a lot of EdU positive cells were observed, which tended to form an inverted V-shaped pattern in the caudal regions of the diencephalon (Fig. 3E, F). These results indicate that the first post-mitotic cells in the ventral diencephalon were generated at E9.5.

Double- label of anti-SSEA-1 and EdU positive cells, while EdU was injected at different embryonic stages

To determine the birthdate of the chiasmatic neurons, EdU positive cells were

double labeled with SSEA-1 antibody, a carbohydrate epitope on early stem cells, expressed prominently on the chiasmatic neurons in mouse embryos. We fixed the day of detecting EdU and SSEA-1 positive cell at E13, but changed the injection day from E9.5 to E11.

When EdU was injected at E9.5 (n=10), EdU labeled cells concentrated to the midline of the ventral diencephalon and tended to form an inverted V-shaped array caudal to the optic chiasm (Fig. 4 A1). Double staining with anti- SSEA-1 showed that the chiasmatic neurons were localized primarily in the territory of the EdU positive cells (Fig. 4 A2, 3). In the merged image, most of the EdU positive cells were observed to localize in the area of chiasmatic neurons (Fig. 4 A3). At higher magnification, EdU positive cells were colocalized with SSEA-1 neurons in this area (Fig. 4 B1-3). From the 60x magnification images taken by the oil lens, it was very clearly that EdU positive staining was located in the nuclei of SSEA-1 neurons (Fig. 5A-D).

When EdU was injected at E10 (n=8), the pattern of EdU labeled cells at the level of the chiasm was similar to that of E9.5 injection. These EdU positive cells were packed together in caudal regions of the diencephalon, but the cell density seems to be smaller when compared with that after E9.5 injection (Fig. 6 A1). In the double labeled pictures, it was found that majority of EdU positive cells were located in the SSEA-1 neuronal array, whereas a number of cells were observed outside the SSEA-1 territory (Fig. 6 A3). At higher magnification, EdU positive cells were colocalized with SSEA-1 neurons in this V-shape array (Fig 6B1-3).

When EdU was injected at E11 (n=10), the pattern of EdU positive cells changed a lot in E13 ventral diencephalon. At the level of the optic chiasm, most EdU positive cells clustered to the anterior parts of the ventral diencephalon. In the

merged image, most EdU positive cells were observed outside the territory of SSEA-1 neurons, whereas only a small number of EdU positive cells remained in the typical "V-shaped" configuration (Fig. 7A1-3). The cells remained in the V-shape were colocalized with SSEA-1 neurons, if looked in a higher magnification (Fig. 7B1-3, Fig. 8A-D).

The birthdate of chiasmatic neurons is around E9.5

Cell counting analyses were performed in this study using the double labeled sections. The double labeled cells from different injection stages were counted on the sections, which contain the optic chiasm, at the level about 200μm above the ventral pial surface. We drew the outline of the SSEA-1 neurons, and then counted the double labeled cells under 400 magnification (Fig. 9A-C). Here we only counted labeled cells with strong EdU label in the nucleus. The spot like EdU staining was not included in the cell counting (indicated by white solid arrow in Fig. 5D).

Cell counting analyses showed that majority of chiasmatic neurons were generated at E9.5, while a fewer number of them were generated at E10 and E11. There was virtually no chiasmatic neurons generated at E9 at all. The number of double labeled cells in the chiasmatic neurons area was significant reduced in E11 injected mice compared with that at E9.5 injected mice ($p<0.01$, Fig. 9A-D).

The distribution of EdU labeled cells in the ventral diencephalon from E14 to E18, when EdU was injected at E9.5

After knowing most chiasmatic neurons at E13 were born on E9.5 and form a characteristic V-shaped array at posterior part of the optic chiasm, we tried to investigate where these E13 chiasmatic neurons go, what their fates are.

1) The distribution of EdU positive cells in the ventral diencephalon at E14

When EdU was injected at E9.5 (n=12), the EdU labeled cells assembled

around the midline and formed a V-shaped structure at E14 (Fig. 10A). But the distribution was more wide spread than that at E13. After double labeling with SSEA-1, most of the EdU labeled cells were observed in the SSEA-1 positive area (Fig. 10B). When examined at a higher magnification, these EdU positive cells had a higher density in the region that close to the midline (indicated by the asterisks, Fig. 10A2). In the merged image, it was clear that the EdU labeled cells in the SSEA-1 positive region were colabeled with the SSEA-1 neurons (Fig. 10B2, 10B3). At 60x magnification using oil lens, we found that the EdU label in the SSEA-1 positive region was confined to the nucleus of the chiasmatic neurons (indicated by open arrows, Fig. 11C). Beside the strongly EdU labeled cells, there was some dotted staining located in the nucleus of chiasmatic neurons (indicated by solid arrows, Fig. 11C). These cells were not included in the following cell counting analyses.

2) The distribution of EdU positive cells in the ventral diencephalon at E15

When EdU was injected at E9.5 (n=13), the EdU positive cells at E15 were found largely close to the midline, and tended to form two arrays on each side of ventral diencephalon caudal to the optic chiasm (indicated by the asterisks, Fig. 12 A1). This distribution was different from that at E14. These EdU positive cells were more restricted to the midline regions. In the merged image, it was found that the pattern of chiasmatic neurons was also changed. Instead of revealing the typical V-shaped array, these chiasmatic neurons extended to the chiasmatic midline and the initial segment of the optic tract (Fig. 12B1). This observation was similar to our previous study (Lin et al, 2005). However, the EdU labeled cells were still detected in the SSEA-1 positive region, just more concentrated at the area close to the midline. These EdU labeled cells in the SSEA-1 positive region were colocalized with the chiasmatic neurons, when examined at a higher magnification (Fig. 12B2, 12B3). It

was clear that EdU staining was still located in the nucleus of the SSEA-1 neurons (indicated by open arrows, Fig. 13C) under the 60x magnification. But there were many dotted staining of EdU, which was also located in the nuclear of chiasmatic neurons (indicated by solid arrows, Fig. 13C).

3) The distribution of EdU positive cells in the ventral diencephalon at E16.

Similar to E15, EdU positive cells at E16 were largely observed in two clusters next to the midline of the ventral diencephalon at the level of the chiasm, when EdU was injected at E9.5 (n=15, indicated by the asterisks, Fig. 14A1). But these clusters appeared smaller than that at E15. In the merged images, most of these EdU staining was still observed to localize in the SSEA-1 positive region. The EdU positive cells in the SSEA-1 region were colabeled with the chiasmatic neurons when observed under higher power (Fig. 14A2 – B3). When examined under oil lens at 60x magnification, only a few EdU labeled cells were observed in the ventral diencephalon at E16 (Fig. 15A). These strong EdU signals were localized in the nuclei of the SSEA-1 neurons (indicated by open arrows), while a lot of light, dotted EdU staining was also observed in the SSEA-1 neurons (indicated by solid arrows, Fig. 15C). Compared with E14 and E15, there were more dotted staining observed in the SSEA-1 region.

4) The distribution of EdU positive cells in the ventral diencephalon at E17 and E18

The distribution pattern of EdU positive cells was very consistent at E17 (n=13) and E18 (n=11), when EdU was injected at E9.5. Similar to E15 and E16, EdU positive cells at E17 and E18 revealed two arrays at each side of the ventral diencephalon close to the midline (indicated by the asterisks, Fig. 16A1, 17A1). In the merged image, EdU labeled cells in the SSEA-1 positive area were still colabeled

with the SSEA-1 neurons (Fig. 16B, 17B).

The chiasmatic neurons generated at E9.5 were decreased from E13 to E16.

Cell counting analyses were performed in this part of study after investigating the distribution of E9.5 born chiasmatic neurons at E13 to E18. The double labeled cells were counted at different embryonic stages on the sections which contain the optic chiasm. We drew the outline of the SSEA-1 positive region on different sections, and counted the doubled labeled cells under 40x magnification (Fig. 18A-D). Only the heavily labeled EdU cells were counted. The light and dotted EdU labeled cells were not included into the counting.

From the results of cell counting analyses, it was found that the chiasmatic neurons at E13, which were born at E9.5, were reduced from E14. Significant reduction of the double labeled cells was observed at E15 ($P<0.05$) and E16 ($P<0.01$).

Identification of chiasmatic neurons with neural stem cell marker

At E13 (n=4), Nestin immunoreactive signal was extensively detected in the ventral diencephalon on the horizontal sections which contain the optic chiasm (Fig. 19 A1, B1). After doing the double staining with SSEA-1, it was found that Nestin immunoreactivity was located at the surface of the chiasmatic neurons in the SSEA-1 positive region. It looked like that the chiasmatic neurons did not overlap with the Nestin positive neural stem cells (Fig. 19A3, B3). When examined at 60x magnification, Nestin was found on the radial processes that span through the SSEA-1 cells. There was very little colocalization, if any (Fig. 20A-C).

Apoptotic cells appeared in the region of chiasmatic neurons from E13

A few apoptotic cells were observed in the area of chiasmatic neurons at E13 (n=3) and E14 (n=4) at the level of the chiasm. At E13, only one caspase positive

apoptotic cell was observed in the ventral diencephalon (indicated by open arrow, Fig. 21A1). As a positive control, many apoptotic cells were detected in the trigeminal ganglion adjacent to the diencephalon (indicated by asterisk, Fig. 21A1). The apoptotic cells were colabeled with SSEA-1 in the ventral diencephalon, when observed under high power (Fig. 21A2-A4). At E14, a few more apoptotic cells were detected in the ventral diencephalon (Fig. 21B1). All the apoptotic cells in the SSEA-1 positive region were colocalized with chiasmatic neurons (indicated by open arrows, Fig. 21B2-B4).

Compared with E13 and E14, many more apoptotic cells were observed in the ventral diencephalon at E15 (n=7, Fig. 22A1, 22B1). Most of these apoptotic cells were located in the SSEA-1 immunoreactive area at the level of optic chiasm (Fig. 22B2). When looked at higher magnification, those apoptotic cells in the SSEA-1 positive area were colabeled with chiasmatic neurons (Fig. 22B3).

Furthermore, we counted the double labeled cells in the SSEA-1 positive region at the level of the optic chiasm, and found that the number of apoptotic cells was increased significantly in this region from E13 to E15 (Fig. 22C). Therefore, more and more chiasmatic neurons became apoptosis from E13 to E15.

Discussion

In this part of experiment, firstly we used EdU to birthdate the chiasmatic neurons in the E13 ventral diencephalon of mouse embryos, when the optic chiasm just formed and the chiasmatic neurons revealed a typical inverted V-shaped array at the chiasm (Lin et al, 2005; Marcus & Mason, 1995; Mason & Sretavan, 1997). After doing the double staining with SSEA-1 antibody and cell counting analyses, we found that most of the chiasmatic neurons at E13 were birthdated at about E9.5. This

gave us a hint that chiasmatic neurons were generated much earlier before the chiasm is formed. They moved out of the ventricular zone after leaving the mitotic cycles, and migrated to the ventral diencephalon, then formed an inverted V-shaped configuration caudal to the future optic chiasm, and got ready to present guidance information to the RGC axons, which was growing through the optic stalk. Secondly, we tried to find the fates of the chiasmatic neurons at E13, which were born at E9.5. Therefore, we fixed the injection day of EdU at E9.5, and then detected the distribution of EdU positive cells at the ventral midline of the chiasm from E14 to E18. It was found that the number of chiasmatic neurons which were born at E9.5 was reduced from E14 and formed clusters on each side of the chiasmatic midline during the later phase of optic chiasm development. In order to explain why some chiasmatic neurons at E13 disappear at the following embryonic stages, the neural stem cell marker and apoptotic cell marker were used to trace the fates of these neurons.

EdU is a good birthdating tool instead of BrdU

As far as we know, the primitive neuroepithelium cells are the precursors of neuronal and neuroglial cells. These primitive neuroepithelium cells, which are also called neural precursor cells, are located at the ventricular zone. These neural precursor cells will start to differentiate into neuroblasts or glioblasts at some point in the CNS development. Under a migration mechanism neuroblasts and glioblasts will differentiate into neurons and glia (Morest & Silver, 2003; Pontious et al, 2008; Tramontin et al, 2003). This suggests that chiasm cells could be differentiated from neuroepithelial cells, and migrate to the ventral diencephalon. In this study, we found that the neuroepithelial cells at the ventricular zone are labeled heavily by EdU. Based on this, EdU can be used to label these neuroepithelial cells first, and allow

tracing of migratory pathway and then the fates of the chiasm cells.

In this study we used EdU instead of BrdU, which is commonly used in birthdating studies. In the BrdU assay, in order to facilitate the binding of anti-BrdU antibody onto the BrdU residues in the DNA, a strong DNA denaturing condition is required. These hash treatments, such as strong acid and heating, help to expose the epitopes hidden within the DNA, but at the same time destroy many other cellular epitopes that are essential for antibody bindings (Buck et al, 2008; Chehrehasa et al, 2009; Salic & Mitchison, 2008).

Similar as BrdU, EdU can incorporate into the DNA during new DNA replications. Unlike BrdU, EdU can react directly with Alexa Fluor, in a copper-catalyzed reaction to form a very stable incorporation without the need of denaturing the DNA. So the EdU protocol can maintain the antibody epitopes for labeling of other cell surface markers. This is why it is easy for us to stain EdU together with other cell markers such as anti-SSEA-1, anti RC2 antibody, for the birthdating studies. Here we used EdU to pulse-label dividing cells in the embryonic mouse brain, and determine when these chiasmatic neurons are generated.

Most of the first differentiated cells assemble at the lower part of ventral diencephalon

In this study, we found that the first postmitotic cells in the mouse ventral diencephalon were generated around E9.5. After leaving the ventricular zone, most of these cells were observed at the ventral part of the diencephalon at E13, about 200μm above the ventral pial surface. Here these early differentiated cells assemble together, and form an inverted V-shaped array. Previous studies have indicated that the optic chiasm of mouse exists at the same level at E13, and the chiasmatic neurons, which were immunoreactive to SSEA-1, formed a characteristic inverted V-shaped

configuration there as well (Lin et al, 2005; Marcus & Mason, 1995; Mason & Sretavan, 1997). A series of double staining experiment in this study showed that most EdU positive cells were colocalized with SSEA-1 neurons in this typical V-shaped array. This observation suggests that the chiasmatic neurons at E13 start to generate at about E9.5. These early born neurons migrate to the ventral diencephalon, and form an inverted V-shaped pattern, after leaving the ventricular zone.

The majority of chiasmatic neurons at E13 are generated at about E9.5

When EdU was injected at E9.5, we found that most of the heavily labeled cells detected at E13 were chiasmatic neurons. As there was no trace of heavily labeled cells when EdU was injected at E9, we conclude that the chiasmatic neurons were first generated at E9.5. However, the birthdate of the majority of chiasmatic neurons is still unknown. So we also investigated the E13 chiasmatic neurons generated at E10 and E11. Immunohistochemistry studies and cell counting analyses showed that the number of new born chiasmatic neurons was reduced from E9.5 to E11. The majority of chiasmatic neurons are born at E9.5. In summary, most of the the ventral diencephalon cells that undergo early differentiation comprise the majority of chiasmatic neurons at E13 in mouse; although still some chiasmatic neurons are born at E10 and E11. Ventral diencephalon cells that undergo later differentiation at E10 and E11 can become other cell types in the ventral diencephalon at E13.

The distribution of chiasmatic neurons born at E9.5 in the ventral diencephalon from E14 to E18

In order to trace the fates of chiasmatic neurons at E13, we investigated the distribution of these chiasmatic neurons in the following embryonic stages. At E14, they still form a V-shaped configuration, but become more spread than that at E13.

The cell density is higher at the region close to the ventral midline. From E15, chiasmatic neurons change their distribution in the ventral diencephalon at the chiasm. They extend anteriorly, and form a rostral part at the midline (Marcus & Mason, 1995; Mason & Sretavan, 1997). Only this rostral part of the chiasmatic neurons will encounter the later born retinal axons and make them turn to ipsilateral or contralateral projections. Starting from E15, the chiasmatic neurons which were labeled from E9.5 tend to concentrate at the ventral midline. These chiasmatic neurons may take part in the midline guidance during the peak and late phase of the optic chiasm formation. As the chiasmatic neurons born at E9.5 are only a small part of the whole chiasmatic neurons at E15 to E18, the other chiasmatic neurons must be generated later than E9.5. So the chiasmatic neurons are renewed during the chiasm formation.

The chiasmatic neurons generated at E9.5 were reduced in number during E13-E16

The results of cell counting analyses showed that the chiasmatic neurons born at E9.5 reduced in number from E14 to E16. Why do some of the earliest born chiasmatic neurons disappear from the chiasmatic region? Where do they go? There are three possibilities. These chiasmatic neuron may migrate away to the other parts of the brain, like in the chick diencephalon (Golden & Cepko, 1996). They may differentiate and become other types of cell, such as one of many hypothalamic nuclei, not only having developmental but also adult function (Mason & Sretavan, 1997). They may represent a population of neurons which exist transiently and may eventually die, like subplate cells in the developing cortex (Allendoerfer & Shatz, 1994)or Cajal-Retzius cells in the hippocampus (Altman & Bayer, 1986). In our experiment, there is no obvious observation that the EdU labeled chiasmatic cells

migrate to other parts of the ventral diencephalon. So we tried to investigate the other two possibilities.

Identification of chiasmatic neurons with neural stem cell marker

In order to investigate whether the chiasmatic neurons have the potential to differentiate or not, we double stain the chiasmatic neurons at E13 with the neural stem cell marker, Nestin. None of the chiasmatic neurons were nestin-positive, almost all the Nestin positive staining was found on the radial processes that span through the chiasmatic neurons. However, SSEA-1 itself is often used as a mouse embryonic stem cell marker and neural stem cell marker (Abramova et al, 2005; Muramatsu & Muramatsu, 2004; Yagi et al, 2010). So it is likely that the earliest born chiasmatic neuron could differentiate in the later stage during development and give rise to some daughter cells. This can cause the original labeled EdU diluted during the differentiation. It corresponds with much more dotted EdU staining appears in the chiasmatic neurons during the later embryonic stage. This can be one reason of why some earliest born chiasmatic neurons disappear during development.

Apoptotic cells appeared in the region of chiasmatic neurons from E13

We also investigated if some of the earliest born chiasmatic neurons died during development. Here, caspase 3, an apoptotic cell marker, was used to dual-label with SSEA-1. At E13, very few apoptotic cells are observed in the region of chiasmatic neurons at the level of chiasm. But a few more apoptotic cells appear in this region at E14. At E15, many apoptotic cells can be detected at the ventral diencephalon, and most of them are located in the SSEA-1 positive region. So, an increasing number of chiasmatic neurons underwent apoptosis from E13 to E15. This may explain partly why the cell number reduced significantly at E15.

In summary, in our experiment we have shown that the earliest born

chiasmatic neurons, which were generated at E9.5, may have the potential to differentiate at late stages and some chiasmatic neurons undergo apoptotic cell death from E14. It is reasonable that some earliest born chiasmatic neurons disappear during development.

Figures

Figure 1 The efficiency of EdU labeling on the mouse embryos. (A) EdU positive cells were detected at the ventricular layer in the ventral diencephalon at E11, when EdU was also injected at E11. (B) The higher magnification of the ventral diencephalon in figure A was showed the morphology of EdU positive cells, which had the strictly nuclear localization. (C) EdU positive cells localized on the ventricular layer in the ventral diencephalon at E13, when EdU was injected at E13. (D) Beside on the ventricular layer, a small number of EdU positive cells were observed in the other region of the diencephalon in the higher power of the ventral diencephalon in figure C.

Scale bar: A, C, D 200μm; B, 100μm.

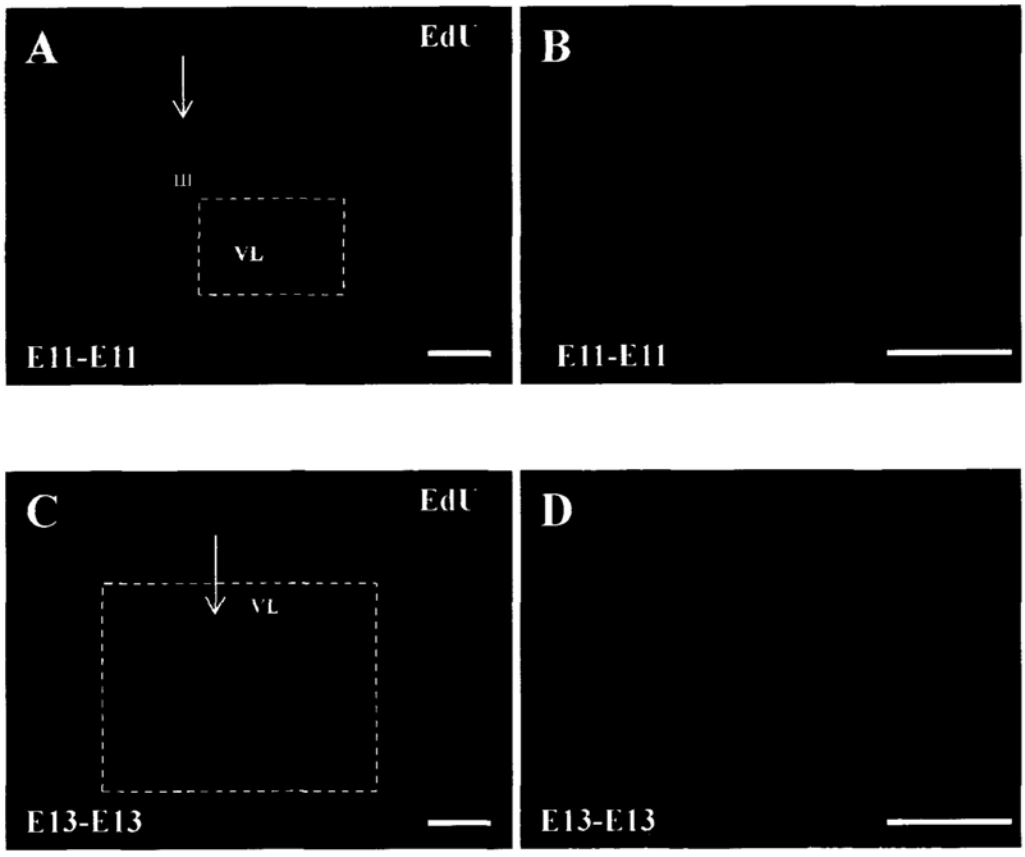
A
EdU
III
VL
E11-E11
B
E11-E11
C
EdU
VL
E13-E13
D
E13-E13

Figure 2 EdU staining in the ventral diencephalon at E13, when the injection was at E9. It was showed that EdU staining on the horizontal section (A) or frontal section (C) of the ventral diencephalon at E13, when the injection was at E9. (B, D) The higher power of ventral diencephalon in figure A and C showed the dot-like staining of EdU. These EdU signals were located extensively on the diencephalon, without forming a cell-like morphology.

Scale bar: A, C, 200μm; B, D, 100μm.

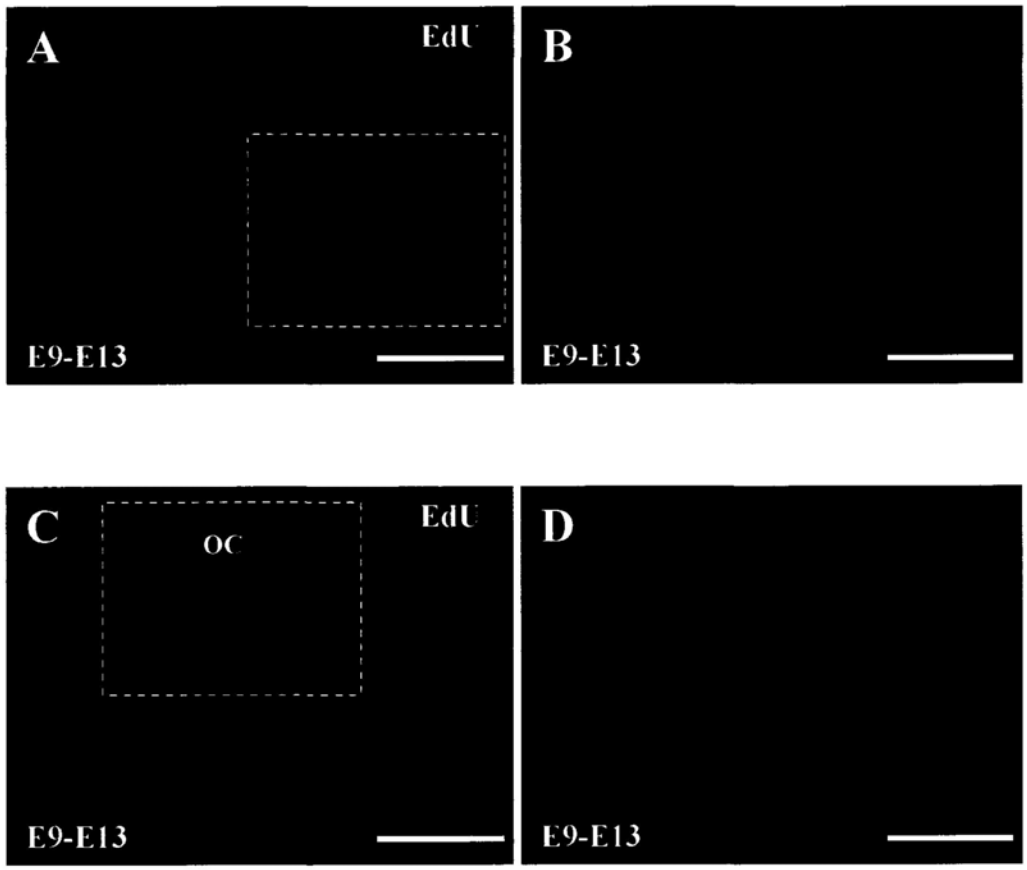
A
EdU
E9-E13
B
E9-E13
C
OC
EdU
E9-E13
D
E9-E13

Figure 3 The distribution of EdU positive cells in the ventral diencephalon at E13, when the injection was at E9.5. (A) showed the EdU staining at the level about 400μm above the ventral pial surface. (B) Only several EdU positive cells were observed on the diencephalon in higher power. C showed the EdU staining at the level about 300μm above the ventral pial surface. (D) At this level, more EdU positives cells were observed than the higher level. E and F showed the EdU staining at the level about 200μm above the ventral pial surface. A lot of EdU positive cells were concentrated at this level, and tended to form an inverted "V-shaped" array (indicated by white line).

Scale bar: A, C, E, 200μm; B, D, F, 100μm.

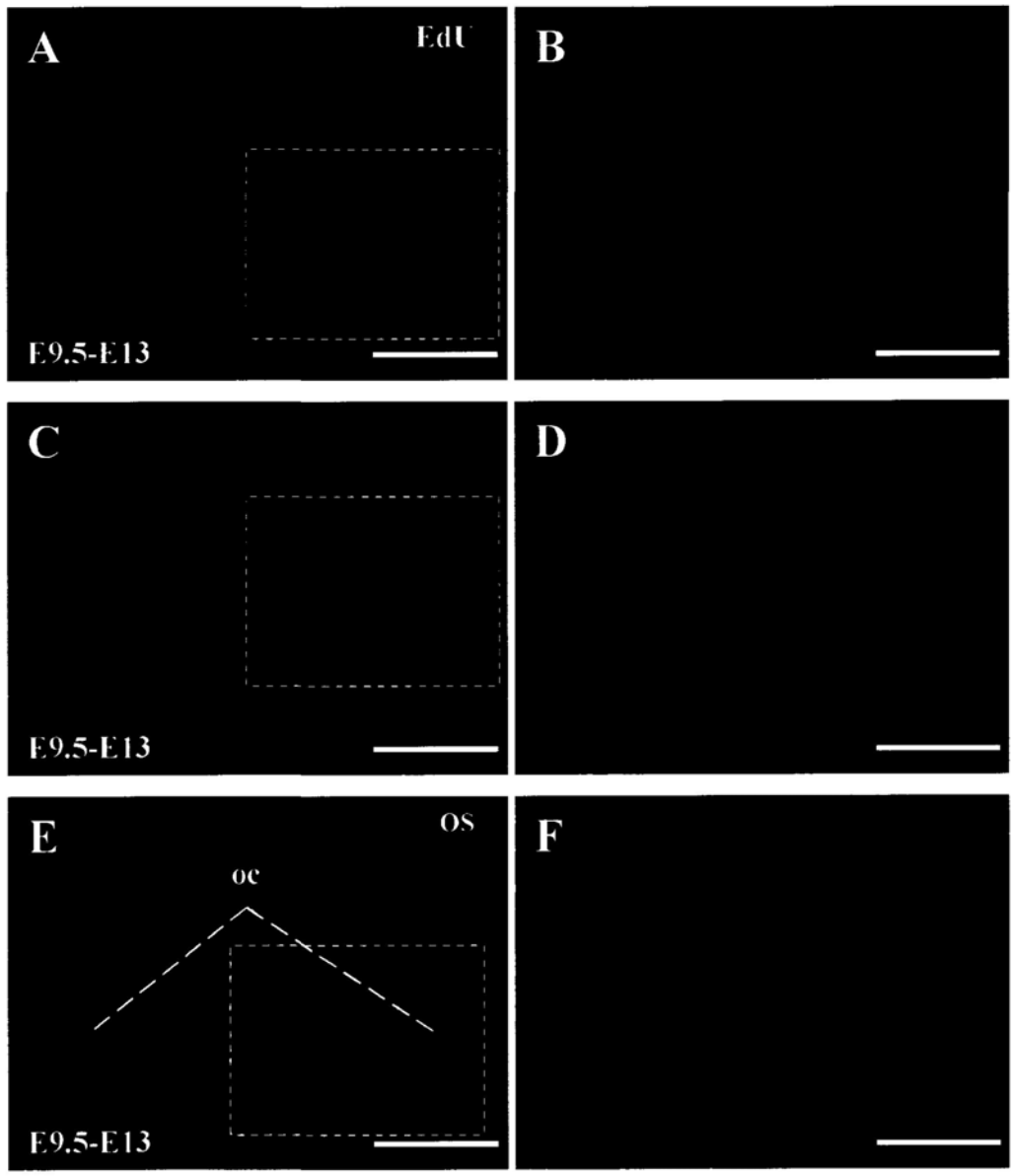
A
EdU
E9.5-E13
B
C
E9.5-E13
D
E
OS
oc
E9.5-E13
F

Figure 4 Co-localization of EdU positive cells and chiasmatic neurons in the ventral diencephalon at E13, when EdU was injected at E9.5. (A) 1 At the level about 200μm above the ventral pial surface, where the optic chiasm (OC) located, a large number of EdU positive cells assembled here, and formed an inverted "V-shaped" outline. 2 In the same section, the characteristic inverted "V-shaped" configuration of the chiasmatic neurons, which was stained by SSEA-1 antibody, was observed. 3 The merged image showed that most of the EdU positive cells were localized in the area of chiasmatic neurons "V-shaped" array. (B) The higher magnification of the "V-shaped" array at figure A was showed that EdU positive cells were colocalized with SSEA-1 neurons in the V-shape region.

Scale bar: A, 200μm; B, 100μm.

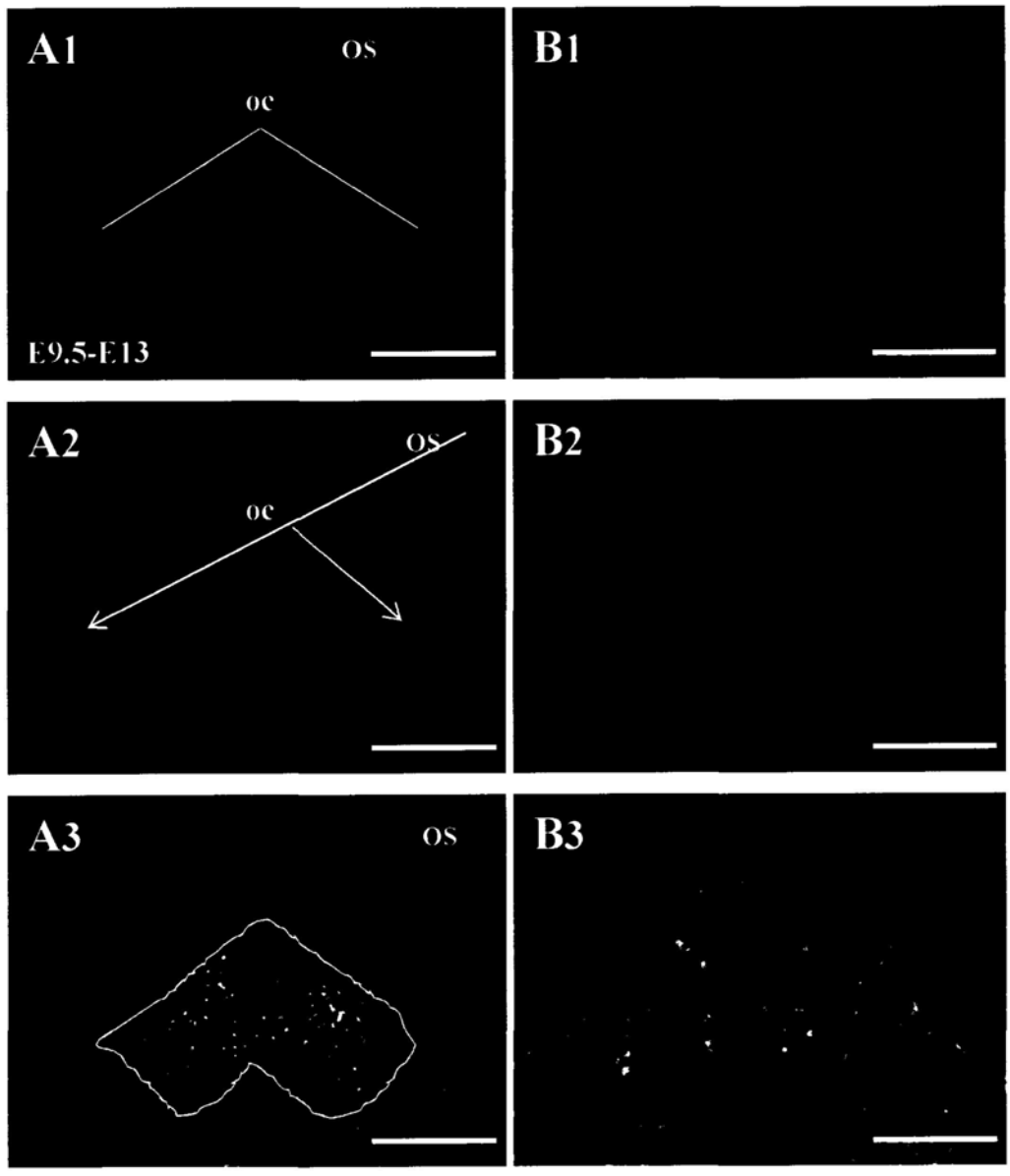
A1
os
oc
E9.5-E13
B1
A2
os
oc
B2
A3
os
B3

Figure 5 EdU positive staining was located in the nuclei of SSEA-1 neurons at E13, when EdU was injected at E9.5. (C) The merged image of A and B showed the colabeling of EdU positive cells and SSEA-1 neurons in higher power of Fig.4. This image was observed by the oil lens. (D) The image was zoomed two times in the white square. It was very clearly that EdU staining was located in the nuclei of the SSEA-1 neurons (indicated by open arrows). The spot like EdU staining, which indicated by white solid arrow, was not recognized as EdU positive cell in the cell counting analyses.

Scale bar: 50μm.

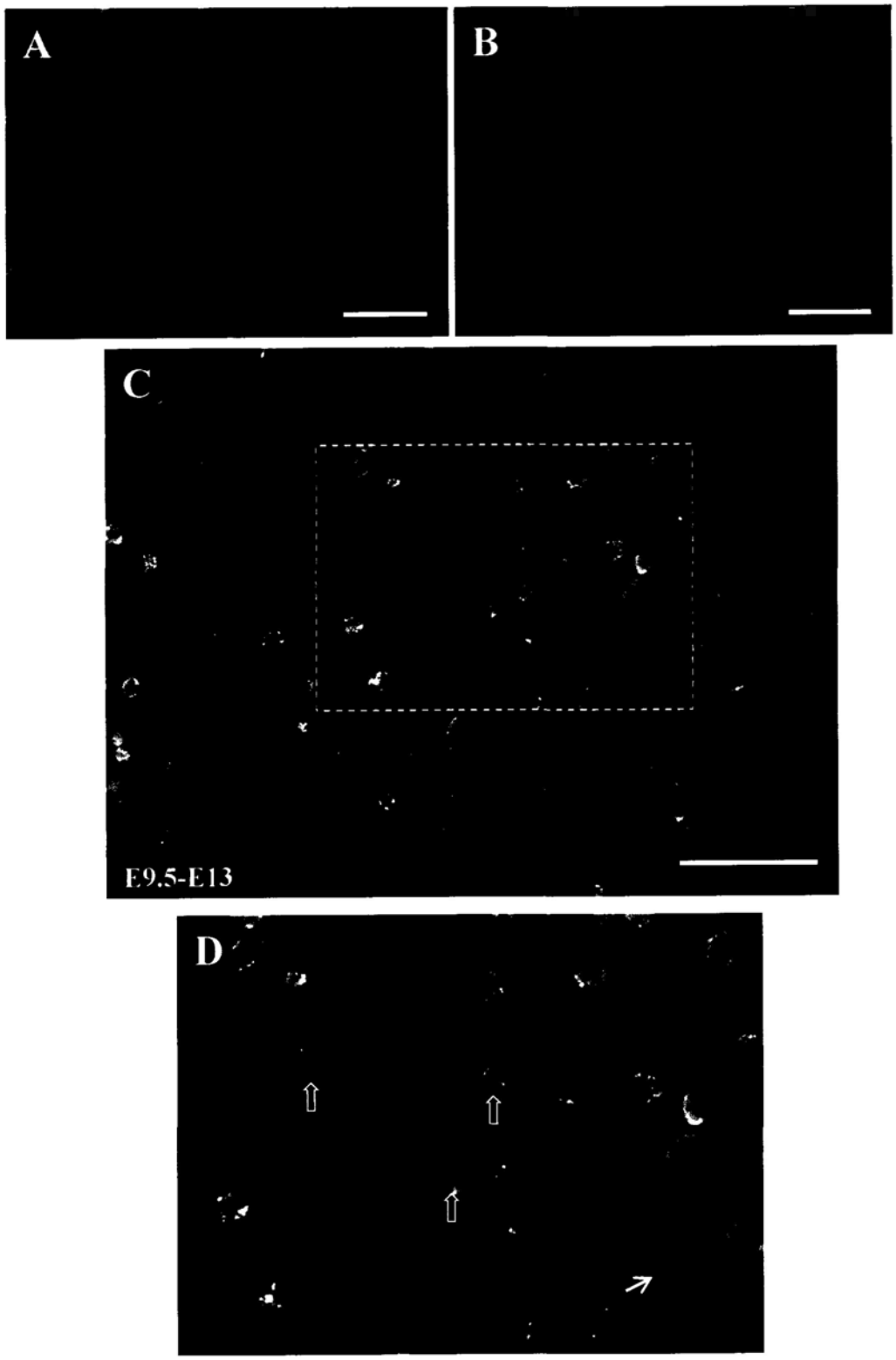
A
B
C
E9.5-E13
D

Figure 6 Co-localization of EdU positive cells and chiasmatic neurons in the ventral diencephalon at E13, when EdU was injected at E10. (A) At E13, the EdU positive cells were still packed together in the caudal region of diencephalon on the level of chiasm, when the EdU was injected at E10. But the density of EdU positive cells seems to be smaller when compared with that after E9.5 injection. In the merged image, most of the EdU positive cells were located in the SSEA-1 neuronal array, whereas some were observed outside the SSEA-1 territory. (B) At higher power of the "V-shaped" array in figure A, EdU positive cells were colocalized with SSEA-1 neurons in this region.

Scale bar: A, 200μm; B, 100μm.

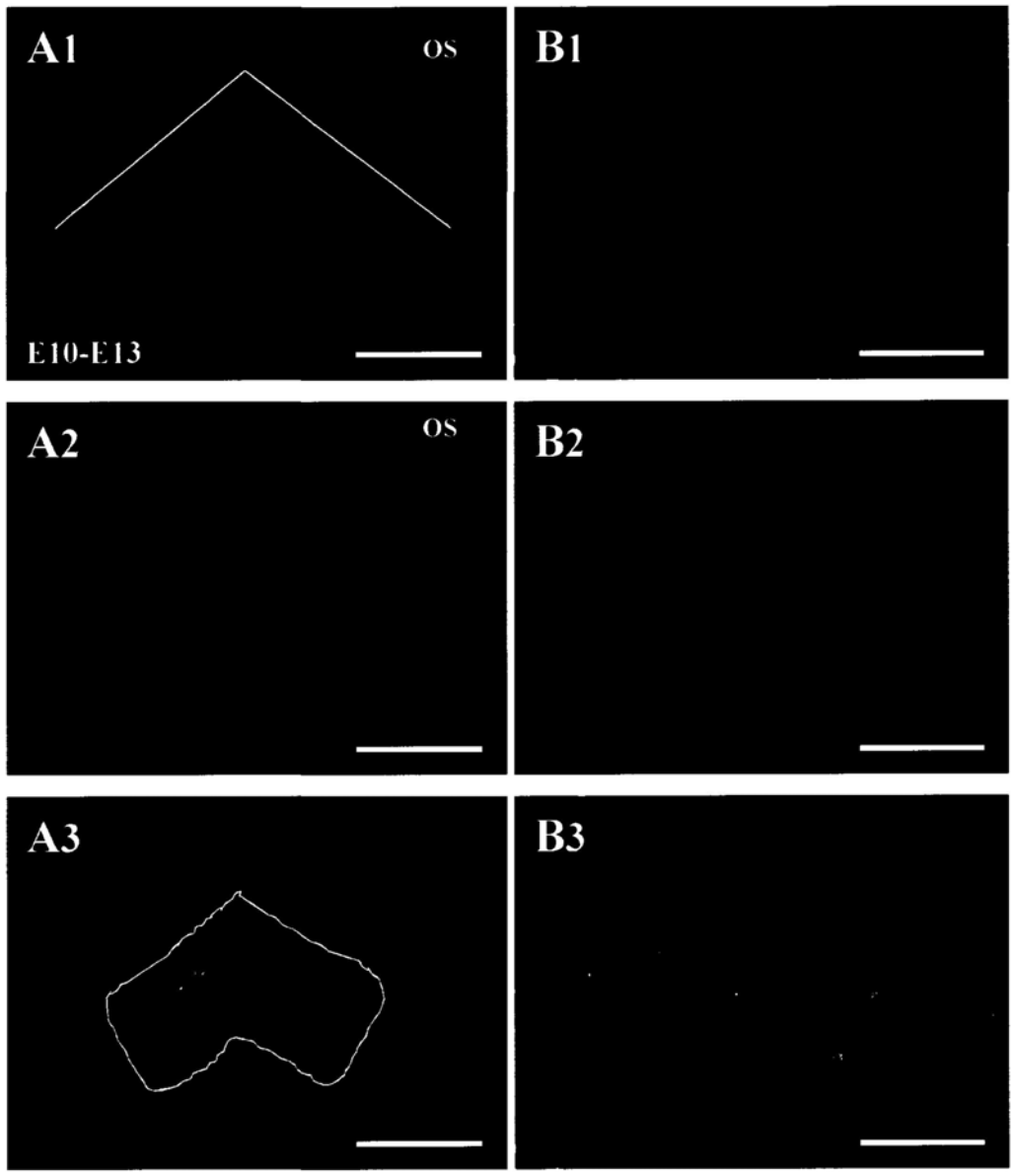
A1
OS
E10-E13
B1
A2
OS
B2
A3
B3

Figure 7 Co-localization of EdU positive cells and chiasmatic neurons in the ventral diencephalon at E13, when EdU was injected at E11. (A) The pattern of the EdU positive cells was quite different from that after EdU E9.5 and E10 injection. The EdU positive cells clustered to the anterior parts of the ventral diencephalon at the chiasm level. In the merged image, most EdU positive cells were observed outside the territory of SSEA-1 neurons, whereas only a small number of EdU positive cells remained in the typical "V-shaped" configuration. (B) At higher power, EdU positive cells in the "V-shaped" array were still colocalized with SSEA-1 neurons.

Scale bar: A, 200μm; B, 100μm.

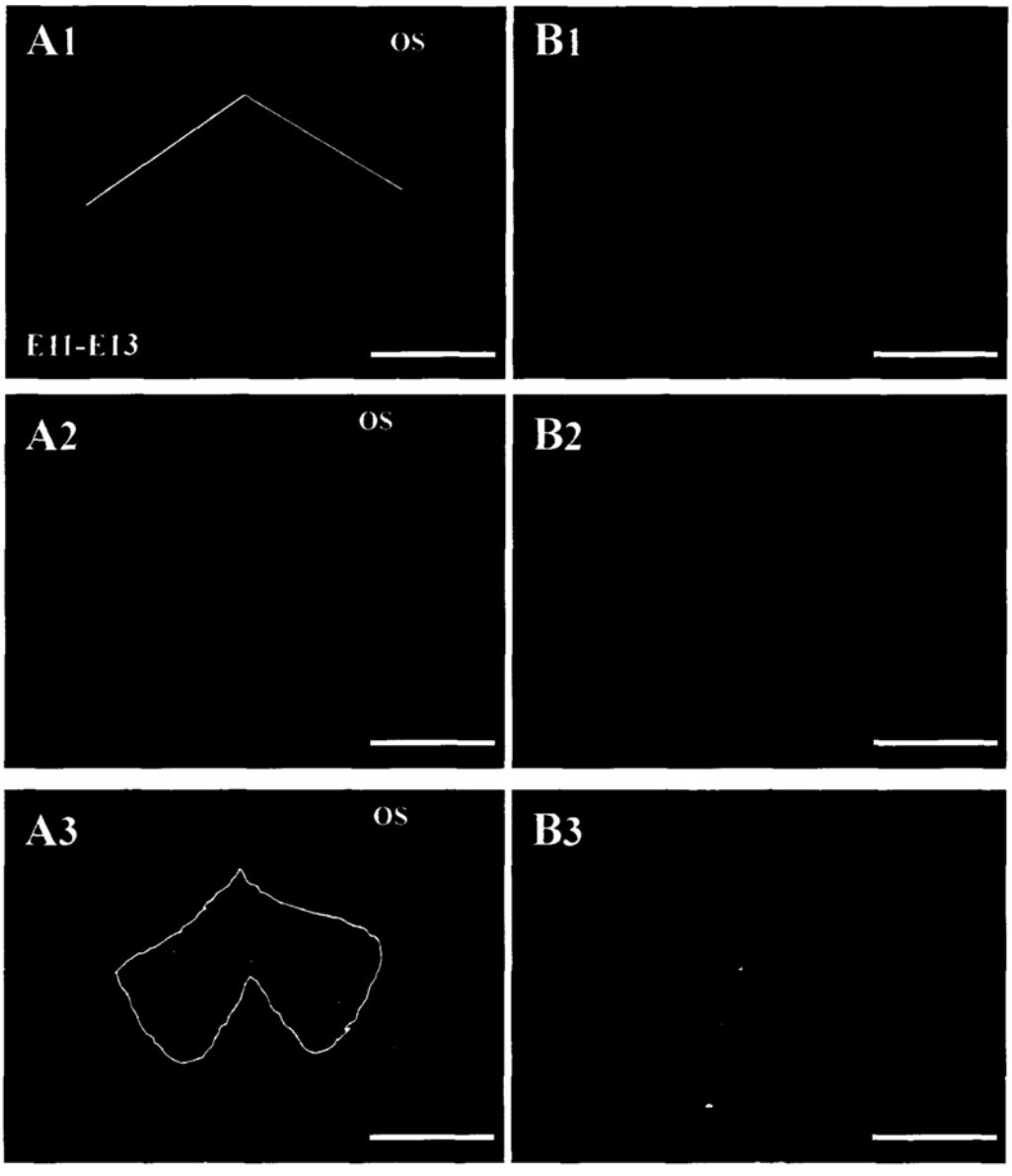
A1
os
E11-E13
B1
A2
os
B2
A3
os
B3

Figure 8 EdU positive signals were located in the nuclei of SSEA-1 neurons at E13, when EdU was injected at E11. (C) The merged image of A and B was observed with oil lens. In this area, which contained half of "V-shaped" chiasmatic neurons, only a few EdU positive cells were inside this area. In the two times zoomed image in the white square, the EdU staining was still located in the nuclei of SSEA-1 neurons. Scale bar: 50μm.

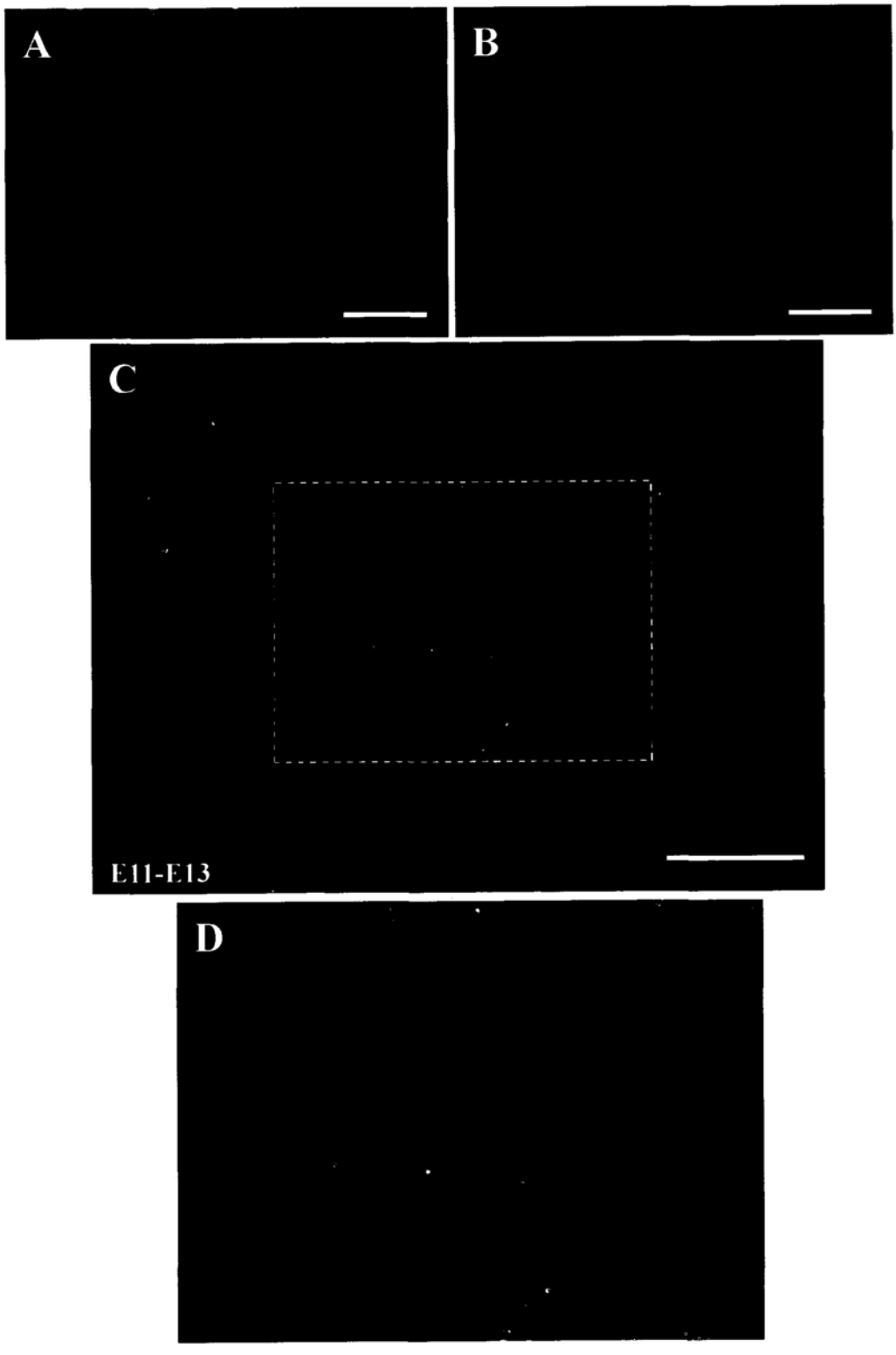
A
B
C
E11-E13
D

Figure 9 The results of cell counting analyses showed that most of the chiasmatic neurons were born at E9.5. (A-C) The double labeled cells were counted at the level 200μm above the ventral pial surface in different sections, where the optic chiasm (OC) located. We drew the outline of the SSEA-1 neurons, and counted the double labeled cells inside. (D) The plot was showed the cell counting results, when EdU was injected at different embryonic stages. When EdU was injected at E9, no EdU positive cell was observed in the ventral diencephalon at E13. Most double labeled cells were found in the E13 diencephalon, when EdU was injected at E9.5. There were fewer double labeled cells on the same level, when EdU was injected at E10 and E11. The number of double labeled cells was significant reduced in E11 injected mice compared with that of E9.5 injected mice.

Scale bar: 200μm.

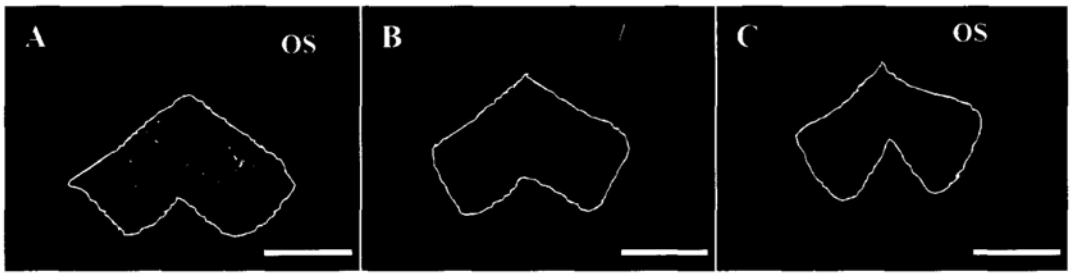

E9.5-E13 **E10-E13** **E11-E13**

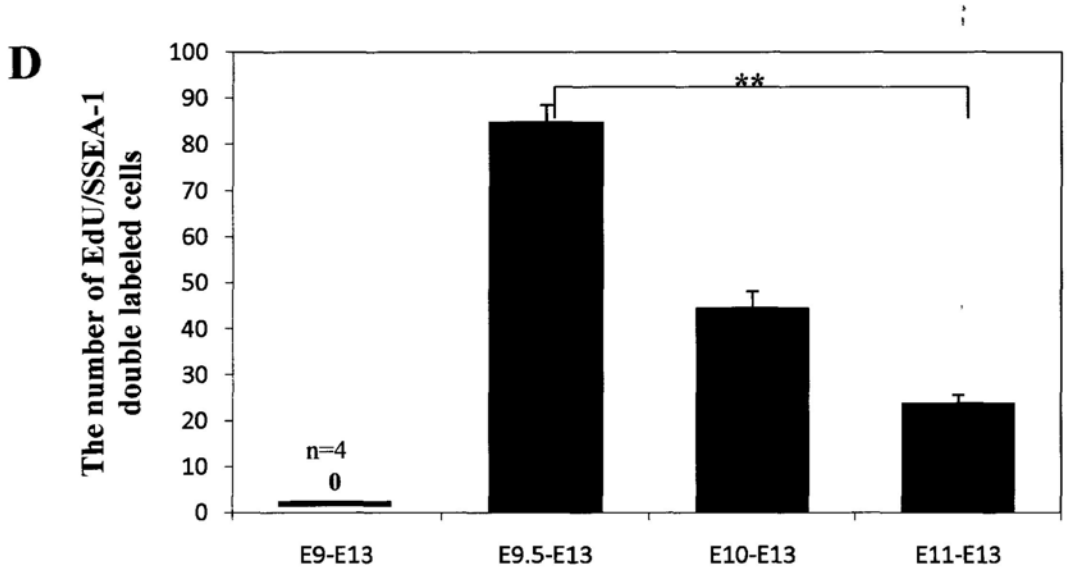

* * $p < 0.01$

Figure 10 Co-localization of EdU positive cells and chiasmatic neurons in the ventral diencephalon at E14, when EdU was injected at E9.5.（A1） When EdU was injected at E9.5, the EdU positive cells at E14 assembled around the midline and formed a V-shaped structure at the level of the optic chiasm. (B1) The merged image showed that these EdU positive cells localized in the SSEA-1 positive area. (A2) At the higher power, these EdU positive cells had higher density in the region that closed to the midline (indicated by the asterisks). (B2) Most of the EdU labeled cells seemed colocalized with the SSEA-1 neurons. (A3 & B3) Under the even higher magnification, it was clear that the EdU labeled cells in the SSEA-1 positive region were colabeled with the SSEA-1 neurons.

Scale bar: A1, A2, B1, B2, 200μm; A3, B3, 100μm.

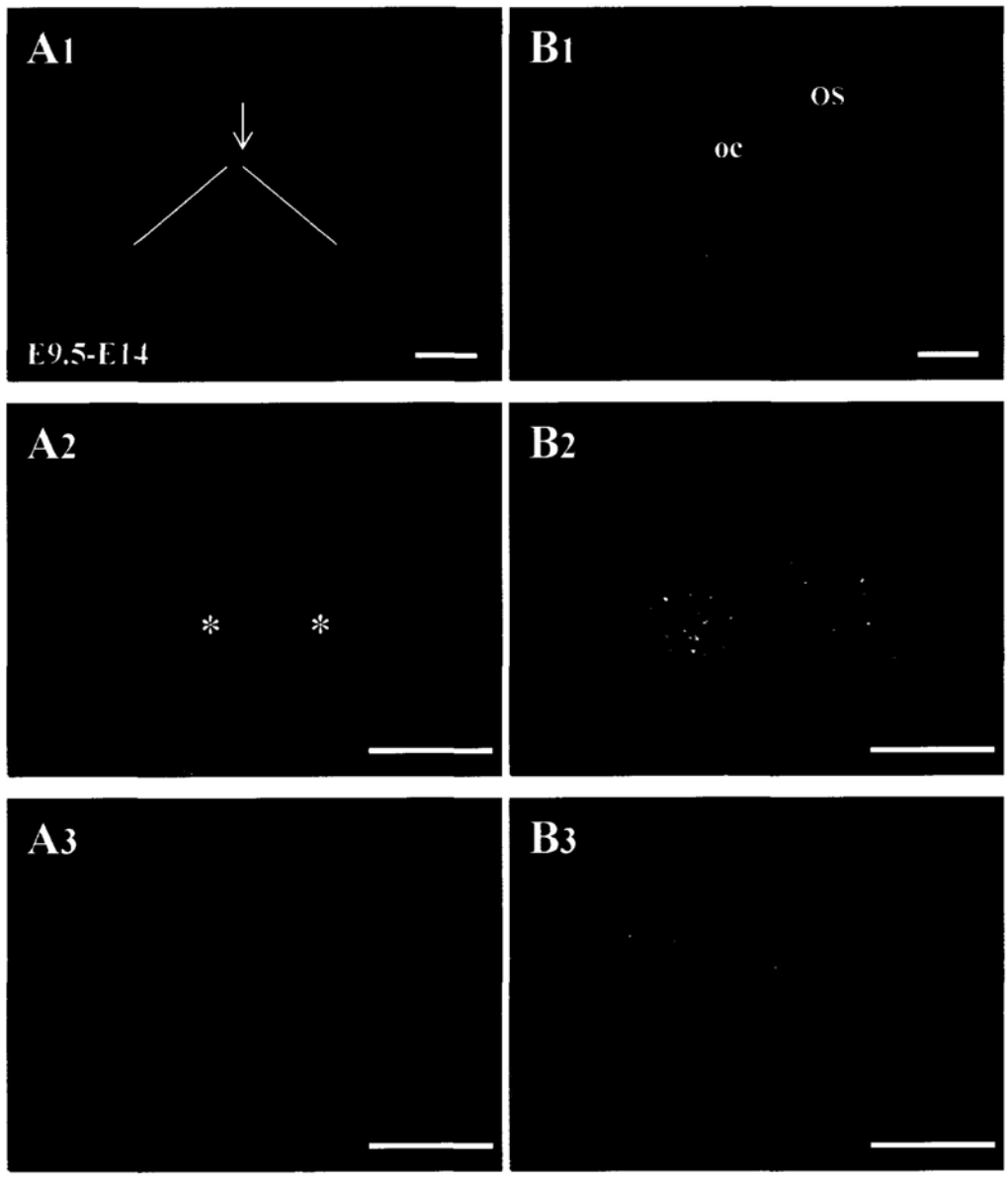
A1
E9.5-E14
B1
os
oc
A2
B2
A3
B3

Figure 11 EdU positive staining was located in the nucleus of SSEA-1 neurons at E14, when EdU was injected at E9.5. (C) The merged image of A and B was showed the colabeling of EdU positive cells and SSEA-1 neurons which was observed under the oil lens. It was clear that EdU staining was located in the nucleus of the SSEA-1 neurons (indicated by open arrows). The dotted EdU staining, which indicated by solid arrows, was not included in the cell counting analyses.

Scale bar: 50μm.

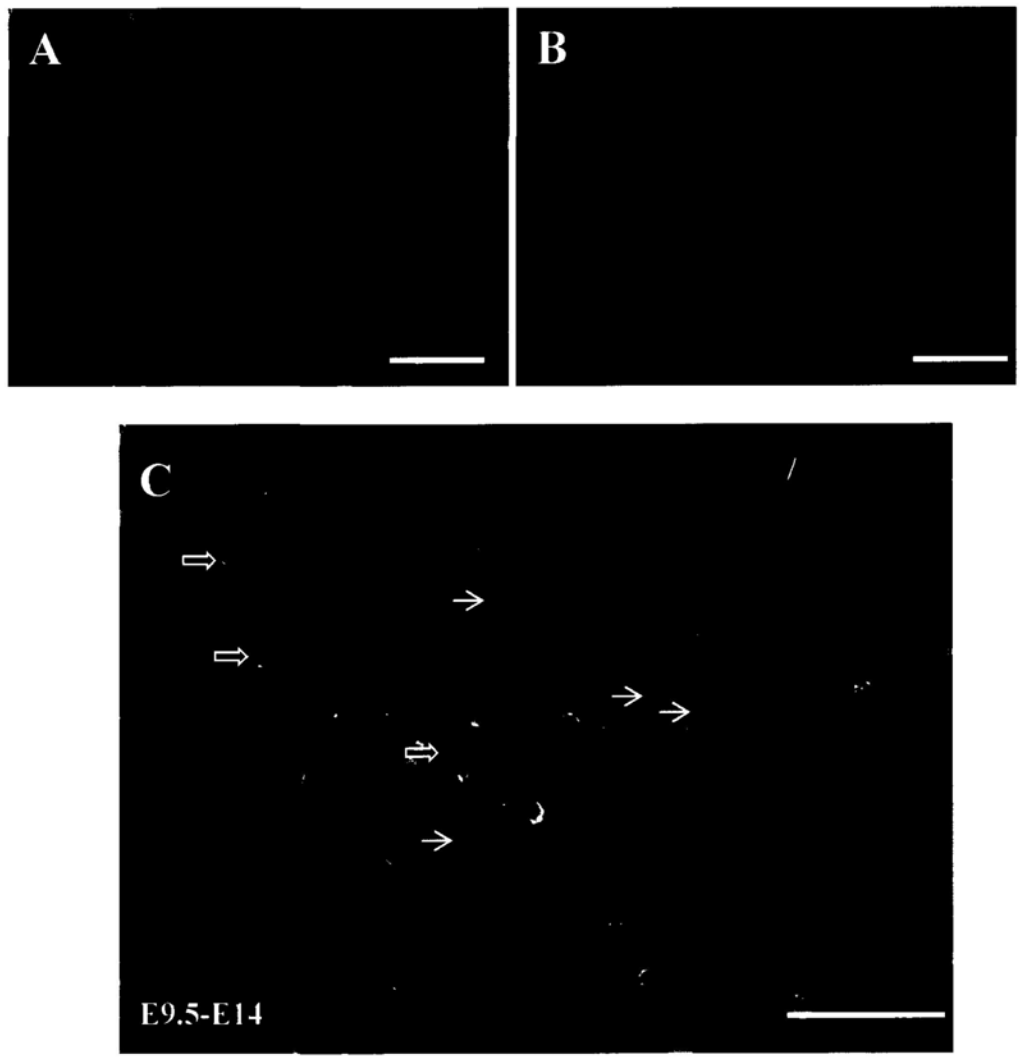
A
B
C
E9.5-E14

Figure 12 Co-localization of EdU positive cells and chiasmatic neurons in the ventral diencephalon at E15, when EdU was injected at E9.5.（A1） When EdU was injected at E9.5, the EdU positive cells at E15 were found largely close to the midline, looked like two stripes at each side on the level of optic chiasm (indicated by the asterisks). (B1) On the merged image, these EdU labeled cells localized in the SSEA-1 positive region. (A2 & B2) The higher power image of the A1 and B1 showed that the EdU labeled cells were widely detected on the SSEA-1 positive region, but more concentrated at the area close to the midline. (A3 & B3) These EdU labeled cells in the SSEA-1 positive region were colocalized with the chiasmatic neurons.

Scale bar: A1, A2, B1, B2, 200μm; A3, B3, 100μm.

Figure 13 EdU positive staining was located in the nucleus of SSEA-1 neurons at E15, when EdU was injected at E9.5. C is the merged image of A and B, which was showed the colabeling of EdU positive cells and SSEA-1 neurons under the oil lens. It was clear that EdU staining was located in the nucleus of the SSEA-1 neurons (indicated by open arrows). But there were many dotted staining of EdU, which was also located in the nuclear of chiasmatic neurons (indicated by solid arrows).
Scale bar: 50μm.

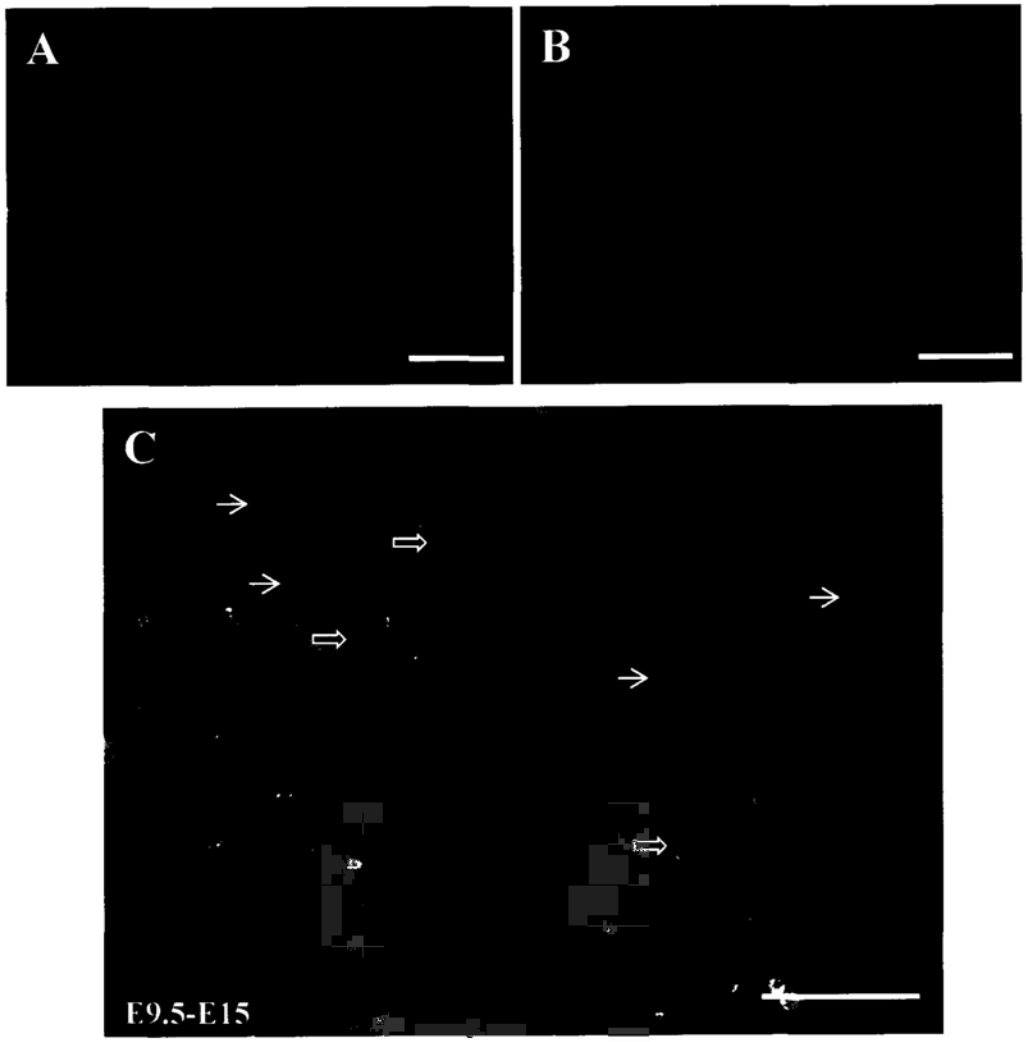
A
B
C
E9.5-E15

Figure 14 Co-localization of EdU positive cells and chiasmatic neurons in the ventral diencephalon at E16, when EdU was injected at E9.5. (A1) Similar to E15, EdU positive cells at E16 were largely observed in two clusters next to the midline of the ventral diencephalon on the level of chiasm, when EdU was injected at E9.5 (indicated by the asterisks). But these cluster appeared smaller than that at E15. (B1) In the merged image, most of these EdU signals were localized in the SSEA-1 positive region. (A2 – B3) At higher magnification, these EdU labeled cells were colabeled with the SSEA-1 neurons.

Scale bar: A1, A2, B1, B2, 200μm; A3, B3, 100μm.

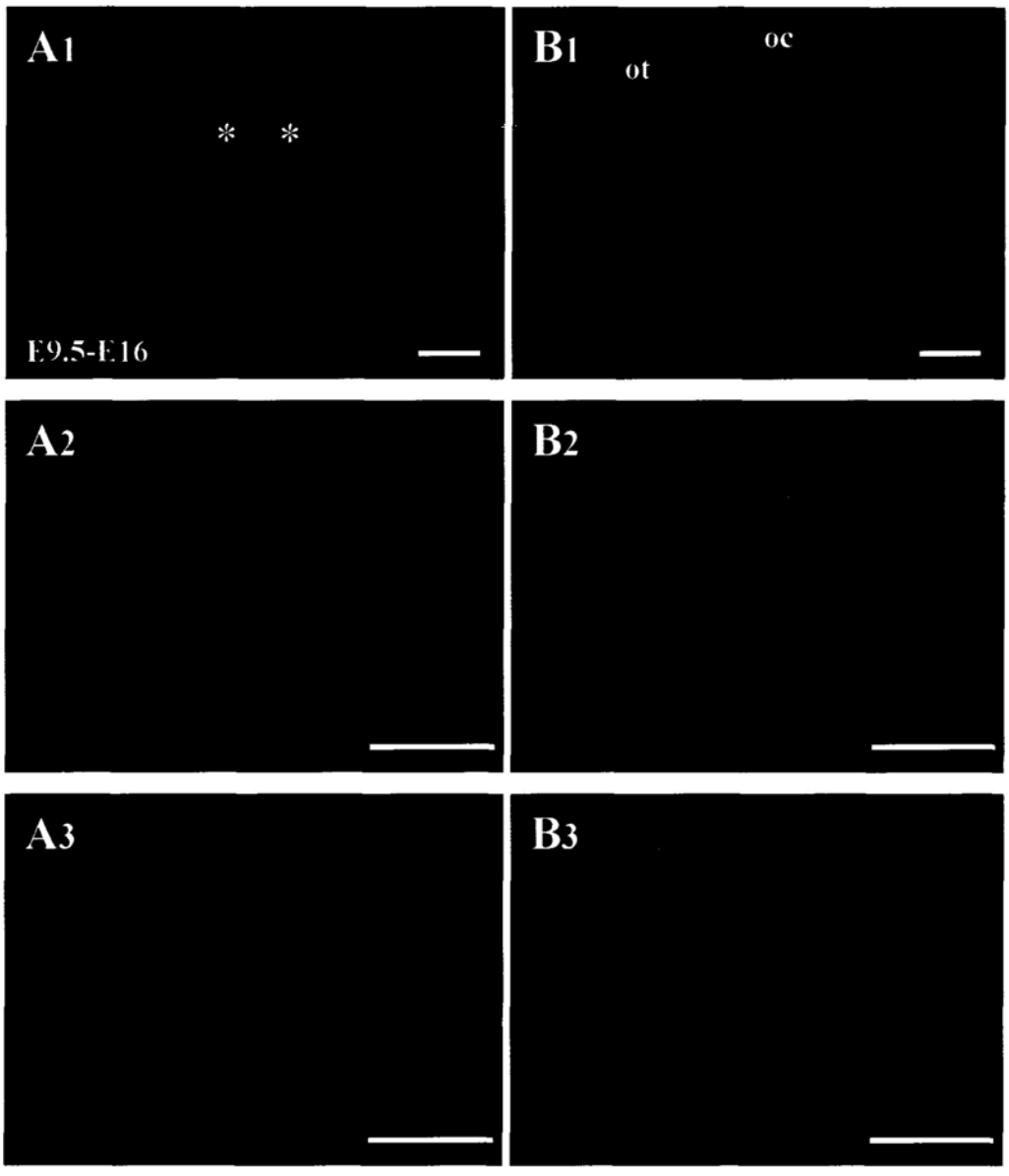
A1
* *
E9.5-E16
B1
oc
ot
A2
B2
A3
B3

Figure 15 EdU positive staining was located in the nucleus of SSEA-1 neurons at E16, when EdU was injected at E9.5. (A) When examined at 60x magnification, only a few EdU labeled cells were observed. (C) In the merged image of A and B, these strong EdU signals were localized in the nuclei of the SSEA-1 neurons (indicated by open arrows), while a lot of light, dot-like EdU staining was also observed in the SSEA-1 neurons (indicated by solid arrows).

Scale bar: 50μm.

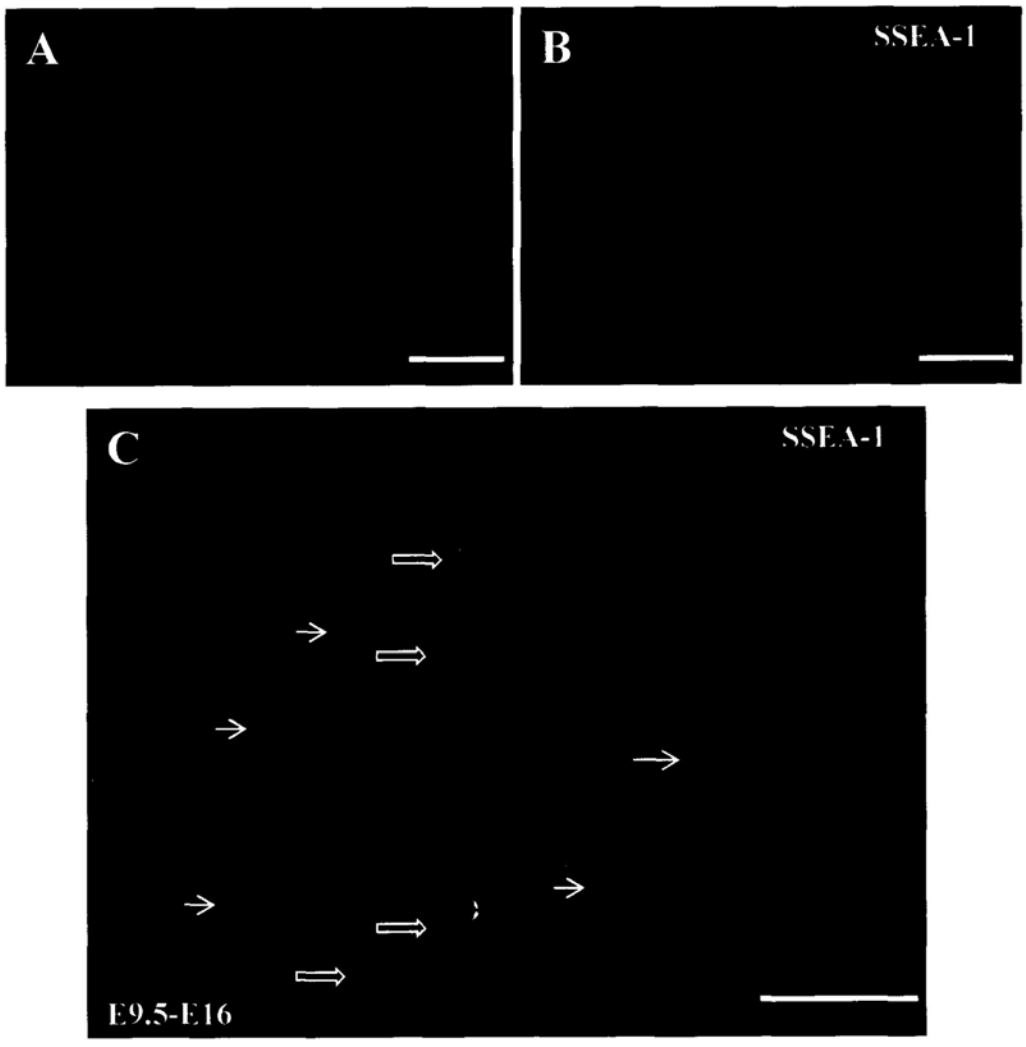
A
B
SSEA-1
C
SSEA-1
E9.5-E16

Figure 16 Co-localization of EdU positive cells and chiasmatic neurons in the ventral diencephalon at E17, when EdU was injected at E9.5. (A1) Similar to E15 and E16, EdU positive cells at E17 revealed two arrays next to the midline at each side of the ventral diencephalon at the level of chiasm, when EdU was injected at E9.5 (indicated by the asterisks). These arrays seemed a little smaller than that at E16. (B1) In the merged image, these EdU staining was localized in the SSEA-1 positive region. (A2 – B3) At higher power, EdU labeled cells were colocalized with the SSEA-1 neurons in the SSEA-1 positive region.

Scale bar: A1, A2, B1, B2, 200μm; A3, B3, 100μm.

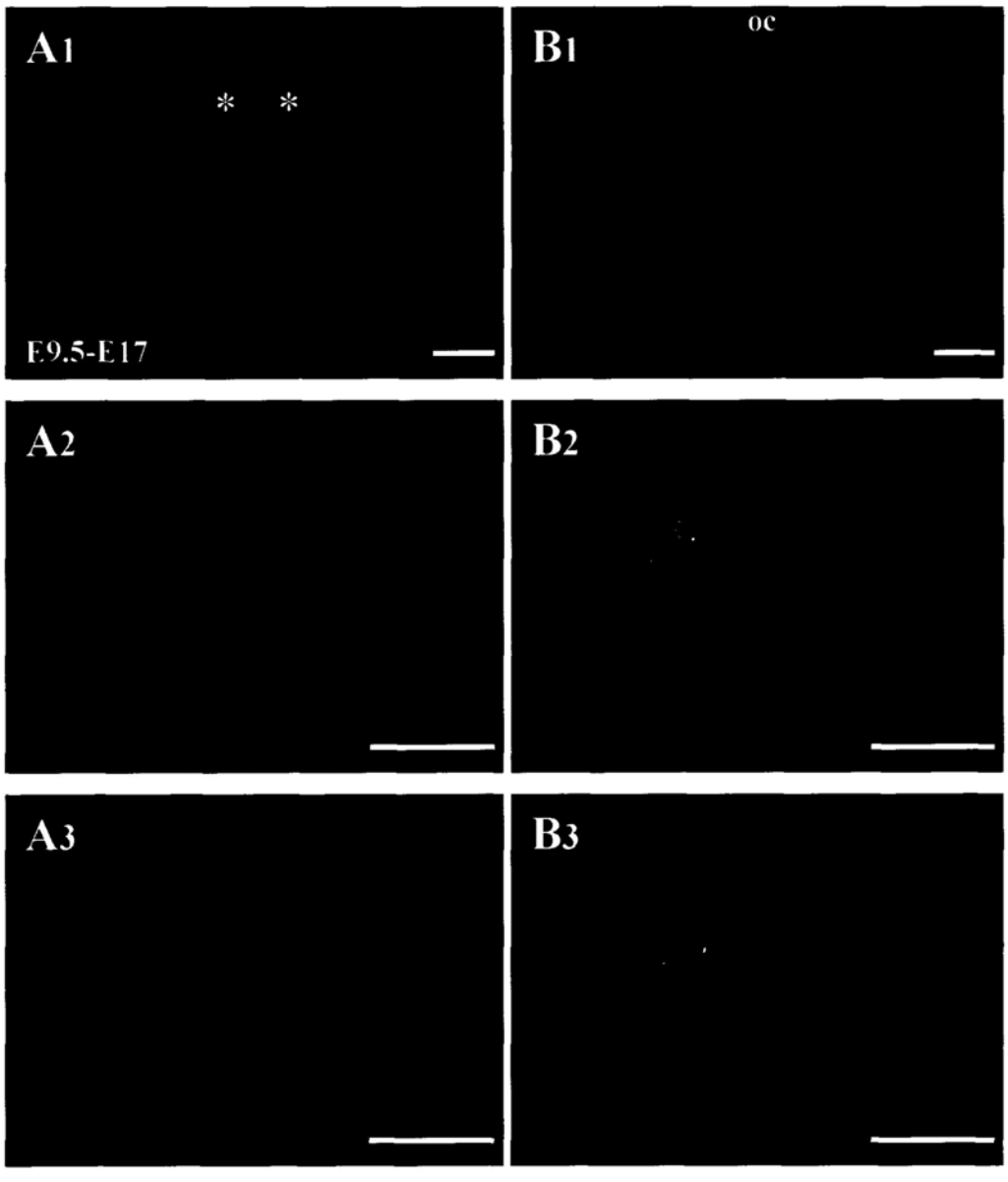
A1
B1
oc
E9.5-E17
A2
B2
A3
B3

Figure 17 Co-localization of EdU positive cells and chiasmatic neurons in the ventral diencephalon at E18, when EdU was injected at E9.5. (A1) Similar to E15 to E17, EdU positive cells at E18 also revealed two arrays at each side of the ventral diencephalon close to the midline at the level of chiasm, when EdU was injected at E9.5 (indicated by the asterisks). (B1) In the merged image, EdU staining was observed in the SSEA-1 positive area. (A2 – B3) At higher power, EdU labeled cells in the SSEA-1 area were still colocalized with the SSEA-1 neurons.

Scale bar: A1, A2, B1, B2, 200μm; A3, B3, 100μm.

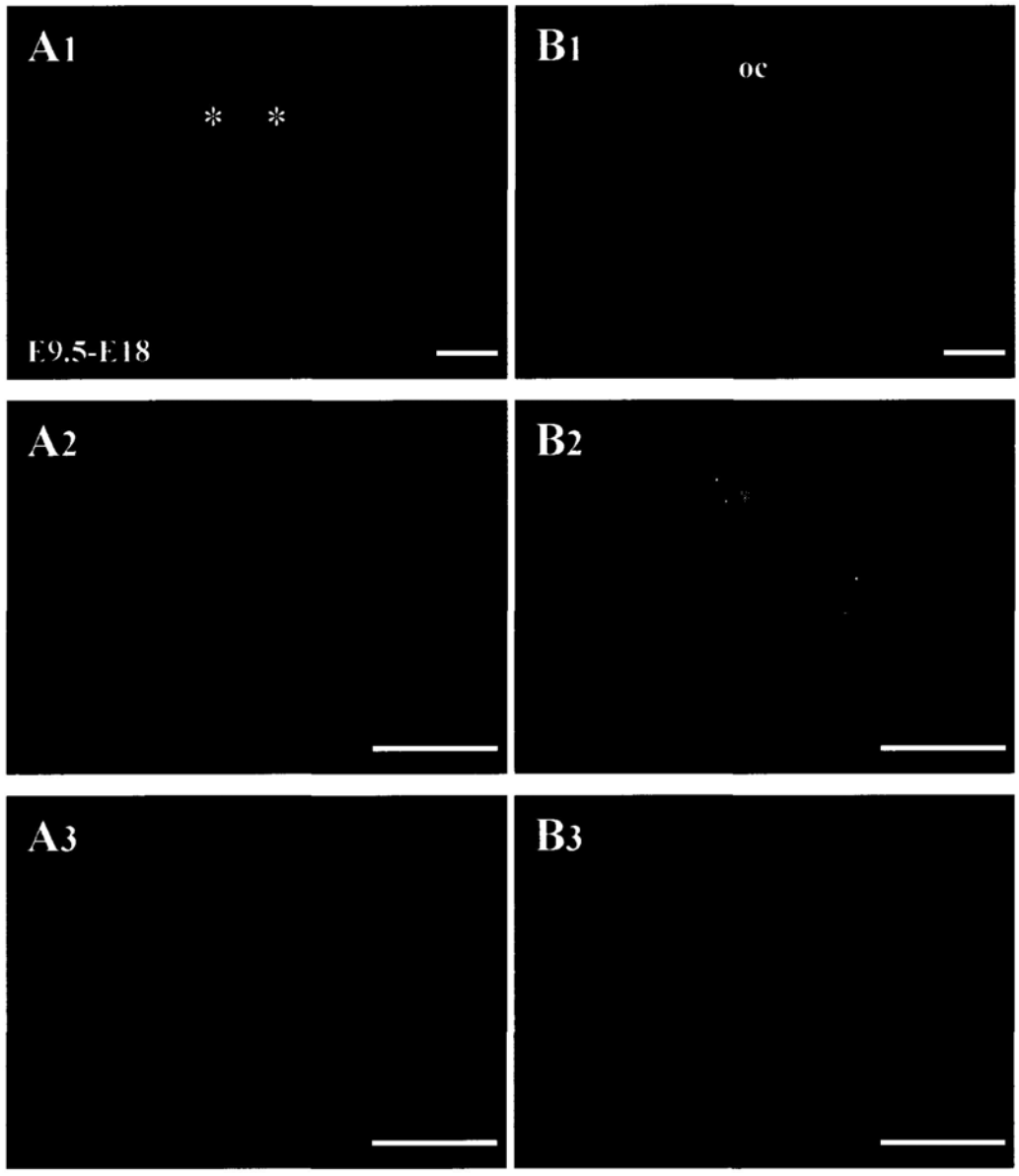
A1
B1
oc
E9.5-E18
A2
B2
A3
B3

Figure 18 The cell counting analyses showed the cell number of chiasmatic neurons from E13 to E16, while these chiasmatic neurons were generated at E9.5. (A – D) The double labeled cells were counted on the level of optic chiasm (OC) at different embryonic stages from E13 to E16. We drew the outline of the SSEA-1 neurons, and counted the double labeled cells inside. (E) The plot was showed the cell counting results at different embryonic stages, when EdU was injected at E9.5. Most double labeled cells were observed on the ventral diencephalon at E13. There were fewer and fewer double labeled cells from E14 to E16. Compared with the double labeled cell at E13, the cell number was reduced significantly at E15 ($P<0.05$) and E16 ($P<0.01$).

Scale bar: 200μm.

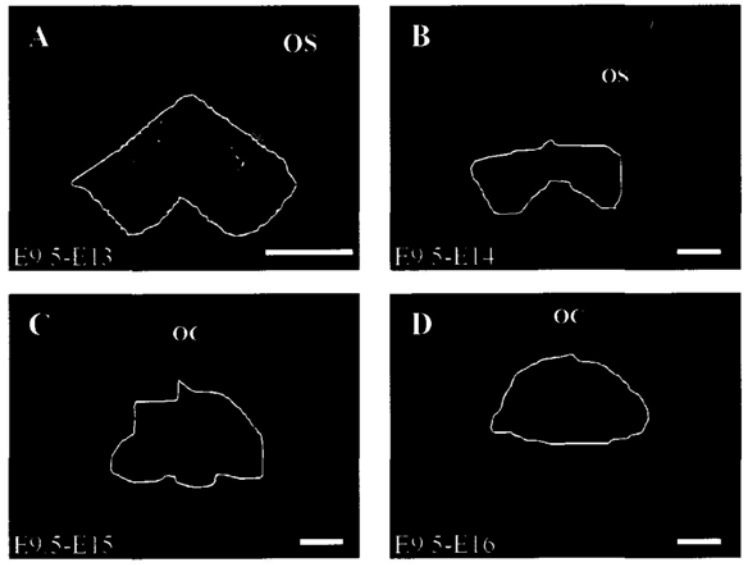
A
OS
E9.5-E13
B
OS
E9.5-E14
C
OC
E9.5-E15
D
OC
E9.5-E16

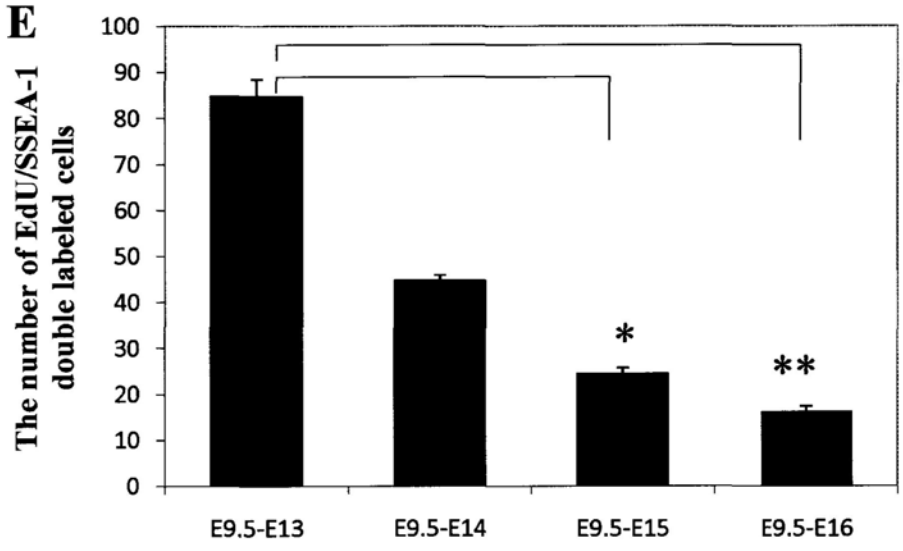
E
The number of EdU/SSEA-1 double labeled cells
100
90
80
70
60
50
40
30
20
10
0
*
**
E9.5-E13
E9.5-E14
E9.5-E15
E9.5-E16

* $P<0.05$

** $P<0.01$

Figure 19 Identification of chiasmatic neurons with neural stem cell marker. (A1 and B1) The pattern of Nestin immunoreactive signals in the ventral diencephalon on the level of optic chiasm at E13. A2 and B2 showed the distribution of SSEA-1 neurons at the same section. (A3 and B3) In the merged image, the chiasmatic neurons did not appear to the Nestin positive neural stem cells.

Scale bar: A, 200μm; B, 100μm.

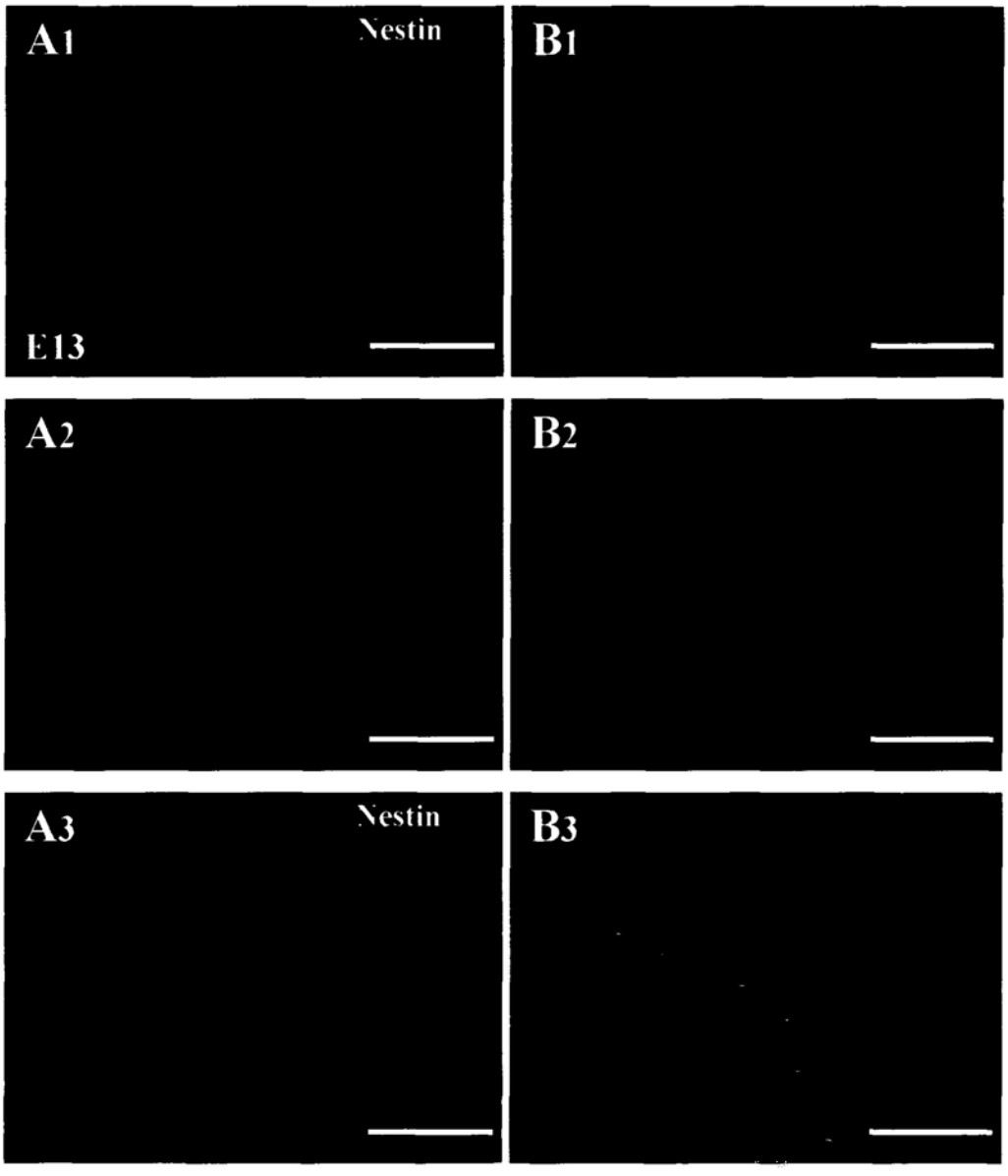
A1
Nestin
E13
B1
A2
B2
A3
Nestin
B3

Figure 20 The higher magnification of confocal photomicrographs revealed that Nestin was found on the radial processes that span through the SSEA-1 neurons. (A) At 60x magnification, Nestin immunoreactive staining was observed on the radial processes. (C) In the merged image, few SSEA-1 positive neurons were colabeled with Nestin immunoreactive cells.

Scale bar: 50μm.

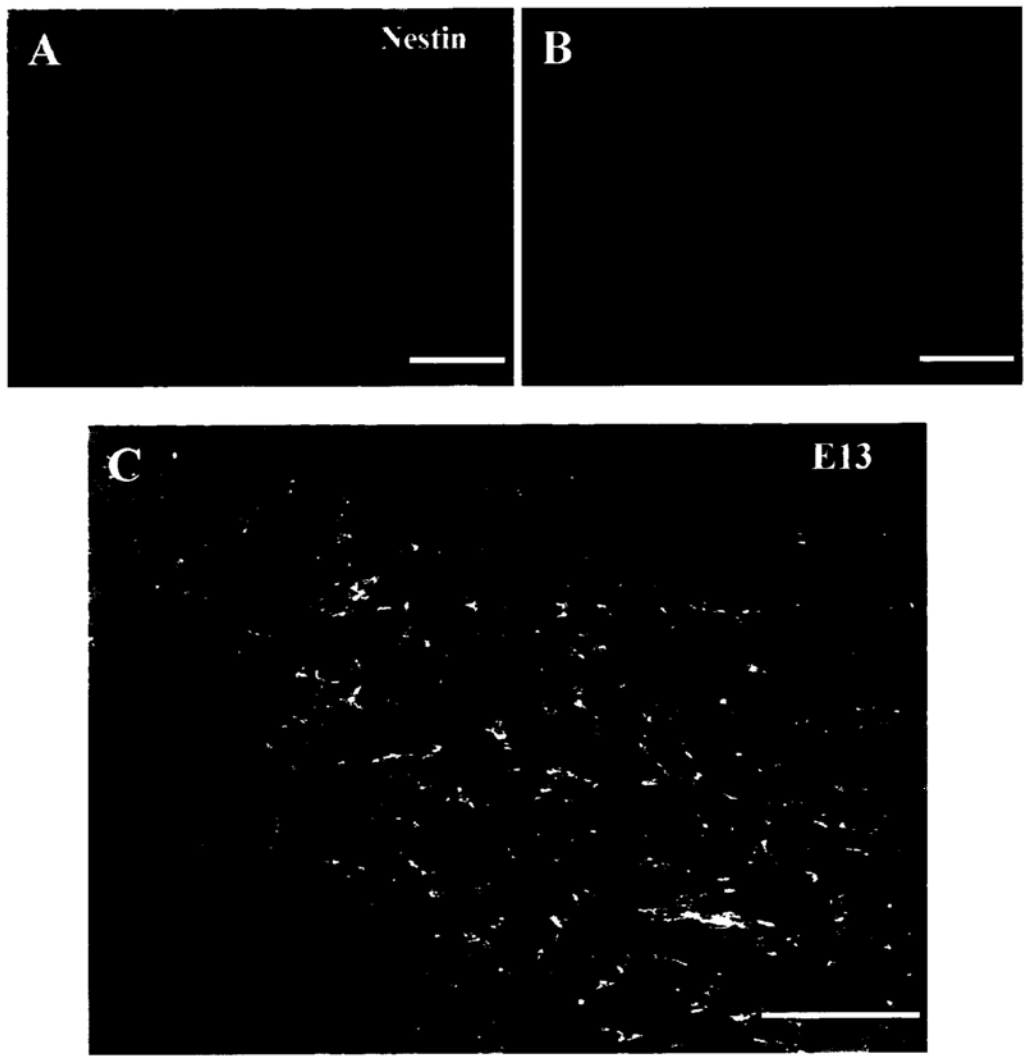
A
Nestin
B
C
E13

Figure 21 A few apoptotic cells were observed in the area of chiasmatic neurons at E13 and E14. (A1) At E13, only one apoptotic cell was observed in the ventral diencephalon (indicated by open arrow). But many apoptosis cells were detected on the trigeminal ganglion close to the diencephalon (indicated by asterisk). (A2 – A4) In the merged image, this apoptotic cell was colabeled with SSEA-1 in the ventral diencephalon. (B1)At E14, a few more apoptotic cells were detected in the ventral diencephalon. (B2 – B4) In the merged image, all the apoptotic cells in the ventral diencephalon were colocalized with SSEA-1 neurons (indicated by open arrows). Scale bar: A1, A2, A3, B1, B2, B3, 200μm; A4, 50μm; B4, 100μm.

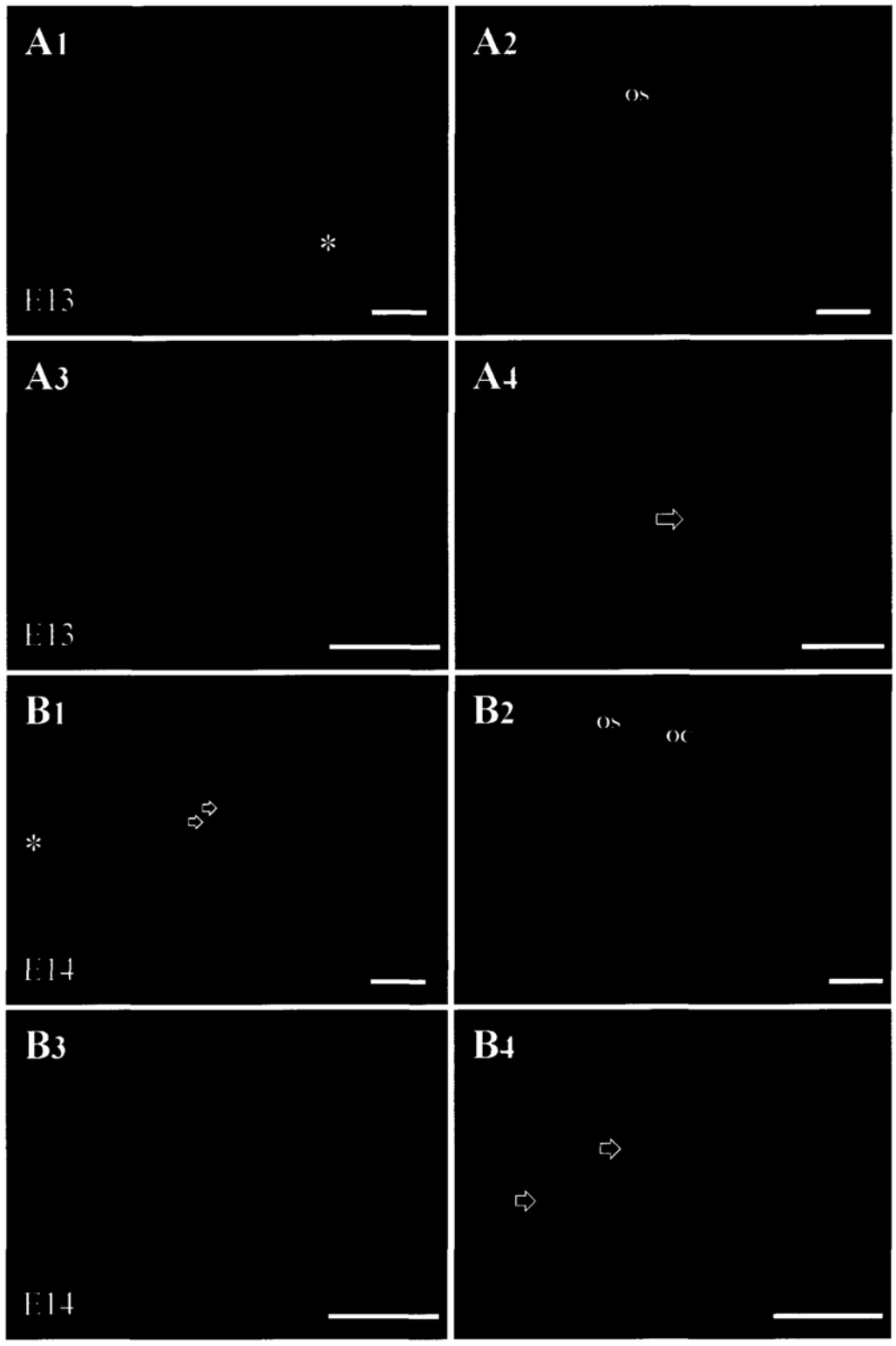
A1
E13
A2
os
A3
E13
A4
B1
E14
B2
os
oc
B3
E14
B4

Figure 22 Many apoptotic cells were observed in the area of chiasmatic neurons at E15. (A1) Compared with E13 and E14, many more apoptotic cells were observed in the ventral diencephalon at E15. (B2) Most of these apoptotic cells were located in the SSEA-1 immunoreactive area at the level of optic chiasm. (A2 – B3) When examined in higher magnification, those apoptotic cells in the SSEA-1 positive area were colocalized with chiasmatic neurons. (C) The plot was showed the cell counting results of apoptotic cells at different embryonic stages. The number of apoptotic cells was increased significantly at E15 compared with that of E13.

Scale bar: A1, A2, B1, B2, 200μm; A3, B3, 100μm.

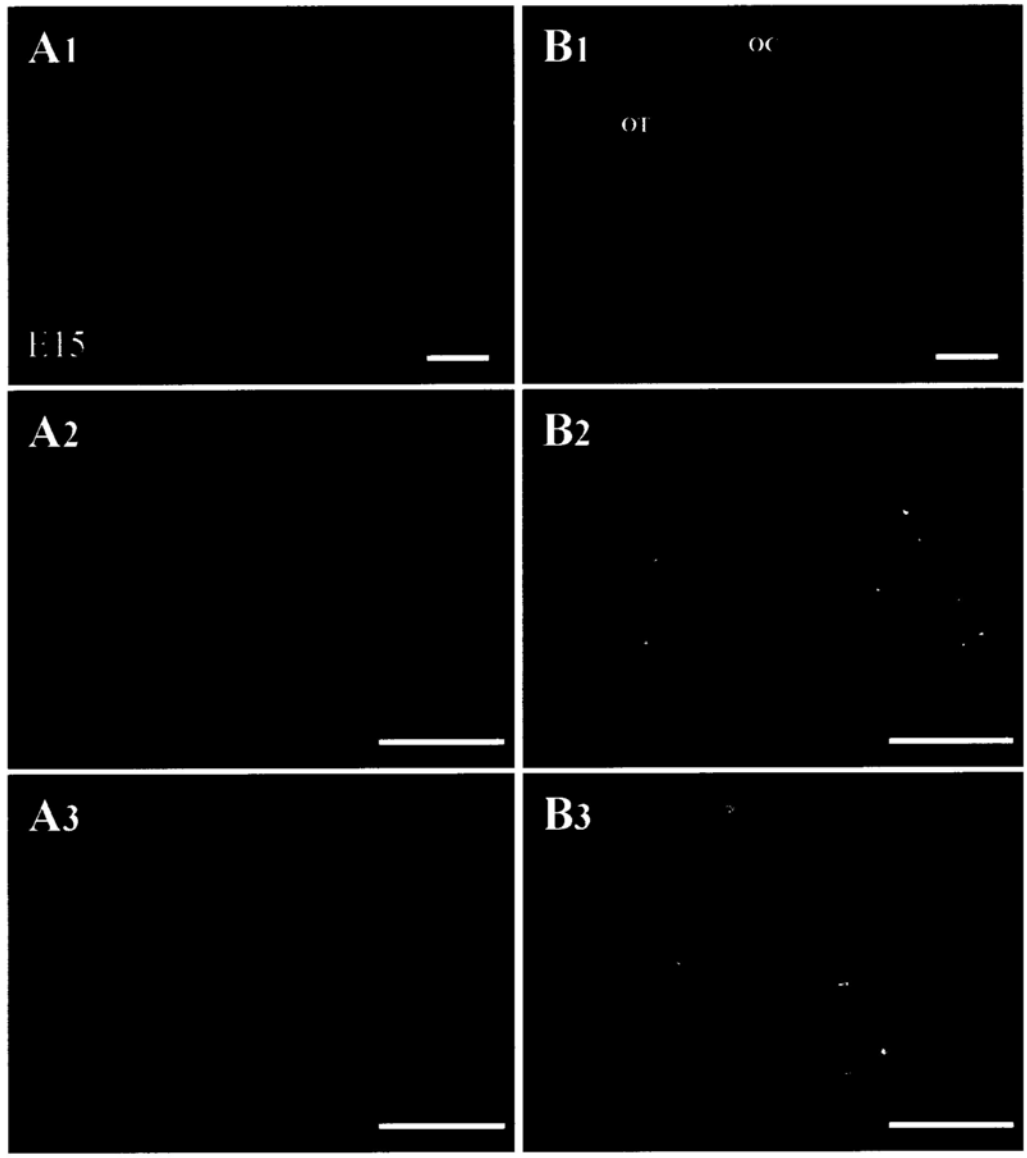
A1
B1
oc
ot
E15
A2
B2
A3
B3

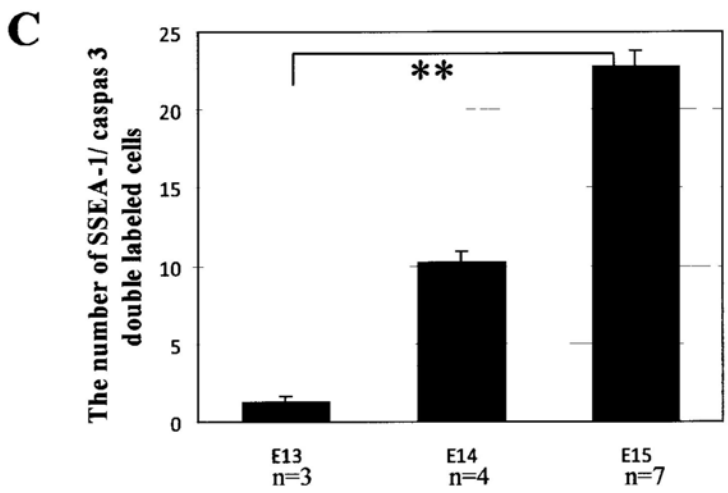
C
The number of SSEA-1/ caspas 3 double labeled cells
25
20
15
10
5
0
**
E13
n=3
E14
n=4
E15
n=7

$P < 0.01$

CHAPTER 3
Birthdating of chiasmatic radial glia in the mouse optic chiasm and tracing their fates

Introduction

Within the mammalian developing optic chiasm there exists two specialized cell arrays, which carries guidance cues and interacts with the RGC axons, to direct axon projection to either ipsilateral or contralateral optic tract. One is the chiasmatic neurons, which was mentioned in the last chapter; the other is the midline radial glia, which form a glia palisade draped along both sides of the chiasmatic midline and can be revealed by the RC2 antibody in the mouse brain at embryonic stage (Marcus et al, 1995; Mason & Sretavan, 1997).

Like radial glia in other parts of the developing brain, the chiasmatic radial glial cells, arising from neuroepithelial cells, have an ovoid cell body located in the ventricular zone and a characteristic bipolar form. They extend an elongated radial process that straddles the chiasmatic midline and a short end foot toward the ventricular surface (Kriegstein & Alvarez-Buylla, 2009; Parnavelas & Nadarajah, 2001).

The guidance mechanisms of the radial glia to the RGC axons are changed at different phases of mouse chiasm development. During the early phase (E12.5-E13.5), the radial glia palisade was more extensive at the midline, about 350-450μm to either side of the midline (Marcus & Mason, 1995). The crossed axons traverse the midline glia zone, but the uncrossed axons grow directly into the ipsilateral optic tract without entering the glia palisade. During the peak phase

(E14-E17), the radial glia palisade becomes more restricted occupying a region about 150-200μm to either side of the midline (Marcus et al, 1995). The uncrossed axons from the VT retina extend to the midline first, then make abrupt turn and project to the ipsilateral optic tract. During the late phase (E17.5-P0), VT axons traverse the glia palisade and grow into the contralateral optic tract (Jeffery, 2001; Mason & Sretavan, 1997; Petros et al, 2008).

Previous study has shown that the chiasmatic radial glial cells are immunoreactive to RC2, a glia marker in mouse embryo from E12 to P0, during the growth period of the RGC axons in the chiasm (Williams et al, 2003). However, when chiasmatic radial glial cells are generated still remains unclear.

In addition why the glia palisade reveals a narrow extension at later stages? It may due to a combination of two factors. First, the width of the basal portion of the ventral diencephalon becomes narrower during development. Second, at the later embryonic stages, the processes of the radial glia become more restricted to the midline (Marcus & Mason, 1995; Petros et al, 2008). The conformation of the chiasmatic radial glia is changed during the chiasm development. How about the radial glia themselves? Little is known about where these chiasmatic radial glia develop into in later development.

In this part of study, using the EdU labeling technique, we try to birthdate chiasmatic radial glia first, then investigated the distribution of EdU labeled cells in the ventral diencephalon from E14 to E18, and try to trace their fates at later stages of development.

Materials and Methods

Animal

Time-mated pregnant pigmented C57 mice.

EdU injections

For birthdating the chiasmatic radial glia, we used the same methods, which were described in chapter 2.

For tracing their fates, we fixed the injection day at E11; then the pregnant mice were allowed to survive up to E14, E15, E16, E17 or E18.

Detecting EdU positive cells

In this part of study we only collected the frontal sections which contain the retinofugal pathway from the eyes to the proximal parts of the optic tract. The detailed procedure was already described in chapter 2.

Double staining of EdU together with radial glial cell marker in the frontal sections of the ventral diencephalon

The frontal sections containing the ventral diencephalon were blocked with 10% normal donkey serum in 0.1M PBS for 90 minutes to reduce the background signals, followed by incubation with RC2 antibody (mouse IgM, 1:5; DSHB, USA) overnight at 4°C. RC2 is a specific marker for the radial glial cells in the mouse diencephalon. After rinsing three times with 0.1M PBS, the frontal sections were incubated with secondary antibodies Cy3-conjugated donkey anti-mouse IgM (1:200, Jackson Laboratories) for 2 hours at room temperature. Finally, the sections were mounted on glass slides with mounting medium (Biomeda). Fluorescent signals on sections were imaged by the confocal microscope (FV300, Olympus Co, Japan). Control sections were prepared with the same procedures but with the absence of the primary antibody. No obvious staining was found in any of these control preparations.

Cell counting and statistical analyses

For birthdating the radial glia, we collected the E13 sections containing the double labeled cells at the level of the optic chiasm, where we can see clearly the RC2-positive palisade. We drew a square, 150μm away from each side of the midline, and 50μm in width, which includes the ventricular zone in the chiasmatic midline at E13. All the double labeled cells were counted in this region. The representative images of the counting samples were showed in Fig.8A-D.

For tracing the fates of chiasmatic radial glia, the double labeled cells were counted at the level of chiasm at different stages from E13 to E15. On the images at 40x magnification, we drew a region which includes the glial palisade in the ventricular zone of the midline, then counted the dual labeled cells in this region (Fig. 17A-D).

In this part of study, Kruskal-Wallis nonparametric ANOVA test of the InStat software (Grapph-Pad Inc., USA) was used to compare the cell number in different groups.

Double staining of chiasmatic radial glia with neural stem cell marker

To examine the characteristic of chiasmatic radial glia, a series of double staining experiment was performed in this study. Frontal sections containing the chiasm were collected in 0.1M PBS and washed with 0.1M PBS for three times. The slices were blocked with 10% normal donkey serum in 0.1M PBS for 90 min to reduce the background signals, and incubated with the primary antibodies against RC2 (1:10) and Nestin (1:1000, mouse IgG, Abcam, UK, cat. No. ab6142) overnight at 4℃. Nestin is a neural stem cell marker, widely used in the CNS (Jose & Krishnan, 2010; Pongpudpunth et al, 2010; Suzuki et al, 2010). After rinsing with 0.1M PBS, the sections were incubated in secondary antibodies at room temperature for 2 hours. The secondaries for RC2 and Nestin were Cyanine 3 (Cy3) conjugated donkey

anti-mouse IgM (1:200) and AF488 conjugated donkey anti-mouse IgG (1:200), respectively. After washing for three times with 0.1M PBS, the sections were mounted on glass slides and took imaged by the confocal microscope.

Double staining of chiasmatic radial glia with cell apoptosis marker

To inveatigate whether there is extensive cell death in the chiasmatic radial glia, they were double stained with caspase 3， the method was similar as described above. Here we used the primary antibodies against RC2 (1:10) and caspase 3 (1:1000, Rabbit IgG, R&D, Cat. No. AF835). The secondaries for RC2 and caspase 3 were Cyanine 3 (Cy3) conjugated donkey anti-mouse IgM (1:200) and AF488 conjugated donkey anti-rabbit IgG (1:200), respectively.

Results

Double- label EdU positive cells with RC2, while EdU was injected at different embryonic stages

In the previous chapter, we birthdated chiasmatic neurons using the double stiaining analyses in horizontal sections of mouse embryo. In this chapter, in order to birthdate the chiasmatic radial glia, EdU positive cells were double labeled with RC2 antibody in frontal sections of E13 ventral diencephalon, while EdU was injected at different embryonic stages.

1) Very few double labeled cells were detected, when EdU was injected at E9.5

When EdU was injected at E9.5 (n=9), only a few EdU positive cells were detected at the dorsal part of the E13 ventral diencephalon at the level of optic chiasm (Fig. 1 A1). The staining was largely at the ventral midline with only a couple of heavily labeled EdU positive cells observed in the ventricular layer, when examined at a higher magnification (Fig. 1 B1). Beside these heavily labeled EdU

positive cells (indicated by short solid arrows, Fig. 1 B1), some punctated staining was also observed in the cells nearby. After double staining with RC2, EdU positive cells were observed at the ventricular zone, where cell bodies of radial glia are located (Fig. 1A3, B3). When observed at 60x magnification using the oil lens, these radial glia cells were characterized by the cell body at the ventricular zone and processes extended from the ventricular to the pial surface (Fig. 2A-C). The long processes straddled the midline of the optic chiasm, and form the glia palisade. In the merged image, it was clear that at the ventricular zone the EdU staining was located at the nucleus of the cell body. There were also some colabeling cells outside the ventricular zone (indicated by open arrows, Fig. 2C), but these cells were not radial glia, as the radial glia have been shown to be located in the ventricular zone (Kriegstein & Alvarez-Buylla, 2009; Malatesta et al, 2008; Parnavelas & Nadarajah, 2001), and these small rounded cells outside the ventricular zone lack the radial glia morphology. So only the colabeled cells within the ventricular zone would be counted in the following cell counting analyses.

2) A few more double labeled cells were detected, when EdU was injected at E10

When EdU was injected at E10 (n=10), more EdU staining was observed around the ventral midline in E13 embryos in frontal sections of the chiasm (Fig. 3 A1, 3B1). Double labeling analyses showed that there was an obvious increase in double labeled cells observed in the ventricular zone when compared with that after E9.5 injection (indicated by square, Fig. 3 A3, B3).

3) EdU injection at E11

When EdU was injected at E11 (n=11), a lot of strongly labeled EdU positive cells were observed, not only in the chiasmatic midline but also in the other regions

of the E13 ventral diencephalon (Fig. 4 A1). At higher magnification, two different kinds of cell could be recognized at the ventral midline based on their morphology (Fig. 4 A2). One had the ovoid cell body located at the ventricular zone of the ventral diencephalon (indicated by short solid arrows); the other had a small rounded cell body located at the ventral half that includes axons in the optic chiasm (indicated by open arrows). After doing the double staining, many colabeled cells were found in the ventricular zone (indicated by square) at the chiasmatic midline (Fig. 4 A3, B3). If examined at 60x magnification, only the EdU positive cells with ovoid cell body located within the ventricular zone were colocalized in RC2 positive radial glia, the small rounded EdU positive cells, which were located near the pial surface, did not show obvious colocalization (Fig. 5A-D).

4) EdU injection at E12

When EdU was injected at E12 (n=8), a large number of strongly labeled EdU positive cells were detected in the ventral diencephalon at E13 (Fig. 6 A1). Similar to the E11 injection, EdU labeled cells in the ventral midline can be divided into two groups, the glia-like group and the neuron-like group (Fig. 6 B1). The double labeling analyses showed that within the ventricular zone, many colabeled cells were detected (Fig. 6 A3, B3). When looked at the 60x magnification, EdU staining was detected in the glia nucleus (Fig. 7A-D).

Many chiasmatic radial glia cells were generated from E11 to E12

Cell counting analyses were performed in this study after doing the double labeling. In this experiment, we set a counting region, 150μm away from each side to the midline, and 50μm in width, which contained the ventricular zone in the chiasmatic midline at E13. Then the frontal images from embryos of different injection day at the level of the optic chiasm were selected for the counting analyses.

We put the counting region on each selected image, and counted all colabeled cells in the region. The counting sample and region were showed in Fig. 8 A-D.

Cell counting results indicated that chiasmatic radial glia cells were generated from E9.5, and the number was significantly increased from E11. There was no significant difference between the number of the newly generated chiasmatic radial glia in E11 and E12 (Fig. 8 E).

Comparison of the distribution of EdU positive cells when EdU was injected at E11 or E12

Here, we tried to investigate which embryonic stage was the birthdate of the major chiasmatic radial glia by comparing the distribution of EdU positive cells in the ventral diencephalon at E13, when EdU was injected at E11 or E12.

The distribution of EdU labeling was very wide-spread in the diencephalon at E13, when EdU was injected at E11. In the double labeled images, except of the ventral midline, the ventricular zone in other parts of the diencephalon around the third ventricle was devoid of EdU labeling. There also were two less labeled regions, which were close to the radial glia palisade at each side (indicated by the asterisks, Fig. 9 A, B).

When EdU was injected at E12, the distribution of EdU positive cells was quite different from that of E11 injection. All the EdU positive cells were gathered to the ventral region of the third ventricle (Fig. 9 C, D). It was similar to that distribution of EdU labeling, when injection and sacrifice on the same day.

For these radial glia which were born at E11, they have two day interval between the injection and sacrifice, when we detected the EdU positive cells at E13, many of them migrated away from the ventricular zone, only those radial glia in the chiasmatic midline domain were still localized in the ventricular zone. For these E12

generated radial glia, they only have one day interval between the injection and sacrifice, and we found all the EdU positive cells still localized near the third ventricle. But it is still difficult to identify at which stage (E11 or E12) had more chiasmatic radial glia cells generated.

It seems like that the E11 generated radial glia make a decision, some of them remain in the chiasmatic midline domain till E13, when the significant numbers of retinal axons have crossed the midline and form the chiasm. So E11 born chiasmatic radial glia cells may play an important role in guiding RGC axons growth in E13 optic pathway.

The distribution of EdU labeled cells at the chiasmatic midline from E14 to E18, when EdU was injected at E11

As we have already found that a number of chiasmatic radial glia cells are born at E11 and these radial glia may play an important role in guiding RGC axons growth in E13 optic pathway, we asked what cell types these early born radial glia will derive to at later stages of prenatal development.

1) The distribution of EdU positive cells at the chiasmatic midline at E14

In frontal sections of the E14 mouse diencephalon, EdU positive cells were concentrated around the midline in the ventricular layer above the optic chiasm (Fig. 10A1), when EdU was injected at E11 (n=10). These EdU positive signals were located in the radial glia palisade, which were revealed by the RC2 antibody (Fig. 10B1). Similar to that at E13, two groups of EdU labeled cells were recognized in the midline region close to the optic chiasm, when observed at higher magnification. The ovoid cells were located at ventricular layer around the third ventricle(indicated by short solid arrows, Fig. 10A2), while the small rounded cell were located at the subventricular layer immediately above the optic chiasm (indicated by open arrows,

Fig. 10A2). Only the ovoid EdU positive cells were colabeled with the radial glia marker at the ventricular zone (Fig. 10B2). The morphology of EdU positive cells and RC2 radial glia were revealed clearly under a 60x objection. EdU had strict nuclear localizationin the radial glia cell body (indicated by open arrows, Fig. 11C, D). Wherease the small rounded cells, which lacking the radial glia morphology, were not overlapped with radial glia marker (indicated by solid arrows, Fig. 11).

2) The distribution of EdU positive cells at the chiasmatic midline at E15

When EdU was injected at E11 (n=14), there were fewer EdU positive staining detected in the ventral midline at E15 than that at E14 (Fig. 12A). These EdU labeled cells were still located in the radial glia palisade (Fig. 12B1, B2). At higher magnification, only the EdU positive cells located in the ventricular zone were colabeled with the RC2 antibody (indicated by solid arrows, Fig. 12B3). When observed under 60x magnification, a few strongly labeled cells were detected in the ventricular zone, and these cells were colabeled with radial glia (indicated by open arrows, Fig. 13). A lot of punctated, dotted EdU signals were observed in the nucleus of RC2 radial glia (indicated by solid arrows, Fig. 13). These lightly labeled cells were not included in the following cell counting analyses.

3) The distribution of EdU positive cells at the chiasmatic midline at E16

When EdU was injected at E11 (n=11), only a few EdU positive cells were detected in the chiasm at E16, whereas a lot of EdU labeled cells were detected in other regions of the diencephalon (Fig. 14A1). These EdU labeled cells at the chiasmatic midline were located in the area of the radial glia palisade, as shown in the merged images (Fig.14B1, B2). At higher magnification, these labeled cells with the rounded cell body were located largely in a globular structure, so called, "glial knot", at the ventral midline (indicated by asterisk, Fig. 14B3).

4) The distribution of EdU positive cells at the chiasmatic midline at E17 and E18

The distribution of EdU positive cells at E17 (n=10) and E18 (n=12) was similar to that at E16, but with fewer positive cells at the chiasmatic midline (Fig. 15 and 16). During these two stages of chiasm formation , the glia palisade became more restricted to the midline domain of the optic chiasm. In the merged images, only a few EdU labeled cells were observed in the ventricular zone at E17 and E18. Almost all labeled cells at the chiasmatic midline were located at the "glial knot" (Fig. 15B3, 16B3).

The chiasmatic radial glia generated at E11 were reduced from E13 to E15 and finally disappeared

Cell counting analyses were performed in this part of study after investigating the distribution of E11 born chiasmatic radial glia at E13 to E18. The EdU and RC2 dual labeled cells were counted on the sections which contain optic chiasm at different embryonic stages from E13 to E16. On the images at 40x magnification, we drew a region which includes the glial palisade in the ventricular zone of the midline, then counted the dual labeled cells in this region (Fig. 17A-D). Similar to the birthdating analyses, we only counted the strongly labeled cells. The light and dotted EdU staining was not included into the cell counting.

Hence, it was found that the number of E11 born chiasmatic radial glia was decreased from E14 and was significant reduced at E15 ($P<0.01$). From E16, these radial glia were almost undetectable in most preparations.

Identification of chiasmatic neurons with neural stem cell marker

At E13 (n=4), immunostaining with Nestin, a marker for neural stem cells, revealed cells with a radial morphology which has long processes extending from the

third ventricle to the pial surface. These Nestin labeled cells were located all over the diencephalon in the frontal sections (Fig. 18A). This pattern was very similar to that of RC2-positive radial glia (Fig. 18B). All the radially oriented Nestin-positive cells were overlapped with the RC2-positive radial glia cells, when observed in the merged image (Fig. 18C).

At E15 (n=3), the distribution of Nestin-positive cells was the same as that at E13, just the localization of optic chiasm was more obvious. The RC2-positive radial glia revealed the same pattern as these neural stem cells. All the radially oriented Nestin-positive cells were colabeled with the radial glial cells (revealed in yellow color, Fig. 19).

No apoptosis cells were observed in the region of the radial glia palisade at E15

At E15 (n=3), only a couple of apoptotic cells immunoreactive to caspase 3 antibody were observed in ventral diencephalon in the frontal sections (Fig. 20A). When examined in the merged image at higher magnification, these apoptotic cells were not located in the radial glia palisade, suggesting that there was no extensive cell death in the ventral diencephalon at E15.

Discussion

In this part of study, first we used EdU birthdating technique to investigate when the E13 chiasmatic radial glia cells were generated. The results of dual-labeling and cell counting analyses showed that the chiasmatic radial glia started to arise from E9.5. However, majority of these radial glia cells was generated during E11 to E12. Compared with the birthdate of chiasmatic neurons, these radial glia in the optic chiasm were born later. These findings suggest that in the developing chiasm, chiasmatic neurons are first arisen from the ventricular zone, and migrate to regions

posterior to the future chiasm (Knabe et al, 2008). In contrast, the chiasmatic radial glia are generated later, and span the chiasmatic midline. Both of these cells are get ready at the future optic chiasm to provide the guidance information to the first arrived RGC axons. There, chiasmatic neurons form a boundary for the early retinal axon growth; the radial glia form a glia palisade given different guidance cues to ipsi- or contralateral projection (Petros et al, 2009).

Second we tried to trace the fates of the chiasmatic radial glial cells at E13, which were birthdated at E11. We fixed the EdU injection day at E11, and investigated the distribution of EdU and RC2 colabeled cells in the ventral diencephalon from E14 to E18. From the observations, we found that these radial glial cells, which were born at E11, became fewer and fewer during the development of optic chiasm and finally disappeared from the chiasmatic midline. What are the reasons causing the reduction of these early born chiasmatic radial glia? In this study, we analyzed the characteristic of these radial glial cells and detected if some of them were dead during the development.

The birthdating schedule of chiasmatic radial glia

In the previous study, we have already shown that chiasmatic neurons are the first differentiated cells in the ventral diencephalon, and are generated principally around E9.5. The birthdating schedule of chiasmatic radial glia is quite different from that of chiasmatic neurons. Although these radial glia cells also start to arise from E9.5, only a couple of cells can be detected at E13. The large number of radial glia cells at the E13 chiasm is born from E11. For the chiasmatic neurons only a few of them are born in E11. As these two group of cells are together to provide guidance cues to early retinal axons, they should be generated prior to the first axon arrival (Guillery et al, 1995; Mason & Sretavan, 1997). The radial glia arise from the

neuroepithelial cells do not need to migrate, still remain in the ventricular zone, just change their morphology (Kriegstein & Alvarez-Buylla, 2009; Tramontin et al, 2003). However, the chiasmatic neurons, which also arise in the ventricular zone, need to migrate to the future chiasm and form the V-shaped array. It may need more time. This may partly explain the reason why the two kinds of chiasm cells have different birthdating schedule.

The birthdate of the major chiasmatic radial glia in E13

In this experiment, we also try to identify when the major chiasmatic radial glia are generated. As many radial glia cells in the chiasm are born on both E11 and E12, the distribution of the EdU positive cells was compared. It was found that when EdU was injected in E11, the expression of EdU was very wide spread. It is quite different from the localized distribution when EdU was injected at E12. The possibilities of the different distributions are as following: two days interval between the injection and sacrifice provides longer time for the cells incorporated EdU to migrate out after birthdate or diluting the EdU when they still keep dividing; one day interval may be too short to do these, so the EdU positive cells remain around the third ventricle. That would cause the overestimate in cell counting. So it is hard to identify at which stage more radial glia are born. As we know the first RGC axons grow into the optic stalk and reach the ventral diencephalon at E12 (Marcus & Mason, 1995). The earliest day of detecting RC2 positive radial gila in the ventral diencephalon is also at E12, but only a few positive cells are observed at the midline (Marcus & Mason, 1995; Williams et al, 2003). In addition, the E11 born radial glia seems make a decision, remaining some of them in the chiasmatic midline domain till E13. It may give us a hint that the chiasmatic radial glia which are generated at E11 may play an important role in guiding RGC axons growth in E13 optic pathway.

Chiasmatic radial glial cells born at E11 finally disappear at the ventral midline

When EdU was injected at E11, there are some EdU and RC2 colabeled cells concentrated in the ventral midline region at E14. This pattern is quite similar to that at E13. At E15, many dotted EdU staining is observed in the nucleus of the radial glia. Although these are colabeled cells, they are not included in the cell counting analyses. As the EdU has already been diluted upon cell divisions, these dual-labeled radial glia are probably not the radial glia observed at E13. From E16, all the dual-labeled radial glial cells disappear from the ventral midline. Only a few EdU labeled cells are located at the "glial knot" at the midline. Cell counting analyses also support these observations.

Where do these early born chiasmatic radial glia go? From the EdU staining pattern, it is possible that these E11 generated chiasmatic radial glia may undergo some developmental changes. Previous studies indicated that at the late embryonic stage, the midline radial glia, like radial glia in the other parts of the brain, start to differentiate into astrocytes, which are immunoreactive to glia fibrillary acidic protein (GFAP) antibody (Bovolenta et al, 1987; Mason & Sretavan, 1997). The radial glia in other parts of the brain have already been proved that they are a population of neural precursor cells (Kriegstein & Alvarez-Buylla, 2009; Malatesta et al, 2008). Radial glia can give rise to both neurons and glia and also serve as scaffold for the migration of new born neurons (Hartfuss et al, 2001; Malatesta et al, 2000; Miyata et al, 2001; Noctor et al, 2001). The radial glia never leave the cycle during development, they undergo interkinetic nuclear movements, dividing asymmetrically to generate mitotic radial glia and postmitotic neurons (Parnavelas & Nadarajah, 2001). In our study, we try to investigate if the chiasmatic radial glia also have this dividing capability.

Identification of chiasmatic radial glia with neural stem cell marker

In order to prove that the chiasmatic radial glia have the potential to differentiate into other cells, we double stain the chiasmatic radial glia with the neural stem cell marker at E13 and E15. The radial glia cells at the chiasmatic midline are colabeled with the Nestin-positive cells both at E13 and E15, suggesting that the chiasmatic radial glia share some characteristic of neural stem cells (Kriegstein & Alvarez-Buylla, 2009; Malatesta et al, 2008). It is very likely that the midline radial glia, like radial gila in other parts of the developing brain, keep dividing and give rise to other cell types. This may explain why the EdU labeled radial glia are reduced gradually at the midline, and EdU was diluted during the rapid division of the midline radial glia.

No apoptosis cells were observed in the region of the radial glia palisade at E15

We also investigated that if there are radial glial cell death during the chiasm development. We double label the RC2-positive radial glia with the apoptotic cell marker caspase 3 at E15. The results showed that there is no apoptotic cell observed in the radial gial palisade, supporting that the reduction in radial glia is not likely caused by an extensive cell death.

In summary, as the early born chiasmatic radial glia become fewer and fewer at the midline, many radial glia must be generated at later embryonic stages to replenish the glia population. The early born radial glia are likely changed into other cell types after finishing their retinal axon guidance mission at the midline.

Figures

Figure 1 Co-localization of EdU positive cells and chiasmatic radial glia in the ventral diencephalon at E13, when EdU was injected at E9.5. (A1) In the frontal section of the E13 ventral diencephalon, EdU positive staining was largely at the ventral midline, when EdU was injected at E9.5. B1 is the higher magnification of the white square region in A1. Beside two heavily labeled EdU positive cells (indicated by short solid arrows), the other staining revealed as spots, and couldn't be recognized as a cell. (A2 & B2) RC2 positive cells revealed as a palisade that straddle the midline of the optic chiasm (OC). (A3 & B3) In the merged image, the heavily labeled EdU positive cells were colocalized with RC2 radial glia.

Scale bar: A, 200μm; B, 100μm.

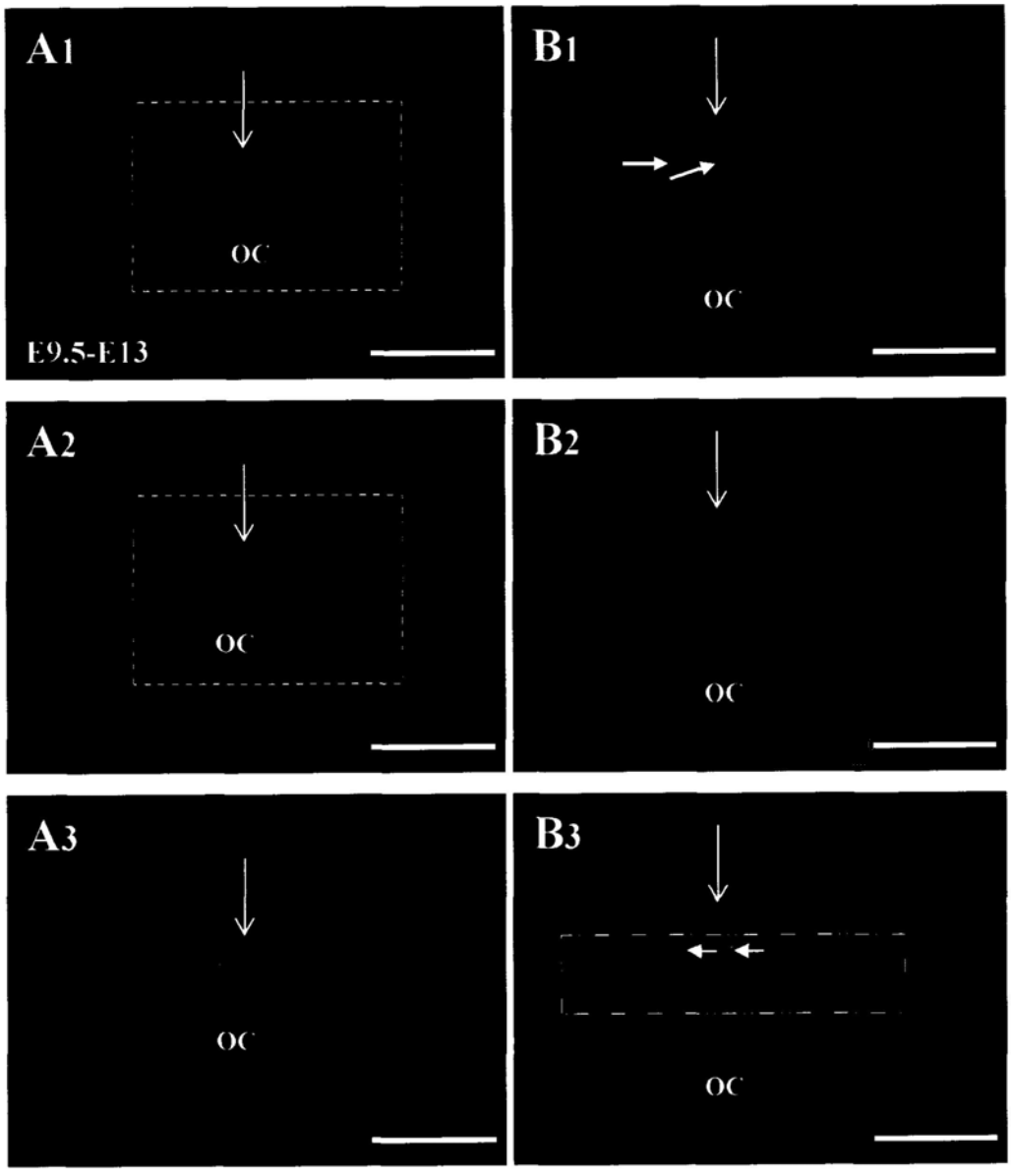
A1
OC
E9.5-E13
B1
OC
A2
OC
B2
OC
A3
OC
B3
OC

Figure 2 EdU positive staining was located in the nuclei of RC2 radial glia at E13, when EdU was injected at E9.5. The EdU and RC2 positive staining was even more clearly when observed at 60x using oil lens. C is the merged image of A and B. In this image, RC2 positive radial glia has the cell body located at the ventricular zone and processes extended from the ventricular to the pial surface. The long processes drape the midline of the optic chiasm, and form the glia palisade. In the ventricular zone (indicated by the square), the EdU positive staining was observed in the nucleus of the glia cell body (indicated by long solid arrow). There were some colabeling cells outside the ventricular zone (indicated by open arrow), but these cells were not radial glia, as the radial glia should be located in the ventricular zone (indicated by the square), and the small rounded cells outside (indicated by short solid arrows) lack the radial glia morphology. So only the colabeled cells within the ventricular zone would be counted in the cell counting analyses.

Scale bar: 50μm.

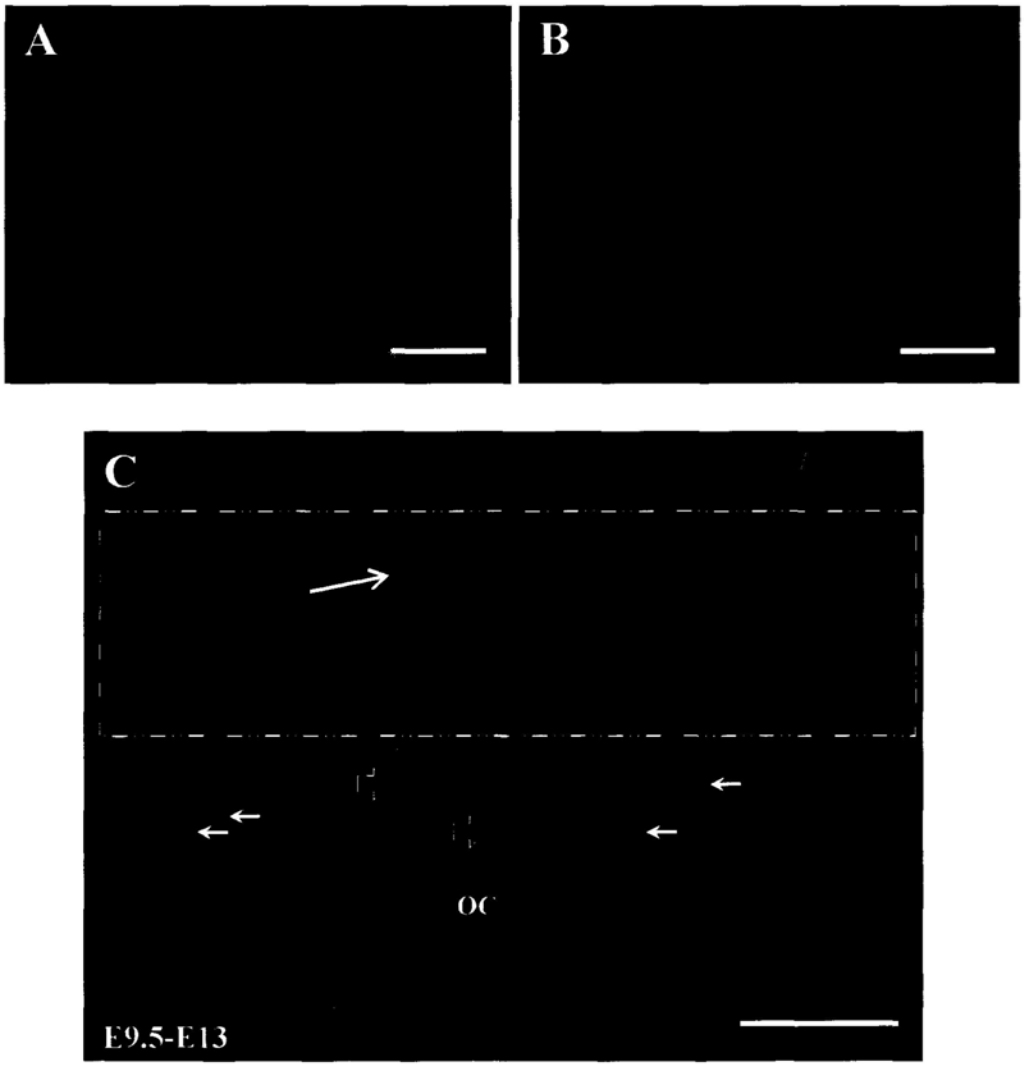
A
B
C
OC
E9.5-E13

Figure 3 Co-localization of EdU positive cells and chiasmatic radial glia in the ventral diencephalon at E13, when EdU was injected at E10. (A1) More EdU staining was observed around at the ventral midline in E13 embryos, when EdU was injected at E10. (B1) The higher power of the square region in A1 showed that there were more heavily labeled EdU positive cells detected when EdU was injected at E10. A2 & B2 showed the chiasmatic midline palisade of the RC2 radial glia. (A3 & B3) The merged images showed that more double labeled cells were observed in the ventricular zone.

Scale bar: A, 200μm; B, 100μm.

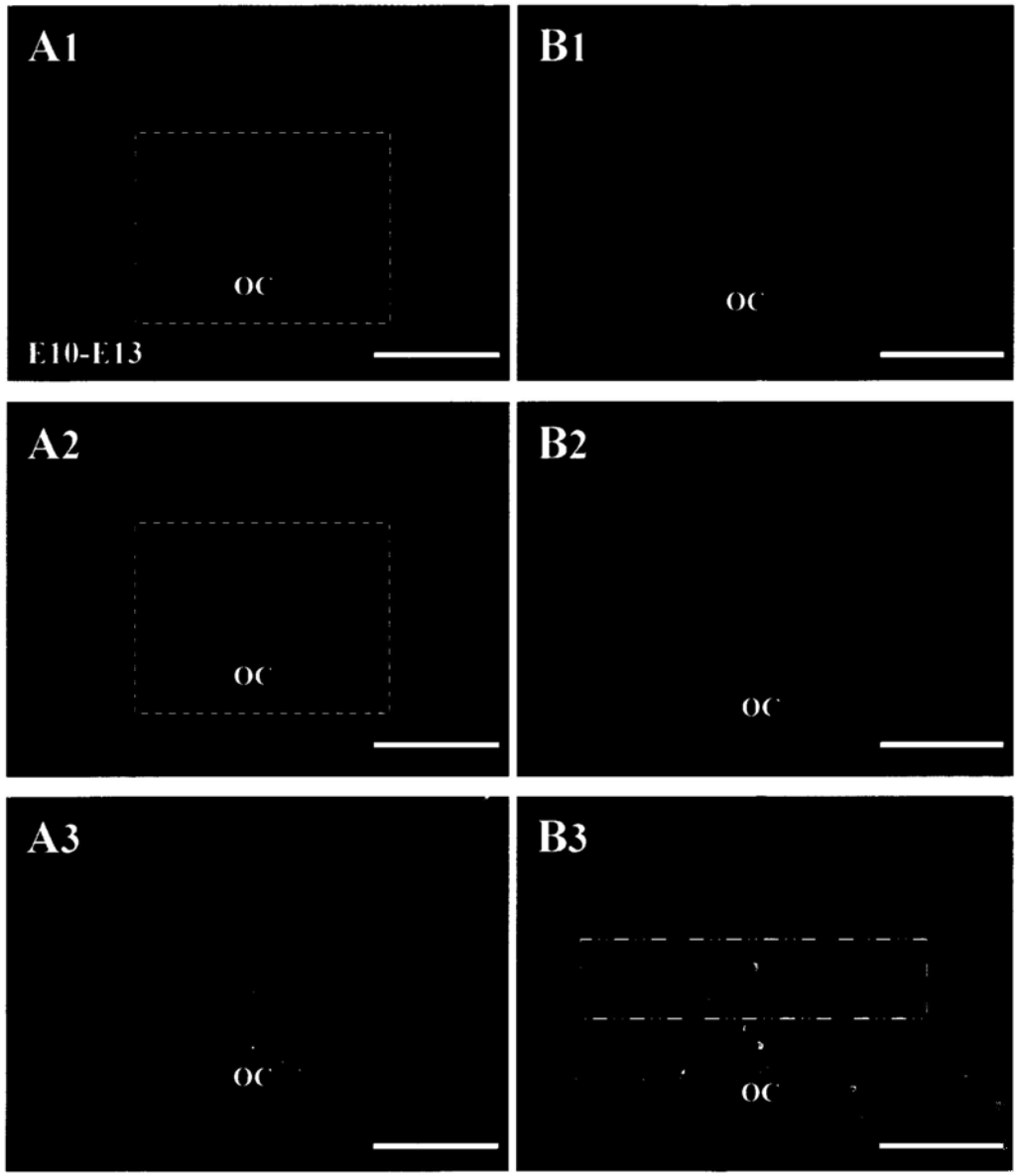
A1
OC
E10-E13
B1
OC
A2
OC
B2
OC
A3
OC
B3
OC

Figure 4 Co-localization of EdU positive cells and chiasmatic radial glia in the ventral diencephalon at E13, when EdU was injected at E11. (A1) A large number of EdU positive cells were detected in the ventral diencephalon at E13, when EdU was injected at E11. (B1) The higher power of the square region in A1 showed that many heavily labeled EdU positive cells were detected at the ventral midline. Based on the cell morphology, these EdU positive cells can be divided into two groups, one had the ovoid cell body located at the ventricular zone of the ventral diencephalon (indicated by short solid arrows), the other had the small rounded cell body located at the ventral half that include axons in the optic chiasm (indicated by open arrows). (A3 & B3) In the merged images, many colabeled cells were located in the ventricular zone (indicated by square) at the chiasmatic midline.

Scale bar: A, 200μm; B, 100μm.

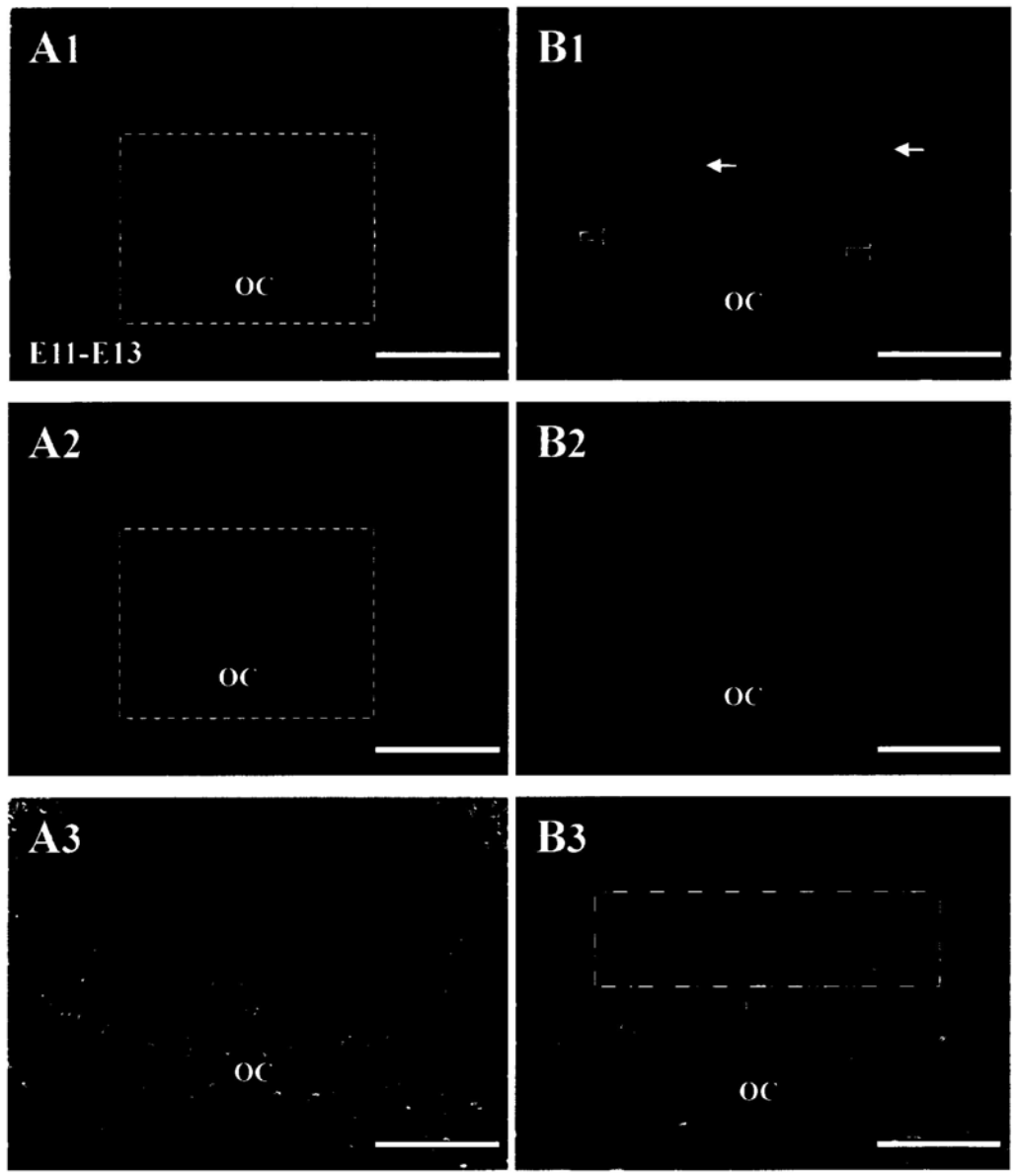
A1
OC
E11-E13
B1
OC
A2
OC
B2
OC
A3
OC
B3
OC

Figure 5 EdU positive staining was located in the nuclei of RC2 radial glia at E13, when EdU was injected at E11. The morphology of EdU positive cells and RC2 radial glia were revealed very clearly in 60x magnification images. C is the merged image of A and B. The EdU heavily labeled cells were colocalized with the RC2 radial glia in the ventricular zone, while the EdU positive cells outside the ventricular zone, which have small rounded cell body, were not RC2 positive. (D) In the two times zoomed image in the white square in C, EdU had strictly nuclear staining in the radial glia cell body.

Scale bar: 50μm.

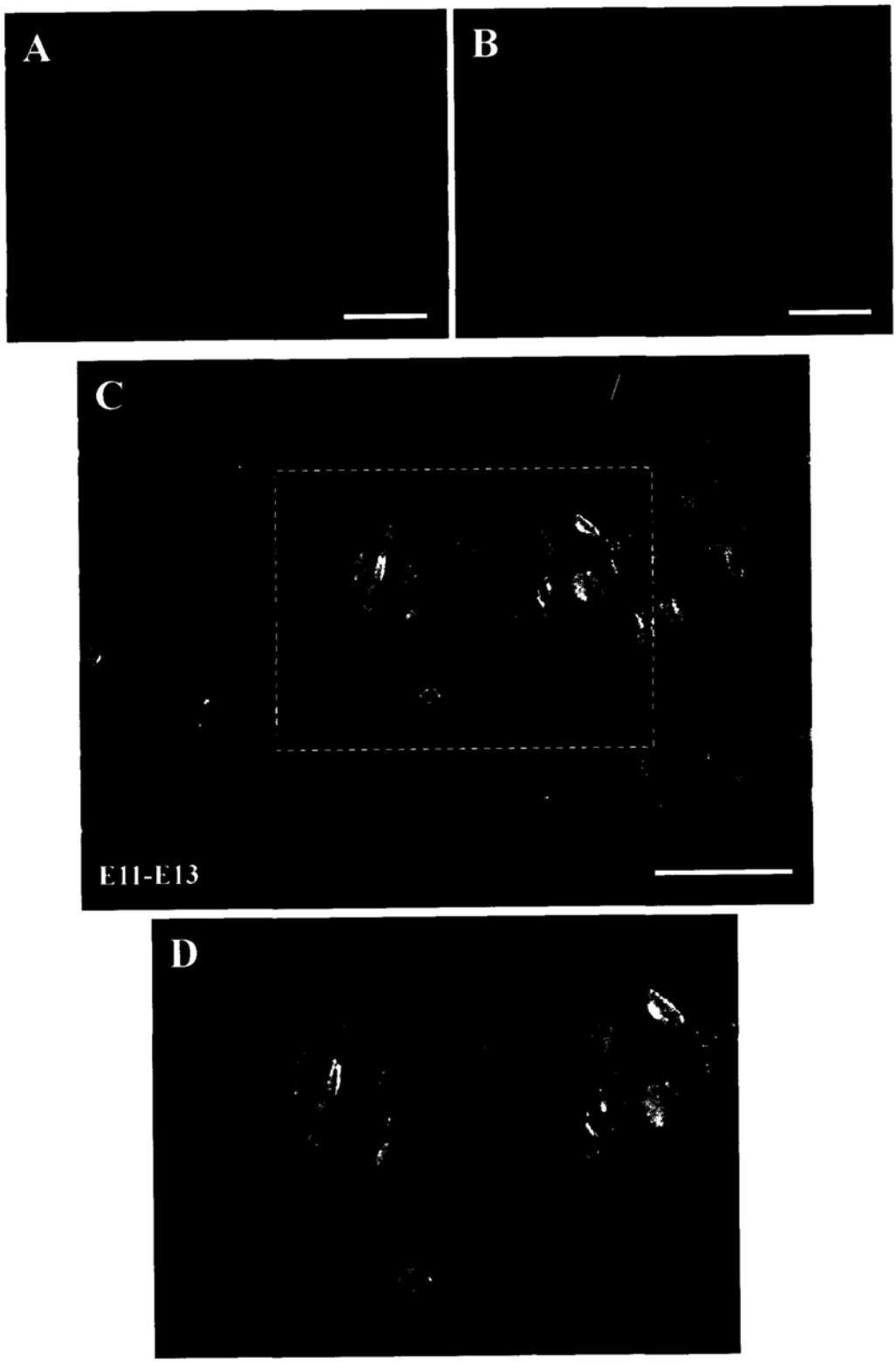
A
B
C
E11-E13
D

Figure 6 Co-localization of EdU positive cells and chiasmatic radial glia in the ventral diencephalon at E13, when EdU was injected at E12. (A1) There are many of EdU heavily labeled cells localized in the ventral diencephalon at E13, when EdU was injected at E12. (B1) At higher magnification, there were two kinds of EdU positive cells located in the ventral midline, the ovoid cells and the rounded cells, indicated by solid arrows and open arrows, respectively. (A3 & B3) In the merged images, many double labeled cells were observed in the region of ventricular zone (indicated by square).

Scale bar: A, 200μm; B, 100μm.

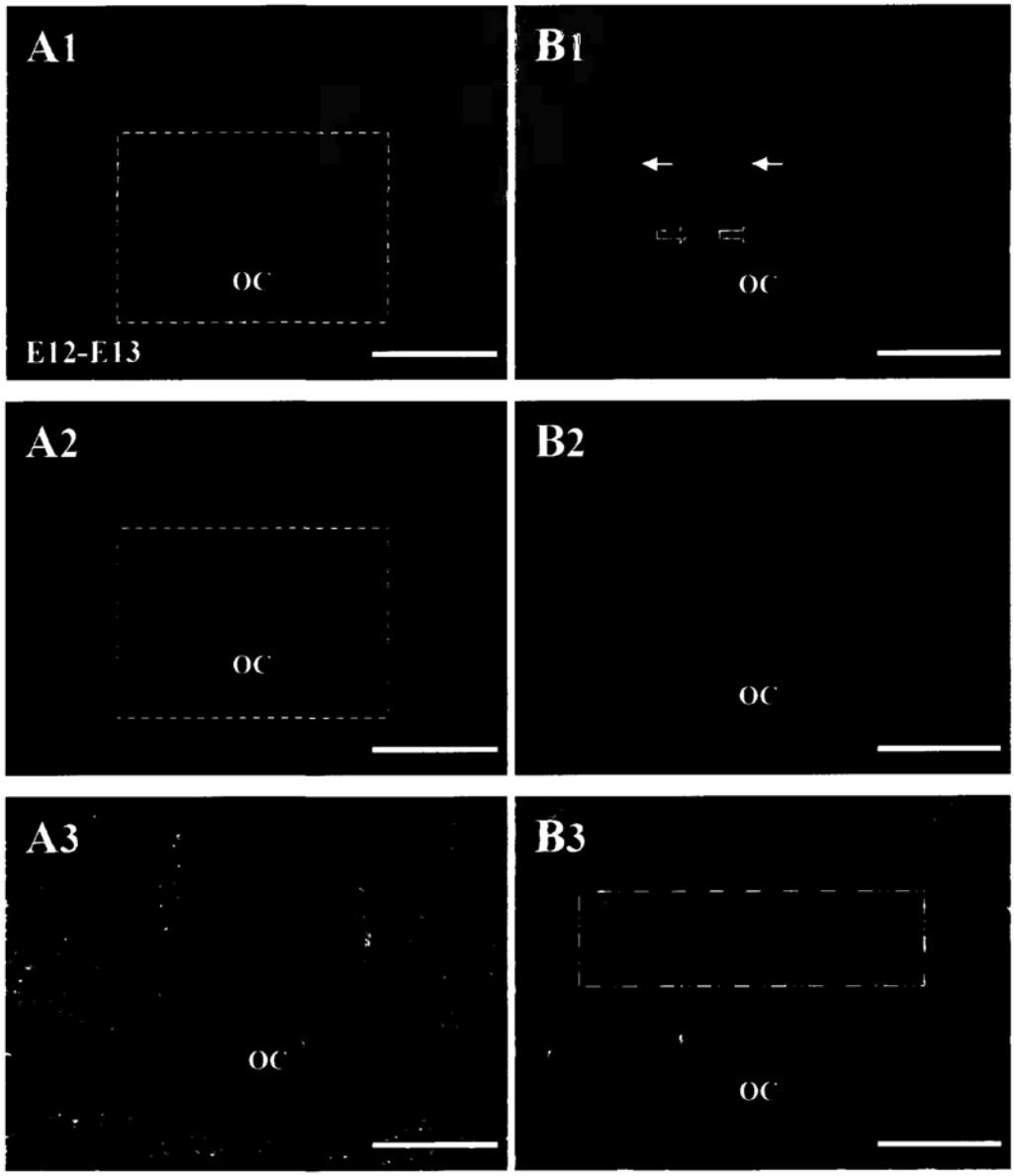
A1
OC
E12-E13
B1
OC
A2
OC
B2
OC
A3
OC
B3
OC

Figure 7 EdU positive staining was located in the nuclei of RC2 radial glia at E13, when EdU was injected at E12. C is the merged image of A and B, observed with oil lens at 60x magnification. D is the two times zoomed image in the white square in C. Here, EdU positive cells were colocalized with RC2 radial glia cells bodies, and EdU staining was detected in the glia nuclei.

Scale bar: 50μm.

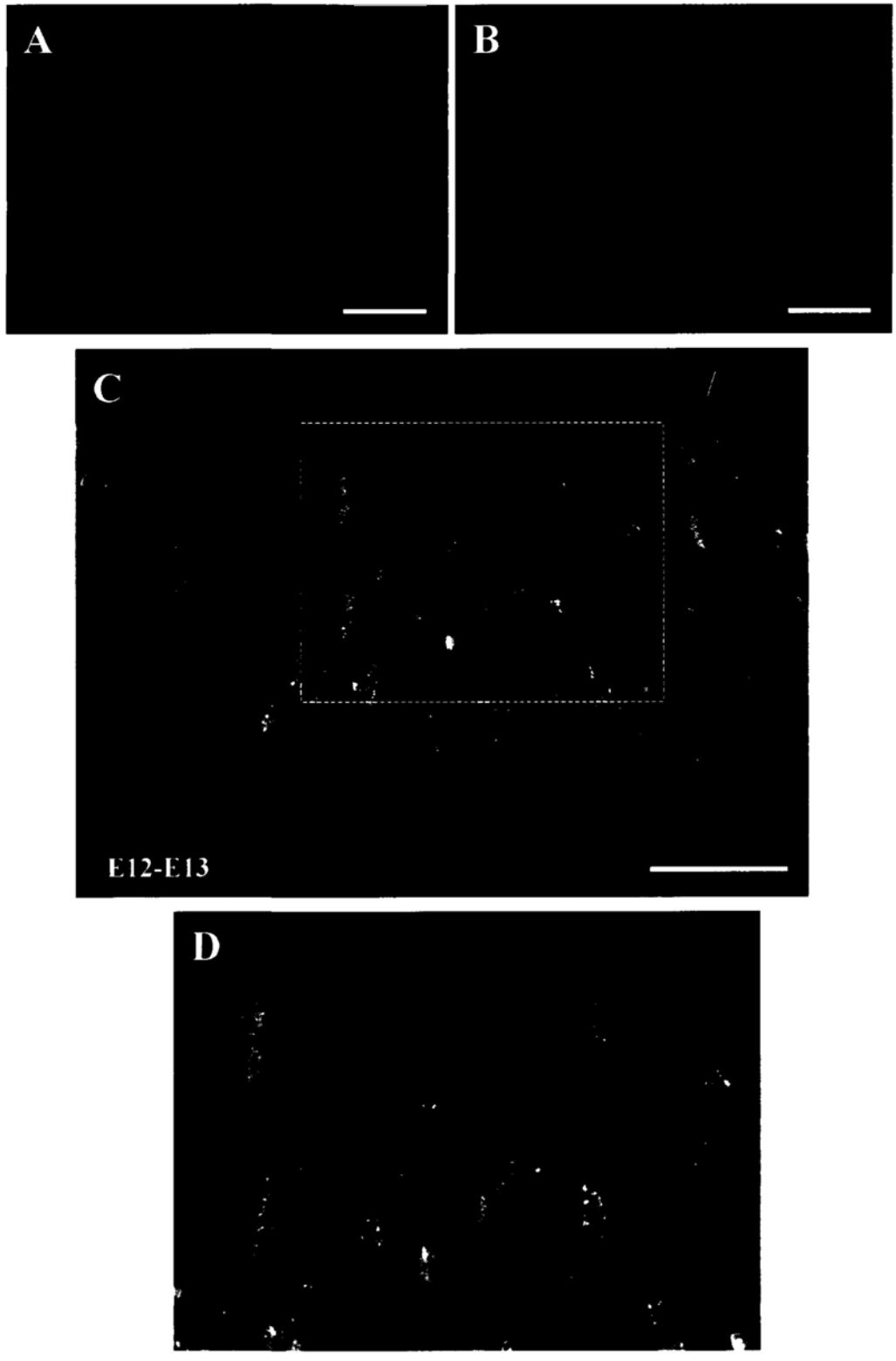
A
B
C
E12-E13
D

Figure 8 The result of cell counting analyses showing that many chiasmatic radial glia cells were generated from E11 to E12. (A-D) We drew a square, 150μm away from each side of the midline, and 50μm in height, which includes the ventricular zone in the chiasmatic midline. Then the square was put on the frontal section images which contain the optic chiasm, and all the double labeled cells were counted in this square of each embryo, which was injected EdU at different stage. (E) The plot was showed the cell counting results, when EdU was injected at different embryonic stages. Many double labeled cells were found on the E13 diencephalon, when EdU was injected at E11 and E12. There were fewer double labeled cells at the level of chiasm, when EdU was injected at E9.5 and E10. The number of double labeled cells was significantly increased at E11 and E12 injected mice compared with that after E9.5 injection.

Scale bar: 100μm.

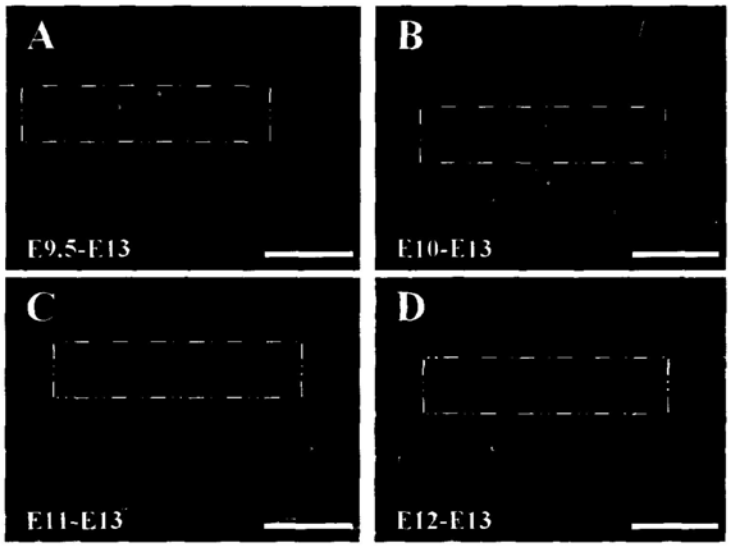
A
E9.5-E13
B
E10-E13
C
E11-E13
D
E12-E13

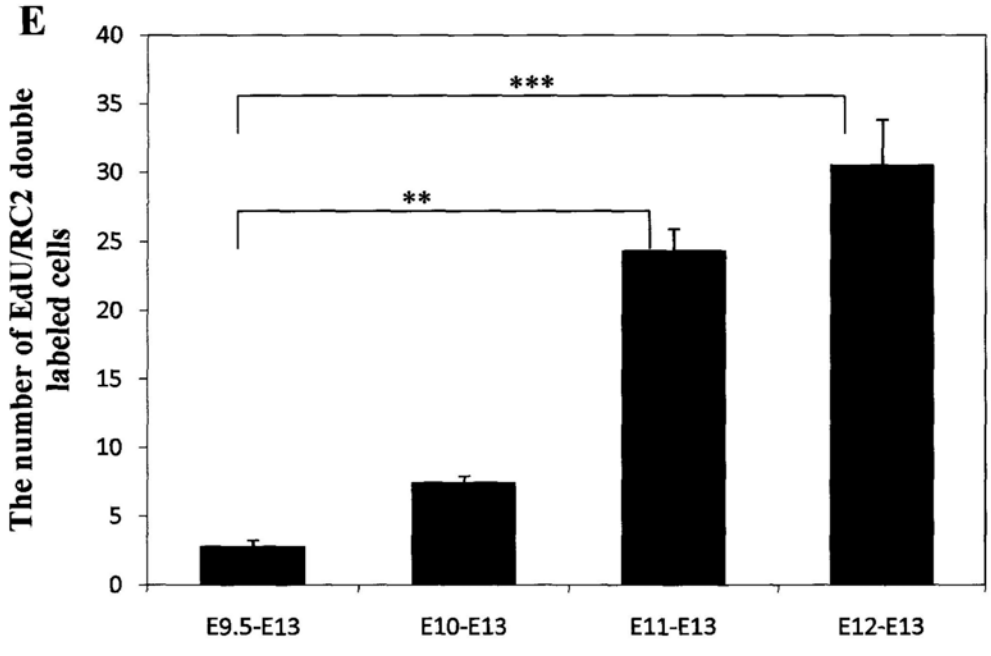
E
The number of EdU/RC2 double labeled cells
40
35
30
25
20
15
10
5
0
***
**
E9.5-E13
E10-E13
E11-E13
E12-E13

* * $p < 0.01$

* * * $p < 0.01$

Figure 9 Comparison of the distribution of EdU positive cells in the diencephalon at E13, when EdU was injected at E11 or E12. (A) The distribution of EdU labeling was wide spread in the diencephalon at E13, when EdU was injected at E11. (B) In the double labeled images, the EdU labeling was absent on the ventricular surface of third ventricle except of the ventral midline. There also were two less EdU labeled areas at each side of the diencephalon which were close to the radial glia palisade (indicated by the asterisks). (C & D) When EdU was injected at E12, all the EdU labeling was gathered to the ventral region of the third ventricle.

Scale bar: 200μm.

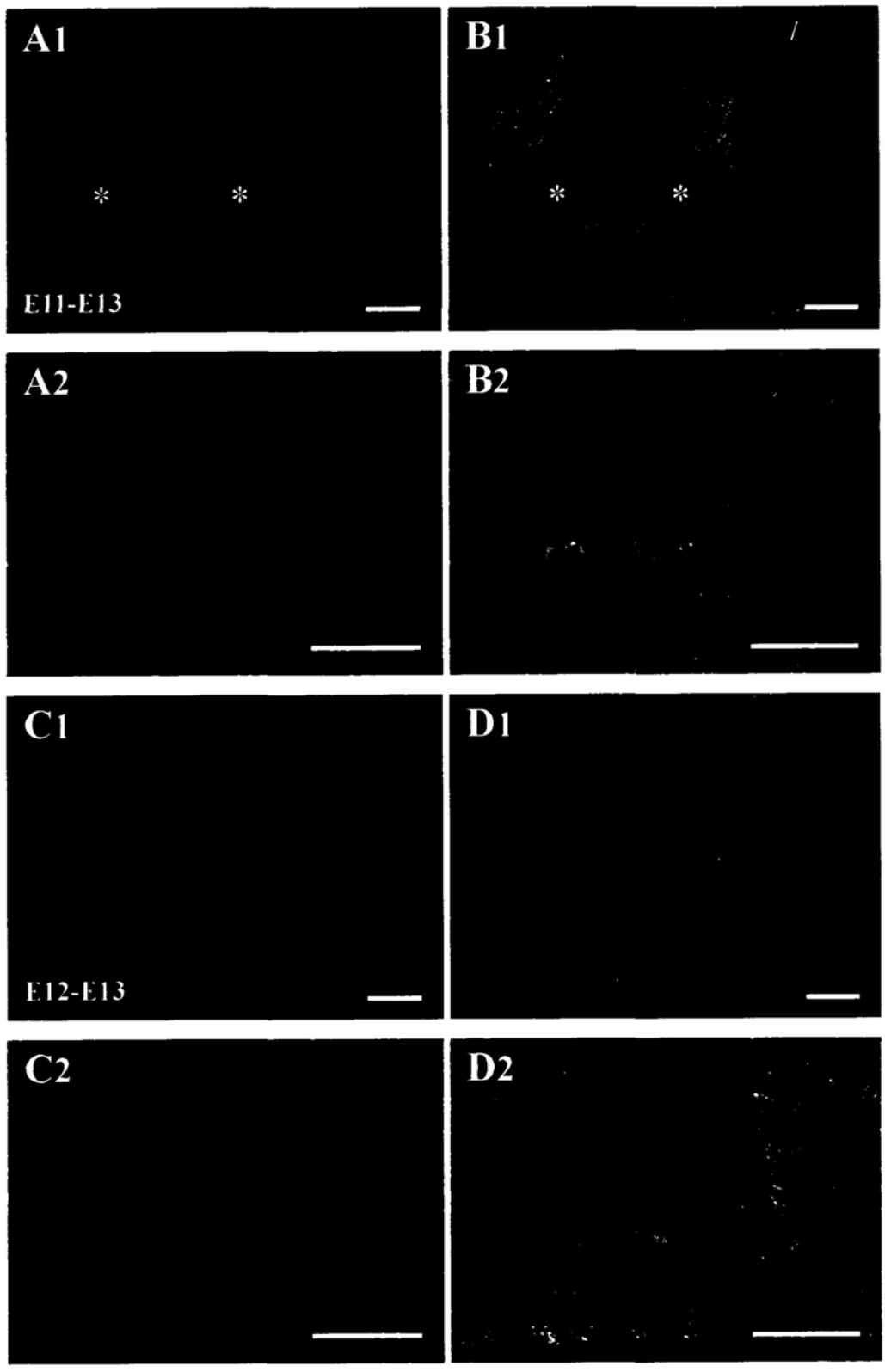
A1
B1
E11-E13
A2
B2
C1
D1
E12-E13
C2
D2

Figure 10 Co-localization of EdU positive cells and chiasmatic radial glia in the ventral diencephalon at E14, when EdU was injected at E11. All these figures are frontal sections, dorsal is to the top. (A1) In the frontal section of the ventral diencephalon, EdU positive cells were concentrated around the midline in the ventricular layer above the optic chiasm (indicated by asterisk). (B1) In the merged image, these EdU positive cells were located in the area of RC2-glia palisade (indicated by square). (A2) At higher magnification, two groups of EdU labeled cells were recognized in the ventral diencephalon based on the cell morphology. One had the ovoid cell body located at the ventricular layer around the third ventricle (indicated by short solid arrows), the other had the small rounded cell body located at the subventricular layer immediately above the optic chiasm (indicated by open arrows). (B2) In the merged image, some colabeled cells were observed in the ventricular zone (indicated by square) at glia palisade.

Scale bar: A1, B1, 200μm; A2, B2, 100μm.

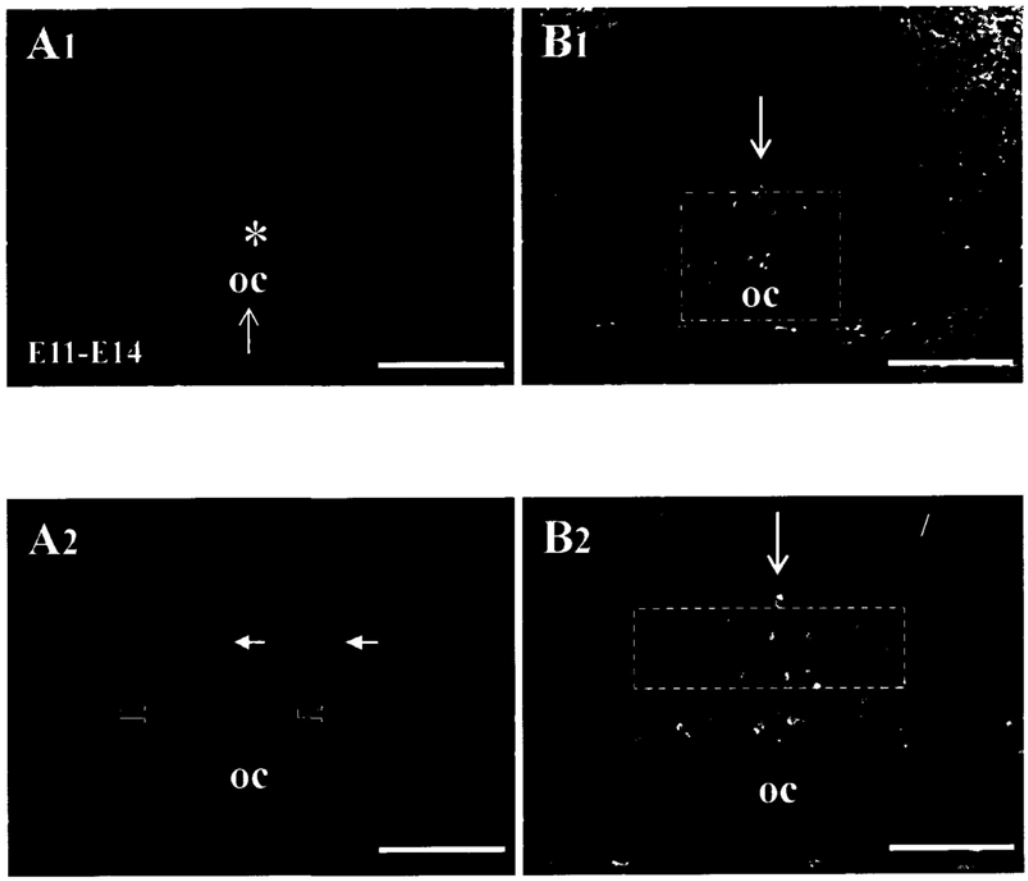
A1
oc
E11-E14
B1
oc
A2
oc
B2
oc

Figure 11 EdU positive staining was located in the nucleus of RC2 radial glia at E14, when EdU was injected at E11. The morphology of EdU positive cells and RC2 radial glia were revealed clear under 60x objection. C is the merged image of A and B. The EdU heavily labeled cells were colocalized with the RC2 radial glia in the ventricular zone (indicated by square). The small rounded cells were lacking the radial glia morpholory. (D) In the two times zoomed image, EdU had strict nuclear localization in the radial glia cell body.

Scale bar: 50μm.

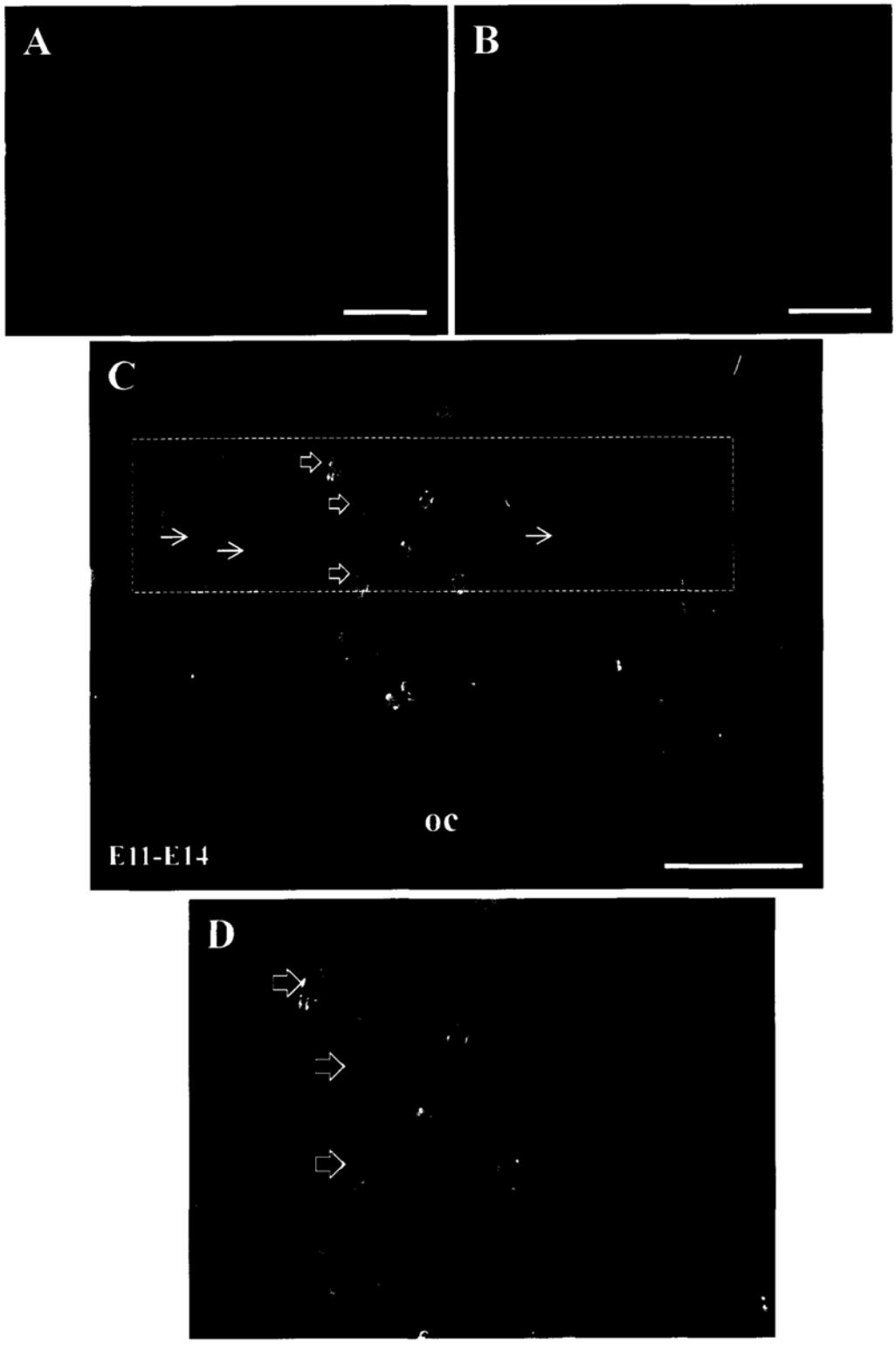
A
B
C
oc
E11-E14
D

Figure 12 Co-localization of EdU positive cells and chiasmatic radial glia in the ventral diencephalon at E15, when EdU was injected at E11. (A1 & A2) When EdU was injected at E11, there were fewer EdU positive staining observed in the ventral midline at E15 than that at E14. (B1& B2) These EdU labeled cells were still located in the radial glia palisade. (A3 &B3) At higher magnification, the EdU positive cells located in the ventricular zone were colabeled with the RC2 radial glia (indicated by solid arrows).

Scale bar: A1, A2, B1, B2, 200μm; A3, B3, 100μm.

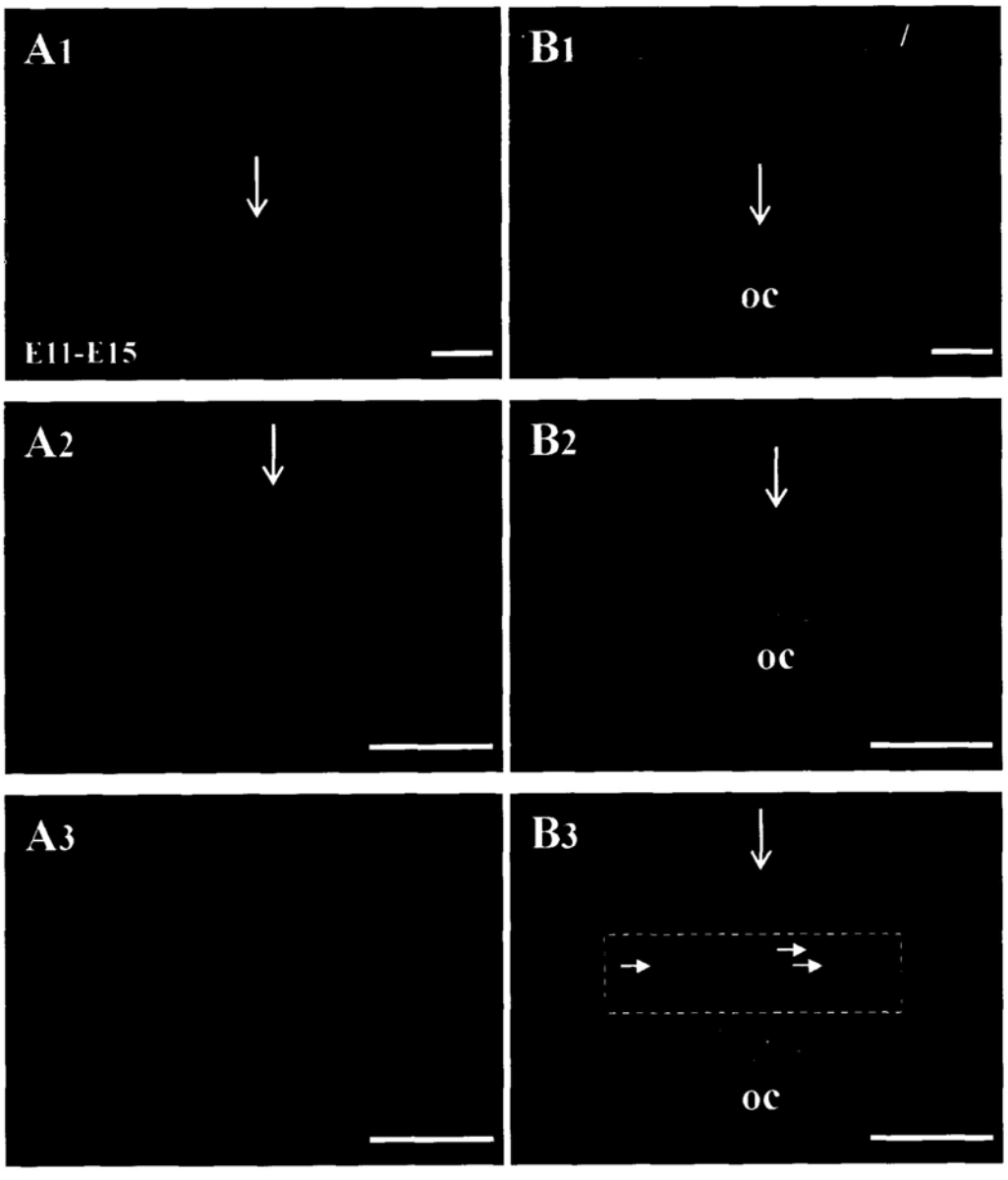
A1
E11-E15
B1
oc
A2
B2
oc
A3
B3
oc

Figure 13 Many dotted EdU signals were observed in the nucleus of RC2 radial glia at E15. C is the merged image of A and B, observed with oil lens under 60x magnification. Only a few strongly labeled cells were detected in the ventricular zone, and these cells were colabeled with radial glia (indicated by open arrows). A lot of punctated, dotted EdU signals were observed in the nucleus of RC2 radial glia (indicated by solid arrows). These lightly labeled cells were not included in the following cell counting analyses.

Scale bar: 50μm.

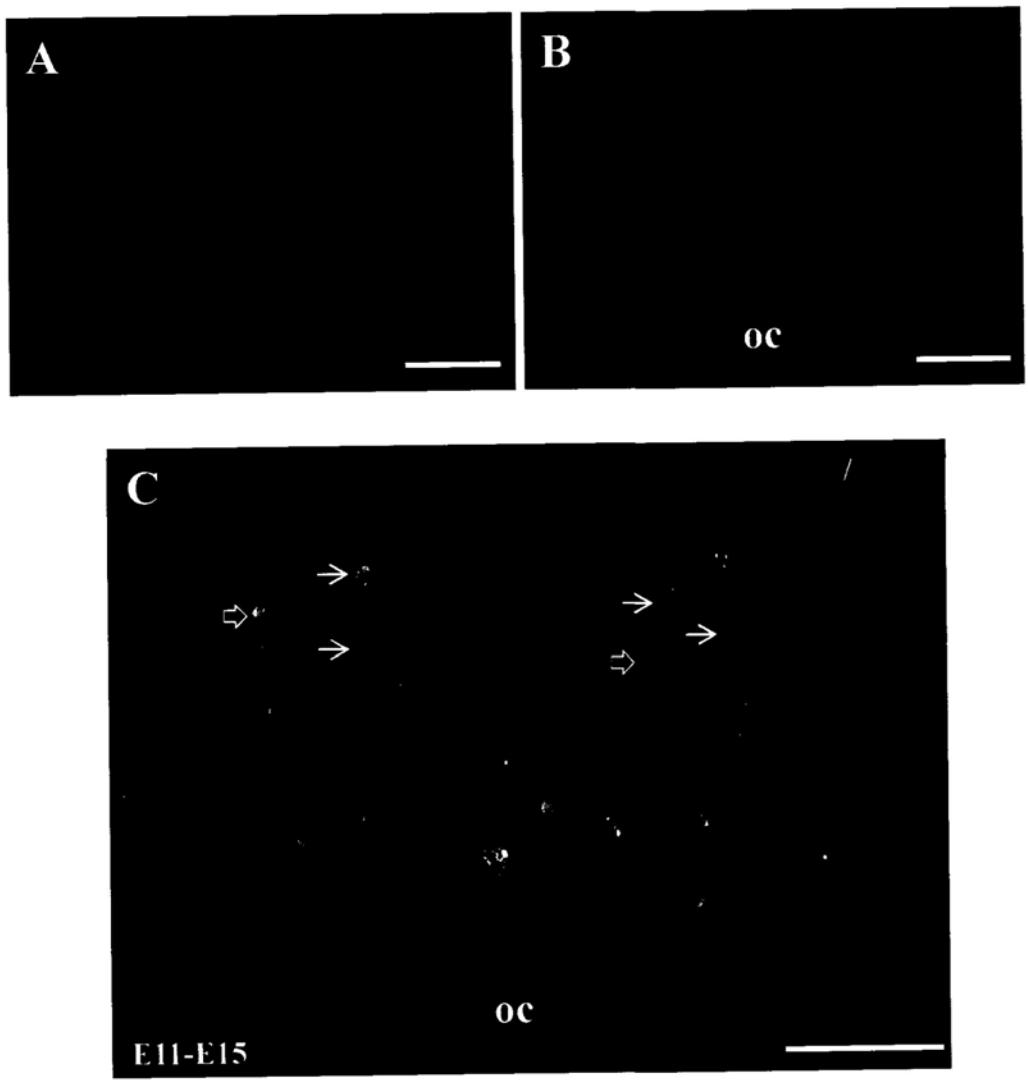
A
B
oc
C
oc
E11-E15

Figure 14 Co-localization of EdU positive cells and chiasmatic radial glia in the ventral diencephalon at E16, when EdU was injected at E11. (A1 and A2) When EdU was injected at E11, only a few EdU positive cell were observed in the chiasm at E16, whereas a lot of EdU labeled cells were detected in other regions of the diencephalon. (B1 and B2) In the merged image, the EdU labeled cells at the chiasmatic midline were located in the area of the radial glia palisade. (A3 and B3) At higher magnification, these EdU labeled cell at the ventral midline were not RC2 positive. These cells with the rounded cell body were located in the "glial knot" (indicated by asterisk).

Scale bar: A1, A2, B1, B2, 200μm; A3, B3, 100μm.

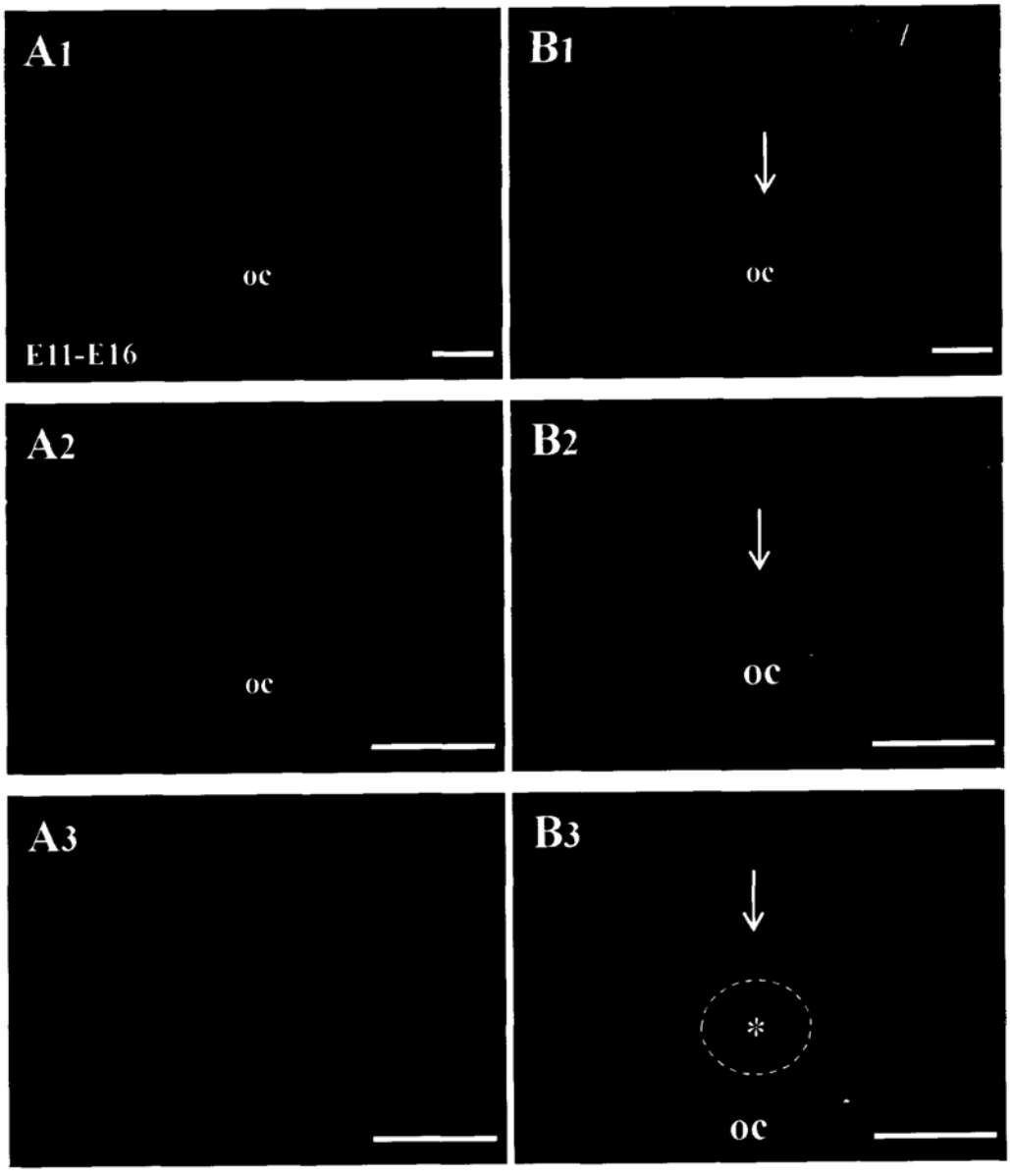
A1
oc
E11-E16
B1
oc
A2
oc
B2
oc
A3
B3
*
oc

Figure 15 Co-localization of EdU positive cells and chiasmatic radial glia in the ventral diencephalon at E17, when EdU was injected at E11. (A1 and A2) The distribution of EdU positive cells was similar to that at E16, but wirh fewer positive cells at the chiasmatic midline. (B1 and B2) The glia palisade became more restricted. In the merged images, at the posterior part of chiasm, only a few the EdU labeled cells were not observed in the ventricular zone. (A3 and B3) At higher magnification, almost all the EdU labeled cells at the chiasmatic midline were located at the "glial knot" (indicated by asterisk).

Scale bar: A1, A2, B1, B2, 200μm; A3, B3, 100μm.

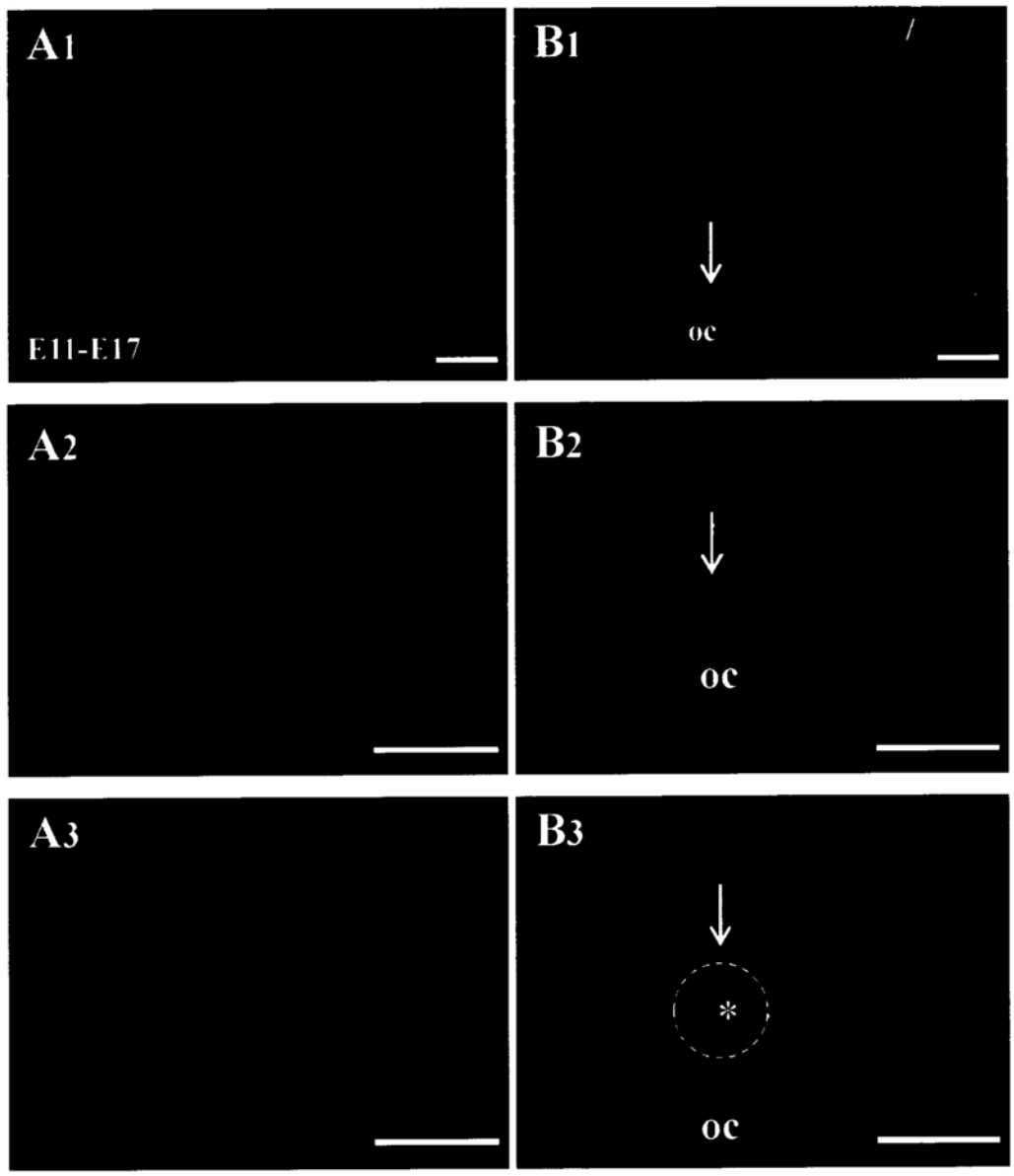
A1
E11-E17
B1
oc
A2
B2
oc
A3
B3
*
oc

Figure 16 Co-localization of EdU positive cells and chiasmatic radial glia in the ventral diencephalon at E18, when EdU was injected at E11. (A1, A2, B1 and B2) The distribution of EdU positive staining and RC2 radial glia was similar to that at E16 and E17, but almost no EdU positive staining were detected at the chiasmatic midline. (A3 and B3) I n the higher power, only a couple of cells were observed in the "glial knot" (indicated by asterisk).

Scale bar: A1, A2, B1, B2, 200μm; A3, B3, 100μm.

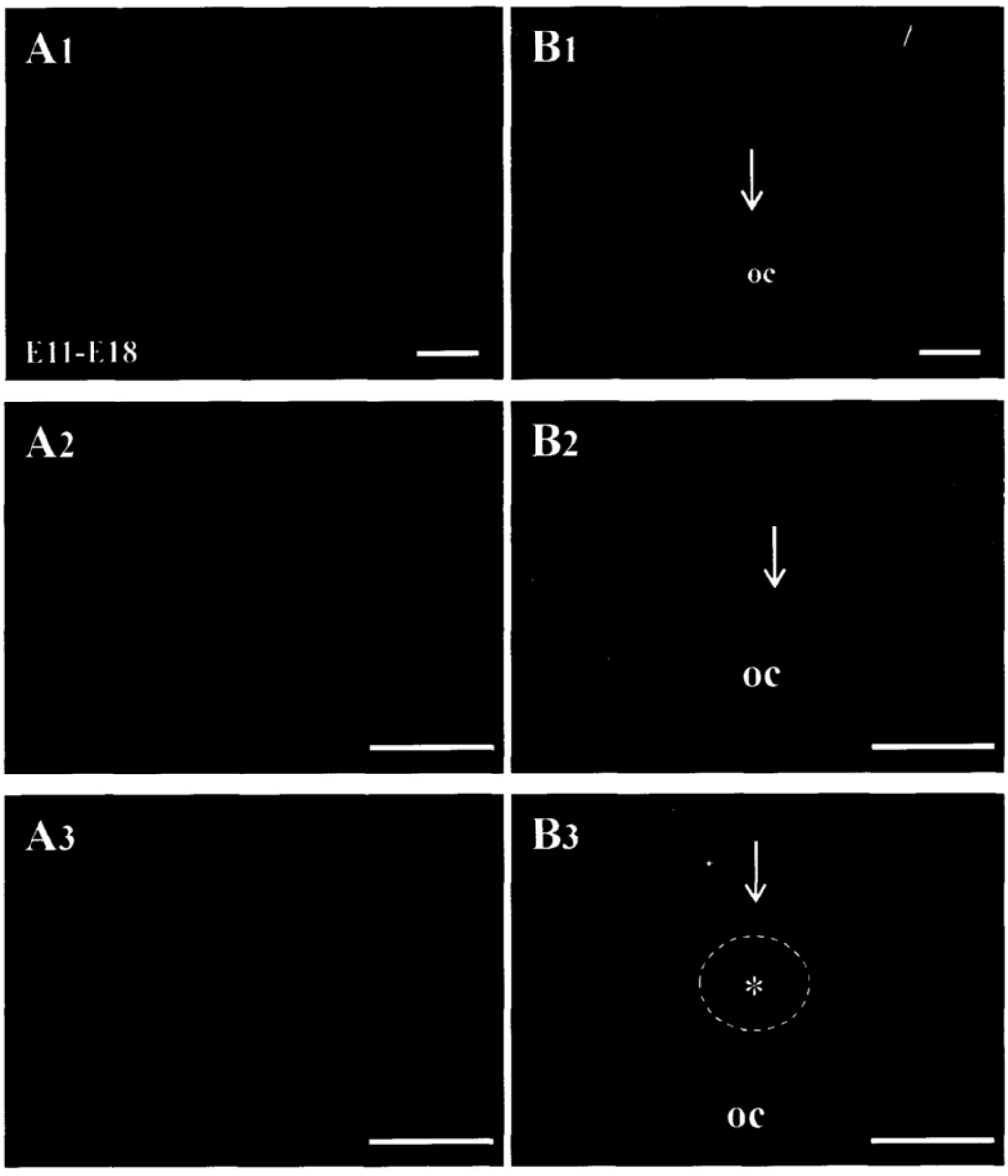
A1
E11-E18
B1
oc
A2
B2
oc
A3
B3
*
oc

Figure 17 The cell counting analyses showed the cell number of chiasmatic radial glia from E13 to E15, when these radial glia cells were generated at E11. (A-D) The EdU and RC2 dual labeled cells were counted on the sections which contain optic chiasm at different embryonic stages from E13 to E16. We drew a region which includes the glial palisade in the ventricular zone of the midline, then counted the dual labeled cells in this region. (E) The plot was showed the cell counting results at different embryonic stages, when EdU was injected at E11. Double labeled cells was decreased from E14 and was significant reduced at E15 ($P<0.01$). From E16, these double labeled cells were almost undetectable in most preparations.

Scale bar: 100μm.

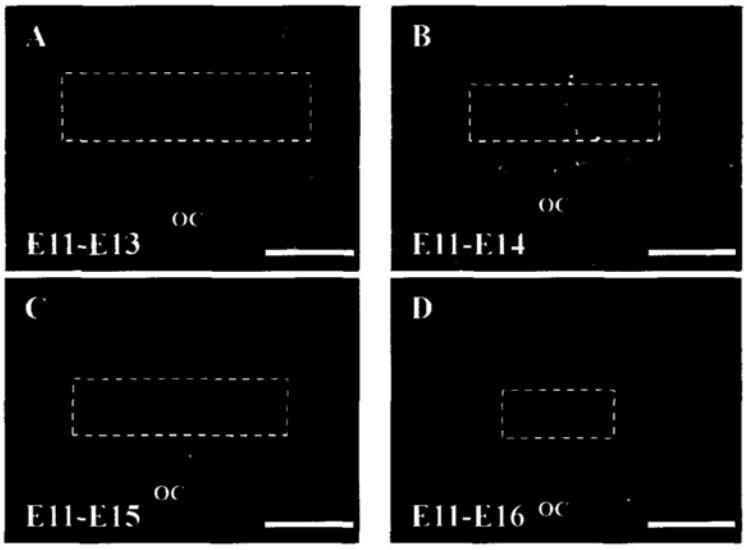
A
OC
E11-E13
B
OC
E11-E14
C
OC
E11-E15
D
E11-E16
OC

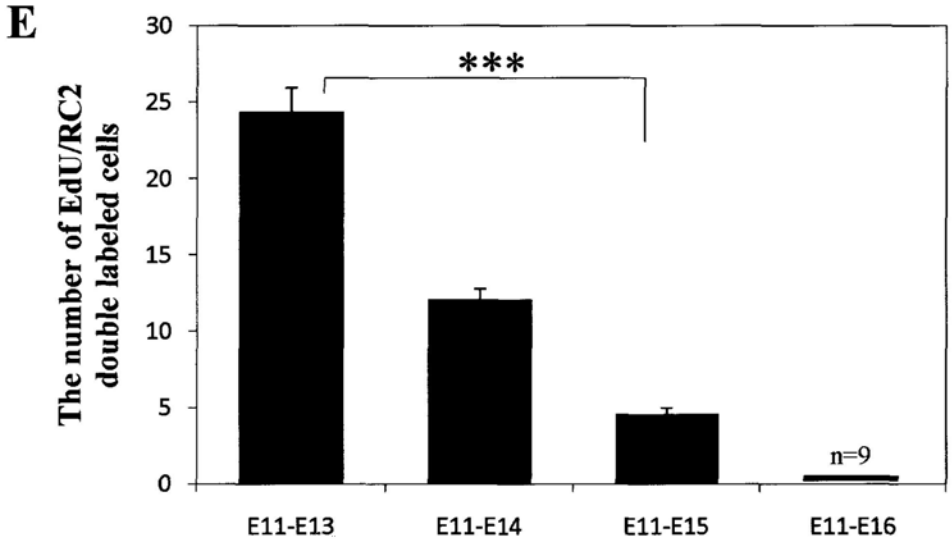
E
The number of EdU/RC2 double labeled cells
30
25
20
15
10
5
0
***
n=9
E11-E13
E11-E14
E11-E15
E11-E16

$* * *$ $p < 0.01$

Figure 18 Identification of chiasmatic neurons with neural stem cell marker at E13. (A) The Nestin-positive cells revealed a radial morphology which were located all over the diencephalon at the frontal section. This pattern was very similar to that of RC2-positive radial glia, which was showed in Fig. B. (C) The merged image of A and B at 60x magnification. All the radially oriented Nestin-positive cells were overlapped with the RC2-positive radial glia cells (revealed in yellow color).
Scale bar: A, B, 200μm; C, 50μm.

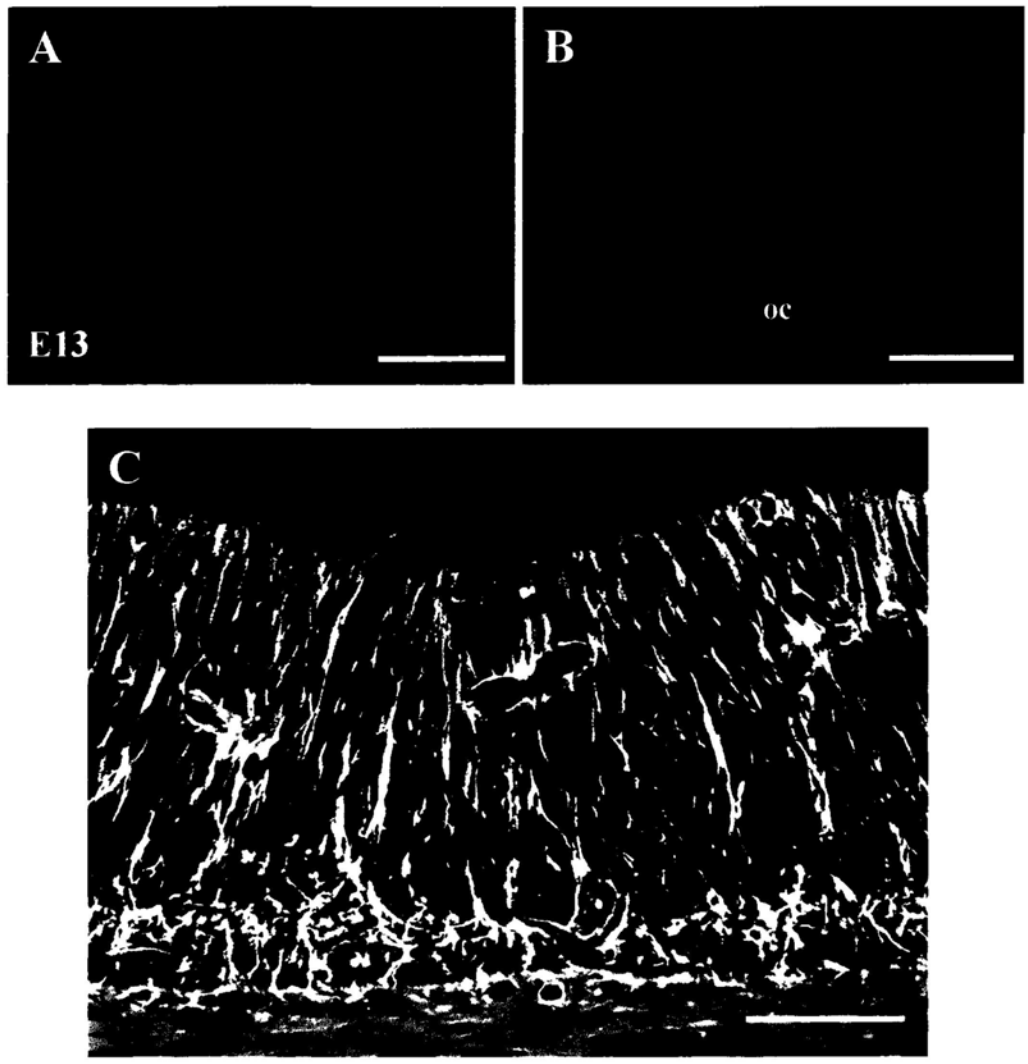
A
E13
B
oc
C

Figure 19 Identification of chiasmatic neurons with neural stem cell marker at E15. (A) The distribution of Nestin-positive cells was the same as that at E13, just the localization of optic chiasm was more obvious. As at E13, this pattern was also very similar to that of RC2-positive radial glia, which was showed in Fig. B. (C) The merged image of A and B at 60x magnification. All the radial oriented Nestin-positive cells were overlapped with the RC2-positive radial glial cells producing a yellow color.

Scale bar: A, B, 200μm; C, 50μm.

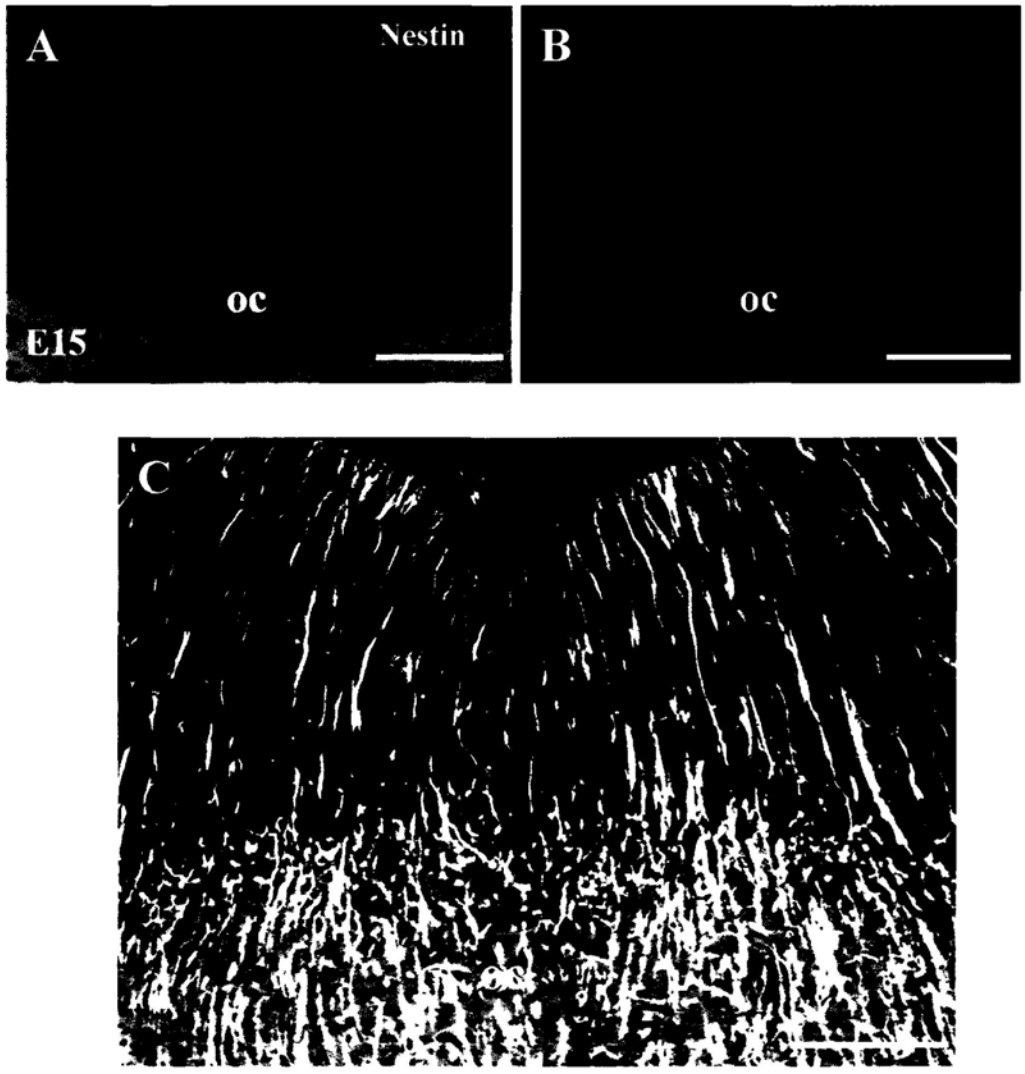
A
Nestin
oc
E15
B
oc
C

Figure 20 No apoptotic cell was observed in the radial glia palisade at E15. (A) Only a couple of apoptotic cells immnoreactive to caspase 3 antibody were observed in ventral diencephalon int the frontal sections. (C) In the merged image at higher magnification, these apoptotic cells were not located in the radial glia palisade.
Scale bar: A, B, 200μm; C, 50μm.

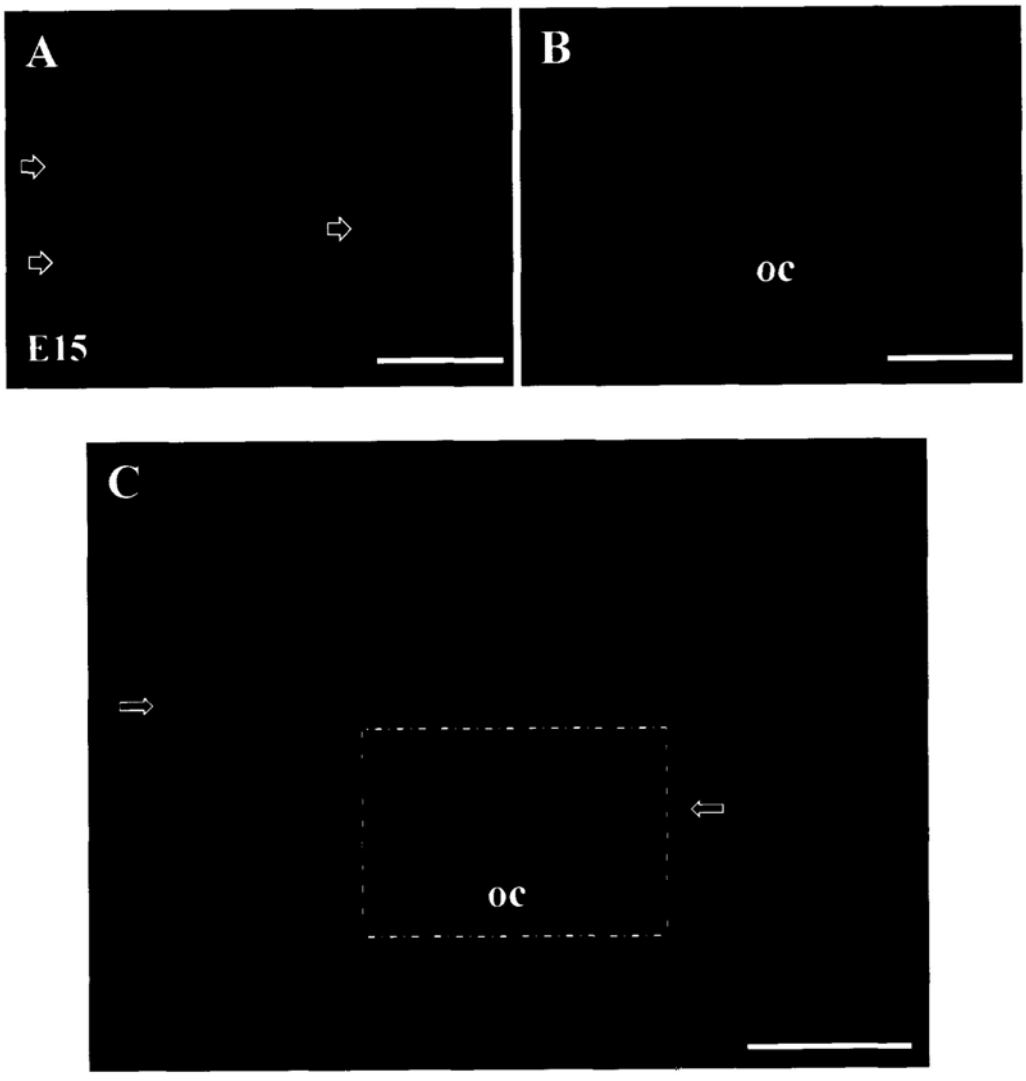
A
E15
B
oc
C
oc

CHAPTER 4

Expression and functions of N-methyl-D-aspartate receptor during development of mouse optic pathway

Introduction

Glutamate is a major excitatory neurotransmitter in the central nervous system (CNS). Glutamate receptors (GluRs) are divided into two classes, one is metabotropic receptors, the other is ionotropic receptors. The metabotropic receptors (mGluRs) are coupled to intracellular second messengers and modulate IP3 and cAMP concentrations. On the other hand ionotropic receptors (iGluRs) are directly coupled to an ion channel, and can be further divided into kainate, α-amino-3-hydroxy-5-methylisoxazole-4-proionate(AMPA),or N-methyl-D-aspartate (NMDA) receptors (Ozawa et al, 1998).

The ionotropic glutamate receptors, which are ligand-gated ion channels, control the majority of excitatory neurotransmission in the CNS (Dingledine et al, 1999). My research mainly focuses on the NMDA receptor. There are seven subtypes of NMDA receptor channel subunits, NMDAR1 (NR1), NMDAR2 (NR2) A-D, NMDAR3 (NR3) A & B. The NMDA receptor exists as heteromeric complexes, and its functional diversity resides in the different assembly of different subunits. The NR1 & NR2 subunits are essential for the ion channel; the function of NR3 subunit is to regulate the activity of NR1/NR2 heteromers (Babb et al, 2005; Nishi et al, 2001). Previous studies have reported that NR1 had a ubiquitous expression in the CNS, whereas the expression of NR2 was quite limited to certain neurons according to

their functions. NR3 showed ubiquitous expression during development, but its expression is restricted in adult (Nishi et al, 2001; Quinlan et al, 1999). NR3A has been reported to play an important role on the development and plasticity of the CNS, through modulating NMDA receptor functions (Das et al, 1998; Sucher et al, 2003; Wong et al, 2002).

Previous studies about NMDA receptor expression and function in the CNS always focused in the postnatal and adult vertebrates. These studies proposed that NMDA receptor is important in the control of protein synthesis at developing synapses, in neuronal plasticity of dendritic spines, neurite elongation and branching and glutamate neurotoxicity. It is expressed in the mammalian developing retina and visual cortex as well (Acosta et al, 2008; Babb et al, 2005; Cuppini et al, 1999; Fletcher et al, 2000; Haberecht et al, 1997; Pickard et al, 2000).

However, until now the expression and functions of NMDA receptor in the embryonic visual system are largely unknown. In this study, we investigated the expression pattern of NMDA receptor in the mouse optic pathway from E13 to E18.

Furthermore, we determined the possible contribution of NMDA receptor to axon outgrowth by using retinal explants culture analyses.

Materials and Methods

Animal

The experimental procedures in this study were approved by the University Animal Ethic Committee. Timed pregnant pigmented C57 mice were obtained from the Laboratory Animals Services Center of the Chinese University of Hong Kong. The day on which the vaginal plug was found was counted as embryonic day 0 (E0).

RT-PCR analysis for all the subunits of NMDA receptor

Total RNA were isolated from adult retina, E13 retina and E13 ventral diencephalon using Trizol reagent (Invitrogen). RNA samples were aliquoted and stored at -80°C until use.

The NMDA receptor subunits and β-actin were amplified using the following sets of primers (from 5' to 3'): NR1 sense, gctgtacctgctggaccgct, NR1 antisense, gcagtgtaggaagccactatgatc; NR2A sense, gctacgggcagacagagaag, NR2A antisense, gtggttgtcatctggctcac; NR2B sense, gctacaacacccacgagaagag, NR2B antisense, gagagggtccacgctttcc; NR2C sense, aaccacaccttcagcagcg, NR2C antisense, gacttcttgcccttggtgag; NR2D sense, cgatggcgtctggaatgg, NR2D antisense, agatgaaaactgtgacggcg; NR3A sense, ccgcgggatgccctactgttc, NR3A antisense, ccagttgttcatggtcaggat (Jakobs et al, 2007); NR3B sense, tgtctcggcacttcaaggtat, NR3B antisense, ggtgttccaccagagttacca (Stepulak et al, 2009), modified for mouse; β-actin sense, gctgtattcccctccatcgtg, β-actin antisense, cacggttggccttagggttcag.

First-strand cDNA templates were synthesized using the ImProm-II™ Reverse Transcription System (Promega). On ice, RNA sample (2μg), Oligo (dT) 15 Primer (2μl) and DEPC water (make the final volume to 5μl) were mixed, then the mixture was incubated at 70°C for 5 minutes and immediately chilled in ice-water. After that the reverse transcription reaction mix was prepared as following: ImProm-II™ 5X Reaction Buffer 4μl, $MgCl_2$ 1μl, dNTP Mix 1μl, Recombinant RNasin® Ribonuclease Inhibitor 0.5μl, ImProm-II™ Reverse Transcriptase 1μl, using DEPC water to make the final volume to15μl. The prepared RNA was added into the reaction mix, then the mixture was incubated at 25°C for 5 min, 42°C for 1 h, 70°C for 15 min.

PCR was performed using GoTaq® Flexi DNA Polymerase (Promega) as follows: 5X Green GoTaq® Flexi Buffer 5μl, $MgCl_2$ 1.5μl, dNTP 0.25μl, upstream

primer 0.5μl, downstream primer 0.5μl, GoTaq® Flexi DNA Polymerase 0.25μl, cDNA sample 1μl, Mili Q 11μl. After initial denaturation at 95°C for 2 min, cDNA was amplified using the following cycling method: first round 9cycles of 95°C for 40 s; 60°C (NR1, NR3A, Beta-Actin) or 61°C (NR2A, NR2B, NR2D) or 56°C (NR2C) or 46°C (NR3B) for 45 s; 72°C for 40 s; second round 19 cycles of 95°C for 40 s; 65°C (NR1, NR3A, β-actin) or 62°C (NR2A, NR2B, NR2D) or 59°C (NR2C) or 50°C (NR3B) for 45 s; 72°C for 40 s; and a final extending of 72°C for 10 min. The PCR products were electrophoresed using 1.5-2% agarose gel containing gel red to visualize the DNA bands. The predicted sizes (in bp) of the PCR-generated products were as follows: 219(NR1), 257(NR2A), 314(NR2B), 464(NR2C), 260(NR2D), 417(NR3A), 186(NR3B), 260(β-actin). Each RT-PCR was repeated at least 3 times to make the results consistently, and representative results are shown.

The mRNA expression analysis of NMDA receptor

The mRNA expression of all NMDA receptor subunits was analyzed from the PCR results. Using Gene Tools software, the quantification of each band was measured. After that a quantity ratio of each target band to the corresponding actin band was obtained. This ratio would be used to represent the mRNA expression of each sample.

Immunohistochemistry for NMDA receptor subunits

Here three NMDA receptor antibodies were used to examine the localization of different NMDA receptor subunits, including NR1 (Rabbit polyclonal, Abcam, Cat. No. ab17345), NR2B (Mouse IgG, BD transduction laboratories, Cat. No.610416) and NR3A (Rabbit polyclonal, Tocris Bioscience, Cat. No. 2059).

Pregnant mice were killed by cervical dislocation, embryos at the stage of E13-E18 were removed via Cesarean section and killed by decapitation. The heads of

the embryos were fixed with 4% paraformaldehyde in 0.1M phosphate buffer (PB, pH 7.4) overnight at 4°C.

The heads were embedded in a gelatin-albumen mixture and sectioned on a vibratome at the thickness of 100μm. Horizontal sections containing the retinofugal pathway from the eyes to the proximal parts of the optic tract were collected in 0.1M phosphate buffer saline (PBS, pH 7.4). Then the horizontal sections were blocked with 10% normal goat serum in 0.1M PBS for 90 min at room temperature to reduce the background signals. The sections were incubated separately with NR1 antibody (1:1000), NR2B antibody (1:100) or NR3A antibody (1:500) overnight at 4°C. On the following day, sections were thoroughly washed with 0.1M PBS and then incubated with Alexa Fluor 488 (AF488) - conjugated secondary antibody (for NR1 and NR3A using goat anti-rabbit IgG 1:200, Jackson Laboratories; for NR2B using goat anti-mouse IgG 1:200, Jackson Laboratories) for 2 hours at RT. After thoroughly washing three times with 0.1M PBS, the sections were mounted on glass slides with mounting medium (Biomeda).

Fluorescent signals on sections were imaged by the confocal microscope (FV300, Olympus Co, Japan). Control sections were prepared with the same procedures but with the absence of primary antibody. No obvious staining was found in any of these control preparations.

Double staining of NR1, NR2B and NR3A with neuronal marker in the E15 retina

To examine the identity of the NR1, NR2B and NR3A positive cells in the retina, a series of double staining experiment was performed in this study. Horizontal sections containing the retina were collected in 0.1M PBS and washed with 0.1M PBS for three times. Then the slices were blocked with 10% normal goat serum in

0.1M PBS for 90 min to reduce the background signals, and incubated with the primary antibodies NR1 (or NR3A) and TuJ-1 (1:500, mouse IgG; Abcam, UK), which was a neuronal marker; or with NR2B and TuJ-1(1:1000, Rabbit polyclonal) overnight at 4℃. After rinsing with 0.1M PBS, the sections were incubated in secondary antibodies at room temperature for 2 hours. The secondaries for NR1, NR3A and TuJ-1 (mouse IgG) were AF488 conjugated goat anti-rabbit IgG and Cyanine 3 (Cy3) conjugated goat anti-mouse IgG, respectively. The secondaries for NR2B and TuJ-1 (Rabbit polyclonal) were AF488 conjugated goat anti-mouse IgG and AF568 conjugated goat anti-rabbit IgG, respectively.

Control sections for this part of study were processed with the same procedures but with the absence of the primary antibodies. No obvious staining was found in these control preparations.

Western blot assays of NMDA receptor

Adult retina, E15 retina and E15 ventral diencephalon were homogenized in a mixed solution of RIPA buffer (Millipore Co, USA) and a protease inhibitor cocktail (1:7; Roche Co, Switzerland) by using a motorized homogenizer (Kontes, USA). The proteins were extracted and quantified with DC protein assay (Bio-Rad Hercules, CA). Samples containing 50μg protein were separated with 7% sodium dodecyl sulfate-polyacrylamide gel electrophoresis (SDS-PAGE) and then transferred to PVDF membrane (Amersham, Sweden) for Western blotting. Membranes were blocked 1 h at RT, in a Tris-buffered saline (TBS) containing 0.1% Tween-20 and 5% non-fat milk power. Inmmunodetection was carried out using primary antibodies against NR1 (1:1000), NR2B (1:100) or NR3A (1:1000) respectively, by incubation overnight at 4℃. After rinsing three times with TBS with 0.1% Tween-20, the membrane was incubated with goat anti-rabbit IgG horseradish peroxidase (HRP;

Jackson Immunoresearch, West Grove, PA) for NR1 and NR3A(1:10000), or goat anti-mouse IgG HRP (1:3000) for NR2B at room temperature. One hour later, the membrane was washed thoroughly with TBS with 0.1% Tween-20 for 2 times, then TBS for one time before adding chemiluminesence reagents. Finally the binding of the antibodies was visualized by using darkroom development techniques.

Preparation of retinal explants and treatment with NMDA receptor antagonists

Retinal explants were prepared from E14 mouse embryos. The eye balls were taken out from the embryos and stored in cold DMEM/F12 medium. After removing the lens and vitreous, retinas with pigmented epithelium were dissected out. The retinas were separated from the pigmented epithelium and cut gently into equal small pieces. Explants were placed with ganglion cell layer down on Poly-DL-Ornithine and laminin coated coverslips, and cultured in DMEM/F12 supplemented with N1, 1% bovine serum albumin and 0.4% methylcellulose (all purchased from Sigma Co, USA) at 37°C. The antagonists of NMDA receptor, Dextrorphan-D-tartrate (RBI, D-127) and (+)-MK-801 hydrogen maleate (RBI, M-107), were added into the culture medium at the start of the culture in various concentrations. After 18 hours, the explants were fixed with pre-warmed 4% paraformaldehyde in 0.1M PB for 30 minutes.

Neurite outgrowth from the whole explants was imaged sequentially using the SPOT Image analysis system (Diagnostic Instruments, Inc) under phase contrast optics (10x, Plan-Neofluar, NA 0.5, from Zeiss, Germany). After that, the images were merged into a montage, on which the whole explant ant its neurites were recognized clearly. To do the image analysis, the software MetaMorph (Universal Imaging Corp, USA) was used. Retinal neurite outgrowths were highlighted by adjusting the threshold, and the pixel was measured in the area, which contained all

the neurite outgrowths from one explant. The data in control groups and the antagonist treated groups were compared by the Kruskal-Wallis nonparametric ANOVA test of the InStat software (Grapph-Pad Inc., USA).

Results

1. Expression of mRNA for NMDA receptor subunits in the mouse adult retina, embryonic retina and embryonic ventral diencephalon

To investigate the mRNA expression of all the NMDA receptor subunits in the mouse embryonic visual pathway, tissues from E13 retina and ventral diencephalon were analyzed. As a comparison, their expression in the adult retina was also examined, because most of the previous studies always focus on the postnatal and adult animals.

The PCR primer pairs of NR1-NR3A were used in the paper written by Jakobs (Jakobs et al, 2007), while the primers of NR3B were modified for mouse according to the paper written by Stepulak (Stepulak et al, 2009). All the subunits of NMDA receptor were expressed in the adult retina (Fig. 1A-D). In the mouse optic pathway, all the subunits were also observed in the E13 retina and ventral diencephalon (Fig. 1A-D). Furthermore, almost all the subunits revealed a different expression at adult retina, E13 retina and E13 ventral diencephalon.

The results of mRNA expression analyses showed an age-dependent and regional specific expression of various NMDA receptor subunits. Here we found that NR1, NR2A, NR2B, NR2D and NR3A revealed a similar expression pattern, they have a higher expression in adult retina and E13 ventral diencephalon but a lower expression in E13 retina. In contrast, NR2C display a higher expression in E13 retina and a lower expression in adult retina and E13 ventral diencephalon. The expression

of NR3B is similar in these three parts (Fig. 1E).

2. Expression of NMDA receptor in the retina and ventral diencephalon in the mouse embryo

1) Expression of NR1 in the mouse retina

The localization of NR1 was first checked in the retina at E13, because the chiasm begins to form at this stage. There was no obvious fluorescent signal in the control sections from E13 embryos (Fig. 2A, n=3). In the sections treated with NR1 antibody, NR1 positive staining was detected on some radically arranged cells in the central retina (Fig. 2B, n=6). In addition, NR1 positive staining was strongly detected in the ciliary margin zone (CMZ), the lens and the blood vessel in the vitreous (Fig. 2B). Under higher magnification, the strongest NR1 immunoreactive signal was observed on the retinal axons at the optic disc (Fig. 2C, indicated by arrows). On the radial cells, NR1 was expressed on both the cell body and the long processes (Fig. 2C, indicated by arrows). At later developmental stage, the expression pattern of NR1 was changed when compared with that at E13. At E14 (n=8) the immunoreactivity of NR1was highly localized on the fiber layer and the inner cell layer of the retina (Fig. 2D). At higher power, prominent staining of NR1 was detected on the retina axons and inner cell layer, meanwhile there was some weaker staining on the radial cells (Fig. 2E). At E15 (n=7) and E18 (n=5), NR1 staining was consistently observed in the retina, and the expression pattern was similar to that at E14. NR1 positive staining was concentrated in the inner cell layer and optic fiber layer (Fig. 2F, G). In the adult retina (n=4), the expression of NR1 was quite extensively, it existed in retinal axons, ganglion cell layer, inner plexiform layer, inner nuclear layer, outer plexiform layer, outer nuclear layer (Fig. 2H).

2) Expression of NR1 in the ventral diencephalon

The expression of NR1 in the ventral diencephalon of the mouse embryo was detected at E13 to E15, and at E18. The positive signal of NR1 was highly expressed in the optic stalk (OS) E13 (Fig. 3A, B; n=6). From the E14 (n=8) to E15 (n=7), the expression of NR1 in the ventral diencephalon was obviously found on the optic stalk and optic tract (OT), while some weak signals were observed at other parts of the ventral diencephalon (Fig. 3C-F). At E18 (n=5) NR1 staining was consistently detected at the OS and OT as well (Fig. 3G). Furthermore, the specificity of NR1 was proved by Western-blot. A band at about 110 kDa (Indicated by arrow) was detected in the adult retina (AR), embryonic retina and ventral diencephalon at E15 (Fig. 3H).

3) Expression of NR2B in the retina and ventral diencephalon

The expression pattern of NR2B in the mouse retina and ventral diencephalon was detected from E13 to E15, the major stages for the formation of the optic chiasm. In control sections at E13 (n=3), no positive signal was detected (Fig. 4A). At E13 retina (n=7), NR2B immunoreactive signal was observed on the radial cell body and their long processes (Fig. 4B). At E14 (n=8), there was some positive staining on the radial cells as well. Furthermore, stronger staining was detected in the fiber layer and inner cell layer in the retina (Fig. 4C). The expression pattern of NR2B in the E15 (n=8) retina was similar to that at E14, the stronger staining was also observed in the inner cell layer (Fig. 4D). From E13 to E15, the expression of NR2B in the ventral diencephalon was almost the same. Positive signals were detected all over the ventral diencephalon. No specific signal was observed on the optic stalk and optic tract (Fig. 4E-G). Western-blot was used to prove the specificity of NR2B antibody. A single band at about 180 kDa (indicated by arrow) was detected in the adult retina and E15 ventral diencephalon, but the band was very weak in the E15 retina (Fig. 4H).

4) Expression of NR3A in the retina and ventral diencephalon

We also examined the NR3A expression in the retina and ventral diencephalon of mouse embryos at E13 to E15. At E13 (n=6), NR3A positive staining was found in the radically oriented cells in the retina (Fig. 5A). At E14 (n=6), beside to the radial cells staining, some weak staining in the retinal axons was detected as well (Fig. 5B). At E15 (n=7), NR3A immunoreactive signal was different from that at E13 and E14. The positive staining on the inner layer was clearly observed but the staining on the radial cells was also detected (Fig. 5C). From E13 to E15, the NR3A immunoreactivity in the ventral diencephalon was observed all over the ventral diencephalon, but was stronger in the optic stalk and optic tract (Fig. 5D-F). Western-blot analyses showed the specificity of NR3A antibody. A band at about 130 kDa (Indicated by arrow) was detected in the adult retina (AR), E15 retina and ventral diencephalon (Fig. 5G).

3. Identity NR1，NR2B and NR3A positive cells in the retina

1) NR1 was expressed on the TuJ-1 positive neurons in the retina

TuJ-1 is a monoclonal antibody, which is the marker of neuron-specific β-tubulin. Retinal ganglion cells are the first neuron type that leaves mitotic cycle during the development and express a neuron-specific β-tubulin isoform (Brittis & Silver, 1994). Therefore TuJ-1 is always used as a ganglion cell marker in the developing retina.

At E15 (n=4), TuJ-1 positive neurons were concentrated in the inner cell layer and optic fiber layer (Fig. 6B). Double staining of NR1 (Fig. 6A) together with TuJ-1showed that NR1 protein was also obviously detected on the TuJ-1 positive cell bodies and their axons (Fig. 6C). So NR1 was highly expressed in the ganglion cells and axons in the mouse retina at E15. In addition, NR1 was observed on some radial

cells and their long processes as well.

2) NR2B was expressed on the TuJ-1 positive neurons in the retina

At E15 retina (n=3), NR2B positive staining was detected on the inner layer, optic fiber layer and some radial cells (Fig. 7A). In the merged image (Fig. 7C), most NR2B positive cells in the inner cells layer were colocalized with TuJ-1 positive neurons.

3) NR3A was expressed on the TuJ-1 positive neurons in the retina

At E15 retina (n=3), NR3A positive signals were also observed on the inner layer, optic fiber layer and some radial cells (Fig. 8A). Double staining study showed that the NR3A positive cells in the inner layer and fiber layer were also TuJ-1 positive (Fig. 8B and 8C). So the expression pattern of NR3A is similar to that of NR1 and NR2B, NR3A was expressed in the ganglion cell bodies and their axons as well, but many radial cells in other parts retina were also NR3A positive.

4. The effects of NMDA receptor antagonists to retinal neurite outgrowth

In order to determine whether the NMDA receptor affects growth of retina axons, we investigated neurite outgrowth from E14 retinal explants in the presence of NMDA receptor antagonists. In this study, two kinds of NMDA receptor antagonists were used, one is Dextrorphan-D-tartrate, the other is MK-801. Both of them are noncompetitive antagonists to NMDA receptor, but have distinct molecular determinants for high-affinity binding. MK-801 with an arylcyclohexylamine structure acts at the NMDA receptor-operated ion channel as an open channel blocker. While Dextrorphan-D-tartrate, which is a kind of benzomorphans, binds to a closed channel, moreover, its recognition site in the ion channel is shallower than that of MK-801 (Carter, 1994; LePage et al, 2005).

1) Dextrorphan-D-tartrate is inhibitory to retinal neurite outgrowth

Here various concentrations of Dextrophan-D-tartrate were used to observe its effect to retinal neurite outgrowth. After 18 h in culture, in control groups of retinal explants, which were treated without addition of Dextrophan-D-tartrate, extensive neurite outgrowth was found (Fig. 9A). When explants were treated with low concentrations (50-200μmole/ml) of Dextrophan-D-tartrate, an obvious reduction in the neurite outgrowth was observed (Fig. 9B-D). Furthermore, under a higher concentration (500 μmole/ml), there was almost no neurite outgrowth coming out from the explants (Fig. 9E). Quantitative analyses showed that retinal neurite outgrowth was significantly inhibited in the presence of 50-500μmole μ /ml Dextrophan-D-tartrate (p<0.05 or 0.001) when compared with corresponding data in control groups cultured without Dextrophan-D-tartrate (Fig. 11A).

2) MK-801 is inhibitory to retinal neurite outgrowth

Similar to Dextrophan-D-tartrate, an obvious reduction in neurite outgrowth was observed as well when explants were treated with MK801 under the concentrations 50-200μmole/ml (Fig. 10A-D). Quantitative analyses showed the same results as that for Dextrophan-D-tartrate treatment. The neurite outgrowth from retinal explant was significantly reduced in the presence of MK-801 (50-200μmole/ml), compared with the controls (p<0.01 or 0.001, Fig. 11B).

Discussion

In this part of study, we have investigated the expression and function of NMDA receptor subunits during development of the mouse optic pathway. The major findings are: (1) All the subtypes of the NMDA receptor are expressed in the mouse optic pathway from E13 to adult. (2) In the developing retina, NR1, NR2B and NR3A were distributed on the radial cells body and their long processes at E13. At

E14 to E15, these three subunits were also expressed in the inner cell layers and optic fiber layer in the retina. The identity studies showed that NR1, NR2B and NR3A are localized on the ganglion cells and their axon. In addition, NR1, NR2B and NR3A were observed on the elongating cells in the retina at E14 to E15. (3) In the developing ventral diencephalon, NR1, NR2B and NR3A were located everywhere, however, NR1 and NR3A had stronger staining on the optic stalk and optic tract. (4) NMDA receptor antagonists, Dextrorphan-D-tartrate and MK-801 can reduce neurite outgrowth from the E14 retinal explants respectively, suggesting that a positive influence of NMDA receptor on the axon growth in the mouse optic pathway.

Expression of mRNA of NMDA receptor subunits in the mouse optic pathway

In this experiment, we detected the mRNA expression of all known subtypes of NMDA receptor in the adult retina, embryonic retina and ventral diencephalon. It was found that all these subunits were expressed in the adult retina, embryonic retina and ventral diencephalon. As we know, the RGC axons begin to enter into the optic stalk at E12, arrive at the ventral midline at E12.5 and begin to form the optic chiasm (Colello & Guillery, 1990; Sretavan, 1990). At E13, a lot of RGC axons have crossed the midline to establish the X-shaped optic chiasm (Sretavan et al, 1994). The NMDA receptor was expressed in the mouse optic pathway from E13 (the earliest stage we observed), so it may play a role in the formation of chiasm and the axon guidance in the chiasm.

After analyzing the PCR results, we found that the quantity of mRNA expression was different at different ages and regions in various subunits. The expression of NR1, NR2A, NR2B, NR2D and NR3A increased from embryo to adult in the retina. They also revealed a higher expression in E13 ventral diencephalon. In contrast, the expression of NR2C was reduced from E13 retina to adult retina, and

was lower in the E13 ventral diencephalon. The expression of NR3B in these three regions was quite similar. Different expression pattern may serve different function during the development. Previous study has shown that NR1 and NR2B reveal an age-depend expression in the CNS during pre- and postnatal development, suggesting they have different functions at different stage (Babb et al, 2005). According to our results, NR2C is like to play an important role in the embryonic retina development because of the higher expression, while NR2B may be more important in the ventral diencephalon development as it has the highest expression there.

However, without doing the Real-time PCR, the analyses of mRNA expression were quite rough. It is hardly to tell which subunit has the highest or lowest expression. Here we just roughly estimate their expression and make some hypotheses accordingly. So Real-time PCR could be done in the future, when we further investigate the different expression pattern of each subunit during the optic pathway development.

Expression of NMDA receptor subunits protein in mouse optic pathway

After knowing the mRNA expression of all the NMDA receptor subunits in E13 optic pathway, we want to investigate the expression of NMDA receptor protein during development of the optic chiasm as well. Here three antibodies for NMDA receptor were used, NR1, NR2B and NR3A. We chose these three subunits to investigate, because NR1 and at least one kind of NR2 were essential of comprising the NMDA receptor, NR3A play an important role on the development and plasticity of the CNS, as a modulator of the NMDA receptor (Das et al, 1998; Sasaki et al, 2002; Sucher et al, 2003; Wong et al, 2002). To date, which subtype of NR2 is more important during optic pathway development still remain largely unknown, we just

select NR2B randomly at the beginning of this study. So the expression of these three subunits may represent a potentially functional NMDA receptor in the developing pathway.

1) Expression of NMDA receptor in the developing retina

At the early stage of retinal development (E13), the distribution of NR1, NR2B and NR3A is quite similar. They are expressed on the radially oriented cells, which have ventricular and vitreal endfeet anchored to the inner and outer surfaces of the retinal neuroepithelium. During development, primitive TuJ-1 positive retinal ganglion cells, which have radial array, lack axons and have ventricular and vitreal endfeet (Brittis & Silver, 1994; Morest & Silver, 2003). Compared with the morphology of NR1, NR2B and NR3A positive cells at E13, they are very likely to be the new-born RGCs. At later stages, from E14 or E15, these receptor subunits are localized in the inner cell layer and fiber layer. Double staining analyses showed that NR1, NR2B and NR3A positive cells were overlapped with TuJ-1 positive neurons. In addition, beside the inner layer and fiber layer, some NR2B and NR3A positive cells are observed on some elongating cells as well. These observations may suggest NR2B and NR3A are also expressed on other cell types from E14 to E15.

There are 4 steps during the early born RGC development: firstly, young RGCs, prior to elaborating an axon, retain a radial configuration, having ventricular and vitreal endfeet anchored to the inner and outer surfaces of the retinal neuroepithelium; secondly, the cell bodies of these neurons move to the vitreal surface; thirdly, these cells finally bud processes; fourthly, these cells lose their endfeet and project axons toward the optic fissure (Brittis & Silver, 1994). According to this, NMDA receptor first locating on the new-born RGCs, then on the inner TuJ-1 neurons, so it may play a role as a modulator of RGC migration in retinal

development. In previous study, it was also shown that glutamate receptor system mediated neuronal migration during brain development (Haberny et al, 2002). Since NR2B and NR3A are also expressed in other cell types, the function of NMDA receptor may be complex.

Actually in this part of study, we also tried to double stain NR2B and NR3A together with Müller glia cell marker (Vimentin) or radial glia cell marker (RC2), but these antibodies did not work well when used together. So there is no good image shown in this chapter. If some good antibodies could be found, we can also identify NR2B and NR3A positive cells with other cell types in the retina.

2) Expression of NMDA receptor in the developing ventral diencephalon

In this study, the extensive expression of NMDA receptor was observed in the mouse ventral diencephalon during development. However, the staining of NR1 and NR3A is stronger in the optic stalk and optic tract. Functional NMDA receptor consists of NR1 and at least one NR2. NR3 is not necessary for the heteromer, but may play a modulatory role in the function (Perez-Otano et al, 2001). It is suspected that functional NMDA receptor exists on the optic axons, and may influence the axon routing at the optic chiasm.

NMDA receptor may have an influence on retinal axon growth

It was shown in this study that NMDA receptor antagonists, both Dextrorphan-D-tartrate and MK-801, significantly inhibited neurite outgrowth from E14 retinal explants, suggesting that NMDA receptor may be involved in modulating axon outgrowth in the mouse optic pathway development. Previous studies indicated that NMDA receptor can promote axon outgrowth in the P19 neurons (Georgiev et al, 2008), immature cerebrocortical neurons (George et al, 2009). In the chick embryo spinal cord, the neuritogenesis can be blocked by MK-801 (Cuppini et al, 1999). All

these studies suggested that NMDA receptor regulated axon outgrowth.

However, most of previous studies investigated the expression and function of the NMDA receptor on the postnatal and adult stage of different vertebrates. The expression and function of NMDA receptor in the mouse embryonic stage are largely unknown. Our study showed that NMDA receptor was expressed on the mouse retina and ventral diencephalon from E13, when the chiasm begin to establish; it may promote the retinal axon growth as well, as using its antagonist can reduce the neurite outgrowth.

Figures

Figure 1 Expression of NMDA receptor subunits in mouse adult retina, embryonic retina and embryonic ventral diencephalon at E13. The mRNA expression of NMDA receptor subunits was determined by RT-PCR using a series of primers, which were showed in the methods. (A-D) All the NMDA receptor subunits were expressed in mouse adult retina, E13 retina and E13 ventral diencephalon. (E) NR1, NR2A, NR2B, NR2D and NR3A revealed a similar expression pattern; they have a higher expression in adult retina and E13 ventral diencephalon but a lower expression in E13 retina. In contrast, NR2C display a higher expression in E13 retina and a lower expression in adult retina and E13 ventral diencephalon. The expression of NR3B is similar in adult retina, E13 retina and E13 ventral diencephalon. Marker: 50bp DNA ladder. The size of PCR-generated products: NR1 (219bp), NR2A (257bp), NR2B (314bp), NR2C (464bp), NR2D (260bp), NR3A (417bp), NR3B (186bp), β-actin (260bp).

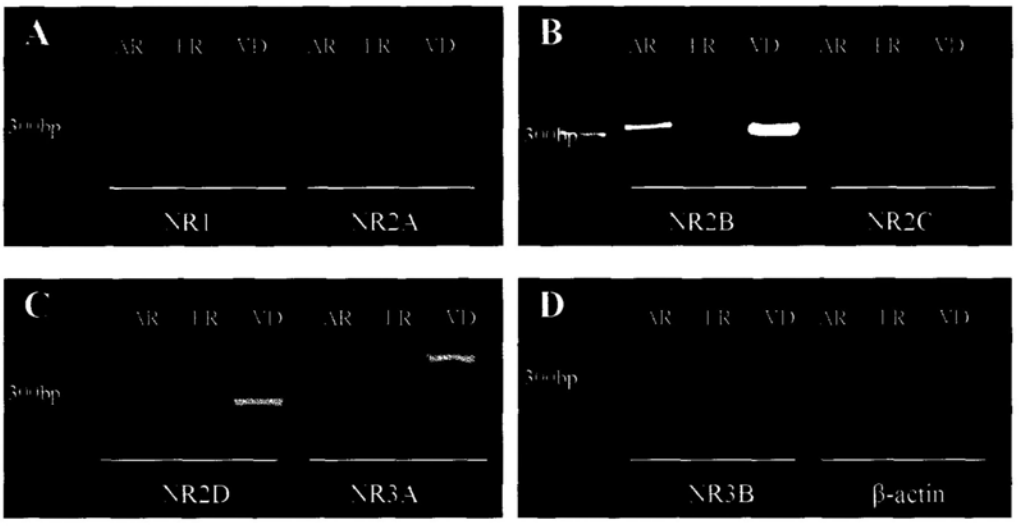
A
AR ER VD AR ER VD
300bp
NR1
NR2A
B
AR ER VD AR ER VD
300bp
NR2B
NR2C
C
AR ER VD AR ER VD
300bp
NR2D
NR3A
D
AR ER VD AR ER VD
300bp
NR3B
β-actin

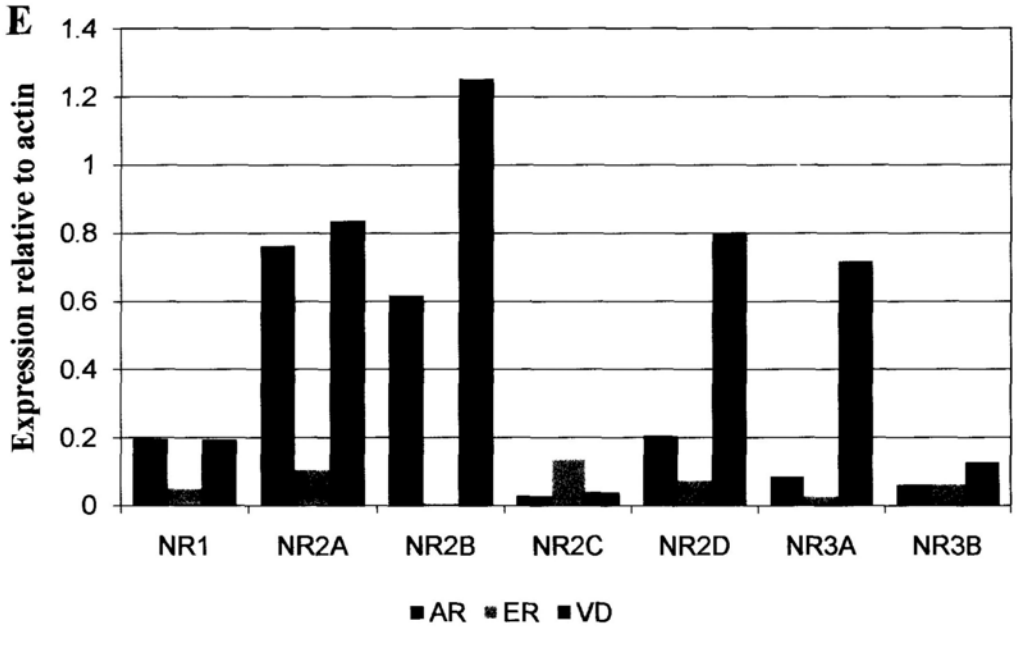
E
Expression relative to actin
1.4
1.2
1
0.8
0.6
0.4
0.2
0
NR1
NR2A
NR2B
NR2C
NR2D
NR3A
NR3B
AR ER VD

Figure 2 Confocal micrographs showed the localization of NMDA receptor 1(NR1) in the retina sections of mouse embryos at E13 to E15; E18 and adult. (A) There was no obvious fluorescent signal in the retina (R) and lens (L) in control sections. (B) At E13, NR1 positive staining was strongly detected in the ciliary margin zone (CMZ) (indicated by white square), the lens and the blood vessel in the vitreous (showed by open arrows). Furthermore, some radial arranged cells in the central retina were NR1 positive as well. (C) High power of the central part of the retina in figure B showed that the strongest NR1 immunoreactive signals were expressed on the retinal axons in the optic disc, the staining was also observed on the radial cells (indicated by solid arrows) which had the long processes spanned the whole thickness of the retina. (D) The NR1 staining in the retina was changed at E14 compared with that at E13. Prominent staining of NR1 protein was observed on the fiber layer and the inner cell layer of the retina. (E) At the higher power of optic disc in figure D, NR1 immunoreactivity was localized at the retinal axons and the inner cell layer (showed by short arrows). There was some weak staining on the radially orientated cells as well (showed by long empty arrows). (F & G) At E15 and E18, the expression pattern of NR1 was quite similar to that at E14. NR1 positive staining concentrated in the inner cell layer and optic fiber layer. (H) The expression of NR1 was more extensive in the adult retina, it existed in retinal axons, ganglion cell layer (RGCL), inner plexiform layer (IPL), inner nuclear layer (INL), outer plexiform layer (OPL), outer nuclear layer (ONL).

Scale bar: A, B, D 200μm; C, E, F, G, H, 100μm.

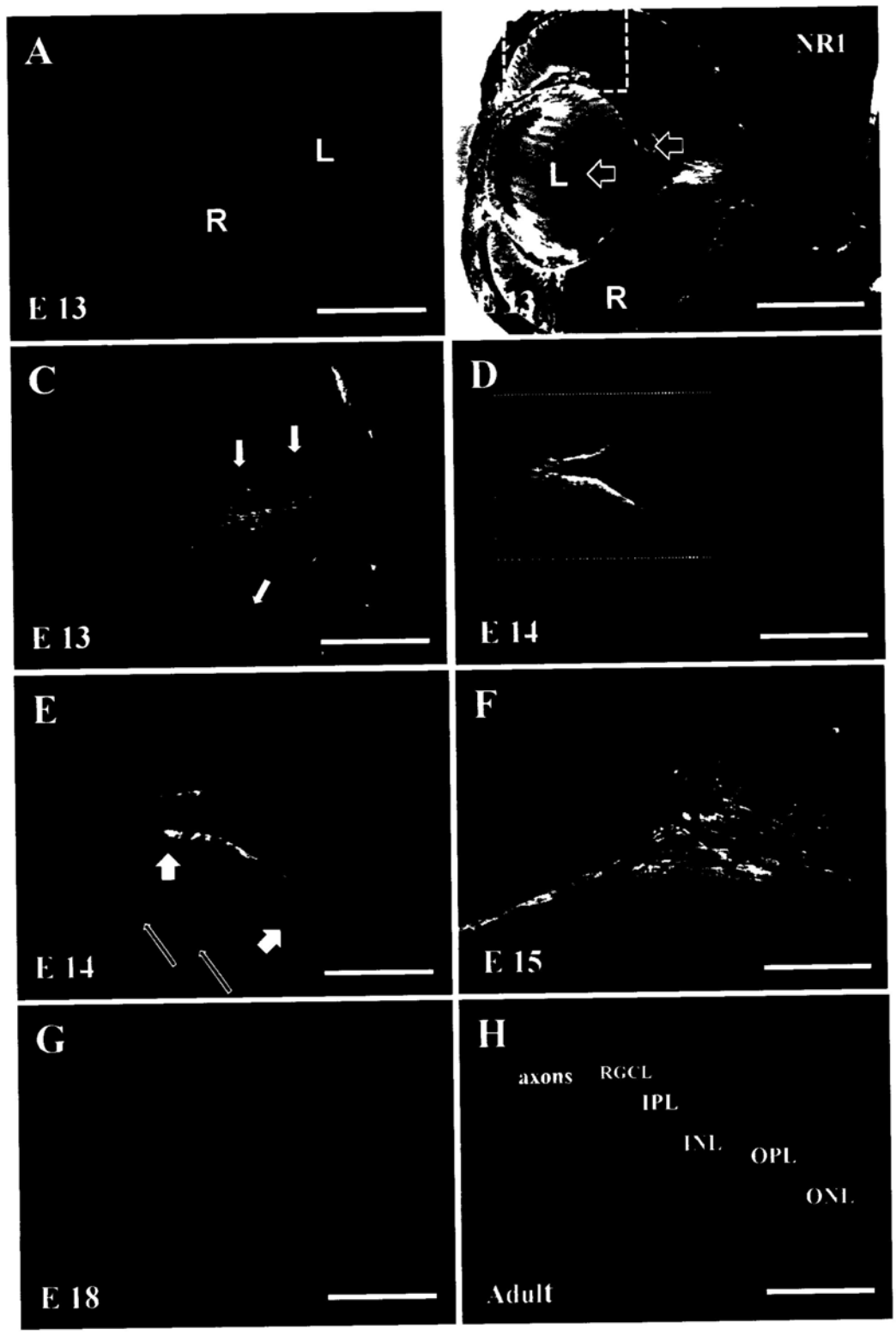
A
L
R
E 13
NR1
L
R
C
E 13
D
E 14
E
E 14
F
E 15
G
E 18
H
axons
RGCL
IPL
INL
OPL
ONL
Adult

Figure 3 Confocal micrographs showed NR1 staining in the ventral diencephalon of mouse embryos at E13 to E15 and E18. (A) At E13, NR1 protein was expressed very extensively in the ventral diencephalon, but the staining was much stronger in the optic stalk (OS). (B) At higher magnification, the strongest NR1 immunoreactive signal was localized on the optic stalk, whereas the weak signals were observed on the other parts of the ventral diencephalon. (C-G) From E14 to E18, the expression of NR1 in the ventral diencephalon was quite similar. The NR1 immunoreactivity was obviously found on the optic stalk and optic tract (OT), while there was also some weak staining extended at other parts of the ventral diencephalon. (H) Western-blot analysis was shown the specificity of NR1 antibody. A band at about 110 kDa (Indicated by arrow) was detected in the adult retina (AR), E15 retina (E15 R) and E15 ventral diencephalon (E15 VD).

Scale bar: 200μm.

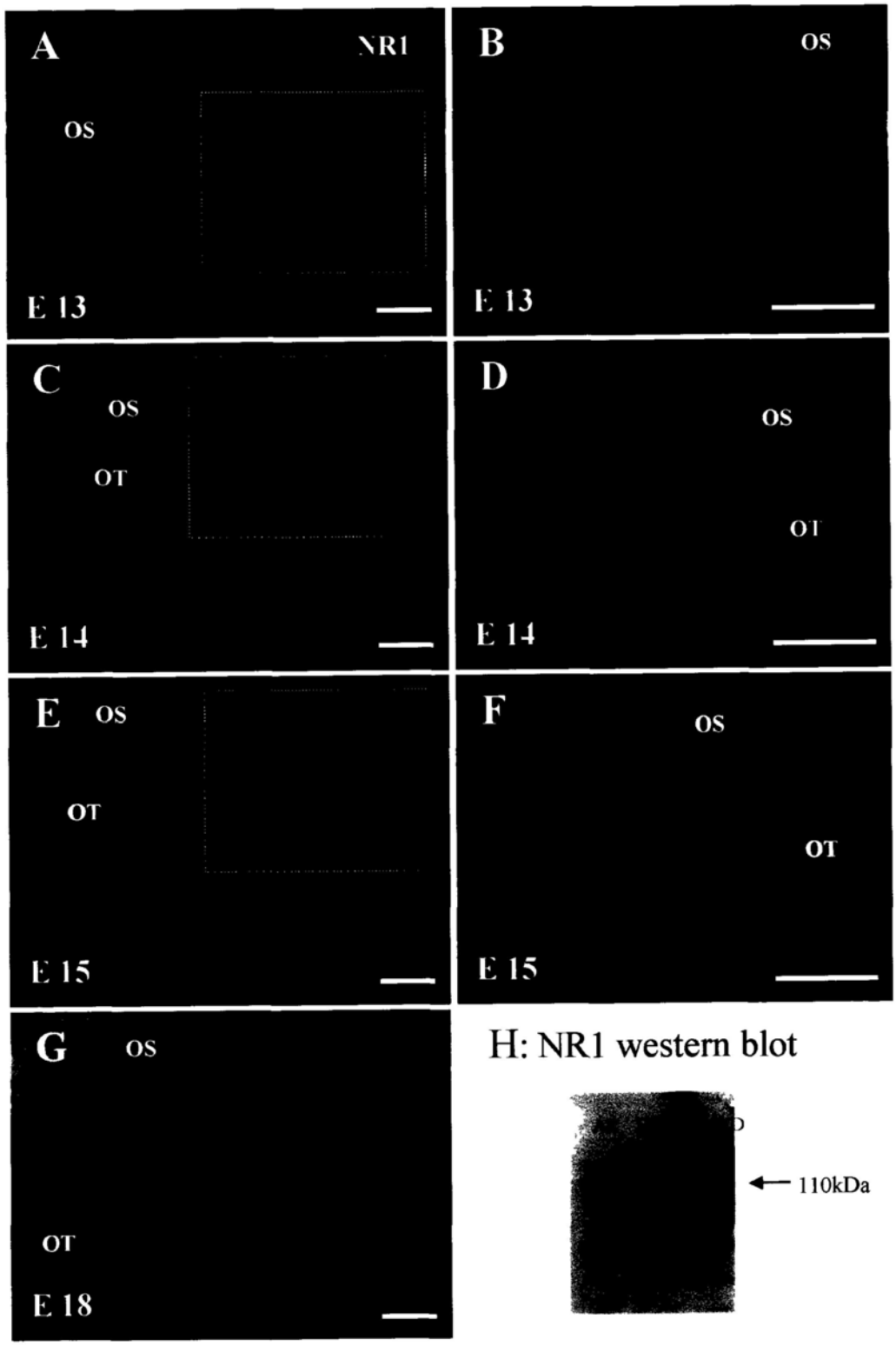
A
NR1
OS
E 13
B
OS
E 13
C
OS
OT
E 14
D
OS
OT
E 14
E
OS
OT
E 15
F
OS
OT
E 15
G
OS
OT
E 18
H: NR1 western blot
110kDa

Figure 4 Confocal photomicrographs showing the localization of NMDA receptor 2B (NR2B) in the retina and ventral diencephalon of mouse embryos at E13 to E15. (A) There was no obvious fluorescent signal in the retina (R) and lens (L) in control sections. (B) At E13, NR2B immunoreactive signal was expressed on the radially orientated cells with the long processes (arrows) (C) At E14, the stronger immunoreactivity of NR2B was detected in the inner cell layer and fiber layer (empty arrows), while the weak positive staining was also observed in the radially orientated cells (long arrow). (D) The NR2B staining at E15 was similar to that at E14, the stronger signal was observed in the fiber layer and inner cell layer. (E-G) From E13 to E15, the expression of NR2B in the ventral diencephalon was almost the same. The staining was detected in the whole ventral diencephalon, no specific signal was observed on the optic stalk and optic tract. (H) Western-blot analysis showing the specificity of NR2B antibody. A single band at about 180 kDa (arrow) was detected in the adult retina (AR) and E15 ventral diencephalon (E15 VD), but the band was very weak in the E15 retina (E15 R).

Scale bar: B, C, D, 100 μm; E, F, G, 200μm.

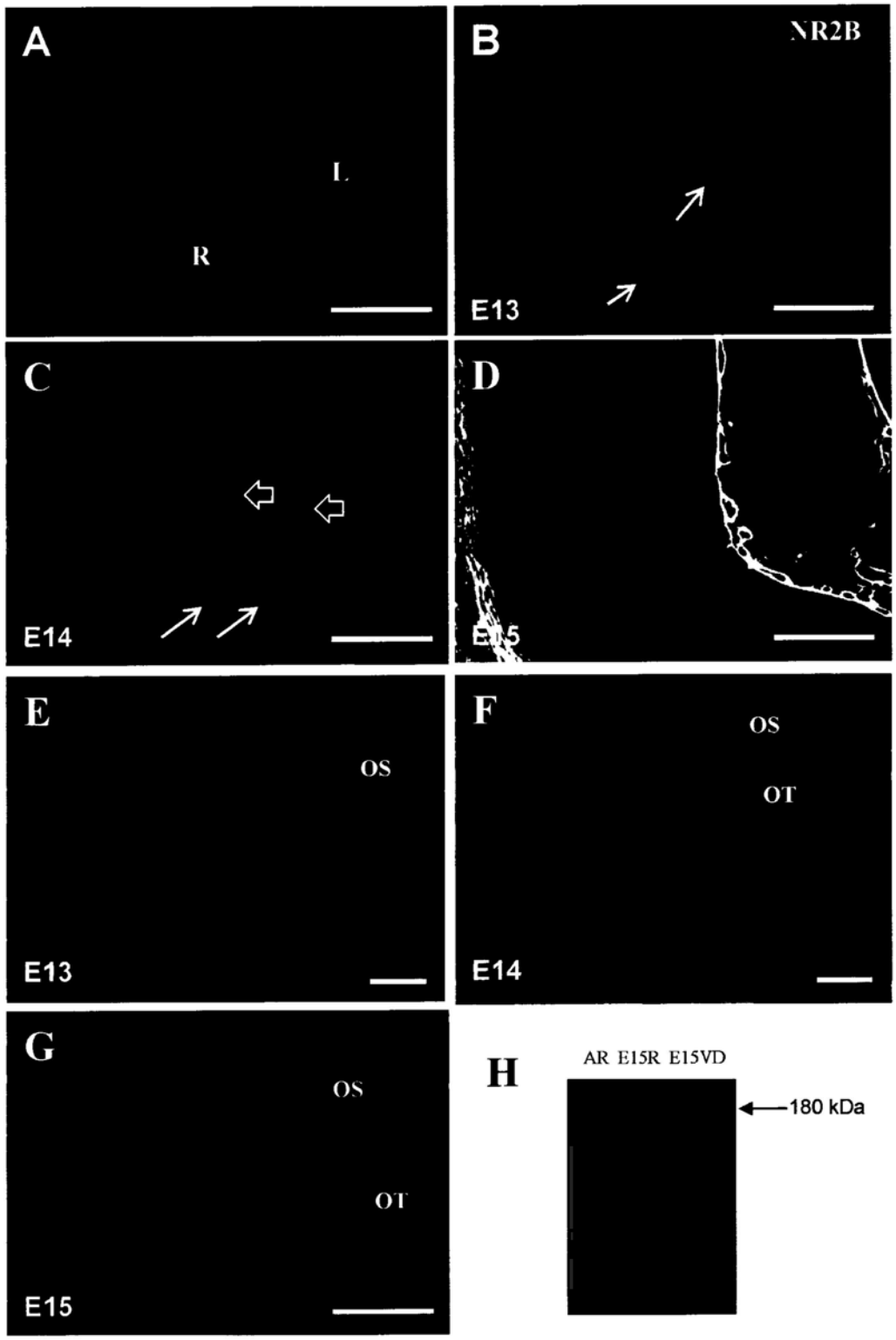
A
L
R
B
NR2B
E13
C
E14
D
E15
E
OS
E13
F
OS
OT
E14
G
OS
OT
E15
H
AR E15R E15VD
180 kDa

Figure 5 Confocal micrographs showed the expression of NMDA receptor 3A (NR3A) in the retina and ventral diencephalon of mouse embryos at E13 to E15. (A) At E13, obviously NR3A positive staining was detected in the radial oriented cells in the retina (showed by empty arrows). (B) NR3A expression at E14 was similar to that at E13. However, there was some weak staining on the retina axons (showed by solid arrows) beside to the radial cells staining. (C) At E15, NR3A immunoreactive signal was quite different from that at E13 and E14. The prominent positive staining was observed on the inner layer (showed by arrows), the expression of NR3A on the retinal axons was very weak. Furthermore, some radial cell staining was also detected on the section. (D to F) From E13 to E15, the NR3A immunoreactivity in the ventral diencephalon was quite similar. The positive staining was observed all over the ventral diencephalon, but a little stronger on the optic stalk and optic tract. (G) Western-blot analyses showing the specificity of NR3A antibody. A band at about 130 kDa (Indicated by arrow) was detected in the adult retina (AR), E15 retina (E15 R) and E15 ventral diencephalon (E15 VD).

Scale bar: A, B, C, 100 μm; D, E, F, 200μm.

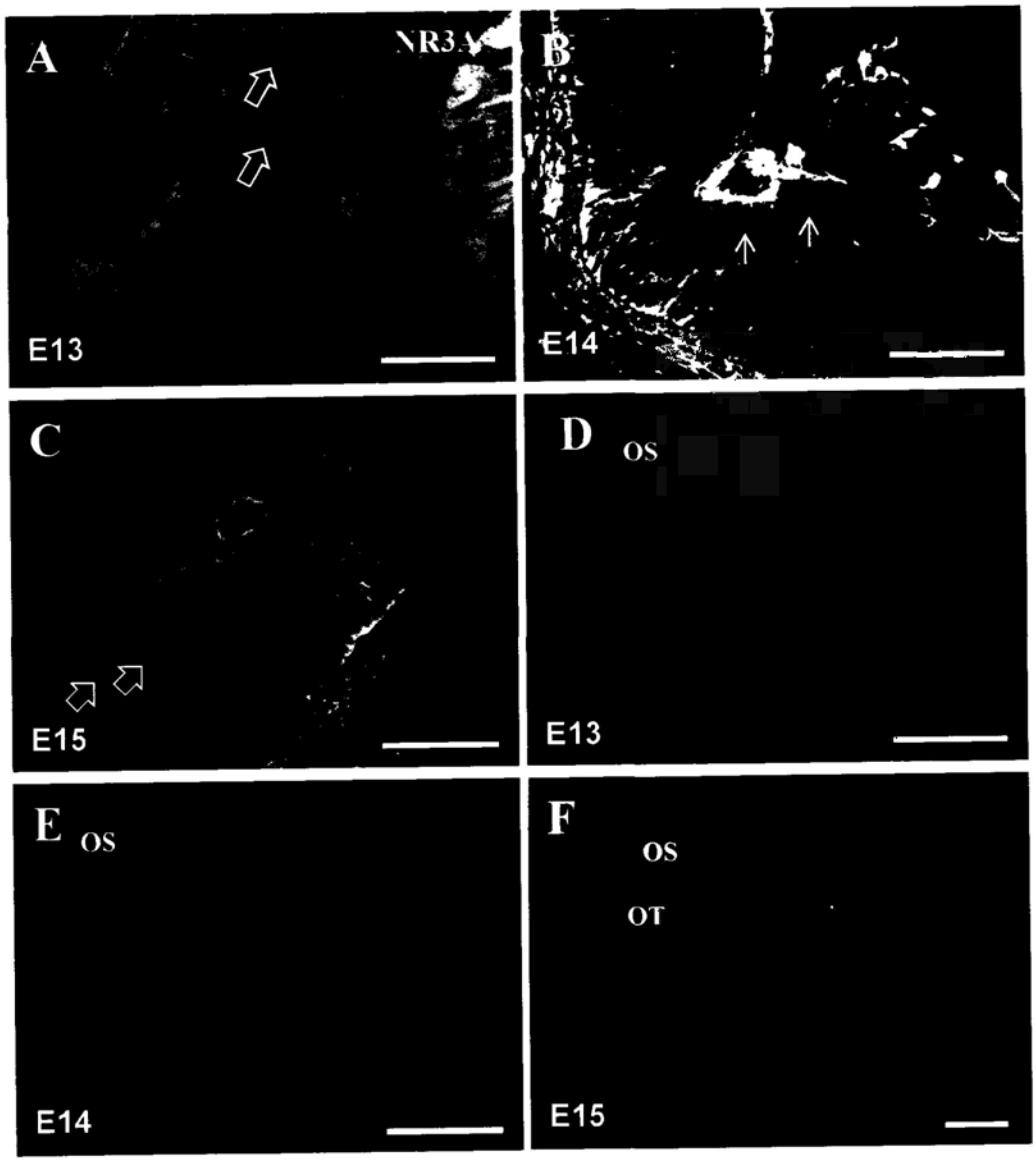
A
NR3A
E13
B
E14
C
E15
D
OS
E13
E
OS
E14
F
OS
OT
E15

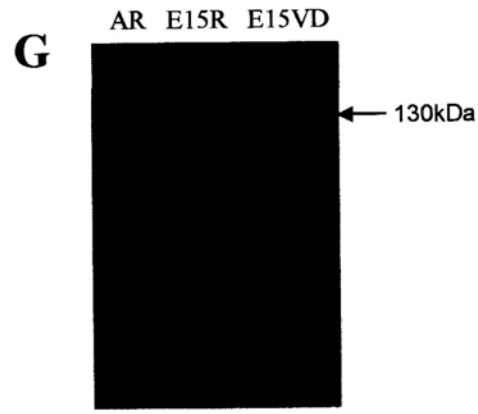
G
AR E15R E15VD
130kDa

Figure 6 Confocal photomicrographs revealed that nearly all the NR1 was distributed in the TuJ-1 positive neurons at E15. (A) NR1 was mainly expressed in the retinal axons and inner cell layer. (B) TuJ-1 positive neurons were located in the retinal axons and inner layer as well. (C) The merged image showed that NR1 positive signals were prominently located on the TuJ-1 immunoreactive signals, indicating that NR1 was expressed in RGCs and their axons.

Scale bar: 100 μm.

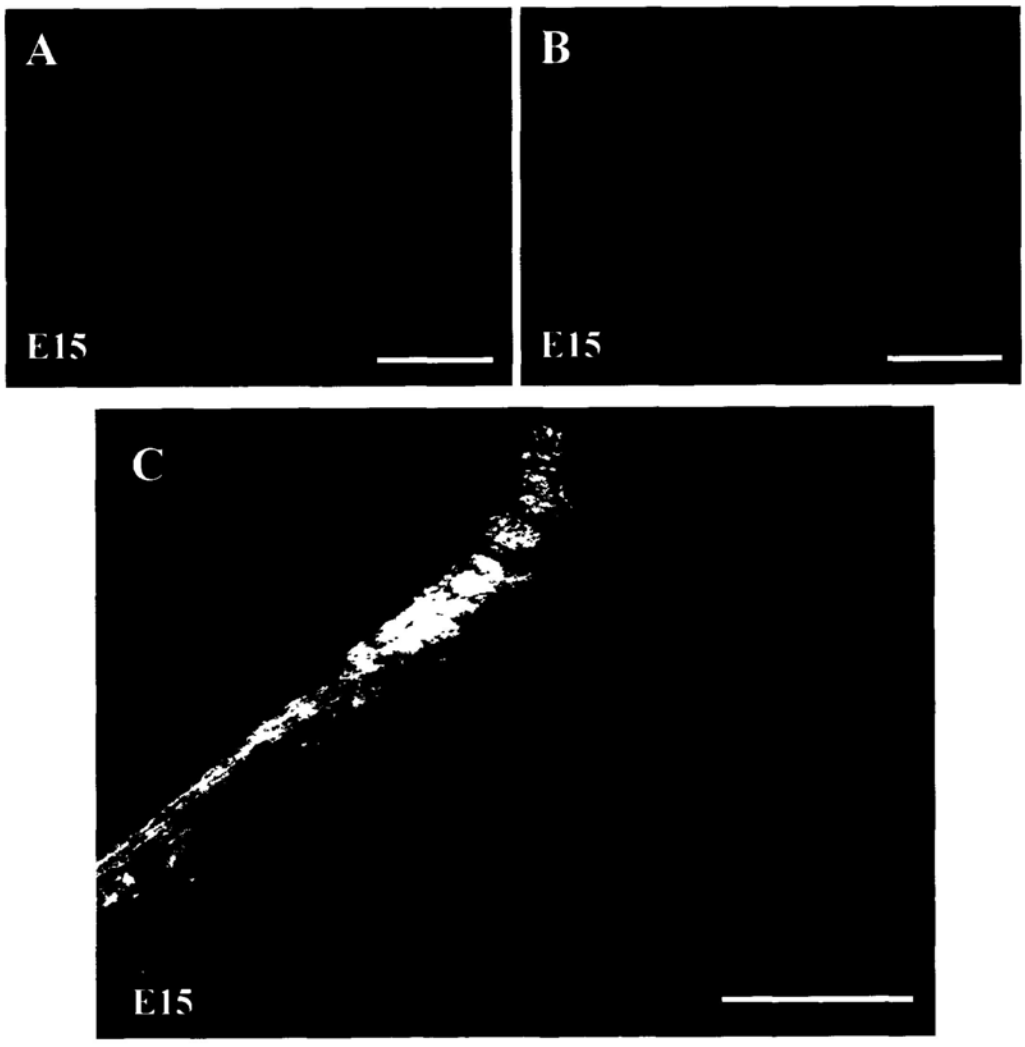
A
E15
B
E15
C
E15

Figure 7 Confocal photomicrographs showed that most NR2B positive cells were not colocalized with TuJ-1 positive neurons at E15. (A) The stronger staining of NR2B was detected in the fiber layer and inner cell layer in the retina, while some radial cells in other parts of retina were also NR2B positive. (B) TuJ-1 positive signals were detected mainly on the retinal axons and the inner cell layer. (C) In the merged image, most NR2B positive cells in the inner cell layer were not colocalized with TuJ-1 positive neurons.

Scale bar: 100 μm.

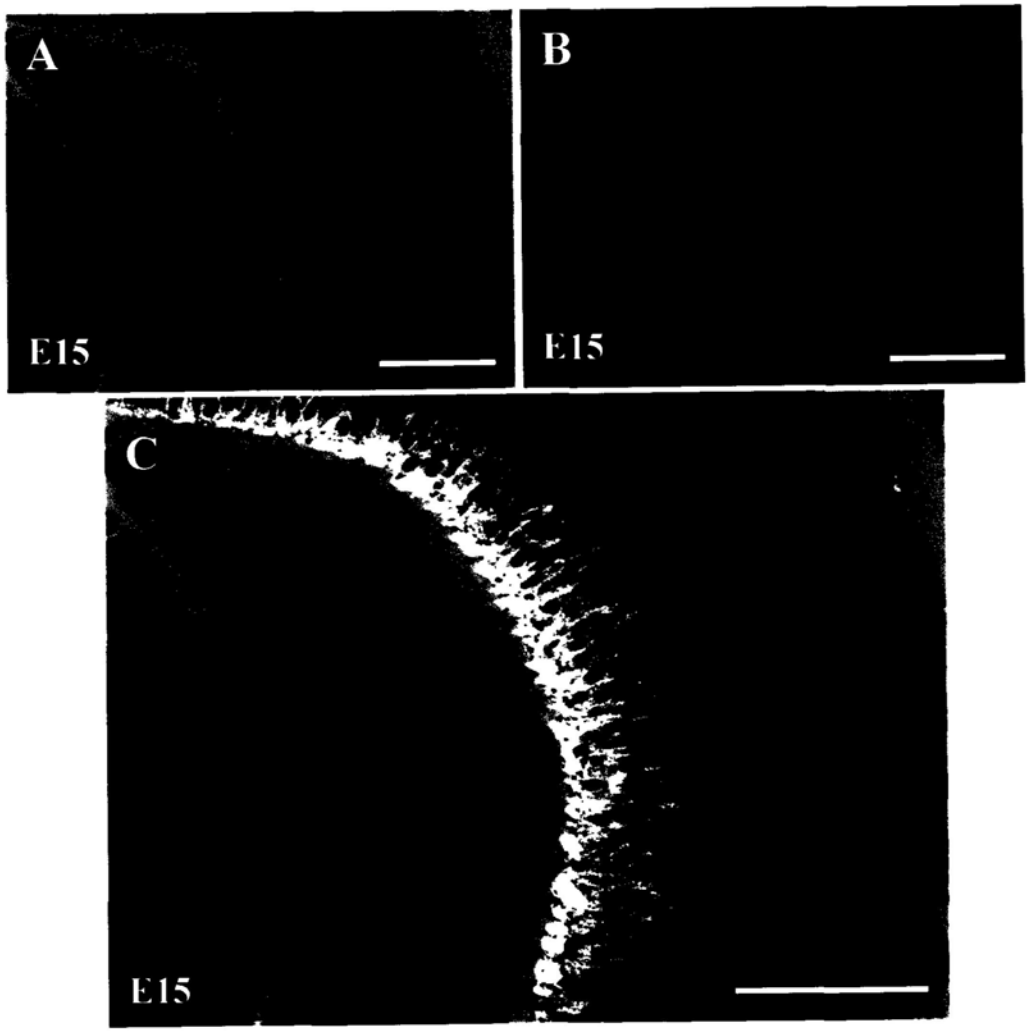
A
E15
B
E15
C
E15

Figure 8 Confocal photomicrographs showing that some of the NR3A positive cells were colocalized with RGCs, which were immunoreactive for TuJ-1 at mouse embryonic retina. (A) Besides on the retinal axons and inner cell layer, NR3A positive staining was also observed on some elongating cells in the E15 retina. (B) TuJ-1 positive signals were detected mainly on the retinal axons and the inner cell layer. (C) The merged image showed that some NR3A was expressed on the RGCs and their axons, which appeared yellow in color.

Scale bar: 100 μm.

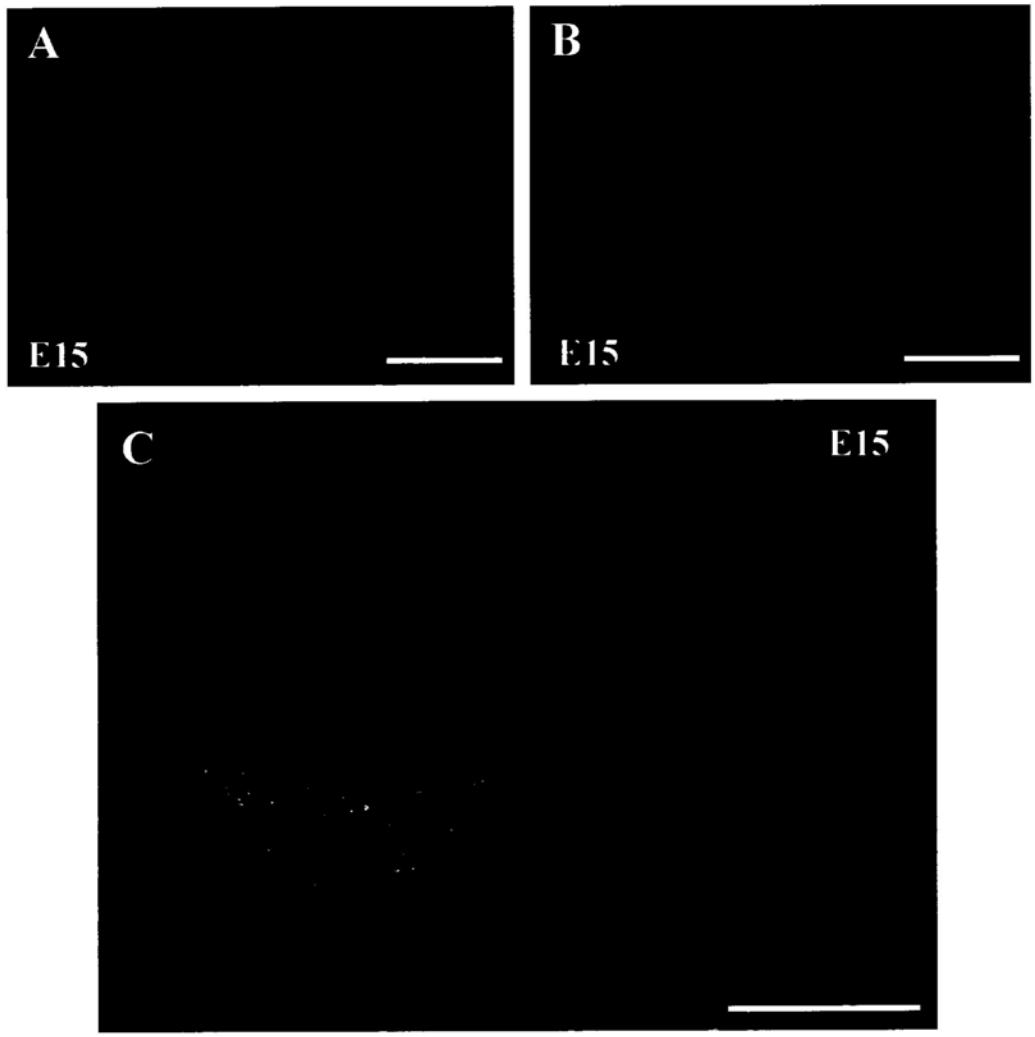
A
E15
B
E15
C
E15

Figure 9 Neurite outgrowth form retinal explant was inhibited by Dextrorphan-D-tartrate. The explants were taken from retina of embryos at E14. In order to enhance the contrast of the neurites, the "Find Edge" filter in the Photoshop was used to obtain all the micrographs. (A) Without addition of Dextrorphan-D-tartrate, the control group of retina explants showed extensive neurite outgrowth after 18h in culture. (B-E) The neurite outgrowth was obviously inhibited by the presence of Dextrorphan-D-tartrate in different concentration from 50μmole/ml to 500μmole/ml.

Scale bar: 500 μm.

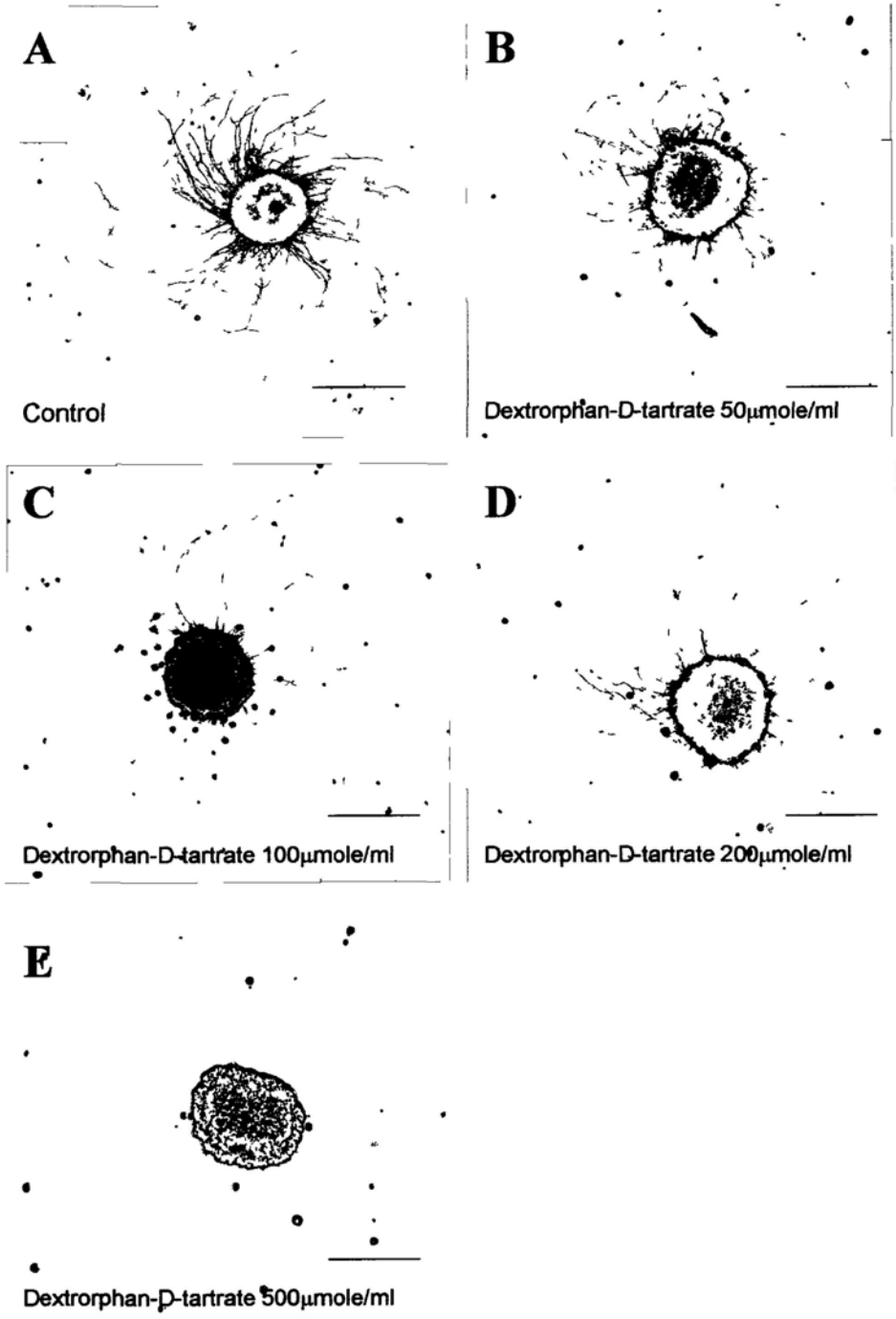
A
Control
B
Dextrorphan-D-tartrate 50μmole/ml
C
Dextrorphan-D-tartrate 100μmole/ml
D
Dextrorphan-D-tartrate 200μmole/ml
E
Dextrorphan-D-tartrate 500μmole/ml

Figure 10 Effects of MK-801 on the outgrowth of neuritis from E14 retinal explants. (A) After 18h in culture, the control explants showed extensive neurite growth. (B-D) In the presence of a serial concentration of MK-801 (50μmole/ml to 100μmole/ml), an obvious reduction in neurite outgrowth was observed in retina explants.

Scale bar: 500 μm.

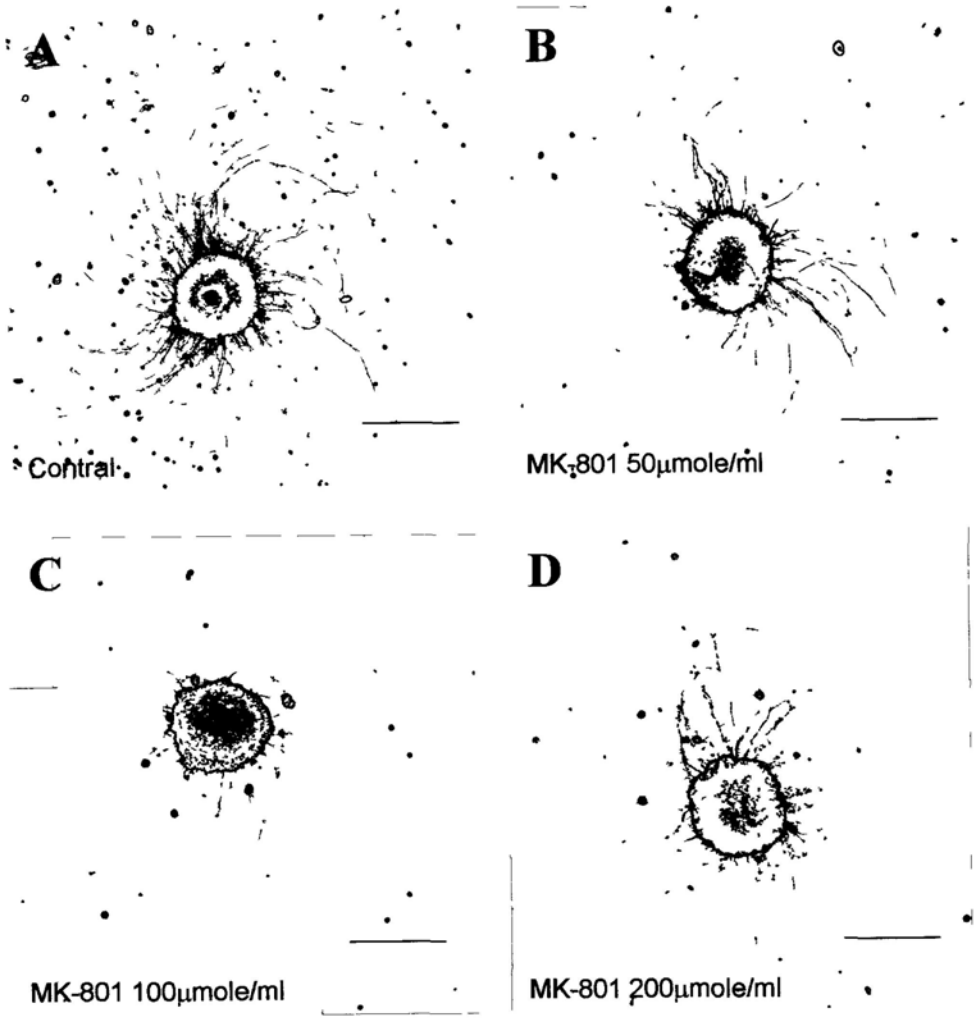
A
Contral
B
MK-801 50μmole/ml
C
MK-801 100μmole/ml
D
MK-801 200μmole/ml

Figure 11 Two plots of the results on the explants culture study, showing the significant reduction effect of different concentrations of Dextrorphan-D-tartrate and MK-801 separately at E14 mouse retina. (A) In the presence of 50-500μmole/ml Dextrorphan-D-tartrate, the neurite outgrowth from the E14 retina was significant inhibited, when compared with controls that were not added Dextrorphan-D-tartrate (indicated by asterisk, $p < 0.05$ or 0.001). (B) The retina neurite outgrowth was significantly reduced by MK-801, in the concentrations 50-200μmole/ml, compared with control groups (indicated by asterisk, $p < 0.01$ or 0.001).

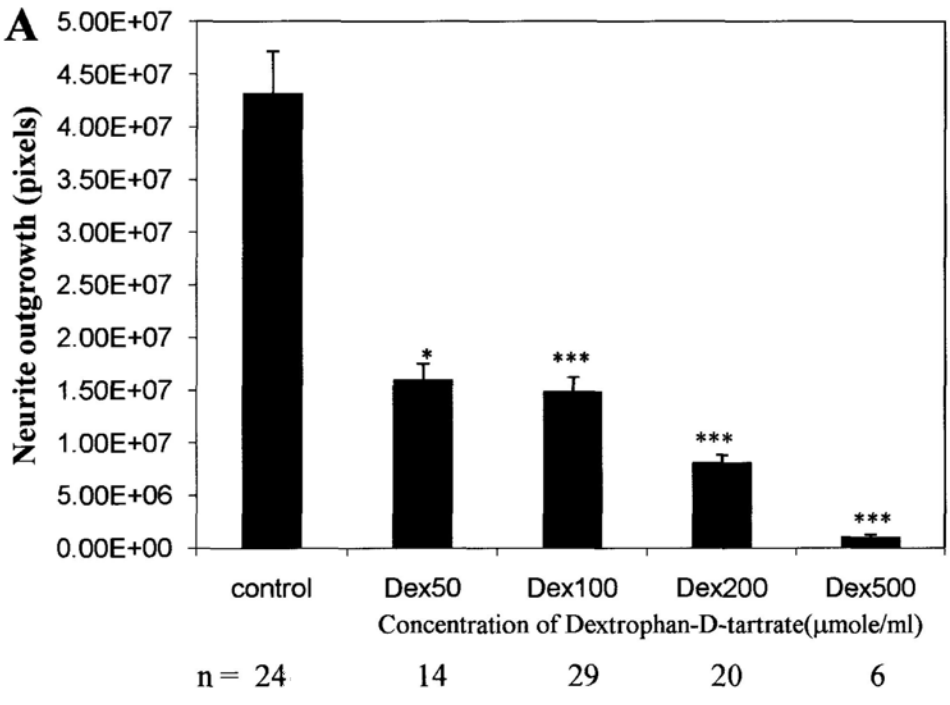

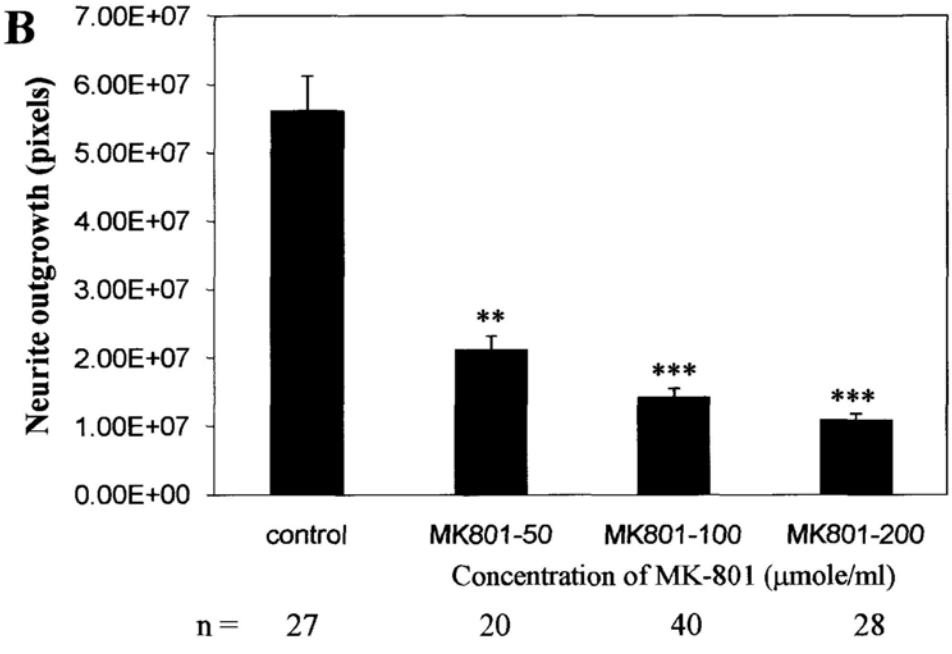

* $P < 0.05$
** $P < 0.01$
*** $P < 0.001$

CHAPTER 5

Routing of retinal axons in the retinofugal pathway of *Sox10*^{Dom} mutant and γA-crystallin mutant embryos

Introduction

Sox10, which is a member of SoxE subfamily, encodes a transcription factor expressed in neural crest cells (NCCs) and plays an important role in neural crest (NC) development (Kapur, 1999). The expression of *Sox10* is observed in NC at premigration stage, maintained transiently in migrating cells, and then lost due to their differentiation. *Sox10* contributes to the formation of NCCs, maintaining their multipotency, specifying a subset of NCCs fates, and differentiating into specific cell types (Kelsh, 2006).

Sox10 mutants are good models to study the essential function of *sox10* during NC development. So far there are two mutations that have been examined in mice: a null mutation which is generated by targeted deletion; and a spontaneous mutation, which is characterized by Dominant megacolon, known as *Sox*^{Dom} (Britsch et al, 2001; Stanchina et al, 2006). *Sox10*$^{Dom/+}$ mutants lack enteric gangalia in their distal large intestine, and display pigmentation defects. *Sox10*$^{Dom/Dom}$ mutants are always dead pre- or perinatally and have several NC deficits, such as a complete lack of enteric nervous system and melanocytes (Britsch et al, 2001; Kapur, 1999; Stanchina et al, 2006). But it is largely unknown if *Sox10* is involved in the optic pathway development.

Crystallins, which belong to the small heat shock protein family, are the

predominant structural proteins in the lens (Andley, 2007). They involve in the transparency and refractive properties of the lens through a uniform concentration gradient (Andley, 2007; Graw, 2009a). Vertebrate lens crystallins can be divided into two major families, α and βγ. γA-crystallins are molecular chaperons, and are essential for delaying age-related cataract (Andley, 2008; Andley, 2009a; Andley, 2009b; Sharma & Santhoshkumar, 2009). In addition, γA-crystallins have been found outside the lens. They are also expressed in the retina, brain, spleen, thymus, skin and so on, but their roles in these tissues still remain unclear (Andley, 2007). βγ-Crystallins are thought to affect the lens development, and exist in the tissues outside the lens as well, suggesting they may have some underlying functions, such as functioning as stress proteins in the retina (Andley, 2007; Graw, 2009b; Sharma & Santhoshkumar, 2009).

The functions of crystallins can be easily investigated using ctystallin mutants, and most studies focused on their functions in the lens (Andley, 2009a; Andley & Reilly, 2010; Gong et al, 2010; Ji et al, 2010). As crystallins are also expressed in the retina, our hypothesis is that crystallins may have some functions in the development of the optic pathway.

In this part of study, using axon routing technique, we investigated the development of optic pathway in the *Sox10*^{Dom} mutant embryos and γA-crystallin mutant embryos.

Materials and Methods

Animal

Sox10^{Dom} mutant embryos have been kindly provided by Prof. Woody Chan, The Chinese University of Hong Kong.

γA-Crystallin mutant embryos have been kindly provided by Prof. MH Sham, The University of Hong Kong.

Routing of retinal axons in the retinofugal pathway

The heads of the mutant embryos were fixed with 4% paraformaldehyde in 0.1M phosphate buffer (PB, pH 7.4) 1-2 days at 4°C. Several granules of DiI (1,1' -Dioctadecyl-3,3,3',3'-etramethylindo-carbocyanine perchlorate, $DiIC_{18}(3)$ from Molecular Probes, OR, USA) were put onto the optic disk of one eye. The heads of these mutant embryos were stored in 2% formalin in dark at room temperature. For the E13 embryos, it took about seven days for the DiI to diffuse along the retinal axons in the retinofugal pathway. For the older embryos, it needed longer time, about 2 weeks in E14 embryos and 3 weeks in E15 embryos. After that, the heads were taken out to remove the tissue and expose the DiI labeled chiasm.

Analyses of retinal trajectory in the optic chiasm

The whole mount preparations of DiI labeled optic pathway were examined by a confocal microscope (FV300, Olympus Co, Japan). The fluorescent signals of the optic pathway were collected by serially capturing projected images. Meanwhile the transmitted images were also captured to show the midline of ventral diencephalon. For analyzing the midline crossing, pixel intensities of all labeled retinal axons and growth cones within a defined region flanking both sides of the midline were measured individually using MetaMorph Software. The ratio of pixel intensity in the post-midline region versus that in the pre-midline region was used to represent the degree of axon crossing in the midline. For $Sox10^{Dom}$ mutant embryos, the axon crossing from E13.5 to E15.5 was analysed in all groups. For γA-crystallin mutant embryos, the axon crossing was only analysed in E13.5 embryos. Instead of analysing midline crossing, we analysed the retino-retinal projection from E14.5 to

E15.5 in γA-crystallin mutant embryos. Here, piexel-intensity of all axons in the two optic stalks was measured, and the ratio of reading in the contralateral stalk versus that in the ipsilateral stalk was used to indicate the extent of growth of retino-retinal projection. In addition, optic pathways of E14.5 and E15.5 mutant embryos were also studied for the uncrossed pathway in all groups. Here, we measured the pixel intensities in a defined region or counted the number of axons in the uncrossed projection in the optic tract. The data obtained from the *Sox10*^{Dom} mutants or γA-crystallin mutants were compared with those from *Sox10* $^{+/+}$ or wild-type controls, using Kruskal-Wallis non-parametric test (GraphPad Inc., USA).

Results

Sox10 did not affect axon midline crossing and uncrossed axons in the chiasm

In the E13.5 ventral diencephalon of *Sox10* $^{+/+}$ embryos (n=7), DiI labeled retinal axons in the optic stalk enter the chiasm first in a caudo-medial direction, and later turn and grow perpendicularly to the midline. After crossing the midline, these axons continue to enter the optic tract (Fig. 1A). *Sox10* $^{Dom/+}$ heterozygous (n=9) and S*ox10*$^{Dom/Dom}$ homozygous (n=5) embryos revealed a similar axon routing pattern in the ventral diencephalon as wild-type embryos (Fig. 1B and C). Statistical analyses of axon crossing in the midline showed that no significant change of crossed pathway were found in *Sox10* $^{+/+}$, *Sox10*$^{Dom/+}$ and *Sox10*$^{Dom/Dom}$ groups (Fig. 1D).

At E14.5, a substantial number of RGC axons had already grown through the optic chiasm in *Sox10* $^{+/+}$ embryos (n=6); most of these axons crossed the midline and projected to the contralateral optic tract, while a number of retinal axons did not cross the midline and made a turn to enter the ipsilateral optic tract (Fig. 2A). In the *Sox10*$^{Dom/+}$ (n=7) and *Sox10*$^{Dom/Dom}$ (n=4) embryos, similar axon trajectories were

observed when compared with wild-type embryos (Fig. 2B and 2C). No significant difference was found by comparing the relative quantities of the crossing axons in these three groups (Fig. 2D). The uncrossed projections in these three groups had no significant difference as well (Fig. 2E).

In E15.5 *Sox10* $^{+/+}$ embryos (n=1), a large number of uncrossed axons were observed in the optic chiasm (Fig. 3A). Similar observation were also found in the *Sox10*$^{Dom/+}$ (n=6) and *Sox10*$^{Dom/Dom}$ (n=3) embryos (Fig. 3B and 3C). There was no significant difference of the crossing axons and uncrossed axons in these three groups (Fig. 3D and 3E).

γA-crystallin mutation did not affect axon routing in the optic chiasm

At E13.5, DiI labeled studies showed a number of retinal axons grew through the optic stalk and crossed the midline to project into the contralateral optic tract in the wild-type group (n=6), γA-crystallin$^{+/-}$ heterozygous group (n=5) and γA-crystallin$^{-/-}$ homozygous group (n=5) (Fig. 4A, 4B and 4C). Statistic comparison of the relative quantities of the axon crossing the midline indicated that there was no significant difference in these three groups (Fig.4D).

In E14.5 optic chiasms, the retino-retinal projection can be seen in the wild-type group (n=2) (indicated by open arrow, Fig. 5A1). A number of uncrossed retinal axons were observed clearly in the ventral diencephalon at this stage as well, when examined in higher magnification (Fig. 5A2). In γA-crystallin$^{+/-}$ heterozygous (n=3) and γA-crystallin$^{-/-}$ homozygous (n=4) groups, DiI labeled retinal axons revealed similar trajectories as in wild-type group (Fig. 5B and 5C). There was no significant difference in relative quantities of retino-retinal projection in these three groups (Fig. 5D). After comparing the number of uncrossed axons in these three groups, no significant change was found in the average number of uncrossed axons

as well (Fig. 5E).

In E15.5 embryos, DiI labeled retinal axons showed similar trajectories in the ventral diencephalon in wild-type (n=6), γA-crystallin$^{+/-}$ (n=4) and γA-crystallin$^{-/-}$ (n=6) groups when compared with that of E14.5. Beside the observation of retino-retinal projection, a large number of uncrossed axons were observed in ipsilateral optic tract (Fig. 6A, 6B and 6C). Still there was no significant difference of relative quantities of retino-retinal projection in these three groups (Fig. 6D). For the quantities of uncrossed axons, there was no significant difference between wild-type and γA-crystallin$^{+/-}$ group (or γA-crystallin$^{-/-}$ group). But significant reduction was found in γA-crystallin$^{-/-}$ group when compared with γA-crystallin$^{+/-}$ group ($P<0.05$, Fig. 6E).

Discussion

In this part of study, we investigated the axon routing in the developing optic pathway in the *Sox10^{Dom}* mutant embryos and γA-crystallin mutant embryos. It was found that the crossing axons and uncrossed axons are quite normal from E13.5 to E15.5 in the *Sox10^{Dom}* mutant embryos. It suggests that *Sox10* may not contribute to axon guidance in the developing optic pathway. For the γA-crystallin mutant embryos, there is no change in the crossing axons at E13.5, when compared with that of wild-type embryos. From E14.5 to E15.5, we investigated the retino-retinal projection in γA-crystallin mutants. Retino-retinal projection is formed by retinal axons transiently grow through the opposite optic nerve, which will disappear shortly after birth (Bunt & Lund, 1981; Tennant et al, 1993; Thanos, 1999). Here, we found that there is no significant difference of the retino-retinal projection at E14.5 and E15.5 between γA-crystallin mutant embryos and wild-type embryos. So

γA-crystallin may not involve in the formation of retino-retinal projection. However, γA-crystallin may play a role in the later uncrossed axons, as a significant reduction in the uncrossed axon at E15.5 in the γA-crystallin$^{-/-}$ group were observed when compared with that in the γA-crystallin$^{+/-}$ group. The function of γA-crystallin in the uncrossed axons may worth to be further investigated.

Figures

Figure 1 Retinal axon routing at the chiasmatic midline of E13.5 *Sox10* $^{+/+}$, *Sox10*$^{Dom/+}$ and *Sox10*$^{Dom/Dom}$ embryos. The confocal micrographs in the left column are images in lower magnification showing the optic stalk, chiasm and optic tract in the whole-mount preparations of the retinofugal pathway, and those in the right column are images in higher magnification showing the details. The midline was indicated by white arrows. (A) DiI labeled retinal axons in the E13.5 ventral diencephalon of *Sox10* $^{+/+}$ embryos showed that retinal axons in the optic stalk enter the chiasm first in a caudo-medial direction, and later turn and grow perpendicularly to the midline. After crossing the midline, these axons continue to enter the optic tract. (B and C) *Sox10* $^{Dom/+}$ heterozygous and *Sox10*$^{Dom/Dom}$ homozygous embryos revealed a similar axon routing in the ventral diencephalon as *Sox10* $^{+/+}$ embryos. (D) The plot showed the statistical analyses of axon crossing in the midline in *Sox10* $^{+/+}$, *Sox10*$^{Dom/+}$ and *Sox10*$^{Dom/Dom}$ groups. There was no significant change of crossed pathway in these three groups.

Scale bar: 200μm.

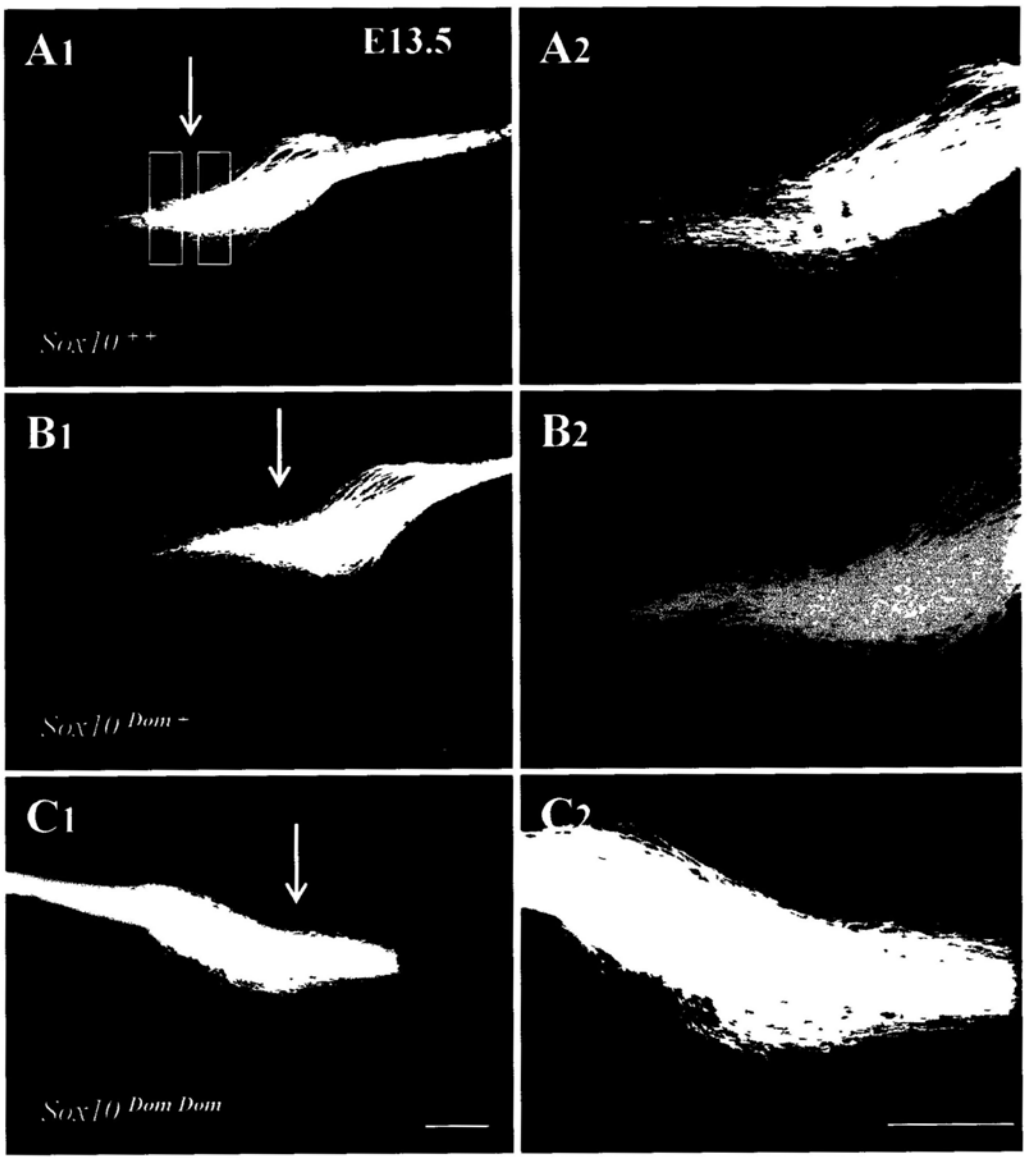
A1
E13.5
A2
Sox10 ++
B1
B2
Sox10 Dom +
C1
C2
Sox10 Dom Dom

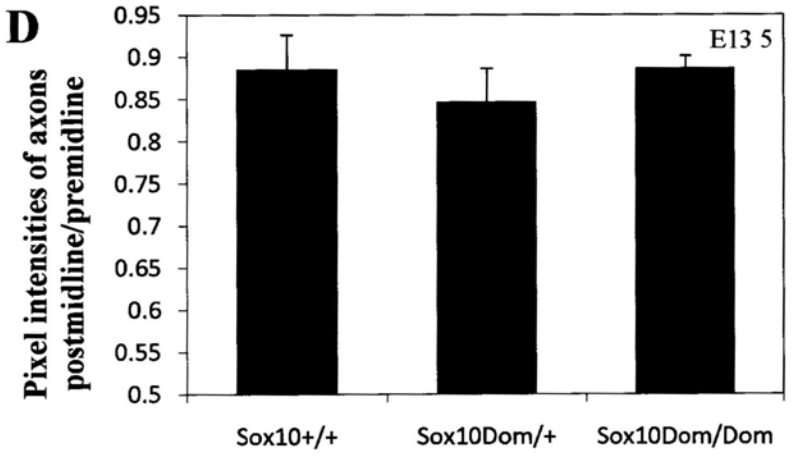
D
Pixel intensities of axons postmidline/premidline
0.95
0.9
0.85
0.8
0.75
0.7
0.65
0.6
0.55
0.5
E13 5
Sox10+/+
Sox10Dom/+
Sox10Dom/Dom

Figure 2 Retinal axon routing at the chiasmatic midline of E14.5 *Sox10* $^{+/+}$, *Sox10*$^{Dom/+}$ and *Sox10*$^{Dom/Dom}$ embryos. The confocal micrographs in the left column are images in lower magnification showing the optic pathway in E14.5 ventral diencephalon, and those in the right column are images in higher magnification showing uncrossed axons. The midline was indicated by white arrows. (A) In E14.5 optic chiasm of *Sox10* $^{+/+}$ embryos, a number of retinal axons did not cross the midline and made a turn to enter the ipsilateral optic tract (indicated by the white square). (B and C) Similar axon routing in the chiasm were observed in the *Sox10*$^{Dom/+}$ and *Sox10*$^{Dom/Dom}$ embryos. (D and E) The plots showed the statistic results of crossing axons and uncrossed axons in *Sox10* $^{+/+}$, *Sox10*$^{Dom/+}$ and *Sox10*$^{Dom/Dom}$ groups. No significant difference was found by comparing the relative quantities of the crossing axons in these three groups. The uncrossed projections in these three groups had no significant difference as well.

Scale bar: 200μm.

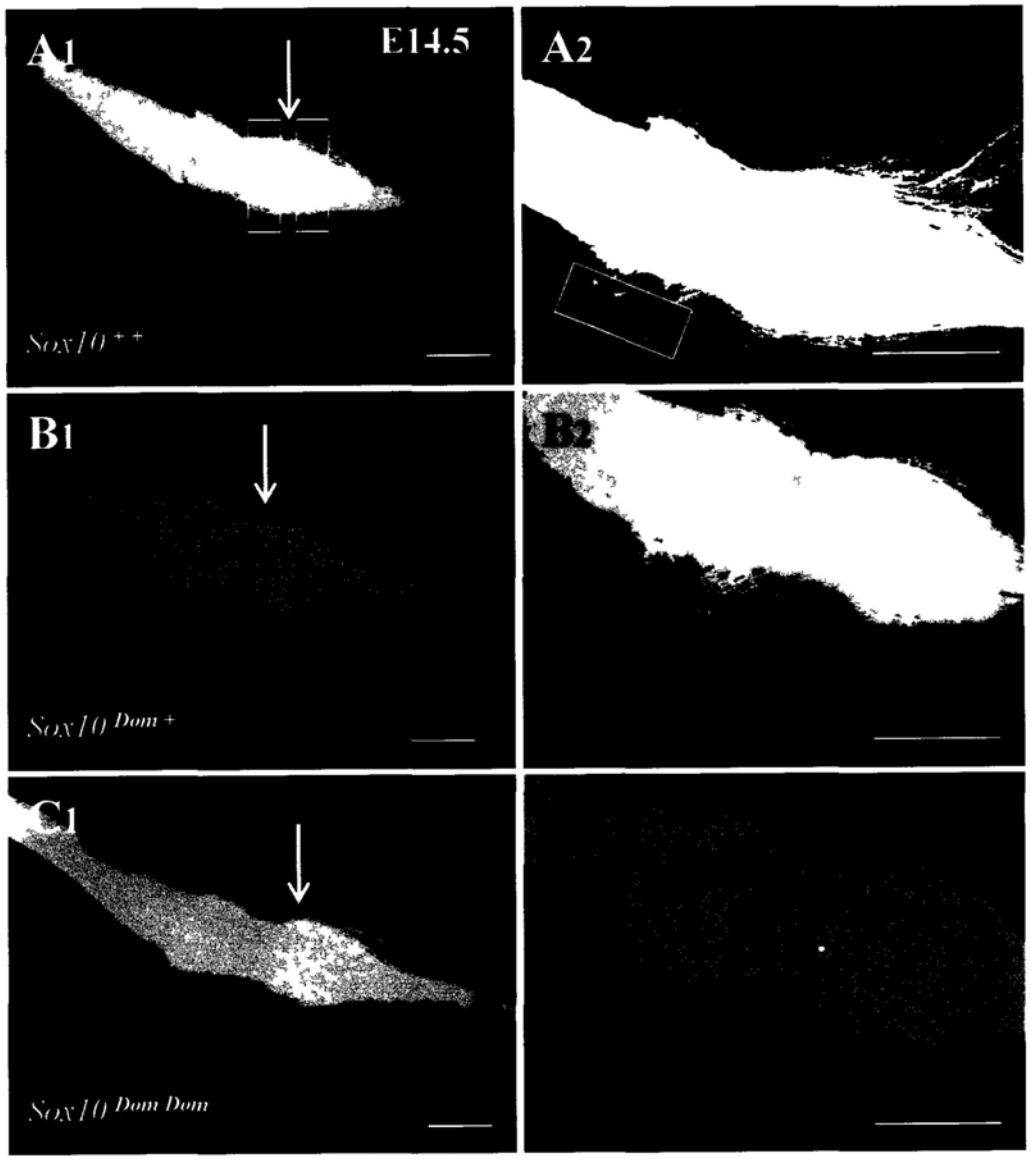
A1
E14.5
A2
Sox10 + +
B1
B2
Sox10 Dom +
C1
Sox10 Dom Dom

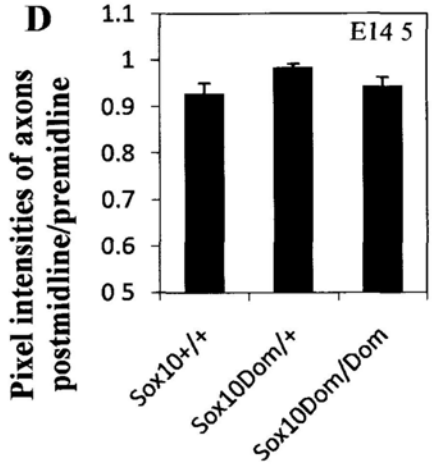
D
Pixel intensities of axons postmidline/premidline
1.1
1
0.9
0.8
0.7
0.6
0 5
E14 5
Sox10+/+
Sox10Dom/+
Sox10Dom/Dom

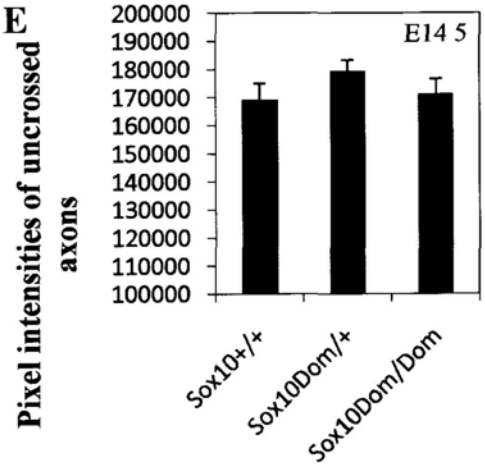
E
Pixel intensities of uncrossed axons
200000
190000
180000
170000
160000
150000
140000
130000
120000
110000
100000
E14 5
Sox10+/+
Sox10Dom/+
Sox10Dom/Dom

Figure 3 Retinal axon routing at the chiasmatic midline of E15.5 wild-type, *Sox10*$^{Dom/+}$ and *Sox10*$^{Dom/Dom}$ embryos. The confocal micrographs in the left column are images in lower magnification showing the optic pathway in E15.5 ventral diencephalon, and those in the right column are images in higher magnification showing uncrossed axons. The midline was indicated by white arrows. (A) In images of DiI labeled optic pathway in E15 ventral diencephalon, a large number of uncrossed axons were observed in the optic chiasm. (B and C) Similar observations were found in the *Sox10*$^{Dom/+}$ and *Sox10*$^{Dom/Dom}$ embryos. (D and E) The plots showed the statistic results of crossing axons and uncrossed axons in *Sox10* $^{+/+}$, *Sox10*$^{Dom/+}$ and *Sox10*$^{Dom/Dom}$ groups. There was no significant difference of the crossing axons and uncrossed axons in these three groups.

Scale bar: 200μm.

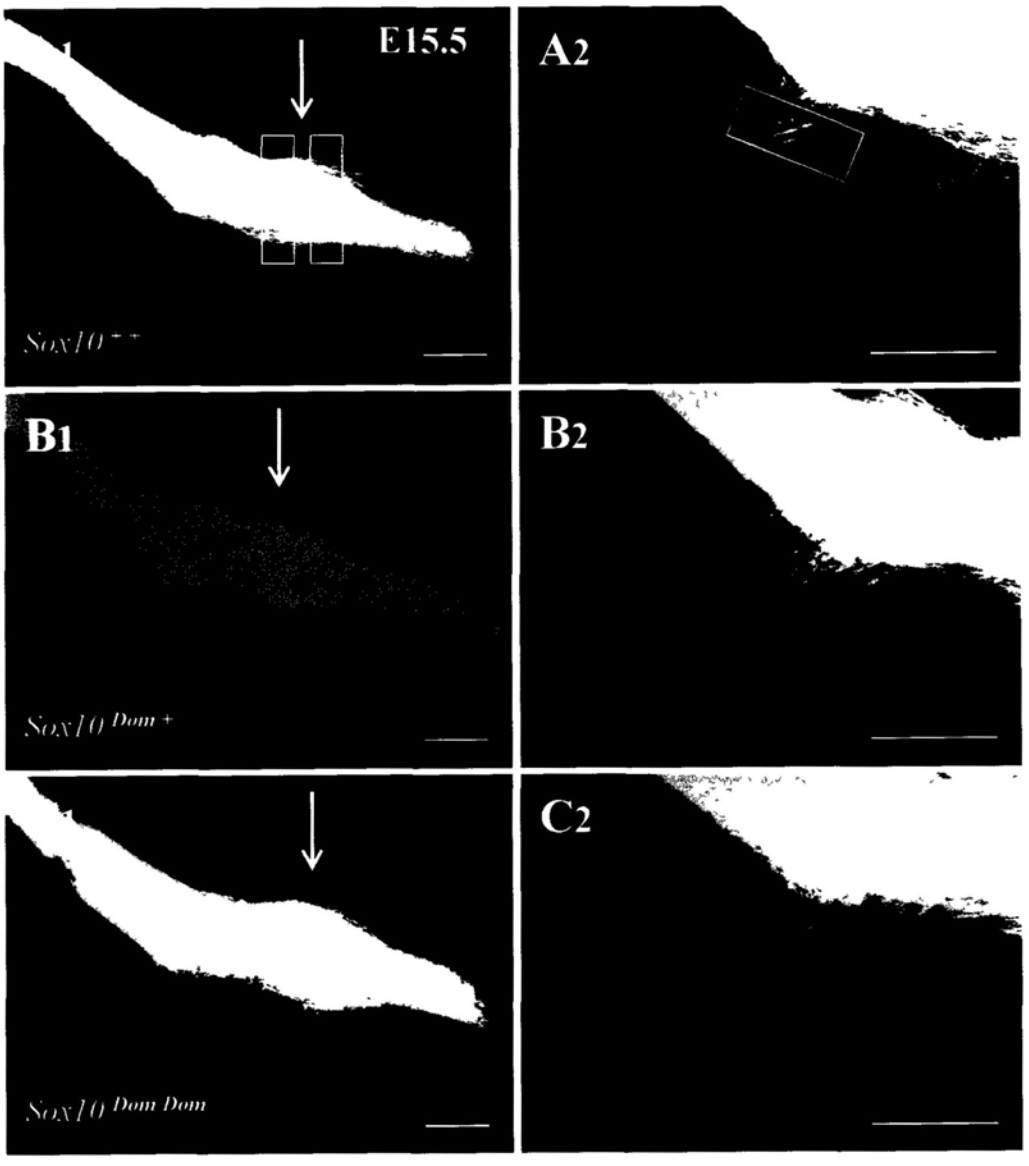
E15.5
A2
Sox10++
B1
B2
Sox10 Dom +
C2
Sox10 Dom Dom

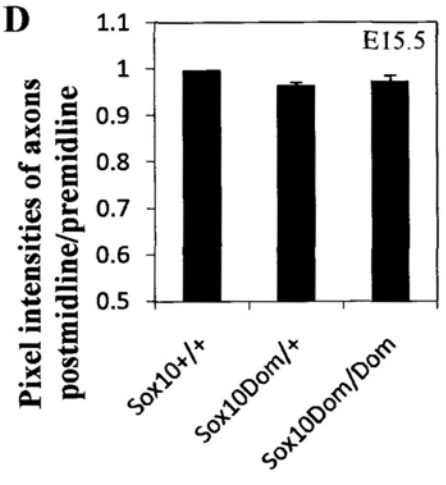
D
E15.5
Pixel intensities of axons postmidline/premidline
1.1
1
0.9
0.8
0.7
0.6
0.5
Sox10+/+
Sox10Dom/+
Sox10Dom/Dom

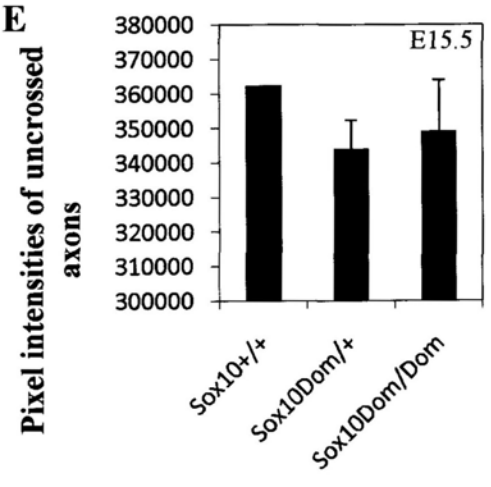
E
E15.5
Pixel intensities of uncrossed axons
380000
370000
360000
350000
340000
330000
320000
310000
300000
Sox10+/+
Sox10Dom/+
Sox10Dom/Dom

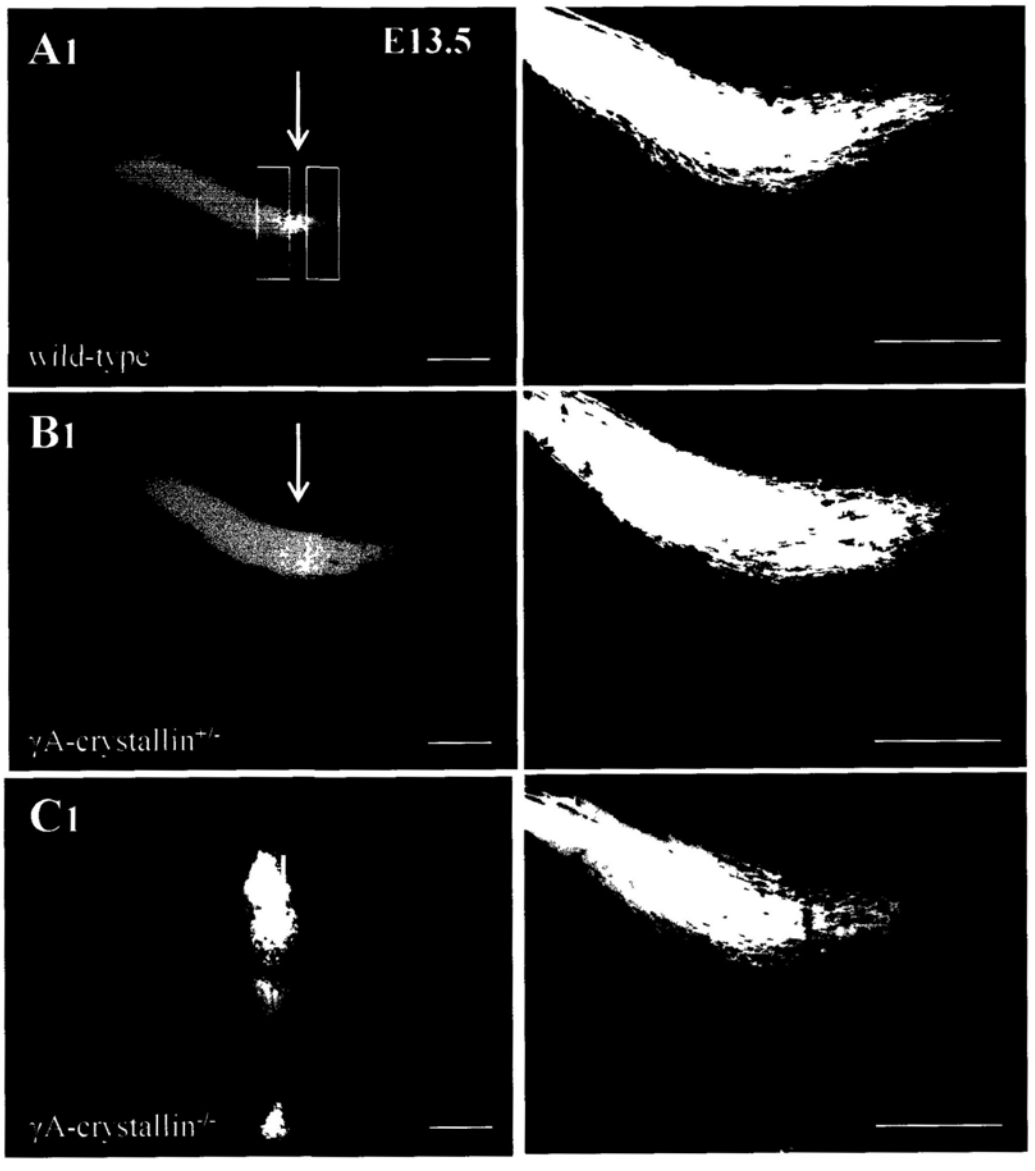
A1
E13.5
wild-type
B1
γA-crystallin+/-
C1
γA-crystallin-/-

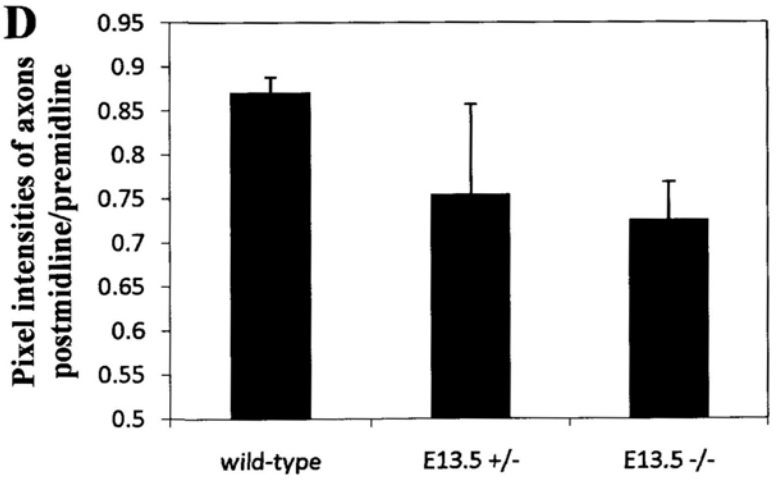
D
Pixel intensities of axons postmidline/premidline
0.95
0.9
0.85
0.8
0.75
0.7
0.65
0.6
0.55
0.5
wild-type
E13.5 +/-
E13.5 -/-

Figure 4 DiI labeled retinal axon trajectories in the optic chiasmatic in E13.5 wild-type, γA-crystallin$^{+/-}$ heterozygous and γA-crystallin$^{-/-}$ homozygous embryos. The confocal micrographs in the left column are images in lower magnification showing the optic pathway in the whole-mount preparations of the retinofugal pathway, and those in the right column are images in higher magnification showing the details. The midline was indicated by white arrows. (A) DiI labeled retinal axon trajectories in the optic chiasm in the wild-type group showed a number of retinal axons grew through the optic stalk and crossed the midline to project into the contralateral optic tract. (B and C) Similar retinal axon trajectories were observed in the γA-crystallin$^{+/-}$ heterozygous and γA-crystallin$^{-/-}$ homozygous groups. (D) The plot showed the statistic comparison of the relative quantities of the axons crossing the midline in wild-type, γA-crystallin$^{+/-}$ and γA-crystallin$^{-/-}$ groups. No significant difference was found in these three groups.

Scale bar: 200μm.

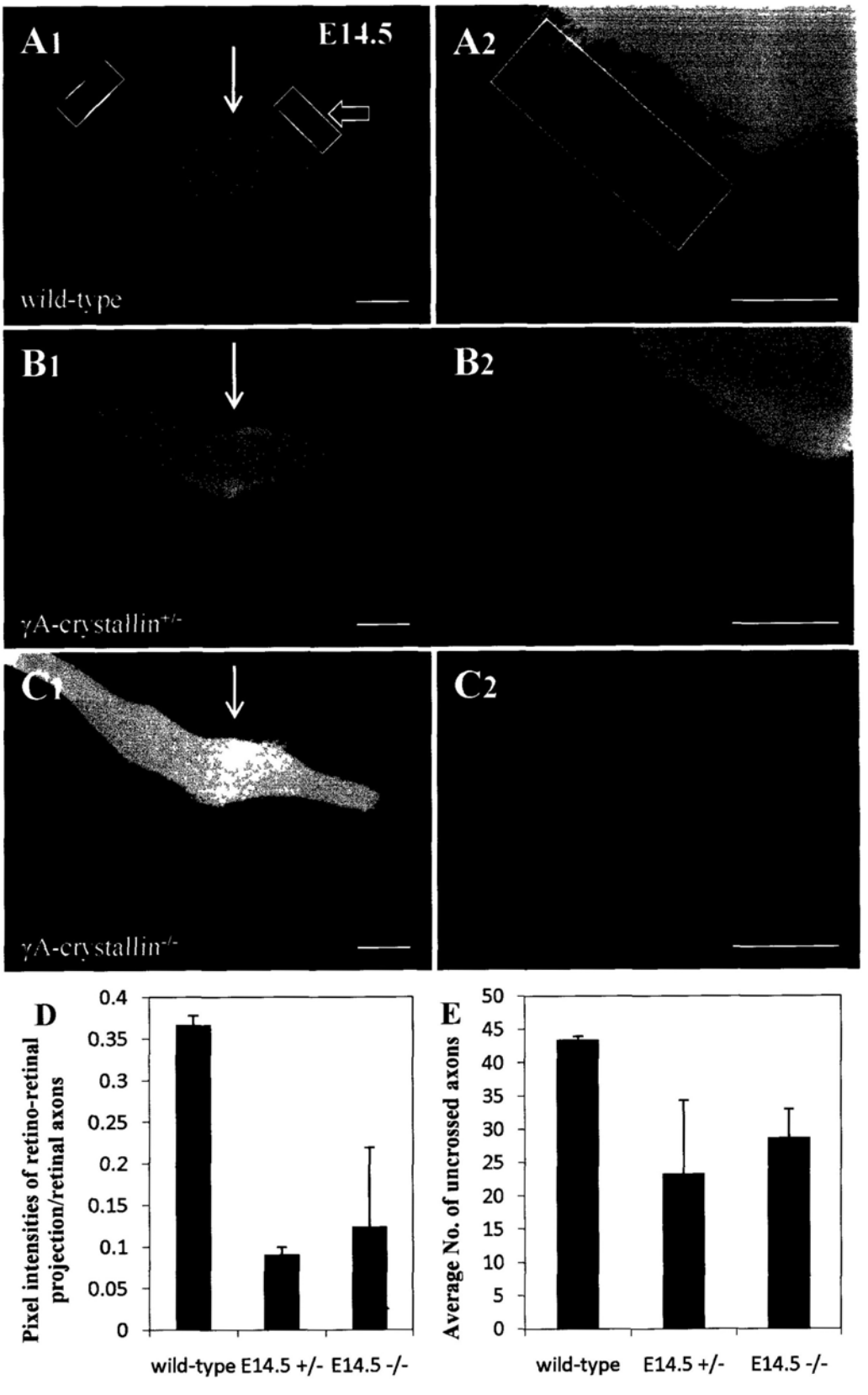
A1
E14.5
A2
wild-type
B1
B2
γA-crystallin+/-
C1
C2
γA-crystallin-/-
D
Pixel intensities of retino-retinal projection/retinal axons
0.4
0.35
0.3
0.25
0.2
0.15
0.1
0.05
0
wild-type
E14.5 +/-
E14.5 -/-
E
Average No. of uncrossed axons
50
45
40
35
30
25
20
15
10
5
0
wild-type
E14.5 +/-
E14.5 -/-

Figure 6 DiI labeled retinal axon trajectories in the optic chiasmatic in E15.5 wild-type, γA-crystallin$^{+/-}$ heterozygous and γA-crystallin$^{-/-}$ homozygous embryos. The midline was indicated by white arrows. (A) In E15.5 wild-type group, DiI labeled retinal axons showed similar trajectories in the ventral diencephalon when compared with that of E14.5 wild-type group. Beside the observation of retino-retinal projection, a large number of uncrossed axons were observed in ipsilateral optic tract. (B and C) Similar observations were found in the γA-crystallin$^{+/-}$ and γA-crystallin$^{-/-}$ groups. (D) Still there was no significant difference of relative quantities of retino-retinal projection in these three groups. (E) For the quantities of uncrossed axons, there was no significant difference between wild-type and γA-crystallin$^{+/-}$ group (or γA-crystallin$^{-/-}$ group). But significant reduction was found in γA-crystallin$^{-/-}$ group when compared with γA-crystallin$^{+/-}$ group ($P<0.05$).

Scale bar: A1, B1, C1, 200μm; A2, B2, C2, 100μm.

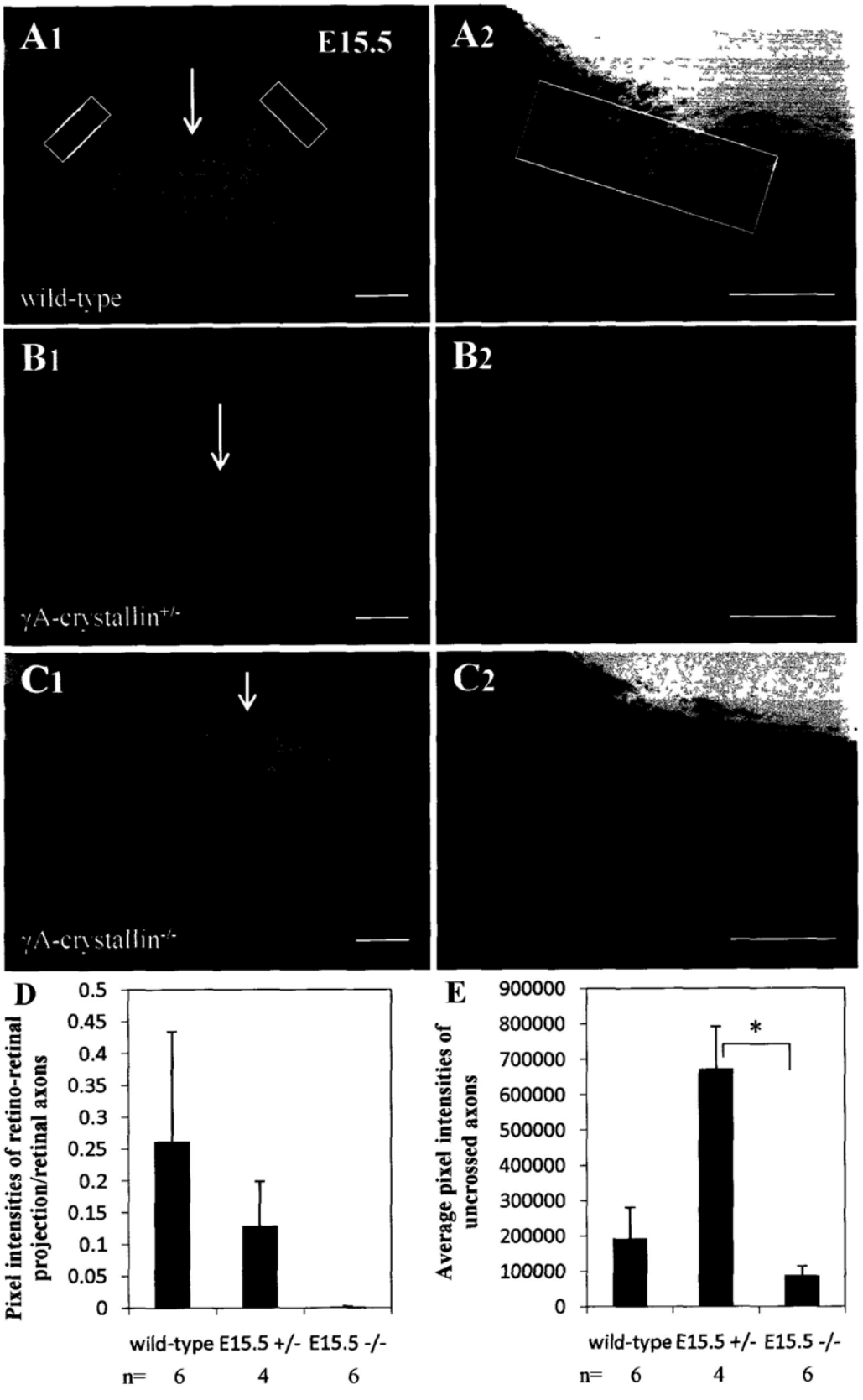
A1
E15.5
wild-type
A2
B1
γA-crystallin+/-
B2
C1
γA-crystallin-/-
C2
D
Pixel intensities of retino-retinal projection/retinal axons
0.5
0.45
0.4
0.35
0.3
0.25
0.2
0.15
0.1
0.05
0
wild-type
E15.5 +/-
E15.5 -/-
n= 6 4 6
E
Average pixel intensities of uncrossed axons
900000
800000
700000
600000
500000
400000
300000
200000
100000
0
*
wild-type
E15.5 +/-
E15.5 -/-
n= 6 4 6

CHAPTER 6
General Discussion

During the development of mouse optic pathway, RGC axons arising from each retina encounter each other at the ventral midline, where they establish an X-shaped axonal intersection—optic chiasm (Mason & Sretavan, 1997). However, RGC axons in each optic never do not merely cross one another at the optic chiasm, they make both contralateral and ipsilateral projections to each optic tract. This structure is crucial for the binocular vision (Guillery et al, 1995; Petros et al, 2008; Sretavan, 1990). The cellular environment of the developing ventral diencephalon is very important for the RGC axon pathfinding at the optic chiasm. There are two groups of cells, so called chiasm cells involved in this cellular environment: one is chiasmatic radial glia which straddle the midline, and the other is chiasmatic neurons which form a typical V-shaped array marking the boundary of crossed and uncrossed RGC axons (Marcus & Mason, 1995; Mason & Sretavan, 1997; Petros et al, 2008). As we know, almost all the cells in the brain are generated from ventricular zone (Morest & Silver, 2003; Pontious et al, 2008). Chiasm cells should also arise from there. But when these chiasm cells are generated, where do they go, and what their fates are still remain largely unknown. In this thesis, using the birthdating technique, we first birthdate chiasmatic radial glia and neurons respectively, and then we try to trace their fates at later stages of development.

In this part of study we use EdU instead of BrdU to birthdate chiasmatic cells and trace their fates. BrdU as an old classic birthdating chemical has a lot of deficiencies, such as long experimental time, complex experimental procedure and destruction of many epitopes after doing the DNA denature (Wojtowicz & Kee,

2006). In contrast, EdU as a new chemical used in birthdating technique make the experiments more effective, it reduces the experiment time, uses an easier procedure and maintains the antibody epitopes (Chehrehasa et al, 2009). So EdU is a good tool to do the birthdate studies.

Here, we birthdate the chiasmatic neurons first, and found that the first postmitotic cells in the mouse ventral diencephalon were generated around E9.5, most of them assemble at the posterior part of chiasm at E13 forming an inverted V-shaped array. Double staining analyses indicate that most of these first postmitotic cells are chiasmatic neurons. In addition, we found that still some chiasmatic neurons are generated at E10, but only a few of them are generated at E11. Cell counting analyses make these observations more consistent, suggesting that the majority of chiasmatic neurons are the first differentiated cells born at E9.5.

After knowing the birthdate of the chiasmatic neurons at E13, we are also curious about where these chiasmatic neurons go, and what their fates are at the later stages of development. So we continue to trace these neurons and try to find out their fates. Therefore, we fixed the injection day of EdU at E9.5, then observe the distribution these E13 EdU labeled chiasmatic neurons from E14 to E18. It was found that these chiasmatic neurons become fewer and fewer from E14 to E18. Based on these finding, we know that chiasmatic neurons are renewed during the chiasm formation, the chiasmatic neurons at later stage than E13 may also generated later. But where do the E13 EdU labeled chiasmatic neurons go? There are three possibilities: they may migrate out of the region of chiasmatic neurons to other part of the brain(Golden & Cepko, 1996); they may differentiated again and become other type of cells(Mason & Sretavan, 1997); they may eventually died after finishing their duties(Allendoerfer & Shatz, 1994; Altman & Bayer, 1986; Mason & Sretavan,

1997). In our experiment, there is no obvious observation that the EdU labeled chiasmatic cells migrate to other part of the ventral diencephalon. So we focus on the other two possibilities. Chiasmatic neurons are inmmunoreactive for SSEA-1 antibody, which is often used as a mouse embryonic stem cell marker and neural stem cell marker (Abramova et al, 2005; Muramatsu & Muramatsu, 2004; Yagi et al, 2010). So chiasmatic neurons may differentiate in the later stage during development and give rise to some daughter cells, causing the original EdU labeling diluted during cell dividing. In addition, we also found that more and more chiasmatic neurons are dead from E13 to E15. So this may be another reason of why many of E13 chiasmatic neurons disappear during development.

Then we birthdated the chiasmatic radial glia and found that chiasmatic radial glia cells also start to rise from E9.5, but only a couple of these early generated cells can be observed at E13. A few more chiasmatic radial glia are generated at E10, but a lot of chiasmatic radial glia cells at the E13 chiasm are born from E11. These observations match to the results of cell counting analyses that the large number of chiasmatic radial glia at E13 is generated from E11.

After birthdating these chiasmatic radial glia, we trace these radial glia and try to find out their fates as well. Therefore, we chose the injection day of EdU at E11. Similar as chiasmatic neurons, these EdU labeled chiasmatic radial glia at E13 become fewer and fewer from E14 to E15, and finally disappear from E16. Where do these chiasmatic radial glia go? It may share the same possibilities with chiasmatic neurons. Still there is no obvious migration of these chiasmatic radial glia observed. So we try to prove the other two possibilities. From E13 to E15, chiasmatic radial glia are Nestin positive, which is classic neural stem cell marker. But be different from chiasmatic neurons, there is no apoptosis cell detected in the radial glia palisade.

Previous study indicated that in the late embryonic stage, the midline radial glia start to differentiate into astrocytes (Bovolenta et al, 1987; Mason & Sretavan, 1997), and radial glia in other parts of the brain have already been proved to be a population of neural precursor cells (Kriegstein & Alvarez-Buylla, 2009; Malatesta et al, 2008) giving rise to both neurons and glia and also serving as scaffold for the migration of new-born neurons (Hartfuss et al, 2001; Malatesta et al, 2000; Miyata et al, 2001; Noctor et al, 2001). So it is very likely that the chiasmatic radial glia, like radial glia in other parts of brain, keep diving during the development causing the original EdU labeling diluted revealed as disappear at the midline.

In this part of study, we have birthdated the chiasmatic neurons and radial glia, and found that these two groups of cells have different birthdating schedule and different fates. However, we only show the possible fates of the chiasm cells. For the chiasmatic neurons, we do not know that they are more likely dead or differentiated during the development. For the chiasmatic radial glia, we still not sure how they differentiate at the midline, what kind of daughter cells they generated. So some further study could be done in the future. We can isolate chiasmatic neurons and radial glia respectively, and test their differentiating abilities in vitro. Using triple staining analyses, we can investigate how many EdU labeled chiasmatic neurons die during the development.

This thesis also contains another part of study-investigating the expression and functions of NMDA receptor during the development of mouse optic pathway. In this part of study, we first detected the mRNA expression of all the receptor subunits and found that all the subunits are expressed in the adult retina, embryo retina and ventral diencephalon and most of them, except NR2C, have a weaker expression in embryo retina and stronger expression in adult retina and embryo ventral

diencephalon. Then we investigated the protein expression of NMDA receptor in the mouse optic pathway. Here we chose three antibodies, NR1, NR2B and NR3A. Actually, we also used NR2A/B and NR2A antibodies, but they did not work very well and these parts of data were not put into this thesis. In the developing retina, NR1, NR2B and NR3A were located on the inner layer and fiber layer in the retina from E14 to E15. Double staining analyses showed that NR1, NR2B and NR3A positive cells were overlapped with TuJ-1 positive neurons. In the developing ventral diencephalon, these three subunits were located everywhere; however, NR1 and NR3A had stronger staining on the optic stalk and optic tract. As NMDA receptor is expressed in the optic pathway, they may also contribute to the axon pathfinding and chiasm development. Using NMDA receptor antagonists, Dextrorphan-D-tartrate or MK-801, a significant reduction of the neurite outgrowth from the E14 retinal explants was observed, suggesting that a positive influence of NMDA receptor on the axon growth at the optic chiasm.

However, through this part of study, it is still not clear if NMDA receptor provides any guidance information to retinal axon projection. To investigate this, we can use NMDA receptor antagonists or antibodies in the brain slice culture, and observe their influence to the axon projection in the chiasm. With the more specific antibodies, we can also detect which subunits are more important for the development of mouse optic pathway.

In the last part of this thesis, we investigated the retinal axon pathway in the ventral diencephalon in the *Sox10*^{Dom} mutant embryos and γA-crystallin mutant embryos. It was found that *Sox10* may not contribute to axon guidance in the developing optic pathway, as retinal axon pathfinding are quite normal in the mutant embryos. γA-crystallin may only play a role in the later uncrossed axons, as a

significant reduction in the uncrossed axon at E15.5 in the γA-crystallin$^{-/-}$ group were observed when compared with that in the γA-crystallin$^{+/-}$ group. But the function of γA-crystallin in the uncrossed axons still remains unclear, may be worth to do further investigations.

References

Abramova N, Charniga C, Goderie SK, Temple S (2005) Stage-specific changes in gene expression in acutely isolated mouse CNS progenitor cells. *Dev Biol* **283:** 269-281

Acosta ML, Bumsted O'Brien KM, Tan SS, Kalloniatis M (2008) Emergence of cellular markers and functional ionotropic glutamate receptors on tangentially dispersed cells in the developing mouse retina. *J Comp Neurol* **506:** 506-523

Allendoerfer KL, Shatz CJ (1994) The subplate, a transient neocortical structure: its role in the development of connections between thalamus and cortex. *Annu Rev Neurosci* **17:** 185-218

Altman J, Bayer SA (1986) The development of the rat hypothalamus. *Adv Anat Embryol Cell Biol* **100:** 1-178

Andley UP (2007) Crystallins in the eye: Function and pathology. *Prog Retin Eye Res* **26:** 78-98

Andley UP (2008) The lens epithelium: focus on the expression and function of the alpha-crystallin chaperones. *Int J Biochem Cell Biol* **40:** 317-323

Andley UP (2009a) AlphaA-crystallin R49Cneo mutation influences the architecture of lens fiber cell membranes and causes posterior and nuclear cataracts in mice. *BMC Ophthalmol* **9:** 4

Andley UP (2009b) Effects of alpha-crystallin on lens cell function and cataract pathology. *Curr Mol Med* **9:** 887-892

Andley UP, Reilly MA (2010) In vivo lens deficiency of the R49C alphaA-crystallin mutant. *Exp Eye Res* **90:** 699-702

Babb TL, Mikuni N, Najm I, Wylie C, Olive M, Dollar C, MacLennan H (2005) Pre- and postnatal expressions of NMDA receptors 1 and 2B subunit proteins in the normal rat cortex. *Epilepsy Res* **64:** 23-30

Birgbauer E, Cowan CA, Sretavan DW, Henkemeyer M (2000) Kinase independent function of EphB receptors in retinal axon pathfinding to the optic disc from dorsal but not ventral retina. *Development* **127:** 1231-1241

Bovolenta P, Liem RK, Mason CA (1987) Glial filament protein expression in astroglia in the mouse visual pathway. *Brain Res* **430:** 113-126

Britsch S, Goerich DE, Riethmacher D, Peirano RI, Rossner M, Nave KA, Birchmeier C, Wegner M (2001) The transcription factor Sox10 is a key regulator of peripheral glial development. *Genes Dev* **15:** 66-78

Brittis PA, Canning DR, Silver J (1992) Chondroitin sulfate as a regulator of neuronal patterning in the retina. *Science* **255:** 733-736

Brittis PA, Silver J (1994) Exogenous glycosaminoglycans induce complete inversion of retinal ganglion cell bodies and their axons within the retinal neuroepithelium. *Proc Natl Acad Sci U S A* **91:** 7539-7542

Brittis PA, Silver J (1995) Multiple factors govern intraretinal axon guidance: a time-lapse study. *Mol Cell Neurosci* **6:** 413-432

Buck SB, Bradford J, Gee KR, Agnew BJ, Clarke ST, Salic A (2008) Detection of S-phase cell cycle progression using 5-ethynyl-2'-deoxyuridine incorporation with click chemistry, an alternative to using 5-bromo-2'-deoxyuridine antibodies. *Biotechniques* **44:** 927-929

Bunt SM, Lund RD (1981) Development of a transient retino-retinal pathway in hooded and albino rats. *Brain Res* **211:** 399-404

Capela A, Temple S (2002) LeX/ssea-1 is expressed by adult mouse CNS stem cells, identifying them as nonependymal. *Neuron* **35:** 865-875

Carter AJ (1994) Many agents that antagonize the NMDA receptor-channel complex in vivo also cause disturbances of motor coordination. *J Pharmacol Exp Ther* **269:** 573-580

Castellani V, De Angelis E, Kenwrick S, Rougon G (2002) Cis and trans interactions of L1 with neuropilin-1 control axonal responses to semaphorin 3A. *EMBO J* **21:** 6348-6357

Chehrehasa F, Meedeniya AC, Dwyer P, Abrahamsen G, Mackay-Sim A (2009) EdU, a new thymidine analogue for labelling proliferating cells in the nervous system. *J Neurosci Methods* **177:** 122-130

Chen C, Regehr WG (2000) Developmental remodeling of the retinogeniculate synapse. *Neuron* **28:** 955-966

Chung KY, Shum DK, Chan SO (2000a) Expression of chondroitin sulfate proteoglycans in the chiasm of mouse embryos. *J Comp Neurol* **417:** 153-163

Chung KY, Taylor JS, Shum DK, Chan SO (2000b) Axon routing at the optic chiasm

after enzymatic removal of chondroitin sulfate in mouse embryos. *Development* **127:** 2673-2683

Clarke RJ, Johnson JW (2006) NMDA receptor NR2 subunit dependence of the slow component of magnesium unblock. *J Neurosci* **26:** 5825-5834

Colello RJ, Guillery RW (1990) The early development of retinal ganglion cells with uncrossed axons in the mouse: retinal position and axonal course. *Development* **108:** 515-523

Constantine-Paton M, Cline HT, Debski E (1990) Patterned activity, synaptic convergence, and the NMDA receptor in developing visual pathways. *Annu Rev Neurosci* **13:** 129-154

Cuppini R, Sartini S, Ambrogini P, Falcieri E, Maltarello MC, Gallo G (1999) Control of neuron outgrowth by NMDA receptors. *J Submicrosc Cytol Pathol* **31:** 31-40

Dakubo GD, Wang YP, Mazerolle C, Campsall K, McMahon AP, Wallace VA (2003) Retinal ganglion cell-derived sonic hedgehog signaling is required for optic disc and stalk neuroepithelial cell development. *Development* **130:** 2967-2980

Dale JK, Vesque C, Lints TJ, Sampath TK, Furley A, Dodd J, Placzek M (1997) Cooperation of BMP7 and SHH in the induction of forebrain ventral midline cells by prechordal mesoderm. *Cell* **90:** 257-269

Dalva MB, Takasu MA, Lin MZ, Shamah SM, Hu L, Gale NW, Greenberg ME (2000) EphB receptors interact with NMDA receptors and regulate excitatory synapse formation. *Cell* **103:** 945-956

Das S, Sasaki YF, Rothe T, Premkumar LS, Takasu M, Crandall JE, Dikkes P, Conner DA, Rayudu PV, Cheung W, Chen HS, Lipton SA, Nakanishi N (1998) Increased NMDA current and spine density in mice lacking the NMDA receptor subunit NR3A. *Nature* **393:** 377-381

Deiner MS, Kennedy TE, Fazeli A, Serafini T, Tessier-Lavigne M, Sretavan DW (1997) Netrin-1 and DCC mediate axon guidance locally at the optic disc: loss of function leads to optic nerve hypoplasia. *Neuron* **19:** 575-589

Demyanenko GP, Maness PF (2003) The L1 cell adhesion molecule is essential for topographic mapping of retinal axons. *J Neurosci* **23:** 530-538

Dingledine R, Borges K, Bowie D, Traynelis SF (1999) The glutamate receptor ion channels. *Pharmacol Rev* **51:** 7-61

Drager UC (1985) Birth dates of retinal ganglion cells giving rise to the crossed and uncrossed optic projections in the mouse. *Proc R Soc Lond B Biol Sci* **224:** 57-77

Ebara M, Yamato M, Aoyagi T, Kikuchi A, Sakai K, Okano T (2004) Temperature-responsive cell culture surfaces enable "on-off" affinity control between cell integrins and RGDS ligands. *Biomacromolecules* **5:** 505-510

Egeland M, Warner-Schmidt J, Greengard P, Svenningsson P (2010) Neurogenic effects of fluoxetine are attenuated in p11 (S100A10) knockout mice. *Biol Psychiatry* **67:** 1048-1056

Ericson J, Muhr J, Placzek M, Lints T, Jessell TM, Edlund T (1995) Sonic hedgehog induces the differentiation of ventral forebrain neurons: a common signal for ventral patterning within the neural tube. *Cell* **81:** 747-756

Erskine L, Herrera E (2007) The retinal ganglion cell axon's journey: insights into molecular mechanisms of axon guidance. *Dev Biol* **308:** 1-14

Erskine L, Williams SE, Brose K, Kidd T, Rachel RA, Goodman CS, Tessier-Lavigne M, Mason CA (2000) Retinal ganglion cell axon guidance in the mouse optic chiasm: expression and function of robos and slits. *J Neurosci* **20:** 4975-4982

Falk J, Bechara A, Fiore R, Nawabi H, Zhou H, Hoyo-Becerra C, Bozon M, Rougon G, Grumet M, Puschel AW, Sanes JR, Castellani V (2005) Dual functional activity of semaphorin 3B is required for positioning the anterior commissure. *Neuron* **48:** 63-75

Feldheim DA, Kim YI, Bergemann AD, Frisen J, Barbacid M, Flanagan JG (2000) Genetic analysis of ephrin-A2 and ephrin-A5 shows their requirement in multiple aspects of retinocollicular mapping. *Neuron* **25:** 563-574

Feller MB (2002) The role of nAChR-mediated spontaneous retinal activity in visual system development. *J Neurobiol* **53:** 556-567

Firth SI, Wang CT, Feller MB (2005) Retinal waves: mechanisms and function in visual system development. *Cell Calcium* **37:** 425-432

Fletcher EL, Hack I, Brandstatter JH, Wassle H (2000) Synaptic localization of NMDA receptor subunits in the rat retina. *J Comp Neurol* **420:** 98-112

Frisen J, Yates PA, McLaughlin T, Friedman GC, O'Leary DD, Barbacid M (1998) Ephrin-A5 (AL-1/RAGS) is essential for proper retinal axon guidance and topographic mapping in the mammalian visual system. *Neuron* **20:** 235-243

Gan L, Wang SW, Huang Z, Klein WH (1999) POU domain factor Brn-3b is essential for retinal ganglion cell differentiation and survival but not for initial cell fate specification. *Dev Biol* **210:** 469-480

Gan L, Xiang M, Zhou L, Wagner DS, Klein WH, Nathans J (1996) POU domain factor Brn-3b is required for the development of a large set of retinal ganglion cells. *Proc Natl Acad Sci U S A* **93:** 3920-3925

Garcia-Frigola C, Carreres MI, Vegar C, Mason C, Herrera E (2008) Zic2 promotes axonal divergence at the optic chiasm midline by EphB1-dependent and -independent mechanisms. *Development* **135:** 1833-1841

George J, Dravid SM, Prakash A, Xie J, Peterson J, Jabba SV, Baden DG, Murray TF (2009) Sodium channel activation augments NMDA receptor function and promotes neurite outgrowth in immature cerebrocortical neurons. *J Neurosci* **29:** 3288-3301

Georgiev D, Taniura H, Kambe Y, Takarada T, Yoneda Y (2008) A critical importance of polyamine site in NMDA receptors for neurite outgrowth and fasciculation at early stages of P19 neuronal differentiation. *Exp Cell Res* **314:** 2603-2617

Giannakopoulos M, Kouvelas ED, Mitsacos A (2010) Experience-dependent regulation of NMDA receptor subunit composition and phosphorylation in the retina and visual cortex. *Invest Ophthalmol Vis Sci* **51:** 1817-1822

Golden JA, Cepko CL (1996) Clones in the chick diencephalon contain multiple cell types and siblings are widely dispersed. *Development* **122:** 65-78

Gong B, Zhang LY, Lam DS, Pang CP, Yam GH (2010) Sodium 4-phenylbutyrate ameliorates the effects of cataract-causing mutant gammaD-crystallin in cultured cells. *Mol Vis* **16:** 997-1003

Graw J (2009a) Genetics of crystallins: cataract and beyond. *Exp Eye Res* **88:** 173-189

Graw J (2009b) Mouse models of cataract. *J Genet* **88:** 469-486

Guillery RW, Mason CA, Taylor JS (1995) Developmental determinants at the mammalian optic chiasm. *J Neurosci* **15:** 4727-4737

Haberecht MF, Mitchell CK, Lo GJ, Redburn DA (1997) N-methyl-D-aspartate-mediated glutamate toxicity in the developing rabbit retina. *J Neurosci Res* **47:** 416-426

Haberny KA, Paule MG, Scallet AC, Sistare FD, Lester DS, Hanig JP, Slikker W, Jr.

(2002) Ontogeny of the N-methyl-D-aspartate (NMDA) receptor system and susceptibility to neurotoxicity. *Toxicol Sci* **68:** 9-17

Hao YL, Hong LP, Chan SO, Dong WR (2007) [Changes of Smoothened expression during retinofugal pathway development in mouse embryos]. *Nan Fang Yi Ke Da Xue Xue Bao* **27:** 293-295

Hartfuss E, Galli R, Heins N, Gotz M (2001) Characterization of CNS precursor subtypes and radial glia. *Dev Biol* **229:** 15-30

Hashimoto M, Mikoshiba K (2004) Neuronal birthdate-specific gene transfer with adenoviral vectors. *J Neurosci* **24:** 286-296

Haupt C, Huber AB (2008) How axons see their way--axonal guidance in the visual system. *Front Biosci* **13:** 3136-3149

Herrera E, Brown L, Aruga J, Rachel RA, Dolen G, Mikoshiba K, Brown S, Mason CA (2003) Zic2 patterns binocular vision by specifying the uncrossed retinal projection. *Cell* **114:** 545-557

Herrera E, Garcia-Frigola C (2008) Genetics and development of the optic chiasm. *Front Biosci* **13:** 1646-1653

Herrera E, Marcus R, Li S, Williams SE, Erskine L, Lai E, Mason C (2004) Foxd1 is required for proper formation of the optic chiasm. *Development* **131:** 5727-5739

Hindges R, McLaughlin T, Genoud N, Henkemeyer M, O'Leary DD (2002) EphB forward signaling controls directional branch extension and arborization required for dorsal-ventral retinotopic mapping. *Neuron* **35:** 475-487

Hopker VH, Shewan D, Tessier-Lavigne M, Poo M, Holt C (1999) Growth-cone attraction to netrin-1 is converted to repulsion by laminin-1. *Nature* **401:** 69-73

Huberman AD, Stellwagen D, Chapman B (2002) Decoupling eye-specific segregation from lamination in the lateral geniculate nucleus. *J Neurosci* **22:** 9419-9429

Ichijo H, Kawabata I (2001) Roles of the telencephalic cells and their chondroitin sulfate proteoglycans in delimiting an anterior border of the retinal pathway. *J Neurosci* **21:** 9304-9314

Inatani M (2005) Molecular mechanisms of optic axon guidance. *Naturwissenschaften* **92:** 549-561

Isa T, Saito Y (2001) The direct visuo-motor pathway in mammalian superior colliculus; novel perspective on the interlaminar connection. *Neurosci Res* **41:** 107-113

Jakobs TC, Ben Y, Masland RH (2007) Expression of mRNA for glutamate receptor subunits distinguishes the major classes of retinal neurons, but is less specific for individual cell types. *Mol Vis* **13:** 933-948

Jaubert-Miazza L, Green E, Lo FS, Bui K, Mills J, Guido W (2005) Structural and functional composition of the developing retinogeniculate pathway in the mouse. *Vis Neurosci* **22:** 661-676

Jeffery G (2001) Architecture of the optic chiasm and the mechanisms that sculpt its development. *Physiol Rev* **81:** 1393-1414

Ji Y, Bi H, Li N, Jin H, Yang P, Kong X, Yan S, Lu Y (2010) Alterations to proteins in the lens of hereditary Crygs-mutated cataractous mice. *Mol Vis* **16:** 1068-1075

Jose A, Krishnan LK (2010) Effect of matrix composition on differentiation of nestin-positive neural progenitors from circulation into neurons. *J Neural Eng* **7:** 036009

Kapur RP (1999) Early death of neural crest cells is responsible for total enteric aganglionosis in Sox10(Dom)/Sox10(Dom) mouse embryos. *Pediatr Dev Pathol* **2:** 559-569

Kelsh RN (2006) Sorting out Sox10 functions in neural crest development. *Bioessays* **28:** 788-798

Knabe W, Washausen S, Happel N, Kuhn HJ (2008) Diversity in mammalian chiasmatic architecture: ipsilateral axons are deflected at glial arches in the prechiasmatic optic nerve of the eutherian Tupaia belangeri. *J Comp Neurol* **508:** 437-457

Kriegstein A, Alvarez-Buylla A (2009) The glial nature of embryonic and adult neural stem cells. *Annu Rev Neurosci* **32:** 149-184

Kruger K, Tam AS, Lu C, Sretavan DW (1998) Retinal ganglion cell axon progression from the optic chiasm to initiate optic tract development requires cell autonomous function of GAP-43. *J Neurosci* **18:** 5692-5705

LePage KT, Ishmael JE, Low CM, Traynelis SF, Murray TF (2005) Differential binding properties of [3H]dextrorphan and [3H]MK-801 in heterologously expressed NMDA receptors. *Neuropharmacology* **49:** 1-16

Li YH, Wang J, Zhang G (2009) Presynaptic NR2B-containing NMDA autoreceptors mediate gluta-matergic synaptic transmission in the rat visual cortex. *Curr Neurovasc Res* **6:** 104-109

Lin L, Chan SO (2003) Perturbation of CD44 function affects chiasmatic routing of retinal axons in brain slice preparations of the mouse retinofugal pathway. *Eur J Neurosci* **17:** 2299-2312

Lin L, Cheung AW, Chan SO (2005) Chiasmatic neurons in the ventral diencephalon of mouse embryos--changes in arrangement and heterogeneity in surface antigen expression. *Brain Res Dev Brain Res* **158:** 1-12

Lin L, Wang J, Chan CK, Chan SO (2007a) Effects of exogenous hyaluronan on midline crossing and axon divergence in the optic chiasm of mouse embryos. *Eur J Neurosci* **26:** 1-11

Lin L, Wang J, Chan CK, Chan SO (2007b) Localization of hyaluronan in the optic pathway of mouse embryos. *Neuroreport* **18:** 355-358

Liu J, Wilson S, Reh T (2003) BMP receptor 1b is required for axon guidance and cell survival in the developing retina. *Dev Biol* **256:** 34-48

Liu X, Chen C (2008) Different roles for AMPA and NMDA receptors in transmission at the immature retinogeniculate synapse. *J Neurophysiol* **99:** 629-643

Macdonald R, Barth KA, Xu Q, Holder N, Mikkola I, Wilson SW (1995) Midline signalling is required for Pax gene regulation and patterning of the eyes. *Development* **121:** 3267-3278

Macdonald R, Scholes J, Strahle U, Brennan C, Holder N, Brand M, Wilson SW (1997) The Pax protein Noi is required for commissural axon pathway formation in the rostral forebrain. *Development* **124:** 2397-2408

Malatesta P, Appolloni I, Calzolari F (2008) Radial glia and neural stem cells. *Cell Tissue Res* **331:** 165-178

Malatesta P, Hartfuss E, Gotz M (2000) Isolation of radial glial cells by fluorescent-activated cell sorting reveals a neuronal lineage. *Development* **127:** 5253-5263

Manitt C, Nikolakopoulou AM, Almario DR, Nguyen SA, Cohen-Cory S (2009) Netrin participates in the development of retinotectal synaptic connectivity by modulating axon arborization and synapse formation in the developing brain. *J Neurosci* **29:** 11065-11077

Mann F, Harris WA, Holt CE (2004) New views on retinal axon development: a navigation guide. *Int J Dev Biol* **48:** 957-964

Marcus RC, Blazeski R, Godement P, Mason CA (1995) Retinal axon divergence in the optic chiasm: uncrossed axons diverge from crossed axons within a midline glial specialization. *J Neurosci* **15:** 3716-3729

Marcus RC, Mason CA (1995) The first retinal axon growth in the mouse optic chiasm: axon patterning and the cellular environment. *J Neurosci* **15:** 6389-6402

Marti E, Takada R, Bumcrot DA, Sasaki H, McMahon AP (1995) Distribution of Sonic hedgehog peptides in the developing chick and mouse embryo. *Development* **121:** 2537-2547

Mason CA, Sretavan DW (1997) Glia, neurons, and axon pathfinding during optic chiasm development. *Curr Opin Neurobiol* **7:** 647-653

McLaughlin T, O'Leary DD (2005) Molecular gradients and development of retinotopic maps. *Annu Rev Neurosci* **28:** 327-355

Meriane M, Tcherkezian J, Webber CA, Danek EI, Triki I, McFarlane S, Bloch-Gallego E, Lamarche-Vane N (2004) Phosphorylation of DCC by Fyn mediates Netrin-1 signaling in growth cone guidance. *J Cell Biol* **167:** 687-698

Messersmith EK, Feller MB, Zhang H, Shatz CJ (1997) Migration of neocortical neurons in the absence of functional NMDA receptors. *Mol Cell Neurosci* **9:** 347-357

Miyata T, Kawaguchi A, Okano H, Ogawa M (2001) Asymmetric inheritance of radial glial fibers by cortical neurons. *Neuron* **31:** 727-741

Morest DK, Silver J (2003) Precursors of neurons, neuroglia, and ependymal cells in the CNS: what are they? Where are they from? How do they get where they are going? *Glia* **43:** 6-18

Muir-Robinson G, Hwang BJ, Feller MB (2002) Retinogeniculate axons undergo eye-specific segregation in the absence of eye-specific layers. *J Neurosci* **22:** 5259-5264

Muramatsu T, Muramatsu H (2004) Carbohydrate antigens expressed on stem cells and early embryonic cells. *Glycoconj J* **21:** 41-45

Nagai T, Aruga J, Minowa O, Sugimoto T, Ohno Y, Noda T, Mikoshiba K (2000) Zic2 regulates the kinetics of neurulation. *Proc Natl Acad Sci U S A* **97:** 1618-1623

Nakagawa S, Brennan C, Johnson KG, Shewan D, Harris WA, Holt CE (2000) Ephrin-B regulates the Ipsilateral routing of retinal axons at the optic chiasm. *Neuron* **25:** 599-610

Nishi M, Hinds H, Lu HP, Kawata M, Hayashi Y (2001) Motoneuron-specific expression of NR3B, a novel NMDA-type glutamate receptor subunit that works in a dominant-negative manner. *J Neurosci* **21:** RC185

Noctor SC, Flint AC, Weissman TA, Dammerman RS, Kriegstein AR (2001) Neurons derived from radial glial cells establish radial units in neocortex. *Nature* **409:** 714-720

Oster SF, Bodeker MO, He F, Sretavan DW (2003) Invariant Sema5A inhibition serves an ensheathing function during optic nerve development. *Development* **130:** 775-784

Ozawa S, Kamiya H, Tsuzuki K (1998) Glutamate receptors in the mammalian central nervous system. *Prog Neurobiol* **54:** 581-618

Pak W, Hindges R, Lim YS, Pfaff SL, O'Leary DD (2004) Magnitude of binocular vision controlled by islet-2 repression of a genetic program that specifies laterality of retinal axon pathfinding. *Cell* **119:** 567-578

Pan L, Yang Z, Feng L, Gan L (2005) Functional equivalence of Brn3 POU-domain transcription factors in mouse retinal neurogenesis. *Development* **132:** 703-712

Parnavelas JG, Nadarajah B (2001) Radial glial cells. are they really glia? *Neuron* **31:** 881-884

Penn AA, Riquelme PA, Feller MB, Shatz CJ (1998) Competition in retinogeniculate patterning driven by spontaneous activity. *Science* **279:** 2108-2112

Perez-Otano I, Schulteis CT, Contractor A, Lipton SA, Trimmer JS, Sucher NJ, Heinemann SF (2001) Assembly with the NR1 subunit is required for surface expression of NR3A-containing NMDA receptors. *J Neurosci* **21:** 1228-1237

Petros TJ, Rebsam A, Mason CA (2008) Retinal axon growth at the optic chiasm: to cross or not to cross. *Annu Rev Neurosci* **31:** 295-315

Petros TJ, Shrestha BR, Mason C (2009) Specificity and sufficiency of EphB1 in driving the ipsilateral retinal projection. *J Neurosci* **29:** 3463-3474

Pickard L, Noel J, Henley JM, Collingridge GL, Molnar E (2000) Developmental changes in synaptic AMPA and NMDA receptor distribution and AMPA receptor

subunit composition in living hippocampal neurons. *J Neurosci* **20:** 7922-7931

Plump AS, Erskine L, Sabatier C, Brose K, Epstein CJ, Goodman CS, Mason CA, Tessier-Lavigne M (2002) Slit1 and Slit2 cooperate to prevent premature midline crossing of retinal axons in the mouse visual system. *Neuron* **33:** 219-232

Pongpudpunth M, Bhawan J, Al-Natour SH, Mahalingam M (2010) Nestin-Positive Stem Cells in Neurofibromas From Patients With Neurofibromatosis Type 1-Tumorigenic or Incidental? *Am J Dermatopathol*

Pontious A, Kowalczyk T, Englund C, Hevner RF (2008) Role of intermediate progenitor cells in cerebral cortex development. *Dev Neurosci* **30:** 24-32

Pratt T, Tian NM, Simpson TI, Mason JO, Price DJ (2004) The winged helix transcription factor Foxg1 facilitates retinal ganglion cell axon crossing of the ventral midline in the mouse. *Development* **131:** 3773-3784

Quinlan EM, Philpot BD, Huganir RL, Bear MF (1999) Rapid, experience-dependent expression of synaptic NMDA receptors in visual cortex in vivo. *Nat Neurosci* **2:** 352-357

Sakai JA, Halloran MC (2006) Semaphorin 3d guides laterality of retinal ganglion cell projections in zebrafish. *Development* **133:** 1035-1044

Salic A, Mitchison TJ (2008) A chemical method for fast and sensitive detection of DNA synthesis in vivo. *Proc Natl Acad Sci U S A* **105:** 2415-2420

Sanchez-Camacho C, Bovolenta P (2008) Autonomous and non-autonomous Shh signalling mediate the in vivo growth and guidance of mouse retinal ganglion cell axons. *Development* **135:** 3531-3541

Sasaki YF, Rothe T, Premkumar LS, Das S, Cui J, Talantova MV, Wong HK, Gong X, Chan SF, Zhang D, Nakanishi N, Sucher NJ, Lipton SA (2002) Characterization and comparison of the NR3A subunit of the NMDA receptor in recombinant systems and primary cortical neurons. *J Neurophysiol* **87:** 2052-2063

Schmidt JT (2004) Activity-driven sharpening of the retinotectal projection: the search for retrograde synaptic signaling pathways. *J Neurobiol* **59:** 114-133

Schmitt AM, Shi J, Wolf AM, Lu CC, King LA, Zou Y (2006) Wnt-Ryk signalling mediates medial-lateral retinotectal topographic mapping. *Nature* **439:** 31-37

Sharma KK, Santhoshkumar P (2009) Lens aging: effects of crystallins. *Biochim Biophys Acta* **1790:** 1095-1108

Singer JH, Mirotznik RR, Feller MB (2001) Potentiation of L-type calcium channels reveals nonsynaptic mechanisms that correlate spontaneous activity in the developing mammalian retina. *J Neurosci* **21:** 8514-8522

Sretavan DW (1990) Specific routing of retinal ganglion cell axons at the mammalian optic chiasm during embryonic development. *J Neurosci* **10:** 1995-2007

Sretavan DW, Feng L, Pure E, Reichardt LF (1994) Embryonic neurons of the developing optic chiasm express L1 and CD44, cell surface molecules with opposing effects on retinal axon growth. *Neuron* **12:** 957-975

Sretavan DW, Kruger K (1998) Randomized retinal ganglion cell axon routing at the optic chiasm of GAP-43-deficient mice: association with midline recrossing and lack of normal ipsilateral axon turning. *J Neurosci* **18:** 10502-10513

Sretavan DW, Pure E, Siegel MW, Reichardt LF (1995) Disruption of retinal axon ingrowth by ablation of embryonic mouse optic chiasm neurons. *Science* **269:** 98-101

Stanchina L, Baral V, Robert F, Pingault V, Lemort N, Pachnis V, Goossens M, Bondurand N (2006) Interactions between Sox10, Edn3 and Ednrb during enteric nervous system and melanocyte development. *Dev Biol* **295:** 232-249

Stellwagen D, Shatz CJ, Feller MB (1999) Dynamics of retinal waves are controlled by cyclic AMP. *Neuron* **24:** 673-685

Stepulak A, Luksch H, Gebhardt C, Uckermann O, Marzahn J, Sifringer M, Rzeski W, Staufner C, Brocke KS, Turski L, Ikonomidou C (2009) Expression of glutamate receptor subunits in human cancers. *Histochem Cell Biol* **132:** 435-445

Sucher NJ, Kohler K, Tenneti L, Wong HK, Grunder T, Fauser S, Wheeler-Schilling T, Nakanishi N, Lipton SA, Guenther E (2003) N-methyl-D-aspartate receptor subunit NR3A in the retina: developmental expression, cellular localization, and functional aspects. *Invest Ophthalmol Vis Sci* **44:** 4451-4456

Suganuma H, Arai Y, Kitamura Y, Hayashi M, Okumura A, Shimizu T (2010) Maternal docosahexaenoic acid-enriched diet prevents neonatal brain injury. *Neuropathology*

Suzuki S, Namiki J, Shibata S, Mastuzaki Y, Okano H (2010) The Neural Stem/Progenitor Cell Marker Nestin Is Expressed in Proliferative Endothelial Cells, But Not in Mature Vasculature. *J Histochem Cytochem*

Tennant M, Bruce SR, Beazley LD (1993) Survival of ganglion cells which form the

retino-retinal projection during optic nerve regeneration in the frog. *Vis Neurosci* **10:** 681-686

Thanos S (1999) Genesis, neurotrophin responsiveness, and apoptosis of a pronounced direct connection between the two eyes of the chick embryo: a natural error or a meaningful developmental event? *J Neurosci* **19:** 3900-3917

Thompson H, Camand O, Barker D, Erskine L (2006) Slit proteins regulate distinct aspects of retinal ganglion cell axon guidance within dorsal and ventral retina. *J Neurosci* **26:** 8082-8091

Thoreson WB, Witkovsky P (1999) Glutamate receptors and circuits in the vertebrate retina. *Prog Retin Eye Res* **18:** 765-810

Torres M, Gomez-Pardo E, Gruss P (1996) Pax2 contributes to inner ear patterning and optic nerve trajectory. *Development* **122:** 3381-3391

Tramontin AD, Garcia-Verdugo JM, Lim DA, Alvarez-Buylla A (2003) Postnatal development of radial glia and the ventricular zone (VZ): a continuum of the neural stem cell compartment. *Cereb Cortex* **13:** 580-587

Trousse F, Marti E, Gruss P, Torres M, Bovolenta P (2001) Control of retinal ganglion cell axon growth: a new role for Sonic hedgehog. *Development* **128:** 3927-3936

Wang SW, Gan L, Martin SE, Klein WH (2000) Abnormal polarization and axon outgrowth in retinal ganglion cells lacking the POU-domain transcription factor Brn-3b. *Mol Cell Neurosci* **16:** 141-156

Wang SW, Mu X, Bowers WJ, Kim DS, Plas DJ, Crair MC, Federoff HJ, Gan L, Klein WH (2002) Brn3b/Brn3c double knockout mice reveal an unsuspected role for Brn3c in retinal ganglion cell axon outgrowth. *Development* **129:** 467-477

Weiner JA, Koo SJ, Nicolas S, Fraboulet S, Pfaff SL, Pourquie O, Sanes JR (2004) Axon fasciculation defects and retinal dysplasias in mice lacking the immunoglobulin superfamily adhesion molecule BEN/ALCAM/SC1. *Mol Cell Neurosci* **27:** 59-69

Wilkinson DG (2000) Topographic mapping: organising by repulsion and competition? *Curr Biol* **10:** R447-451

Williams SE, Grumet M, Colman DR, Henkemeyer M, Mason CA, Sakurai T (2006) A role for Nr-CAM in the patterning of binocular visual pathways. *Neuron* **50:** 535-547

Williams SE, Mann F, Erskine L, Sakurai T, Wei S, Rossi DJ, Gale NW, Holt CE, Mason CA, Henkemeyer M (2003) Ephrin-B2 and EphB1 mediate retinal axon divergence at the optic chiasm. *Neuron* **39:** 919-935

Williams SE, Mason CA, Herrera E (2004) The optic chiasm as a midline choice point. *Curr Opin Neurobiol* **14:** 51-60

Wojtowicz JM, Kee N (2006) BrdU assay for neurogenesis in rodents. *Nat Protoc* **1:** 1399-1405

Wong HK, Liu XB, Matos MF, Chan SF, Perez-Otano I, Boysen M, Cui J, Nakanishi N, Trimmer JS, Jones EG, Lipton SA, Sucher NJ (2002) Temporal and regional expression of NMDA receptor subunit NR3A in the mammalian brain. *J Comp Neurol* **450:** 303-317

Wong RO (1999) Retinal waves and visual system development. *Annu Rev Neurosci* **22:** 29-47

Xiang M, Zhou L, Macke JP, Yoshioka T, Hendry SH, Eddy RL, Shows TB, Nathans J (1995) The Brn-3 family of POU-domain factors: primary structure, binding specificity, and expression in subsets of retinal ganglion cells and somatosensory neurons. *J Neurosci* **15:** 4762-4785

Yagi H, Yanagisawa M, Kato K, Yu RK (2010) Lysosome-associated membrane protein 1 is a major SSEA-1-carrier protein in mouse neural stem cells. *Glycobiology*

Zelina P, Avci HX, Thelen K, Pollerberg GE (2005) The cell adhesion molecule NrCAM is crucial for growth cone behaviour and pathfinding of retinal ganglion cell axons. *Development* **132:** 3609-3618